This is to certify that the
dissertation entitled

FREQUENCY AND TIME DOMAIN BACKCALCULATION OF FLEXIBLE PAVEMENT LAYER PARAMETERS

presented by

Yigong Ji

has been accepted towards fulfillment
of the requirements for the

Ph.D. degree in Civil Engineering

Major Professor's Signature

5/4/2005

Date

FREQUENCY AND TIME DOMAIN BACKCALCULATION OF FLEXIBLE PAVEMENT LAYER PARAMETERS

By

Yigong Ji

A DISSERTATION

Submitted to
Michigan State University
In partial fulfillment of the requirements
For the degree of

DOCTOR OF PHILOSOPHY

Department of Civil and Environmental Engineering

April 2005

ABSTRACT

Frequency and Time domain Backcalculation of Flexible Pavement Layer Parameters

By Yigong Ji

In this study, new algorithms method for backcalculating flexible pavement layer parameters based on dynamic interpretation of FWD deflection time histories using frequency and time-domain solutions have been developed. The backcalculation procedure is based on the modified Newton-Raphson method originally adopted in the MICHBACK program. Singular value decomposition (SVD), in conjunction with scaling techniques is employed in solving for the inverse problem. The frequency-domain method uses real and imaginary deflection basins as the measured quantities, while the time-domain method uses either the peak deflections and corresponding time lags or traces of the deflection time histories as the measured quantities to be matched by the backcalculation procedure.

The new associated program called DYNABACK has been written in the FORTRAN 77 language, and offers two options: (i) frequency-domain analysis, and (ii) time-domain analysis. The new program has been incorporated into the Windows™ based MFPDS program, which allows for user–friendly features including interactive input and output screens, and the ability to view and process the deflection data before analyzing it.

The new program was theoretically verified using synthetic data. Numerical examples show that the proposed methods are able to backcalculate layer moduli and thicknesses

accurately from synthetically generated FWD data. The applicability of the new program to interpret field tests was evaluated using measured deflection time history data from several FWD tests conducted in Michigan and elsewhere. The analyses included the comparison of backcalculated layer moduli and damping ratios with MICHBACK results for various pavement sections and load levels. The backcalculation was done in both frequency and time domains, where the time-domain solution included backcalculating layer moduli and thicknesses. The data were obtained from tests involving KUAB and Dynatest FWD machines. Most pavement sections were analyzed as three- and four-layer systems with some sections involving a stiff layer at shallow depth. The results indicate that dynamic backcalculation of layer parameters using field data presents some serious challenges. The frequency-domain method can lead to large errors if the measured FWD records are truncated before the motions fully decay in time, and the time-domain method when simultaneously backcalculating layer moduli and thicknesses produces mixed results.

ACKNOWLEDGMENTS

For his excellent support and advice in both academic and research works, I would like to express my gratitude to my major advisor Dr. Karim Chatti, whose assistance and guidance made this work feasible.

The author would like to express his utmost appreciation to Dr. Ronald S. Harichandran for his constant guidance and encouragement through the course of this study.

I am also indebted to the other members of the committee, Dr. Gilbert Y. Baladi and Dr. Haydar Radha for their suggestions.

The contributions, suggestions and discussions of several graduate students, especially Hyung S. Lee and Zhihui Huang are greatly appreciated.

I am thankful to the Michigan Department of Transportation for providing me with the funding during my graduate studies.

Finally I would like to thank my wife, Liping Feng, for her love and patience, and my parents and family for their support and understanding. They are always there for me.

TABLE OF CONTENTS

LIST OF TABLES

LIST OF FIGURES

CHAPTER 1 - INTRODUCTION

1.1 General

The falling weight deflectometer (FWD) is a commonly used device for evaluating the structural condition of pavements. Considerable effort has been expended over the years to interpret FWD deflection basins for determining rehabilitation strategies. This is usually done through static backcalculation in which layer moduli are determined by matching the peak deflections measured under a known load with deflections generated through a theoretical model of the pavement.

1.2 Problem Statement

Over the years, many backcalculation procedures for pavement parameters have been developed. At present, pavement layer moduli can be backcalculated from FWD data using static and dynamic methods. Static methods use only the peak values of the FWD response time histories, while dynamic methods use more of the information contained within the time histories. Since the FWD imparts a dynamic load, viscoelastic pavement properties and dynamic effects such as inertia and damping will affect the pavement response. Static backcalculation neglects these effects and is therefore less accurate than dynamic backcalculation. Furthermore, dynamic backcalculation uses the richer information contained within the FWD response time histories and may therefore have the potential to backcalculate a greater number of parameters than static backcalculation.

The above considerations indicate a need for dynamic backcalculation of the layer moduli. The purpose of this study is to develop such a tool. Dynamic backcalculation should characterize pavement materials more accurately, and thus lead to a better prediction of the pavement response using the mechanistic-empirical method of design.

1.3 Research Objective

The objective of this project is to develop a robust dynamic backcalculation computer program, whose results are not sensitive to the seed values of layer moduli. In addition, the algorithm should be able to compute the layer thicknesses and damping ratios accurately.

The resulting program needs to be user-friendly, providing various options to the user to view and preprocess the load and deflection time histories and deflection basins. This should provide an advanced backcalculation tool to pavement engineers in the context of a mechanistic based design methodology.

Upon verifying the robustness of the new dynamic backcalculation program, it will be possible to incorporate it in the Michigan Flexible Pavement Design System (MFPDS) computer software.

1.4 Report Layout

This report is organized as follows:

Chapter 2 provides a review of relevant literature on the analysis of asphalt concrete pavements. Various backcalculation methods of layer moduli and their merits and

limitations are presented. Also some of the difficulties related with the backcalculation process and error sources are discussed.

Chapter 3 describes the forward analysis program. The response of viscoelastic multi-layered pavement system due to a FWD loading is presented. The pavement is modeled as a system of horizontal layers whose material is assumed to be isotropic and linearly elastic with a hysteretic type damping. The complex response method is introduced, and the steady state as well as the transient response analyses using frequency-domain analysis is discussed.

Chapter 4 introduces an efficient iterative method for dynamic backcalculation of pavement layer properties using the relative difference between measured and computed deflections. A modified Newton method and its application to the backcalculation of pavement layer properties are presented for both frequency and time-domain backcalculation.

Chapter 5 presents the structure and features of the DYNABACK program.

Chapter 6 presents the validation results of the DYNABACK program using theoretical deflection time histories. Important aspects of convergence characteristics and uniqueness of solutions are examined. Sensitivity analyses for the various layer parameters are conducted, and the effects of imprecision in deflections and duration of deflection records are studied.

Chapter 7 contains the evaluation of the DYNABACK program using measured FWD test data from pavements across the State of Michigan as well as other sites.

Chapter 8 includes a summary of the findings and some recommendations for future research.

CHAPTER 2 - LITERATURE REVIEW

2.1 General

Falling Weight Deflectometers (FWD) are widely used to evaluate the structural properties of flexible pavements nondestructively. Backcalculation of pavement properties from FWD data is usually carried out by matching the measured deflections under a known load with theoretical deflections generated by an analytical model of the pavement by varying the elastic moduli. Such procedures usually use error minimization techniques to minimize either the absolute or the squared error, with or without weighing factors.

At present, pavement layer moduli can be backcalculated from the FWD deflection basin using the peak values of the deflection time histories (static backcalculation) or using the FWD full time history (dynamic backcalculation). However, the deflection basin under a static load is different from that under dynamic or impulse loads because of viscoelastic pavement properties and dynamic effects such as inertia, damping, and resonance. Dynamic analysis would therefore provide a more accurate estimation of the pavement modulus.

However, the interpretation of data still remains problematic. This is due to the limitations associated with the mechanical models incorporated into the backcalculation procedures and the uniqueness of inverse solutions. The net effect of these limitations is to increase the uncertainty associated with the values of the estimated in-situ mechanical properties. Such uncertainties will contribute to reducing an engineer's confidence in

their ability to properly evaluate the structural integrity of the pavement and estimate its remaining life. Nevertheless, during the past few decades, there was a significant improvement in the area of pavement modeling and NDT techniques. In the following sections, the development of pavement models and backcalculation schemes will be reviewed and discussed.

2.2 Static Material Characterization

2.2.1 Layered elastic model

The simplest way to characterize the behavior of flexible pavements is based on Boussinesq's solution that models a flexible pavement as a homogeneous, isotropic, and elastic half-space. Later, Burmister (1943) presented a method for determining stress, stain and displacement in a two layer system. Based on Burmister's method, Acum and Fox (1951) presented the solution for a three-layered pavement system. Since then, a large number of computer programs have been developed for calculating the analytical response of multi-layered flexible pavements to different load and layer interface conditions, including CHEVRON (Warren and Dieckmann, 1963), BISAR (Dejong et al,1973), ELSYM5 (Kopperman, 1985), and KENLAYER (Huang, 1993). Finite element analysis is another method that can model a layered elastic system, in which the layered pavement is divided into many small "elements". The stress state in each element is calculated using the theory of elasticity. Programs such as MICH-PAVE (Yeh, 1989) and ILLI-PAVE (Raad and Figueroa, 1980) have been developed using the finite element method. Other approaches, such as the equivalent thickness method based on the equivalent layer theory were introduced by Odemark (1949) and Ullidiz (1987).

2.2.2 Nonlinear elastic model

It is well known that granular materials and subgrade soils are nonlinear with their elastic modulus varying with the level of stress. Various constitutive equations have been developed to describe the behavior of nonlinear elastic materials. Computer programs that can handle non-linear behavior within the layered elastic theory include KENLAYER (Huang, 1993) and NELAPAVE (Irwin, 1994). The finite element computer programs MICHPAVE and ILLIPAVE can model non-linear material behavior more accurately.

2.3 Static Backcalculation Methods

Most of the commonly used backcalculation programs are generally based on static forward models. Exiting static backcalculation methods can be separated into three major groups depending on the techniques used to reach the solution.

The first group is based on iteration techniques, which repeatedly use a forward analysis method within an iterative process. The layer moduli are repeatedly adjusted until a suitable match between the calculated and measured deflection basins is obtained. A number of computer programs, such as BISDEF (Bush, 1985), BOUSDEF (Roesset, 1995), CHEVDEF (Bush, 1985), and COMCOMP (Irwin, 1994), have been developed for back-calculation analysis using this method.

The second group is based on searching a database of deflection basins. A forward calculation scheme is used to generate a database, which is then searched to find a best match for the observed deflection basin. The program MODULUS (Uzan, 1994) is one

such example. It uses deflection databases generated from the forward program BISAR, and a Hook-Jeeves pattern search algorithm within a three-point Lagrange interpolation technique to backcalculate a set of layer moduli.

The third group is based on the use of regression equations fitted to a database of deflection basins generated by a forward calculation scheme. The LOADRATE program (Chua, 1984) belongs to this category and uses regression equations generated from a database obtained by using the ILLIPAVE (Raad, 1980) nonlinear finite element program.

A thorough literature review on static backcalculation can be found elsewhere (Mahmood, 1993).

2.4 Dynamic Properties of Paving Materials

2.4.1 Asphalt Concrete

Laboratory tests indicate that the stress-strain curves for asphalt concrete materials under harmonic load exhibit a hysteresis loop as shown in Figure 2.1(Sousa, 1986). The elliptical shape shows that asphalt concrete properties are linear viscoelastic materials at low strains. The viscoelasicity can be expressed in terms of a modulus and a damping ratio which can be determined from stress or strain-controlled sinusoidal testing (Sousa, 1986). Experimental results plotted in Figure 2.2 through Figure 2.4 show that the dynamic modulus increases with frequency between 0.5 and 20 Hz, while it decreases with higher temperature. The figures also show that dynamic modulus (slope) is less affected by frequency at lower temperatures. On the other hand, damping increases with

higher temperature, and it decreases with higher frequency. Poisson's ratio increases with increasing of temperature, and decreases with increasing frequency. Also it is well known that aging makes asphalt concrete lose its viscoelasticity and become more brittle with time.

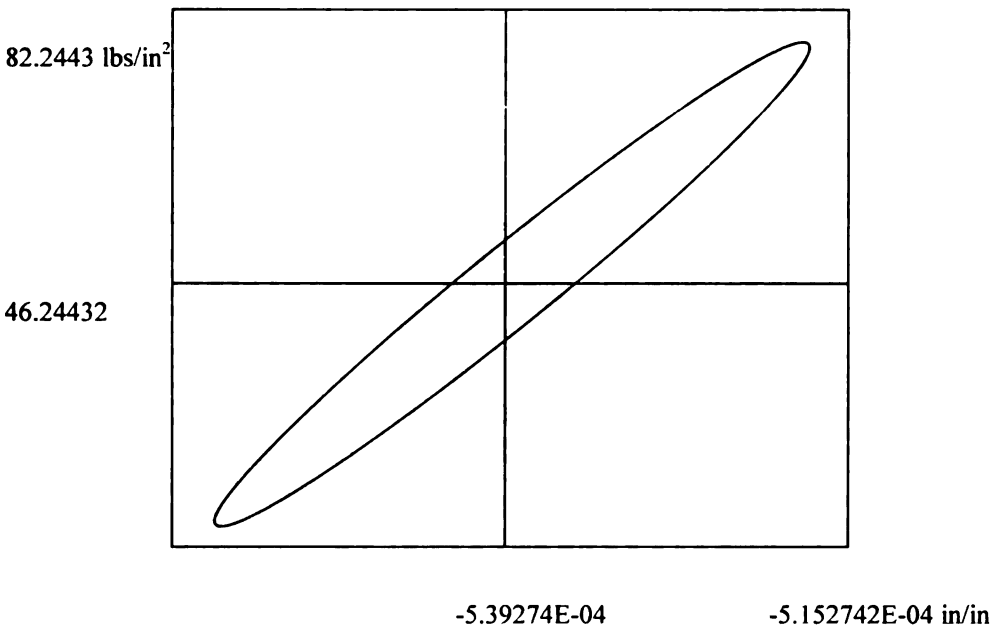

Figure 2.1 A typical hysteresis loop of asphalt concrete at 25 ° C (from Sousa, 1986)

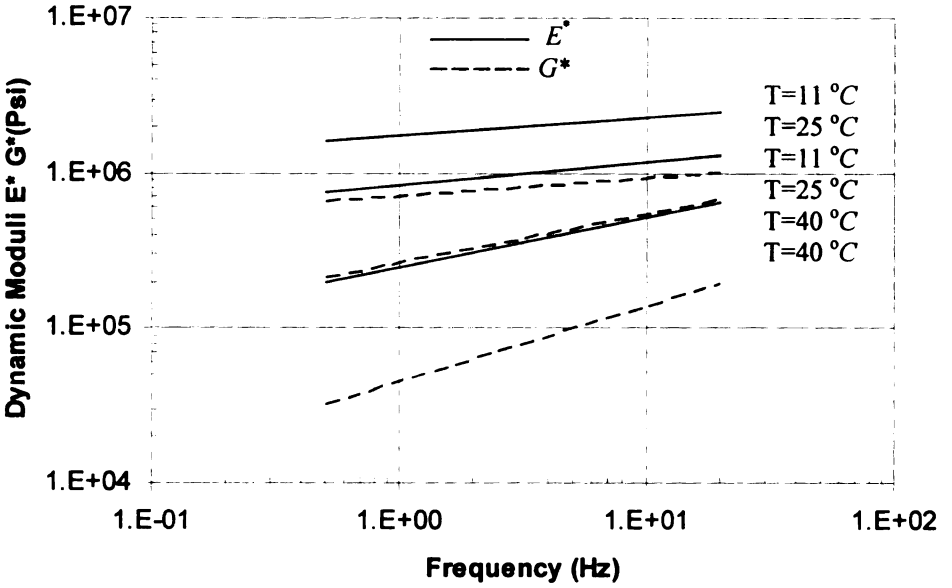

Figure 2.2 Influence of frequency and temperature on the dynamic moduli of asphalt concrete in compression and shear (from Sousa, 1986)

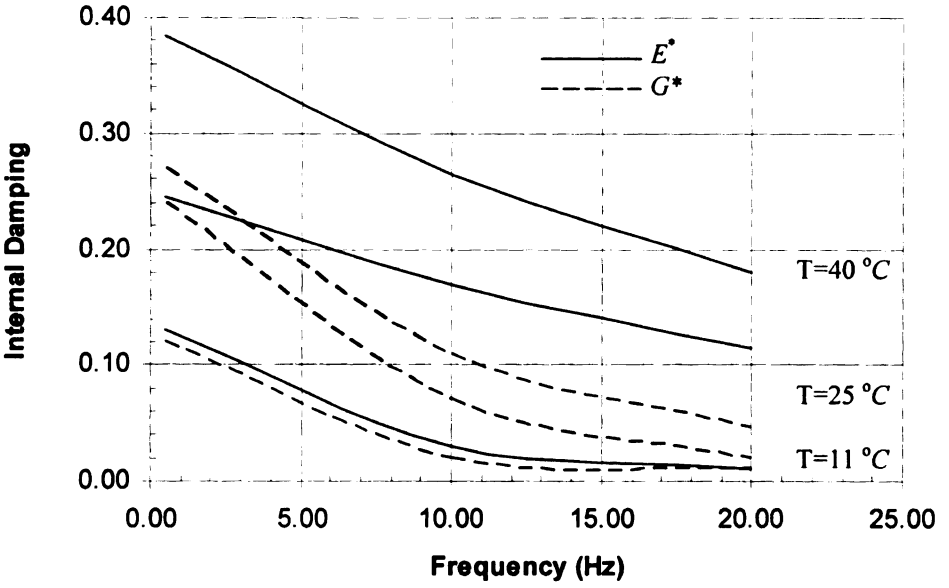

Figure 2.3 Influence of frequency and temperature on the damping ratio of asphalt concrete (from Sousa, 1986)

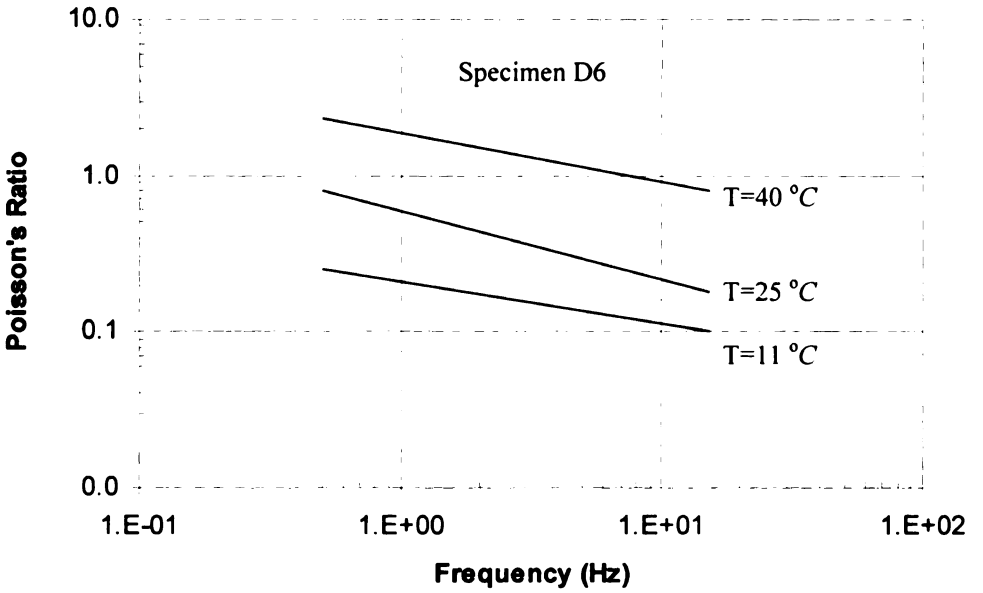

Figure 2.4 Influence of frequency and temperature on the damping ratio of asphalt concrete (from Sousa, 1986)

2.4.2 Granular Materials

Granular materials are commonly used for the construction of bases and subbases. Due to the non-linearity of granular materials, the modulus and damping ratio of the base and the subbase is dependent on three main factors: (1) the strain level; (2) the confining pressure; and (3) the relative density (Harding and Drnevich, 1972) (Seed, Wong, and et al, 1986). Figure 2.5 (Sousa, 1986) shows the dynamic shear modulus as a function of frequency at three strain levels (0.01, 0.1 and 1.0 percent) conducted with three different levels of effective mean stress (26, 20 and 16. in. Hg). The figure shows that the shear modulus decreases with increasing strain level; i.e., it exhibits no-linear behavior. However, the modulus is independent of frequency. These results are in excellent agreement with the results presented by seed and Idriss (1968).

Figure 2.6 (Sousa, 1986) shows that the internal damping increases with increasing strain levels, in addition scattering of data in the figure shows that frequency have a effects on damping ratio.

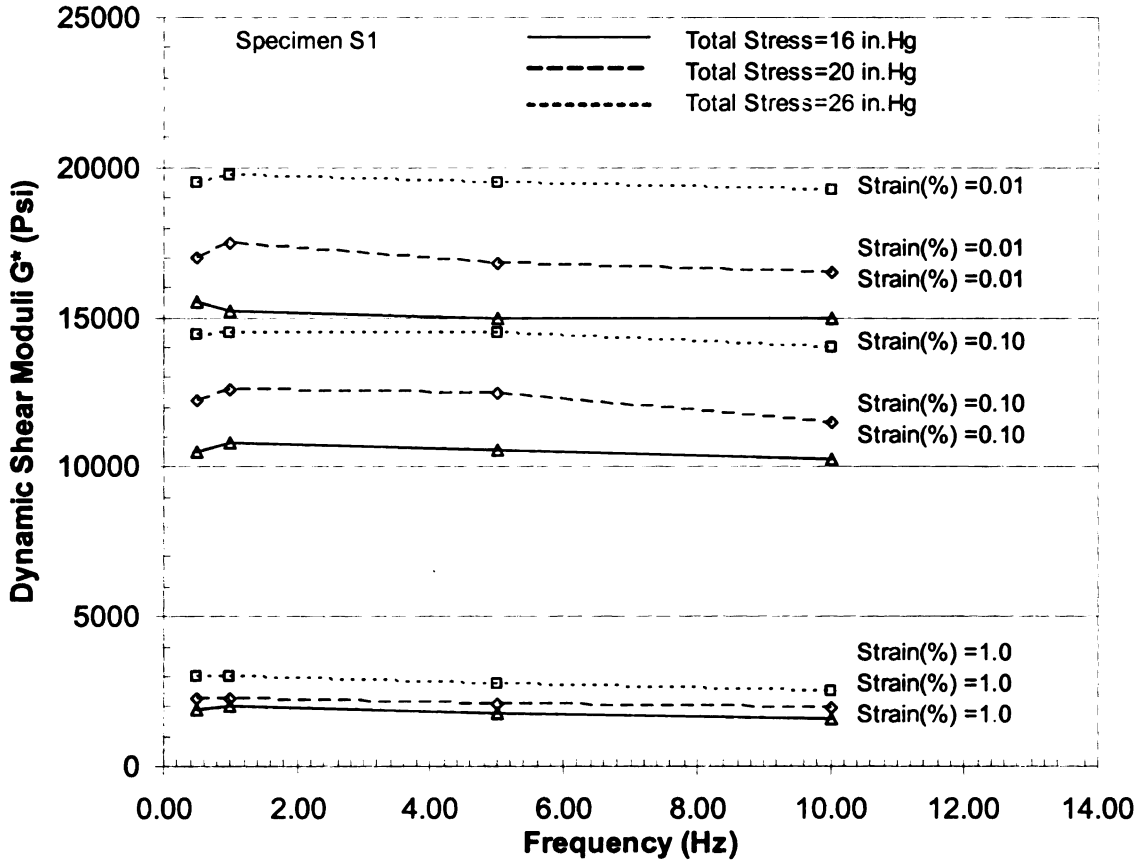

Figure 2.5 The relationship between dynamic shear modulus and frequency for Montery sand #0, 90 percent relative density (from Sousa, 1986)

Figure 2.6 (Sousa, 1986) shows that the internal damping increases with increasing strain levels, in addition scattering of data in the figure shows that frequency have a effects on damping ratio.

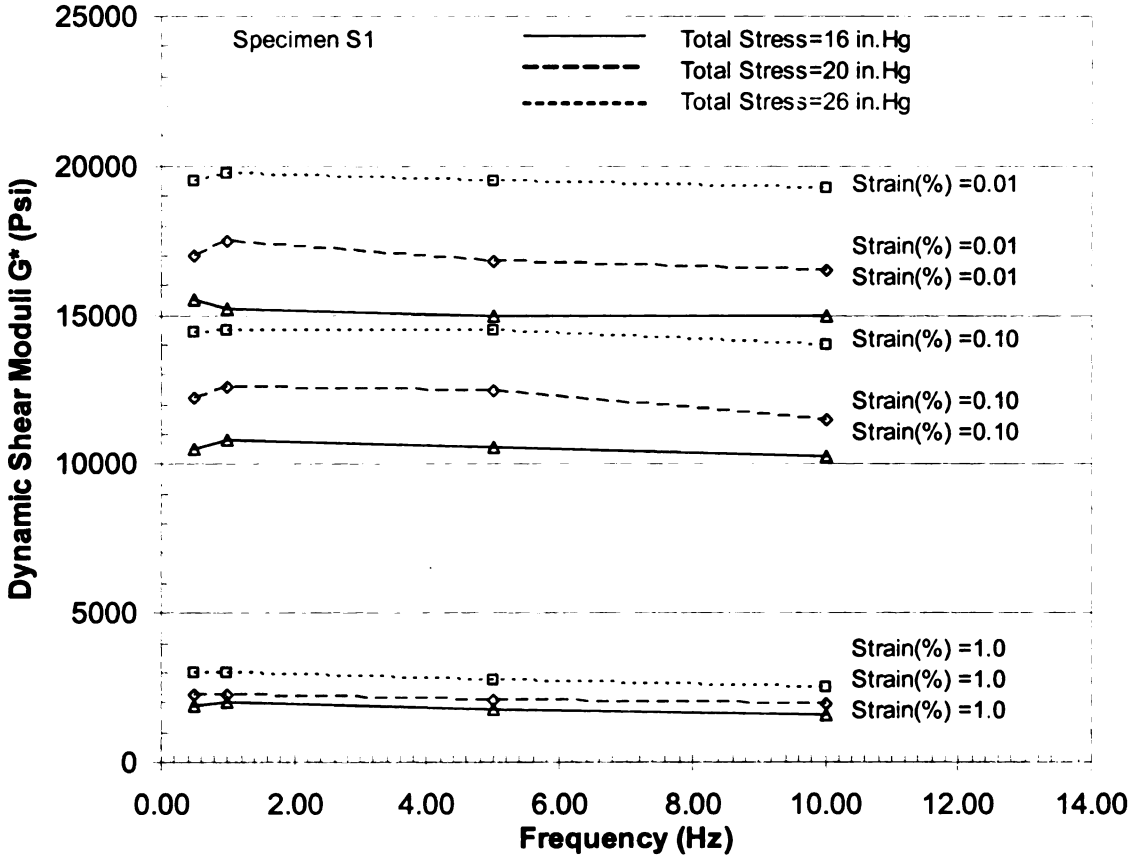

Figure 2.5 The relationship between dynamic shear modulus and frequency for Montery sand #0, 90 percent relative density (from Sousa, 1986)

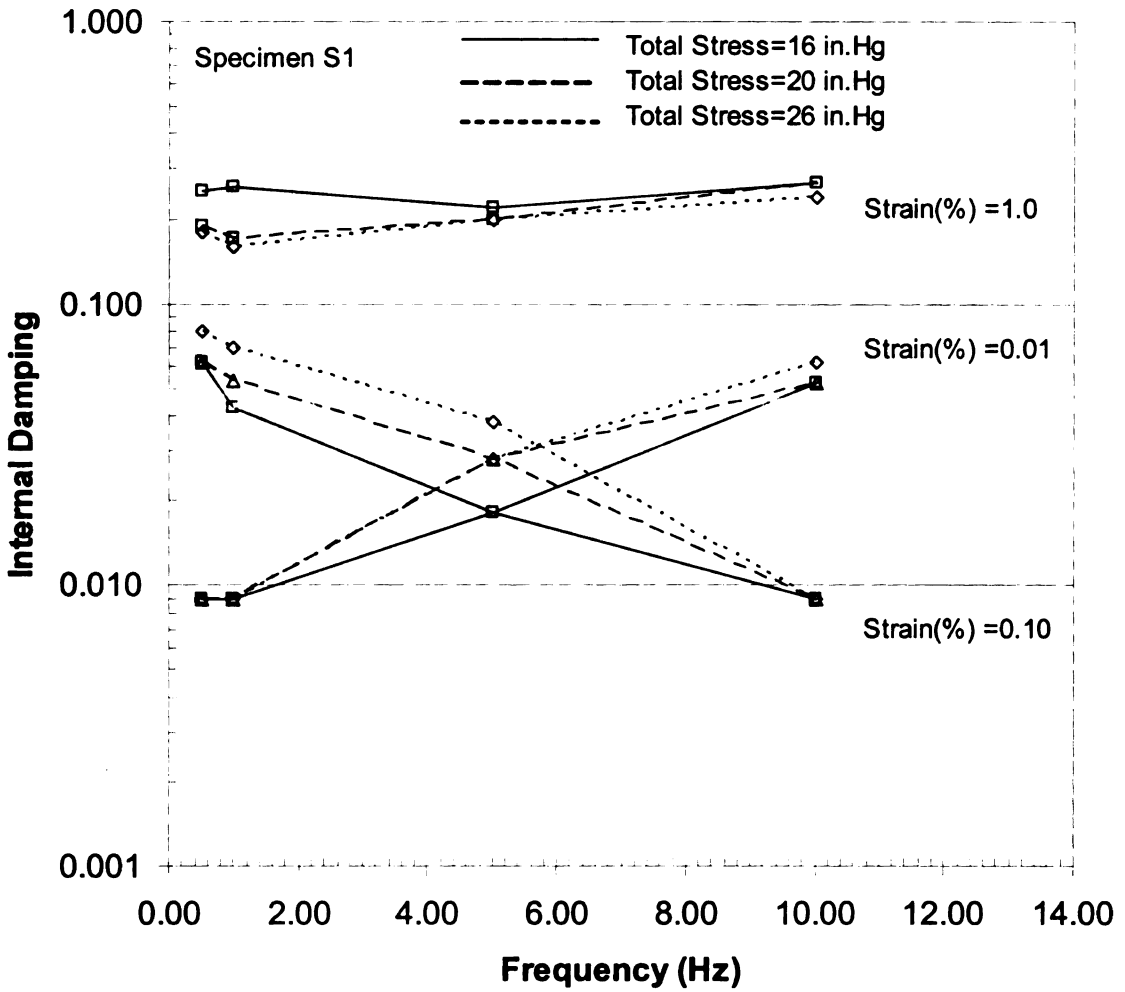

Figure 2.6 The relationship between internal damping and frequency for Montery sand #0, 90 percent relative density (from Sousa, 1986)

2.4.3 Fine-grained Soil

Determination of hysteretic stress-strain loops in soils can be obtained from triaxial compression tests, simple shear tests or torsional shear tests conducted under harmonic loading conditions. Dynamic properties of a Vicksburg silty clay are shown in Figure 2.7 and Figure 2.8. These figures illustrate that the internal damping increases with

increasing strain amplitude and decreases with increasing frequency; however frequency of loading does not affect the dynamic shear modulus of clay.

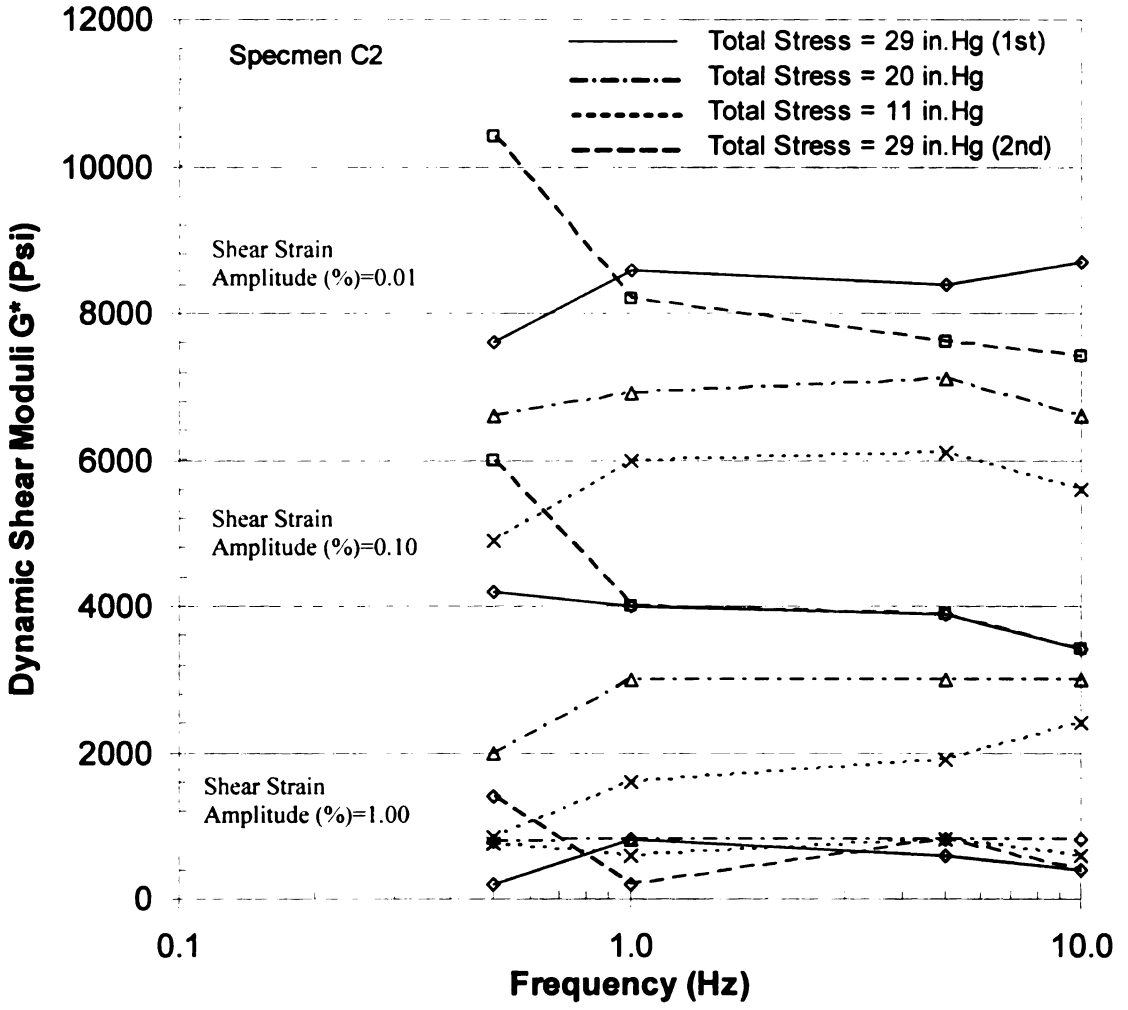

Figure 2.7 The influence of frequency of loading on the dynamic shear modulus of Vicksburg silty clay (from Sousa, 1986)

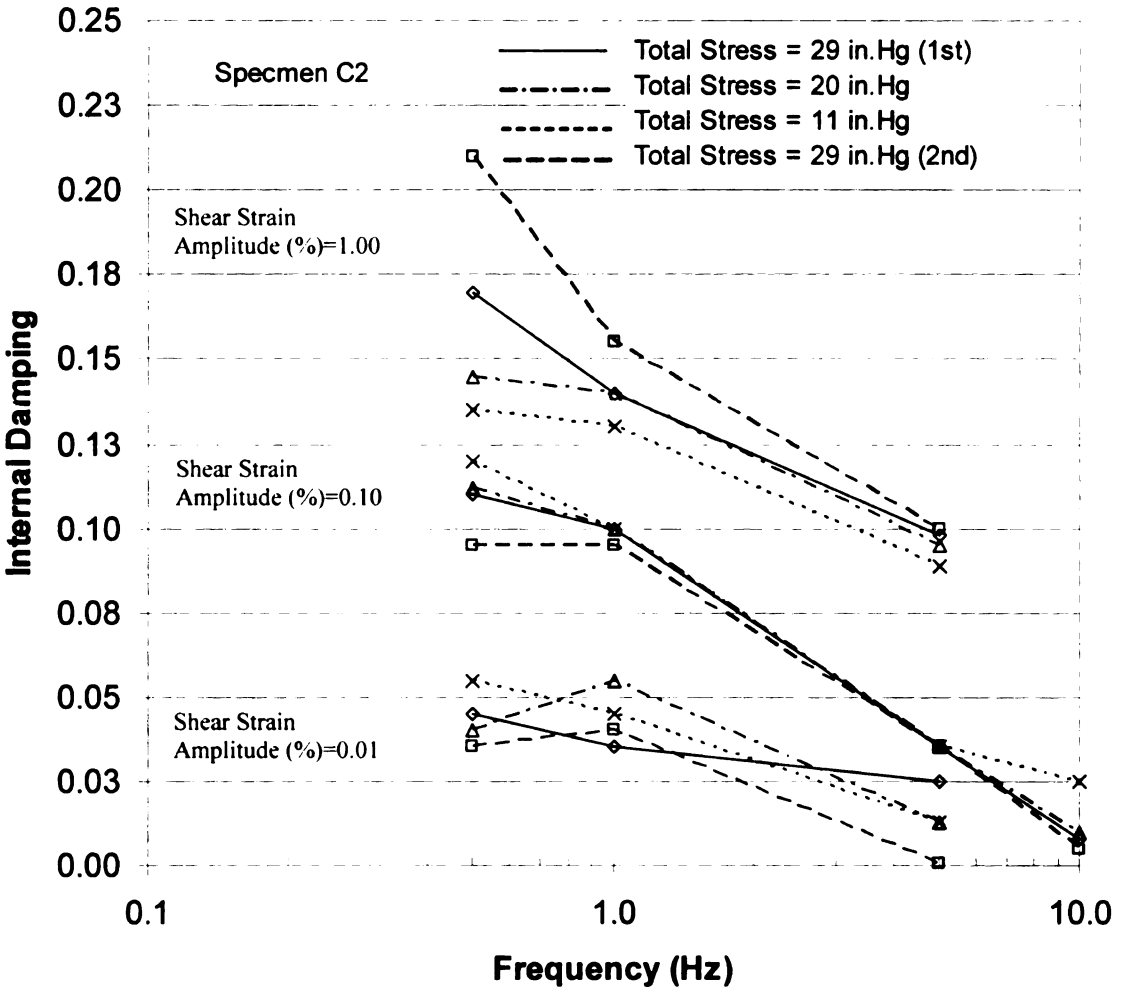

Figure 2.8 The influence of frequency of loading on the damping ratio of Vicksburg silty clay (from Sousa, 1986)

2.5 Viscoelastic Material Characterization

Viscoelastic material response is comprised of elastic and viscous responses corresponding to the behavior of a solid and a liquid, respectively. There are two general methods to characterize viscoelastic materials (Huang, 1993): (i) by mechanical models, and (ii) by a creep compliance curve.

2.5.1 Mechanical Models

The behavior of an asphalt concrete material can be modeled using a combination of springs and dashpots (Huang, 1993). The most basic models include the Maxwell and Kelvin models. The Maxwell model consists of a linear spring and a viscous damper in series. The Kelvin model consists of a linear spring and a viscous damper in parallel. More complex viscoelastic models include the standard solid model and the Burger's model. The standard solid model combines Kelvin and spring models in series, while Burger's model consists of Kelvin and Maxwell models in series. Figure 2.9 shows the various mechanical models described above, with σ, E, and λ denoting stress, elastic modulus, and viscous fraction, respectively.

Maxwell Model

The response from the Maxwell model is the least realistic; under constant stress loading (creep), it consists of an instantaneous strain, which is recoverable, followed by a linearly increasing strain, which is irrecoverable. The equation characterizing the response behavior of Maxwell model (Huang, 1993) is:

$$\sigma + \frac{\eta}{E}\dot{\sigma} = E\frac{\eta}{E}\dot{\varepsilon} \tag{2.1}$$

For viscous damping of Maxwell model, the elastic modulus is replaced by the complex modulus (Haddad, 1995):

$$E^* = E_{real} + iE_{\mathrm{Im}} = E\left(\frac{\omega^2\xi^2}{1+\omega^2\xi^2} + i\frac{\omega\xi}{1+\omega^2\xi^2}\right) \tag{2.2}$$

in which $\xi = \frac{\lambda}{E}$, and ω is the circular frequency.

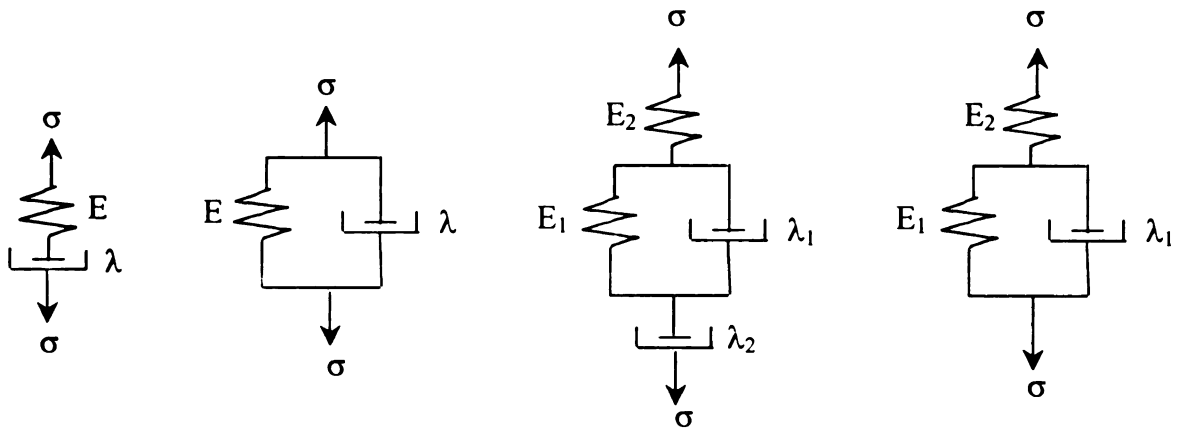

(a) Maxwell (b) Kelvin (c) Burgers (d) Standard Solid

Figure 2.9 Mechanical models

Kelvin Model

The response from the Kelvin model is more realistic than that for the Maxwell model; under constant stress loading (creep), the strain starts at zero, increases non-linearly (with an exponential term) approaching a maximum value corresponding to the elastic response. The Kelvin model is usually used to simulate viscous or hysteretic (material) damping. For viscous damping, the elastic modulus is replaced by the complex modulus:

$$E^* = E(1 + i\omega\xi_d) \tag{2.3}$$

in which E is the spring constant, ω is the circular frequency and ξ_d is the damping ratio (equal to the ratio of the dashpot constant to the spring constant). Note that in this case,

the real part of the modulus is constant and equal to the elastic modulus while the imaginary part of the modulus (representing damping) varies linearly with increasing frequency.

Burger Model

Burger's model, also called the Four-parameter fluid model, consists of both a Maxwell component and a Kelvin component in series. The complex modulus can be written as (Al-Khoury, 2001):

$$E^*(\omega) = \frac{\omega^2\left[p_1 q_1 - q_2\left(1 - p_2\omega^2\right)\right] + i\omega\left[p_1 q_2 \omega^2 - q_1\left(1 - p_2\omega^2\right)\right]}{p_1\omega^2 + \left(1 - p_2\omega^2\right)^2} \quad (2.4)$$

where

$$p_1 = \frac{\lambda_1}{E_1} + \frac{\lambda_1}{E_2} + \frac{\lambda_2}{E_2} \quad p_2 = \frac{\lambda_1\lambda_2}{E_1 E_2}$$

$$q_1 = \lambda_1 \quad q_2 = \frac{\lambda_1\lambda_2}{E_2}$$

The complex shear modulus and the complex Lame's constant can be determined as (Al-Khoury, 2001):

$$G^*(\omega) = \frac{3K\left(i\omega q_1 - \omega^2 q_2\right)}{9K\left(1 + i\omega p_1 - \omega^2 p_2\right) - i\omega q_1 + \omega^2 q_2} \quad (2.5)$$

$$\lambda^*(\omega) = K - \frac{2}{3}G^*(\omega)$$

where K is the bulk modulus.

For hysteretic damping, the complex modulus is constant with frequency, and can (for small damping) be written as:

$$E^* = E(1 + 2i\xi_d) \tag{2.6}$$

The best model (among the four models described above) for describing the response of asphalt concrete is the Burger's model. While not perfectly suited for real material behavior, its strain response under constant stress shows many of the characteristics observed under creep testing in the laboratory. It is important to note, however, that both the real and imaginary parts of the complex modulus are zero at zero frequency and vary non-linearly with increasing frequency. The Poisson's ratio is also complex and frequency dependent in this case.

Olard and Di Benedeho (2003) proposed a general "2S2P1D" model which simulates better the viscoelastic aspect of both asphalt and mixtures.

Note that the SAPSI program (Chen, 1987) allows for the elastic and shear moduli as well as the Poisson ratio to be complex and frequency dependent, thus allowing for describing the response according to any viscoelastic model (i.e., Kelvin, Burger's or any other model).

2.5.2 Creep Compliance Model

The asphalt concrete material may be modeled by using a power law model. Such a model describes the stress-strain relationship for an asphalt concrete mixture as a creep

compliance function. For the purpose of backcalculation, Magnuson et al (1991) used a three-parameter model:

$$D(t) = D_0 + D_1 t^m \tag{2.7}$$

where, $D_0 = 1/E_0$ (Elastic response term)

D_1 = Creep compliance constant (for viscous term)

m = Exponent for nonlinear time dependence

2.6 Dynamic Forward Computation Programs

Most dynamic backcalculation methods use dynamic damped-elastic finite-layer or finite element models for their forward solutions. The finite layer solutions are based on Kausel's formulation (Kausel, 1982) which subdivides the medium into discrete layers that have a linear displacement function in the vertical direction and satisfy the wave equation in the horizontal direction. The solution is based on the premise that if the sublayer thickness is small relative to the wavelength of interest, it is possible to linearize the transcendental functions and reduce them to algebraic expressions. Examples of programs containing such solutions include UTFWIBM (Roesset, 1987) and UTFWD (Chang, 1992), GREEN (Kang, 1998), and SAPSI (Chen, 1987). The computer program SCALPOT (Magnuson et al, 1991) models the asphalt concrete layer as a viscoelastic material using a two-parameter power law model, while the SAPSI program allows the layer material properties to be complex and frequency-dependent. Al-Khoury et al. (Al-Khoury, 2001) developed an efficient forward solution for the dynamic analysis of flexible pavements using the spectral element technique for the simulation of wave

propagation in layered systems. The method is able to model each layer as one element without the need for subdivision into several sublayers.

Finally, Endiran developed a non-linear dynamic model in DYNARK computer program (Endiran, 1999) which accounts for non-linearities in granular material as well as subgrade soil.

2.7 Dynamic Backcalculation Methods

Dynamic backcalculation methods are based on either frequency or time domain solutions. For the former procedure, the applied load and measured deflection time histories are transformed into the frequency domain by using the Fast Fourier Transform (FFT). Backcalculation of layer parameters is done by matching the calculated steady-state (complex) deflection basin with the frequency component of the measured sensor deflections at one or more frequencies. In time domain backcalculation, the measured deflection time histories are directly compared with the predicted results from the forward program. One of the advantages of this method is that matching can be achieved for any time interval desired. Uzan compared both methods and concluded that time domain backcalculation is preferred over frequency domain backcalculation (Uzon, 1988). A number of computer programs have been developed for dynamic backcalculation of flexible pavement layer parameters. Each program employs a particular forward model and a specific backcalculation scheme. A brief overview of the programs developed so far is mentioned below.

Uzan (Uzan,1994) presented two dynamic linear backcalculation procedures, one in the time domain and the other in the frequency domain. Both approaches use the program UTFWIBM as the forward model and Newton's method as the backcalculation solution.

PAVE-SID (Magnuson, 1991) is a computer program that uses the SCALPOT program to generate frequency response curves; a system identification technique is applied for matching computed frequency data in order to extract pavement properties. SCALPOT computes the dynamic response of a horizontally layered viscoelastic half-space to a time dependent surface pressure distribution.

BKGREEN (Kang,1998) models the pavement as a layered elastic system in terms of dynamic Green flexibility influence functions using Kausel's formulation of discrete Green functions for dynamic loads in linear viscoelastic layered media (1981). Backcalculation is done at multiple frequencies, and the set of layer moduli is determined using a non-linear least squares technique. The solution can experience some computational difficulties at certain frequencies due to the numerical complications associated with implementing infinite integration in computer codes.

Al-Khoury et al. (2001) developed an axisymmetric layered solution as a forward model using the spectral element technique, and used the modified Levenberg-Marquardt and Powell hybrid methods for solving the resulting system of nonlinear equations.

Losa (2002) used the SAPSI program as the forward solution and a nonlinear least squares optimization technique (Levenberg-Marquardt method) for backcalculating layer parameters at multiple frequencies. The solution assumes the asphalt concrete and

subgrade moduli to be frequency dependent, while the base modulus is assumed to be constant with frequency.

FEDPAN (1991) is a finite element program that can perform both static and dynamic backcalculation for three-layer pavement systems using the CHEVDEF backcalculation algorithm (Bush, 1985). This program can simulate the effects of pavement inertia and damping in the dynamic analysis, and material nonlinearity in the static analysis.

Matsui et al. (1998) modeled the flexible pavement as an axisymmetric linear elastic system using the FEM method, in conjunction with Ritz vectors to improve computational efficiency. The backcalculation method was the Gauss-Newton method coupled with the singular value decomposition (SVD) method with truncation.

Finally, Meier and Rix (1995) developed an artificial neural network solution that has been trained to backcalculate pavement layer moduli for 3-layer flexible pavement systems using synthetic dynamic deflection basins. The dynamic pavement response was calculated using an elastodynamic Green function solution based on Kausel's formulation (Kausel and Roesset, 1981).

The various dynamic backcalculation programs are summarized in Table 2.1 along with their inverse method and the corresponding forward analysis programs. Table 2.2 summarizes the advantages and disadvantages for each method.

Table 2.1 Dynamic backcalculation programs

Program	Domain	Inverse Method	Forward Program	Author, Year
BKGREEN	Frequency-domain	Nonlinear least-square optimization	GREEN	Kang Y. V. (1998)
No name	Frequency-domain and time-domain	Newton's method	UTFWIBM	Uzan J. (1994)
PAVE-SID	Frequency-domain	System Identification (SID)	SCALPOT	Magnuson (1991)
FEDPAN	Time-domain	Linear least squares	SAP IV	Ong (1991)
No name	Frequency-domain	Levenberg-Marquardt method	SAPSI	Losa (2002)
No name	Frequency-domain	Newton's method	LAMDA	Al-Khoury (2002)
No name	Time-domain	Gauss-Newton method	FEM	Matsui K (1998)

Table 2.2 Advantages and disadvantages for dynamic backcalculation programs

Author	Advantages	Disadvantages
BKGREEN	1 multi-frequencies (three frequencies) 2 can handle thin layers 3 potentially more layers	1 no thickness backcalculation 2 backcalculation is limited to the narrow frequency range (0-5Hz) 3 fixing damping ratio (2%) 4 constant AC modulus 5 blow up in numerical calculation at some frequencies
Uzan J.	1 creep moduli for AC 2 both time domain and frequency domain 3 full time history match (75 points) in time domain 4 multi-frequency backcalclation (13 frequencies)	1 no thickness backcalculation 2 fixing damping ratio (2-5%)
Magnuson	1 creep moduli for AC 2 backcalculates up to 8 parameters including creep compliance	1 no thickness backcalculation 2 fixing damping ratio (2-5%)
Ong	1 FEM method 2 can handle thin layers 3 potentially more layers	1 no thickness backcalculation 2 constant modulus for every layer 3 fixing damping ratio (5%)
Losa	1 thickness backcalculation 2 AC frequency-dependent	1 blow up in numerical calculation at some frequencies
Al-Khoury	1 Considered Kelvin, Maxwell, and Burger Models for AC	1 no thickness backcalculation 2 verification only for theoretical data
Matsui K.	1 traces of time history are used 2 Rize vectors are introduced to reduce the number of system equations	1 no thickness backcalculation 2 time consuming

CHAPTER 3 - FORWARD PROGRAM

3.1 Introduction

The forward program SAPSI (Chen, 1987) models the pavement structure as a system of layers that are infinite in the horizontal direction and underlain by an elastic half-space. The materials are assumed to be isotropic and linearly elastic with hysteretic damping. Full interface bonding is assumed at the layer interfaces. The mass densities and elastic moduli change with depth, from layer to layer, but are assumed to be constant within each layer. For the present application, the top layer represents the asphalt surface which is supported by the base, subbase and subgrade.

3.2 Analysis Methods

The forward program uses the complex response method, which uses the notation of complex algebra to express the response of a pavement system to a harmonic excitation force. The main assumption of this method is that if the forcing function is expressed in the complex form then the steady-state response should have the same function of frequency. This method of dynamic analysis is based on Fourier transformation. To simplify the analysis, a transient mode of loading can be represented by a series of harmonic loads with different frequencies and magnitudes using Fourier transformation. Once the responses to steady-state loadings are obtained in terms of frequency and magnitude, the response to a transient load in the time-domain can be obtained through the inverse Fourier transform.

3.2.1 Modeling of Viscoelasticity

In viscoelasticity, the behavior of materials is expressed in terms of a complex modulus, E^*, which couples the elastic and the viscous part of the response. The modulus and damping ratio of soils are assumed to be independent of frequency, whereas those of asphalt concrete (AC) are allowed to vary with frequency.

3.2.1.1 Hysteretic Damping

According to this model the complex modulus can be written as follows:

$$E^* = E\left(1 - 2\beta^2 + 2i\beta\sqrt{1-\beta^2}\right) \tag{3.1}$$

where $i = \sqrt{-1}$, E is Young's modulus of elasticity, and β is the hysteretic damping ratio.

For very low damping ($\beta << 1$), the complex modulus can be expressed as:

$$E^* \cong E(1 + i2\beta) \tag{3.2}$$

3.2.1.2 Viscous Damping

Asphalt concrete can be achieved using the Kelvin model, which consists of a spring and a dashpot in parallel, as shown in Figure 3.1. The spring represent the stress component ($E\varepsilon$), while the dashpot represents the strain component that is proportional to the stain rate ($\eta\dot{\varepsilon}$).

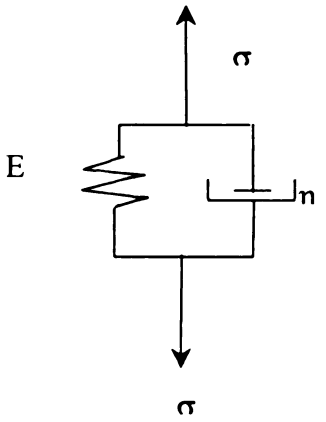

Figure 3.1 Linear Kelvin's model

The stress-strain relationship for Kelvin's model is expressed as

$$\sigma = E\varepsilon + \eta\dot{\varepsilon} \tag{3.3}$$

The steady-state response of the system to harmonic forcing function can be expressed as

$$u = Ue^{i\omega t}$$

$$\varepsilon = \frac{\partial u}{\partial x} = \frac{\partial U}{\partial x} e^{i\omega t} \tag{3.4}$$

$$\dot{\varepsilon} = \frac{\partial u}{\partial x \partial t} = i\omega \frac{\partial U}{\partial x} e^{i\omega t}$$

Substituting equation (3.4) in equation (3.3), we obtain

$$\sigma = E\frac{\partial u}{\partial x} + i\omega \frac{\partial^2 u}{\partial x \partial t} = \left(E\frac{\partial U}{\partial x} + i\omega\eta \frac{\partial U}{\partial x} \right) e^{i\omega t} = (E + i\omega\eta)\varepsilon\, e^{i\omega t} \tag{3.5}$$

Therefore

$$E^* = (E + i\omega\eta) = E_{\mathrm{Re}} + E_{\mathrm{Im}} \tag{3.6}$$

where E_{Re} and E_{Im} are the real part and imaginary part of the modulus in the frequency domain, respectively.

3.2.2 Steady-State Response

The steady-state solution of a layered system subjected to a harmonic vertical disk load is adopted from the SAPSI model (Chen, 1987). For a uniformly distributed vertical pressure q acting over a circular area with radius *a*, the load vector in the axisymmetric spatial domain may be expressed as:

$$\{p\} = \begin{Bmatrix} p_r \\ p_z \end{Bmatrix} = q \begin{Bmatrix} 0 \\ 1 \end{Bmatrix} \qquad 0 \le r \le a \tag{3.7}$$

In the wave number domain the load can be expressed as:

$$\{\bar{p}\} = \int_0^\infty -r \begin{bmatrix} J_1(kr) & 0 \\ 0 & J_0(kr) \end{bmatrix} \begin{Bmatrix} p_r \\ p_z \end{Bmatrix} dr\, d\theta = \frac{qa}{k} J_1(ka) \begin{Bmatrix} 0 \\ 1 \end{Bmatrix} \tag{3.8}$$

where, k is the wave number, r is the radial distance to the center of the load, and J_0 and J_1 are Bessel functions of zeroth and first degrees, respectively.

The displacement vector can be expressed as:

$$\{U\} = \begin{Bmatrix} u \\ w \end{Bmatrix} = \int_0^\infty -r \begin{bmatrix} J_1(kr) & 0 \\ 0 & J_0(kr) \end{bmatrix} \{\bar{U}\} dk \tag{3.9}$$

The displacements $\{\bar{U}\}$ and force $\{\bar{p}\}$, in the wave number domain are related by

$$[K]\{\bar{U}\} = \{\bar{p}\} \tag{3.10}$$

where, $[K] = [A]k^2 + [B]k + [G] - \omega^2[M]$, and the respective matrices can be found elsewhere (Kausel, 1981).

The closed form expression for the vertical displacement of the surface layer can be obtained as

$$w = qa \sum_{s=1}^{2N} \phi^1_{z,s} \phi^1_{z,s} I_{1s} \tag{3.11}$$

where $\phi^1_{z,s}$ denotes the vertical displacement at the surface load in the s^{th} mode.

$$\{\phi^1_z\} = \{\phi^1_{z,s}\} \qquad s = 1,2,\ldots,2N$$

$$I_{1s} = \int_0^\infty \frac{1}{\left(k^2 - k_s^2\right)} J_0(kr) J_1(ka) dk$$

$$= \frac{\pi}{2ik_s} J_0(k_s r) H_1^{(2)}(k_s r) - \frac{1}{k_s^2 a} \qquad \text{for} \quad 0 \le r \le a$$

$$= \frac{\pi}{2ik_s} J_1(k_s r) H_0^{(2)}(k_s r) - \frac{1}{k_s^2 a} \qquad \text{for} \quad r \ge a$$

Consider a pavement with m surface deflections. Let the vector $\{ w \}$ represent the calculated surface deflections due to a harmonic vertical load. For each frequency ω, the steady-state equation (3.10) of motion can be written as:

$$[K]\{w\} = \{\bar{p}\} \tag{3.12}$$

where $\{w\} = \{w_1 \quad w_2 \quad \cdots \quad w_{m-1} \quad w_m\}$, and $w_j = w_j^1 + iw_j^2$ with w_j^1 and w_j^2 representing the elastic and viscous response, respectively.

Although SAPSI had been verified by Chen (1987) using simple analytical solutions, it was decided to compare the SAPSI results with those obtained using another dynamic layered solution: the computer program GREEN by Kang (1998). The validation was done by comparing SAPSI results with published deflection data by Kang (1998). A three-layer pavement system resting over a subgrade is subjected to a 44.5 kN (10,000 lb) load on a 300 mm diameter plate. The layer properties of the pavement section are presented in Table 3.1. The dynamic deflections at offset distances of 0, 225, 300, 525, 750 and 1350 mm were calculated using SAPSI and GREEN. Figure 3.2 shows the results for three different frequencies: 0.25, 8 and 25 Hz. Excellent agreement exists at all frequencies, except for the farthest sensor at 25 Hz. It is believed that for this particular case, the result from SAPSI is more reasonable than that from GREEN because there is no reason for the far sensor deflection to be higher than the 6th sensor. Given that the FWD analysis is in the frequency range from 0 to 30 Hz, it can be concluded that the program SAPSI is suitable as a forward program.

Table 3.1 Profile used for comparing SAPSI and GREEN solutions

Layer Name	Thickness (in)	Unit Weight (pcf)	Poisson Ratio	Damping Ratio	Modulus (ksi)
AC	3	140	0.35	0.0	300
Base	6	125	0.40	0.0	45
Subbase	12	125	0.40	0.0	21
Subgrade	∞	110	0.45	0.0	7.5

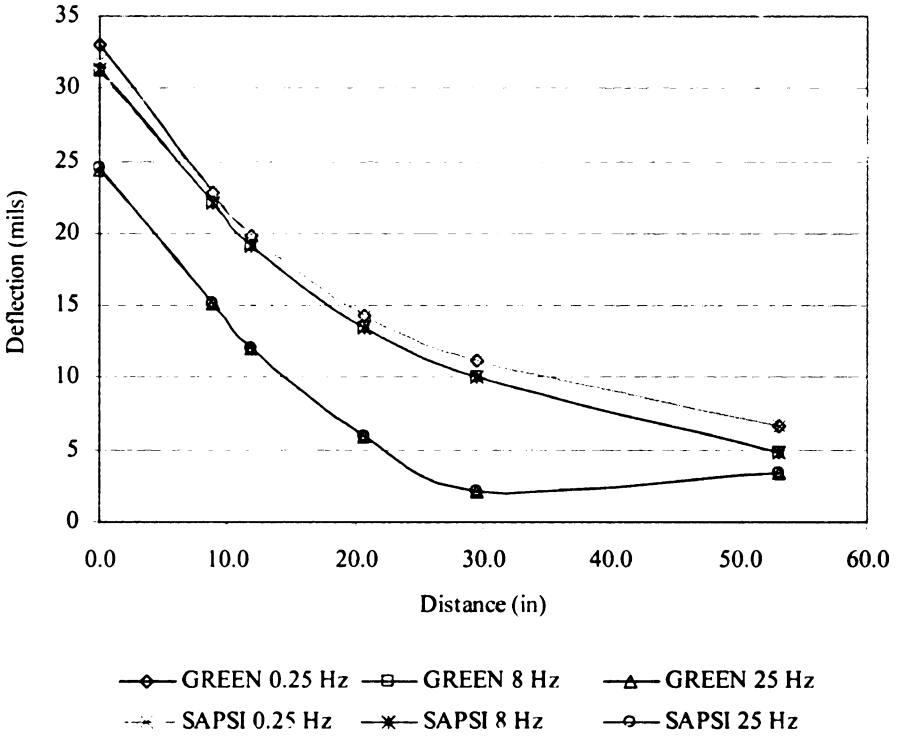

Figure 3.2 Comparisons of dynamic deflection basins from SAPSI and GREEN computer programs

3.2.3 Transient Response

For an arbitrary transient excitation such as that corresponding to a FWD test, the time history of the specified force can be decomposed into different frequency components using a Fourier transform. Responses corresponding to each frequency are calculated and combined to obtain the displacement time history.

3.2.3.1 Frequency-domain Solution

The first step of the analysis is to decompose the excitation function p(t) into its different frequency components $P(\omega)$ by means of the discrete Fourier Transform, which is evaluated numerically by using the Fast Fourier Transform (FFT) algorithm. In order to use this algorithm, the basic load-time history input needs to be specified at N points with a constant time interval over the duration T. In other words, the load-time history can be expressed as:

$$P(t) = p(s \cdot \Delta t) \tag{3.13}$$

where Δt is the time interval T/N. The load-time history can be expressed as:

$$P(t) = \mathrm{Re} \sum_{s=0}^{N/2} p(\omega_S) \exp(i\omega_S t) \tag{3.14}$$

where the frequencies are defined as $\omega_S = 2\pi/(N\Delta t)$, and $p(\omega_S)$ are complex load amplitudes defined as follows:

$$p(\omega_S) = \frac{1}{N} \sum_{n=0}^{N-1} p(n\Delta t) \exp(-i\omega_S n\Delta t) \quad \text{for} \quad s = 0 \ \text{and} \ s = \frac{N}{2}$$

$$p(\omega_S) = \frac{1}{N} \sum_{n=0}^{N-1} p(n\Delta t) \exp(-i\omega_S n\Delta t) \quad \text{for} \quad s = 1,2 \cdots \frac{N}{2} - 1$$

The second step is to obtain the transfer function $H_i(\omega)$, which is defined as the response of the pavement system due to a harmonic excitation with unit amplitude. In this case, the

transfer function is the displacement due to a harmonic unit load applied at the surface of the pavement system. The third step is to obtain the displacement by multiplying the Fourier Transform of the force with the transfer function:

$$U_i(\omega_S) = H_i(\omega_S) * p(\omega_S) \tag{3.15}$$

which is evaluated for the entire range of frequencies. Finally, the displacement time history can be obtained using an Inverse Fourier Transform that is evaluated numerically. It should be noted that unlike the continuous Fourier Transform, the Discrete Fourier Transform (FFT algorithm) assumes that the input function is periodic with a period T_p. When using the FFT algorithm, the values of the basic parameters involved (e.g. number of sampled points N, time increment Δt and total period T_p) have to be selected properly so that a compromise can be reached between the accuracy of results and the cost of computation. It should be noted that the transfer function does not need to be computed for all frequencies, as interpolation techniques can be used effectively to reduce computation time.

3.2.3.2 Interpolation Scheme

In order to calculate the response time history, SAPSI performs the following steps: (1) The load time history is transformed to the frequency-domain using the Fast Fourier Transform (FFT). (2) The unit response functions are computed at several particular frequencies. (3) The unit response functions at other frequencies are estimated using an interpolation scheme. (4) The load and unit response functions are multiplied in the

frequency-domain to obtain the response of the pavement in the frequency-domain. (5) The inverse FFT is applied to yield the pavement response in the time-domain.

The FWD load time history is sampled typically at every 0.1 ms or 0.2 ms. In order to obtain the time lag between the peak load and computed peak response accurately, a 0.01 ms sampling interval was used in the analysis, with linear interpolation of the load and measured deflections. Since the load has practically no contribution from the harmonics with frequencies above 75 Hz, the steady-state response is computed in the range from 0 to 75 Hz. To reduce the computational effort of the time-domain backcalculation, responses are computed at a limited number of frequencies (usually less than 10) and an interpolation scheme is used to obtain the response at other frequencies.

The interpolation technique was developed by Tajirian (1981) to estimate the response at all frequencies from the calculated response at a limited number of frequencies. The technique is based on the frequency response function of a two-degree of freedom system. The response of each degree of freedom subjected to a harmonic load has the following general form:

$$U(\omega) = \frac{c_1\omega^4 + c_2\omega^2 + c_3}{\omega^4 + c_4\omega^2 + c_5} \tag{3.16}$$

where $U(\omega)$ is the response at frequency ω, which will be calculated using equation (3.15), and c1, c2, c3, c4 and c5 are constants. Thus, if the response of the system is known at five frequencies, the five constants may be obtained by solving the following equation:

$$\begin{bmatrix} \omega_1^4 & \omega_1^2 & 1 & -\omega_1^2 U_1 & -U_1 \\ \omega_2^4 & \omega_2^2 & 1 & -\omega_2^2 U_2 & -U_2 \\ \omega_3^4 & \omega_3^2 & 1 & -\omega_2^2 U_3 & -U_3 \\ \omega_4^4 & \omega_4^2 & 1 & -\omega_2^2 U_4 & -U_4 \\ \omega_5^4 & \omega_5^2 & 1 & -\omega_2^2 U_5 & -U_5 \end{bmatrix} \begin{Bmatrix} c_1 \\ c_2 \\ c_3 \\ c_4 \\ c_5 \end{Bmatrix} = \begin{Bmatrix} \omega_1^4 U_1 \\ \omega_2^4 U_2 \\ \omega_3^4 U_3 \\ \omega_4^4 U_4 \\ \omega_5^4 U_5 \end{Bmatrix} \tag{3.17}$$

3.2.3.3 Summary of Procedure for Calculating Transient Response

The summary of the transient response computations is as follows:

1. The FWD load and deflection data are read, and if necessary, interpolated to obtain values at every 0.01 ms.

2. The time history of the load is filled with zeros beyond the recorded time and transformed to the frequency-domain using the FFT algorithm.

3. The computer program SAPSI is used to compute the unit response functions of the pavement at several frequencies. Both real and imaginary components of the responses are obtained.

4. The unit response function at 0 Hz is estimated from that at 0.01 Hz, and those at other frequencies are interpolated from values computed at the several frequencies spanning from 1.52 to 76.29 Hz.

5. The load and unit response vectors are filled with zeros for the frequencies beyond 75 Hz.

6. The deflections in the frequency-domain are obtained by multiplying the load and unit response functions at all frequencies.

7. The deflection time histories are computed by using the inverse FFT of the deflection vector in the frequency-domain.

3.2.3.4 Dynamic Response of a Pavement System due to an FWD Load

In order to illustrate the typical behavior of the pavement system subjected to a FWD load and the type of information that can be extracted from its dynamic response, a typical flexible pavement with bedrock presented in Table 3.2 was analyzed. Figures 3.2 and 3.3 show the real and imaginary parts of the transfer functions, respectively, for different sensors. It can be observed that as the frequency increases, the displacement increases until they reach a peak at the same frequency for all sensors. The low amplitudes of displacement at high frequencies are the result of inertial effects. The interpolation scheme mentioned previously is used in this calculation. Figures 3.4 and 3.5 show the real part and the imaginary part of the Fourier Transform of the load, respectively. The direct Fourier transform of the displacements is obtained by multiplying the frequency component of the load by the transfer functions for different sensors and are shown in Figures 3.6 and 3.7. The displacement time histories of the different sensors are obtained using an Inverse Fourier Transform, and are shown in Figure 3.9.

It is noted that SAPSI program uses real and imaginary parts of modulus as input parameters. The difference between the hysteretic and the viscous damping models is that the former model employs the damping ratio to simulate the viscoelastic property, while the latter model uses the imaginary part of the modulus. Since the elastic modulus and

damping ratio can be expressed in term of the real and imaginary part of the complex modulus according to equation (3.1), and the Kelvin model has real and imaginary parts already according to equation (3.6), the SAPSI computer program is suitable for both models.

Table 3.2 Pavement profile characteristics

Layer Name	Thickness (inch)	Unit Weight (pcf)	Poisson Ratio	Damping Ratio	Modulus (ksi)
AC	8	145	0.3	0.05	200
Base	12.13	135	0.35	0.03	24
Subgrade	54.69	120	0.40	0.02	18
Stiff layer	∞	145	0.15	0.05	500

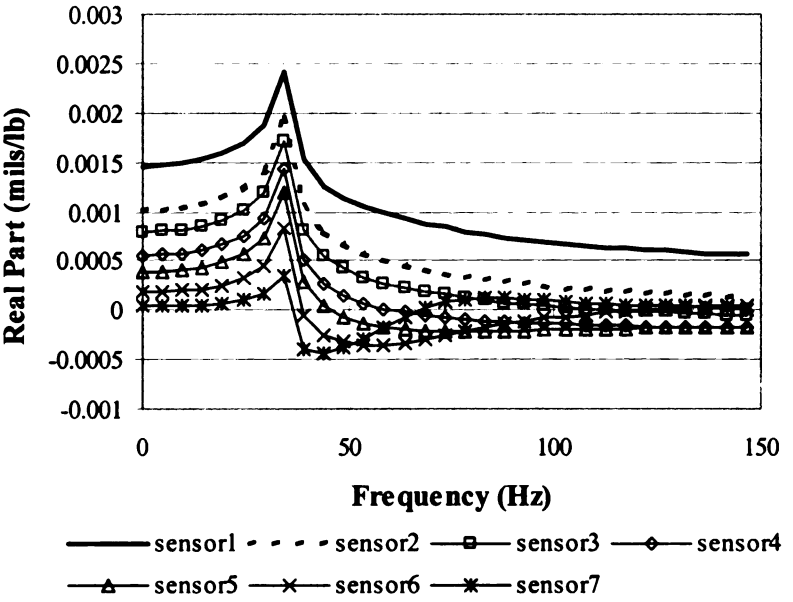

Figure 3.3 Real part of the displacement transfer function

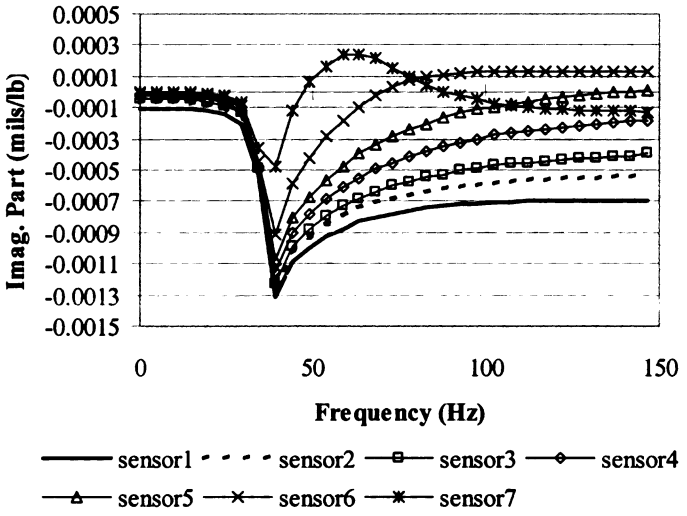

Figure 3.4 Imaginary part of the displacement transfer function

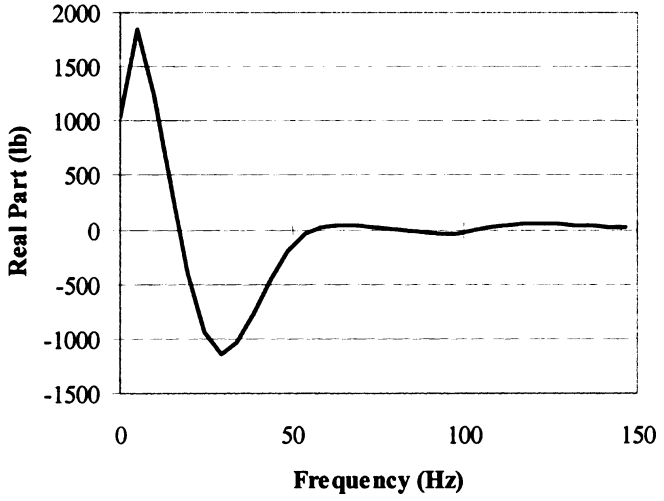

Figure 3.5 Real part of the load

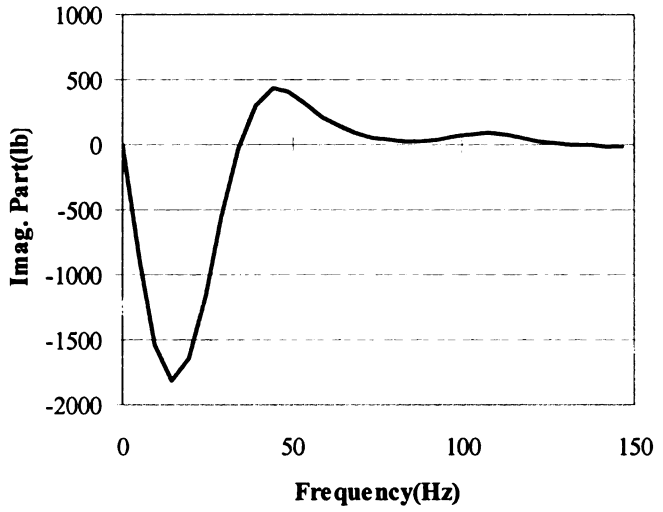

Figure 3.6 Imaginary part of the load

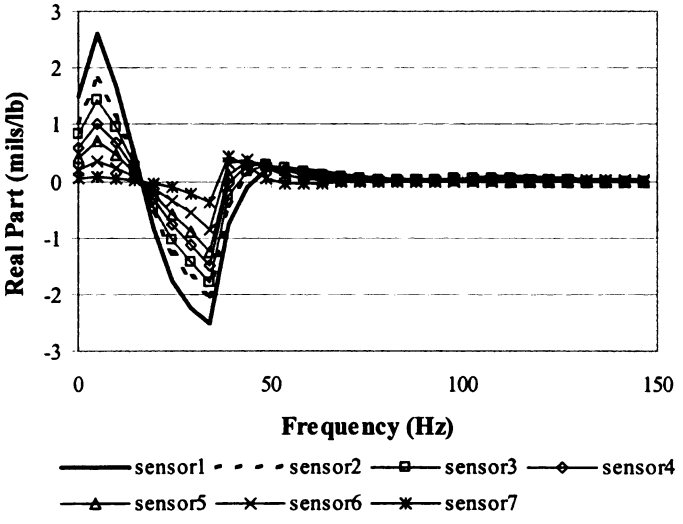

Figure 3.7 Real part of sensor displacements

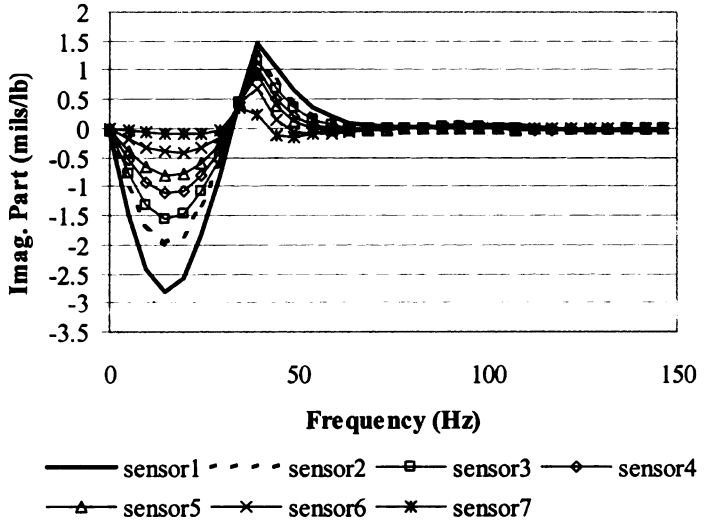

Figure 3.8 Imaginary part of sensor displacements

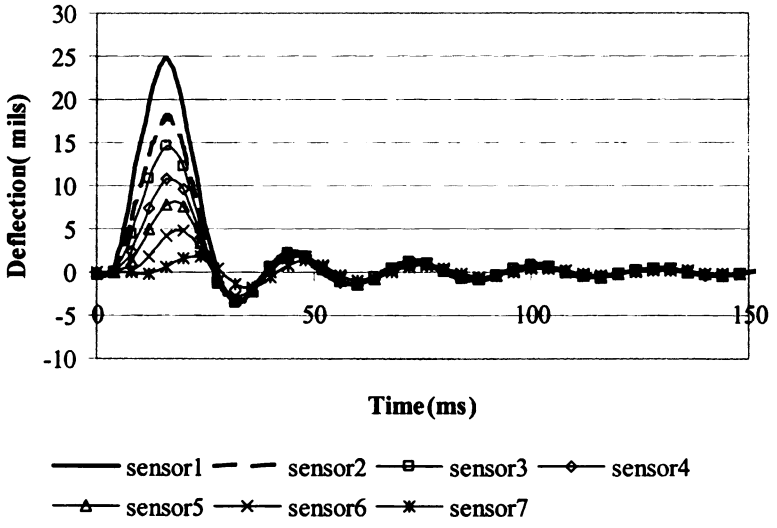

Figure 3.9 Sensor deflection time histories

3.3 Estimating Depth-to-Stiff Layer (DSL) and Subgrade Modulus

3.3.1 Estimating Depth to Stiff Layer (DSL)

To determine the depth to bedrock and the depth to ground water table, one-dimensional wave propagation theory was used as suggested by Roesset et al (1995). Two equations were developed: Equation 3.18 for saturated and Equation 3.19 for unsaturated subgrade. Equation 3.18 can be used only for bedrock, while Equation 3.19 can be used for both bedrock and ground water table. Both equations were initially developed by Roesset et al (1995), and modified in this research. The profiles used in the verification analysis are shown in Tables 3.3 through 3.5. Two different profiles with three different shear wave velocities were used for the verification of Equation 3.18 and one profile with three different shear wave velocities was used for the verification of Equation 3.19. During the verification analysis, the coefficient for Equation 3.18 (saturated subgrade) was modified because there was a significant difference between the actual and calculated depth to bedrock using the coefficient proposed by Roesset (1995).

$$D_b = \frac{V_s * T_d}{1.35} \quad \text{for saturated subgrade with Bedrock} \tag{3.18}$$

$$D_b = \frac{V_s * T_d}{(\pi - 2.24 * \upsilon)} \quad \text{for unsaturated subgrade with Bedrock or Ground Water Table} \tag{3.19}$$

where, V_s = S - wave velocity of subgrade material

T_d = Natural period of free vibration

υ = Poisson ratio of subgrade

Table 3.3 Profiles used in the analysis of saturated subgrade with bedrock

	Layer Name	Thickness (in)	Unit Weight (pcf)	Poisson Ratio	Damping Ratio	S-wave velocity (fps)	P-wave velocity (fps)	Elastic Modulus (ksi)
Profile 1	AC	6	145	0.3	0.05	2217	4150	400
	Base	6	140	0.35	0.03	700	1460	40
	Subbase	6	130	0.35	0.03	629	1310	30
	Subgrade	h*	135	0.495	0.02	500	5020	21.8
			135	0.495	0.02	600	6000	31.4
			135	0.495	0.02	765	5000	50.8
	Bedrock	∞	150	0.2	0.05	3590	5860	1000
	Layer Name	Thickness (in)	Unit Weight (pcf)	Poisson Ratio	Damping Ratio	S-wave velocity (fps)	P-wave velocity (fps)	Elastic Modulus (ksi)
Profile 2	AC	1	145	0.3	0.05	2217	4150	690.4
	Base	12	125	0.35	0.03	700	1460	67.4
	Subgrade	h*	110	0.495	0.02	500	5020	17.8
			110	0.489	0.02	750	5110	39.8
	Bedrock	∞	150	0.2	0.05	3590	5860	1000

* Thickness of subgrade layer is varied from 3.5 ft to 31.5 ft

The results of the verification analyses are shown in Figures 3.9 through 3.18. Deflection- time histories were calculated using the SAPSI program. The natural period of the profiles and the peak time delay between the 6^{th} and 7^{th} sensors (r = 3 ft and 5 ft, respectively) were then determined from the deflection time records. Since the shear wave velocity, unit weight and Poisson's ratio of the subgrade are known, the depth to stiff layer or the depth to ground water table can be calculated using the equations. The results indicated that the depth to bedrock and depth to ground water table could be accurately predicted using these two equations.

Table 3.4 Profile used in the analysis of unsaturated subgrade with bedrock

Layer Name	Thickness (in)	Unit Weight (pcf)	Poisson Ratio	Damping Ratio	S-wave velocity (fps)	Elastic Modulus (ksi)
AC	6	145	0.3	0.05	2217	400
Base	6	140	0.35	0.03	700	40
Subbase	6	130	0.35	0.03	629	30
Subgrade	h*	110	0.35	0.02	500	16
		110	0.35	0.02	600	23
		110	0.35	0.02	700	31.4
Bedrock	∞	150	0.2	0.05	3590	1000

* Thicknesses of subgrade layer is varied from 3.5 ft to 31.5 ft

Table 3.5 Profile used in the analysis of unsaturated subgrade with GWT

Layer Name	Thickness (in)	Unit Weight (pcf)	Poisson Ratio	Damping Ratio	S-wave velocity (fps)	P-wave velocity (fps)	Elastic Modulus (ksi)
AC	6	145	0.3	0.05	2217	4150	400
Base	6	140	0.35	0.03	700	1460	40
Subbase	6	130	0.35	0.03	629	1310	30
Subgrade	h*	110	0.35	0.02	300	-	5.8
GWT	∞	135	0.495	0.02	500	5000	21.6
		135	0.49	0.02	700	5000	42.6

* Thicknesses of subgrade layer is varied from 3.5 ft to 31.5 ft

(a)

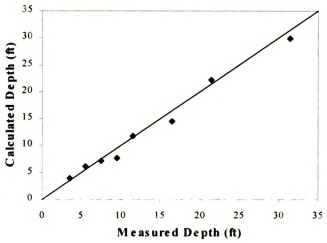

(b)

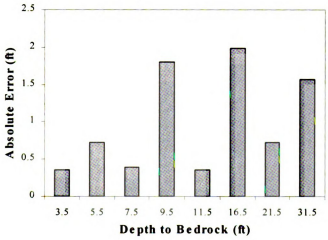

(c)

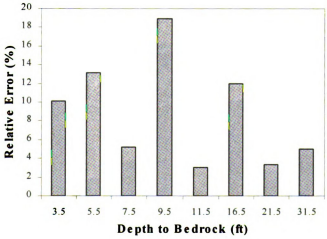

Figure 3.10 Comparison of predicted and actual depth-to-bedrock

(a)

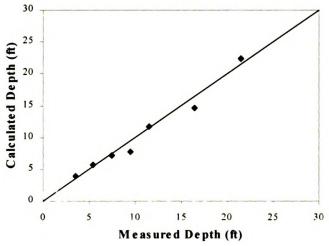

(b)

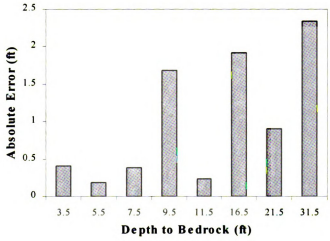

(c)

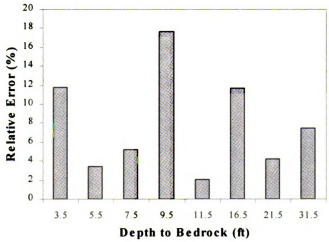

Figure 3.11 Comparison of predicted and actual depth-to-bedrock

(a)

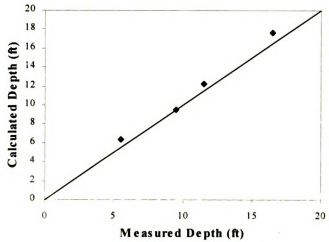

(b)

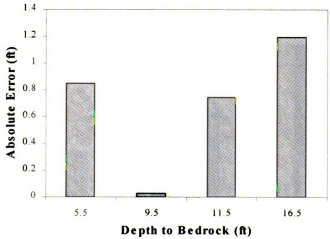

(c)

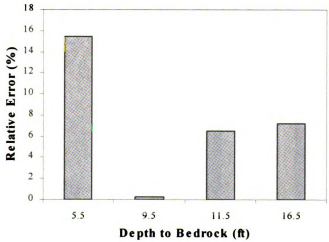

Figure 3.12 Comparison of predicted and actual depth-to-bedrock

(a)

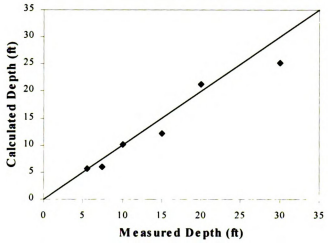

(b)

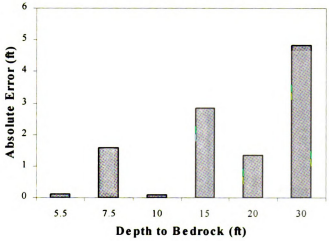

(c)

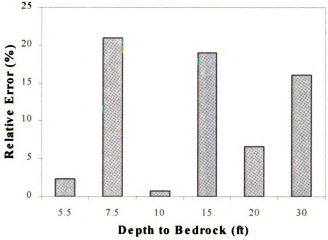

Figure 3.13 Comparison of predicted and actual depth-to-bedrock

(a)

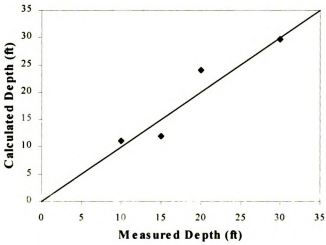

(b)

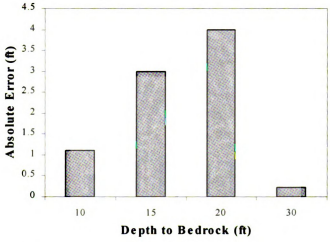

(c)

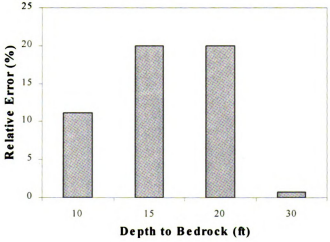

Figure 3.14 Comparison of predicted and actual depth-to-bedrock

(a)

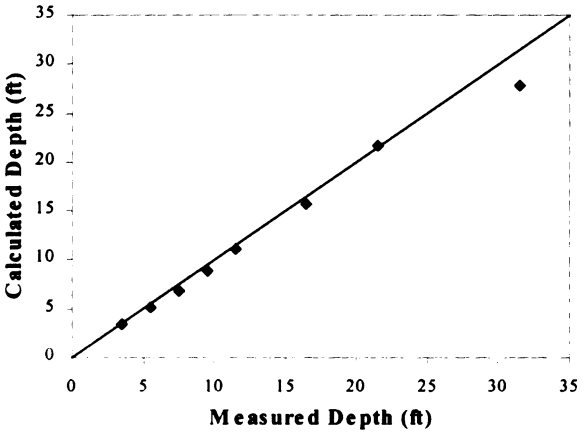

(b)

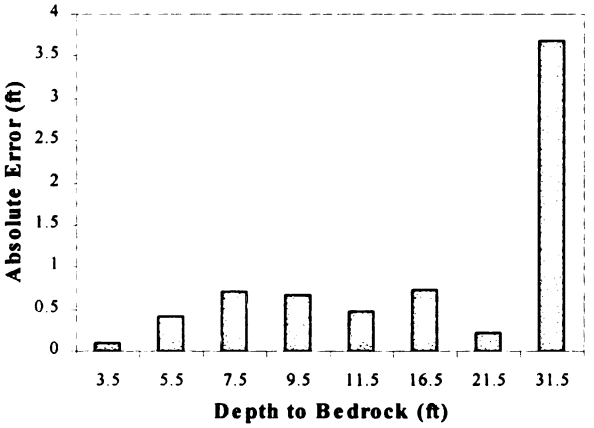

(c)

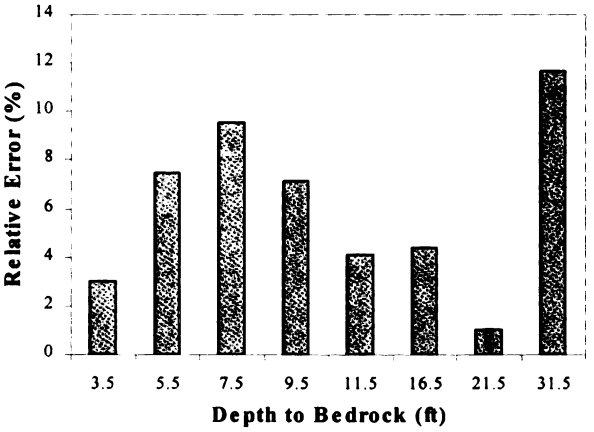

Figure 3.15 Comparison of predicted and actual depth-to-bedrock

(a)

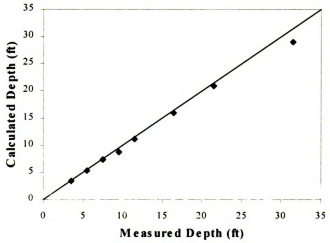

(b)

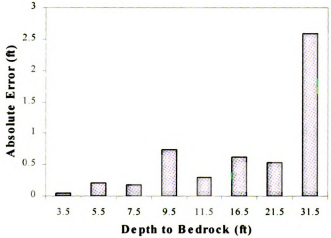

(c)

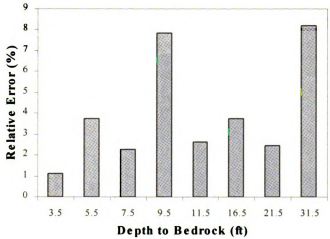

Figure 3.16 Comparison of predicted and actual depth-to-bedrock

(a)

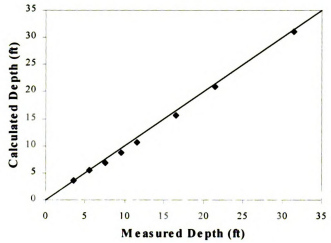

(b)

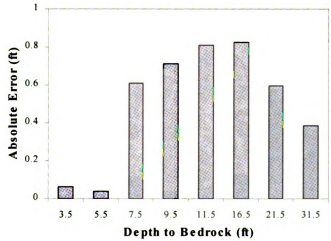

(c)

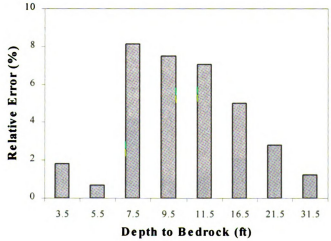

Figure 3.17 Comparison of predicted and actual depth-to-bedrock

(a)

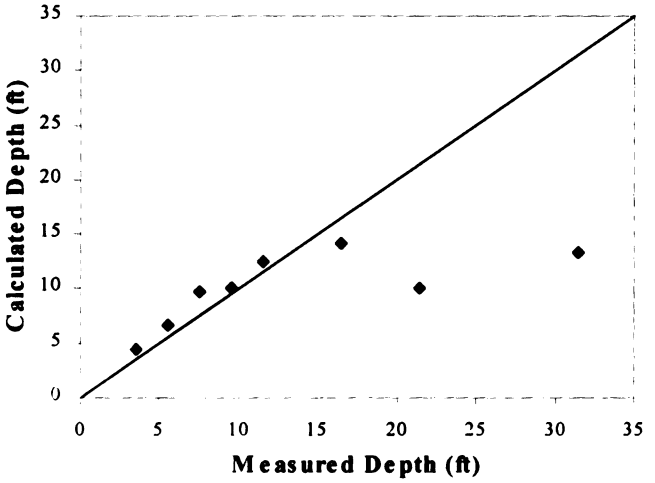

(b)

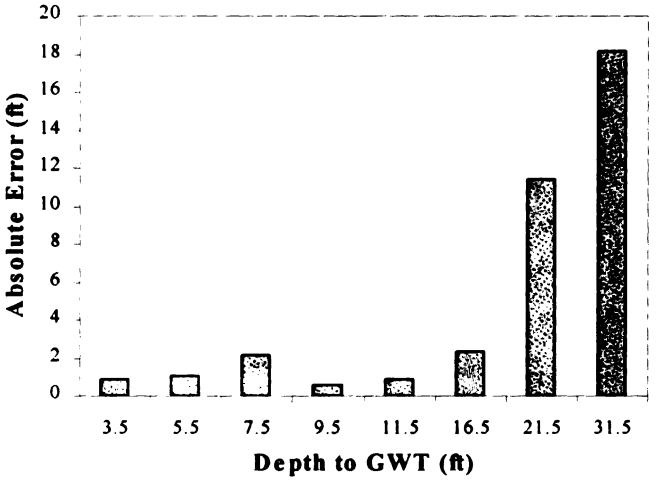

(c)

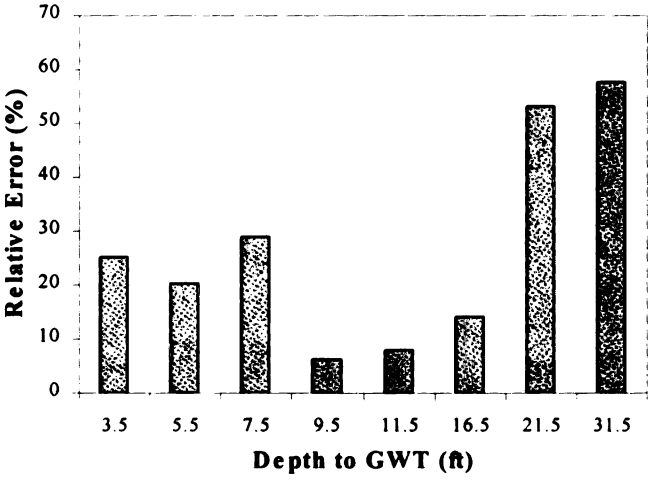

Figure 3.18 Comparison of predicted and actual depth-to-watertable

(Poisson's Ratio=0.495, Vs=500 ft/s)

(a)

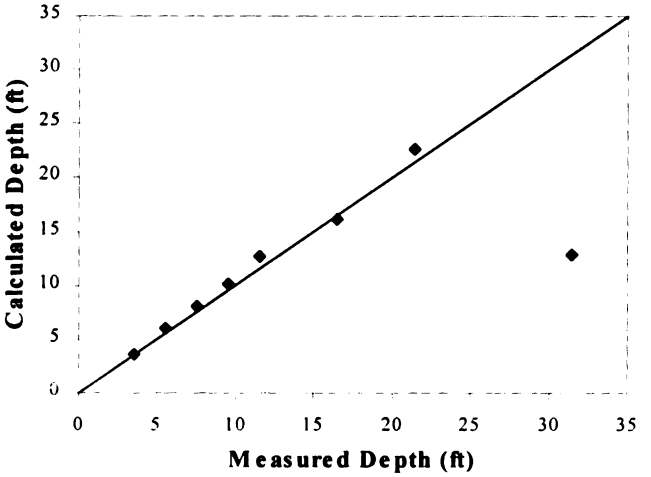

(b)

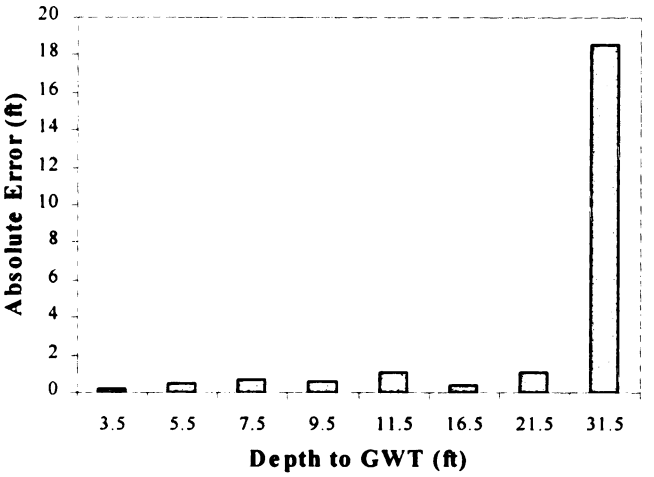

(c)

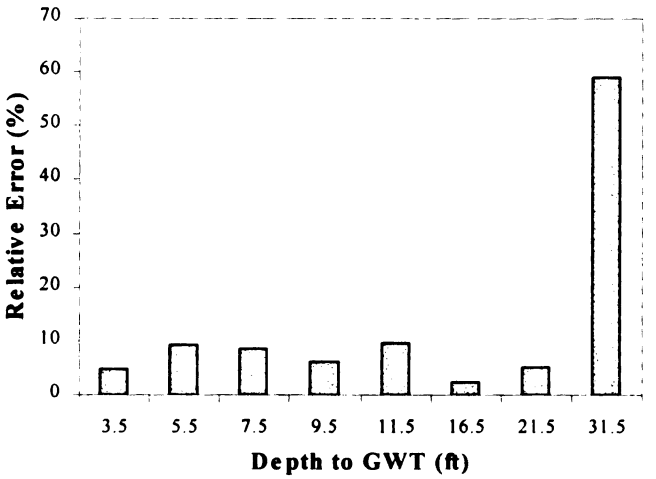

Figure 3.19 Comparison of predicted and actual depth-to-water table

(Poisson's Ratio=0.495, Vs=700 ft/s)

3.3.2 Estimating Subgrade Modulus

The procedure for estimating the depth-to-stiff layer, described in section 3.3.1 requires the knowledge of the subgrade modulus values. However, in the analysis of field data, subgrade properties (shear-wave velocity, unit weight and Poisson ratio) are not generally known, and therefore need to be either measured or assumed. Two different methods were considered for estimating the elastic modulus of the subgrade:

- Using the shear wave velocity as estimated from the time difference between two specified sensors (r = 3 ft and 5 ft)
- Using the base damage index (BDI) and shape factor (F2) proposed by Lee et al (1998).

In the first method, using the time difference between two specified sensors, the shear-wave velocity can be calculated, and two other properties (Poisson's ratio and unit weight) are assumed with typical values; using these values, the elastic modulus of the subgrade can then be calculated.

In the second method, BDI and F2 are calculated using Equations 3.16 and 3.17 and then combined with Equation 3.18, which calculates the surface deflection at a distance r from the applied load for a single layer system. Finally, the elastic modulus of the subgrade is calculated using Equation 3.19, assuming a typical value for Poisson's ratio of the subgrade

$$\text{Base Damage Index: } BDI = \delta_1 - \delta_2 \qquad (3.16)$$

$$\text{Shape Factor: } F2 = \frac{\delta_1 - \delta_3}{\delta_2} \tag{3.17}$$

where: δ_1 = Deflection at a distance of 12 in from the load

δ_2 = Deflection at a distance of 24 in from the load

δ_3 = Deflection at a distance of 36 in from the load

The results of the analysis showed that the second method was more accurate than the first method. Therefore, only the second method is used in the new backcalculation program. Figures 3.19 through 3.26 only show the results of the analysis using the second method.

$$\delta_r = \frac{P\left(1-\nu^2\right)}{E_{sg}} f(r) \tag{3.18}$$

where, δ_r =surface deflection at offset, r, from the applied load

P = Applied load

E_{sg} = Subgrade modulus

ν = Subgrade Poisson's ratio

$f(r) = \frac{1}{r}$, with r being the distance from the applied load

$$E_{sg} = \frac{F2 \cdot P(1-\nu^2) f(3)}{4BDI - \delta_1 F2} \tag{3.19}$$

3.3.3 Using the Subgrade Modulus and Depth-to-Stiff Layer Estimates in the Backcalculation Algorithm

In the backcalculation algorithm, the subgrade modulus is first estimated using Equation 3.19. An improved estimate of the depth-to-stiff layer or the depth-to- ground-water-table can then be obtained using the new value for the subgrade modulus. The total duration of the deflection should be several times larger than the actual duration of the load to insure that all free vibrations have attenuated. Although the appropriate value depends on the fundamental natural period of the system and the amount of damping, a duration of 0.15 to 0.2 second is generally sufficient to determine the natural period, Td, of the pavement system.

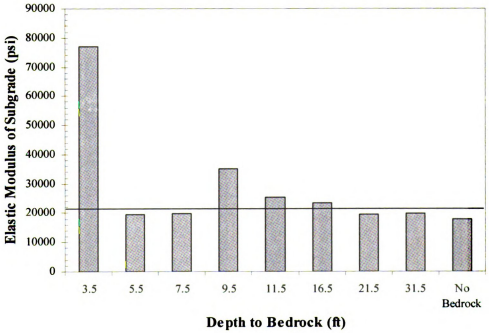

Figure 3.20 Results of analysis for elastic modulus of subgrade calculation

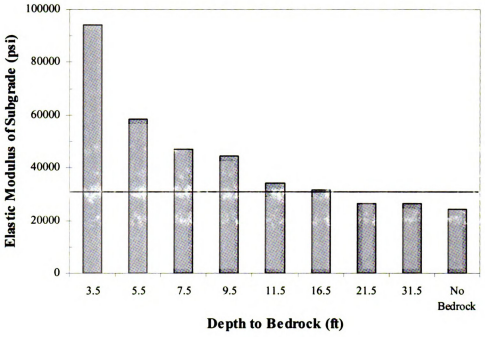

Figure 3.21 Results of analysis for elastic modulus of subgrade calculation

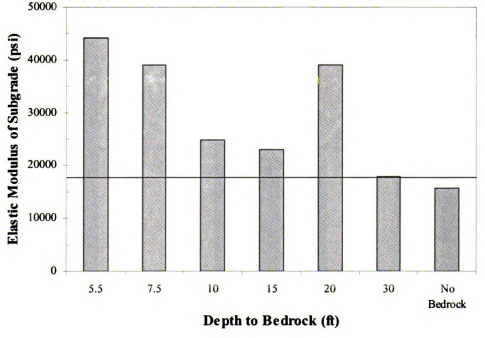

Figure 3.22 Results of analysis for elastic modulus of subgrade calculation

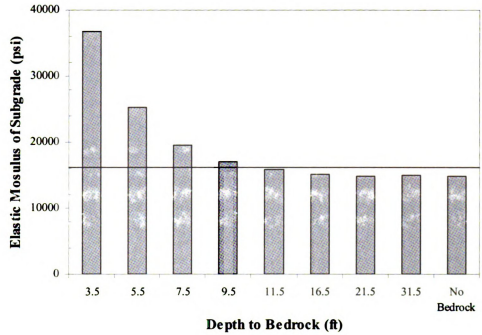

Figure 3.23 Results of analysis for elastic modulus of subgrade calculation

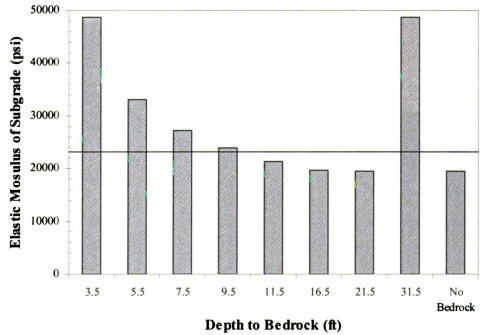

Figure 3.24 Results of analysis for elastic modulus of subgrade calculation

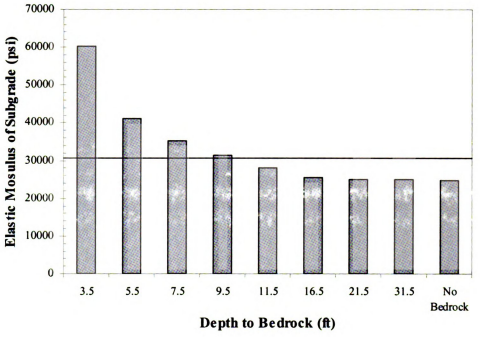

Figure 3.25 Results of analysis for elastic modulus of subgrade calculation

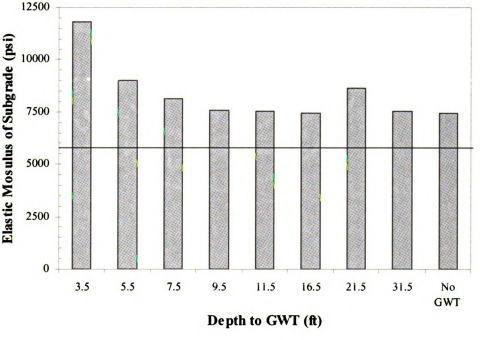

Figure 3.26 Results of analysis for elastic modulus of subgrade calculation

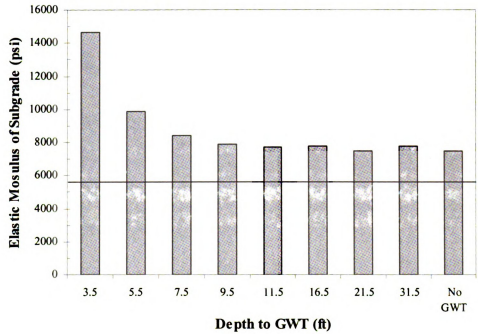

Figure 3.27 Results of analysis for elastic modulus of subgrade calculation

CHAPTER 4 - INVERSE SOLUTION

4.1 Introduction

Backcalculation of pavement layer parameters is an inverse problem, where some of the layer parameters are estimated by matching the theoretical prediction to the measured deflections such that the measured system response (in the form of the deflection basin) is matched by the theoretical predictions.

In FWD test interpretation, the input is the impulse load applied to the pavement structure by the Falling Weight Deflectometer; the output is the deflection time histories at the different sensors, and the system is the pavement structure. The theoretical formulation for computing the response of the pavement structure due to the FWD load has been presented in chapter 3. The dynamic response of the pavement structure depends on the elastic modulus, damping ratio, thickness, Poisson's ratio and mass density of each layer.

Current methods of interpretation of FWD test results use the maximum displacement at each sensor to define a deflection basin, which is interpreted as having resulted from a statically applied load. This approach neglects the dynamic nature of the test. When the time histories of the load and displacements are recorded, the additional information available provides substantial insight into the properties of the system and can improve the accuracy of the backcalculation results.

The number of deflection measurements must exceed (or, theoretically, at least be equal to) the number of parameters that are to be backcalculated. Most backcalculation schemes allow for backcalculating 3 to 5 parameters, these being layer moduli. Some schemes

allow for backcalculating the depth to stiff layer; however, none of the available backcalculation solutions allows for backcalculating both layer moduli and thicknesses.

In this study, two new methods based on dynamic interpretation of deflection time histories using frequency and time-domain solutions are developed. The methods allow for theoretically backcalculating the layer moduli, damping ratios and thicknesses for a three to five- layer system. The backcalculation procedure is based on the modified Newton-Raphson method originally adopted in the MICHBACK program (1993). The new program offers two options: (i) frequency-domain and (ii) time-domain backcalculation.

4.2 Frequency-domain backcalculation

In the frequency-domain solution, the modified Newton-Raphson method is extended to include complex valued deflection gradients, and the gradient matrix can be expanded to handle multiple frequencies simultaneously. In addition, methods for estimating the depth to stiff layer and the seed subgrade modulus, proposed by Roesset (1995) and Lee et al. (1998), respectively, have been adopted with some modifications and are implemented in the new program.

4.2.1 Multi-frequency backcalculation

In this option, the AC modulus is frequency-dependent, while the other layer moduli are assumed to be constant with frequency. The damping of the AC layer is solved by using the real and imaginary parts of the backcalculated complex moduli, while damping ratios of the base and subgrade layers are assumed.

The ability of the new solution to analyze complex deflection basins at multiple frequencies simultaneously allows for increasing the number of parameters that can be backcalculated. Currently, the computer program uses deflection basins from three frequencies. This enables the backcalculation of twelve parameters:

- Modulus of the asphalt concrete layer at three frequencies; (3)
- Damping ratio of the asphalt concrete layer at three frequencies; (3)
- Moduli for the base, subbase and subgrade layers; (3)
- Thicknesses for the AC, base and subbase layers. (3)

For the case of a stiff layer at shallow depth, the base and subbase layers can be combined into one layer, and the program can calculate the depth-to-stiff layer as a third thickness. In this option, the user may also choose not to backcalculate layer thicknesses.

4.2.2 Single-frequency backcalculation with thickness backcalculation

In this option, all parameters are allowed to vary with frequency since they are backcalculated at different (independent) frequencies. However, given the reduced amount of information (only one complex deflection basin), only eight parameters can be backcalculated (the damping ratios of the base and subgrade are assumed):

- Modulus of the asphalt concrete layer at a given frequency; (1)
- Damping ratio of the asphalt concrete layer at a given frequency; (1)
- Moduli for the base, subbase and subgrade layers; (3)
- Thicknesses for the AC, base and subbase layers. (3)

Similarly to the multi-frequency backcalculation, the base and subbase layers can be combined into one layer when a stiff layer is suspected to exist at shallow depth, and the program can calculate the depth-to-stiff layer as a third thickness. Also in this option, the user may choose not to backcalculate layer thicknesses.

4.2.3 Single-frequency backcalculation without thickness backcalculation

In this option, layer thicknesses are assumed, and the moduli and damping ratios of all layers are backcalculated at each frequency. This leads to eight backcalculated parameters at each frequency;

Moduli of the AC, base, subbase and subgrade layers; (4)

Damping ratio of the AC, base, subbase and subgrade layers. (4)

4.3 Time-domain backcalculation

In the time-domain backcalculation, the gradient matrix is expanded by including gradients of peak deflections and their corresponding times (or traces of time history). The details of the inverse solution are described in section 4.5.

4.3.1 Time-domain backcalculation without thickness backcalculation

In this option, layer thicknesses are assumed, and the moduli and damping ratios of all layers are backcalculated using ~~since~~ either peak deflections and their corresponding time lags or traces of time history. This leads to backcalculating as many as eight parameters. The first option is to backcalculate the following:

- Moduli of the AC, base, subbase and subgrade layers; (4)
- Damping ratios of the AC, base, subbase and subgrade layers.(4)

The second option is to backcalculate:

- Modulus of the asphalt concrete layer (1)
- Damping ratio of the asphalt concrete layer (1)
- Moduli for the base, subbase and subgrade layers.(3)

This option is more realistic when using field data.

4.3.2 Time-domain backcalculation with thickness backcalculation

In this option, all parameters are allowed to vary, and as many as eight parameters can be backcalculated:

- Moduli of AC, base and subgrade layers; (3)
- Damping ratios of AC, base and subgrade layers; (3)
- Thicknesses of AC and base layers. (2)

The other option backcalculates:

- Modulus of the asphalt concrete layer; (1)
- Damping ratio of the asphalt concrete layer; (1)
- Moduli for the base, subbase and subgrade layers; (3)
- Thicknesses for the AC, base and subbase layers. (3)

In all options mentioned above, a least square optimization algorithm or singular value decomposition (SVD) is used to mach the measured and computed deflection

4.4 FWD Data Processing

Modeling the dynamic response of the pavement subjected to an FWD pulse requires calculating the time history of surface deflections $U_i(t)$ that would be recorded at receivers *i* due to a transient uniform disk load *P(t)* applied to the pavement structure. The full-time histories of the load and deflection are used in the analysis. Because the FWD load is transient in nature and not harmonic, the Fourier transform is used to represent the transient load as a series of harmonic loads with different amplitudes at different frequencies. The same transformation is done for the deflection time histories.

As a first step the excitation *P(t)* is decomposed into its different frequency components $P(\omega)$ by means of a Fourier transform. This is evaluated numerically using the Fast Fourier Transform (FFT) algorithm. The second step is to obtain the Fourier transform of the different sensor displacements, $U_i(\omega)$.

It should be noted that unlike the continuous Fourier Transform, the Discrete Fourier Transform (FFT algorithm) assumes that the input function is periodic with a period Tp. When using the FFT algorithm, the values of the basic parameters involved (e.g. number of sampled points, N; time increment, Δt; and total period, T_p) have to be selected properly so that a compromise can be reached between the accuracy of results and the cost of computation. Finally, it should be noted that the transfer function does not need to

be computed for all frequencies, as interpolation techniques can be used effectively to reduce computation time.

An example load pulse is shown in Figure 4.1. In this example, data are sampled every 0.77 ms and the sampling time is 100 ms. Deflection time histories from all seven sensors are shown in Figure 4.2. The load and deflection functions in the frequency-domain are shown in Figure 4.3 and Figure 4.4. Figure 4.5 shows the real and imaginary parts of the transfer functions due to a unit harmonic load as a function of frequency.

4.5 Inverse Solution

The objective of any back-calculation solution is to find a set of layer parameters such that the calculated deflection basin will match the measured one within a specified tolerance. To accomplish this, it repeatedly adjusts the parameter values until a suitable match is obtained. The discussion below describes the solution in terms of the modulus being the backcalculated parameter. The same method can be applied to thickness (in lieu of the modulus); however, it is not included herein for the sake of brevity.

The dynamic backcalculation solution developed in this research is an extension of the solution used in the MICHBACK program (1993). It uses the modified Newton method to obtain a least squares solution of an over determined set of equations. In the MICHBACK solution, these sets of equations are real-valued and correspond to the peak deflection values, since the backcalculation scheme uses a static solution (CHEVRONX) to predict the deflection basin. In the frequency-domain solution, the equations are complex-valued and correspond to the steady-state solution at one or multiple

frequencies. In the time-domain solution, the real-valued equations are expanded to correspond to the peak transient deflections and their corresponding time lags relative to the peak load.

4.5.1 Frequency-domain Backcalculation

Frequency-domain backcalculation uses the harmonic (steady-state) solution in SAPSI to predict the deflection basin at any given frequency. In this case, the equations become complex-valued, and they can be expanded to include deflection basins at multiple frequencies.

Newton's method consists of approximating the non-linear curve relating the complex deflections $\{U(\omega)\} = \left\{ \overline{w}_1^m \quad \overline{w}_2^m \quad \cdots \quad \overline{w}_{m-1}^m \quad \overline{w}_m^m \right\}$ by a series of straight lines tangent to the curve at the estimate of the complex modulus $\hat{E}^i$. The complex deflection is defined as $\overline{w}_i^m = w_i^1 + iw_i^2$ where the real part of the deflection corresponds to the elastic response and the imaginary part describes the viscous response. The complex modulus is defined as $E = E^1 + iE^2$. The slope of the straight line is used to obtain the increment, ΔE_i, which is added to $\hat{E}^i$ to obtain the improved modulus estimate $\hat{E}^{i+1}$.

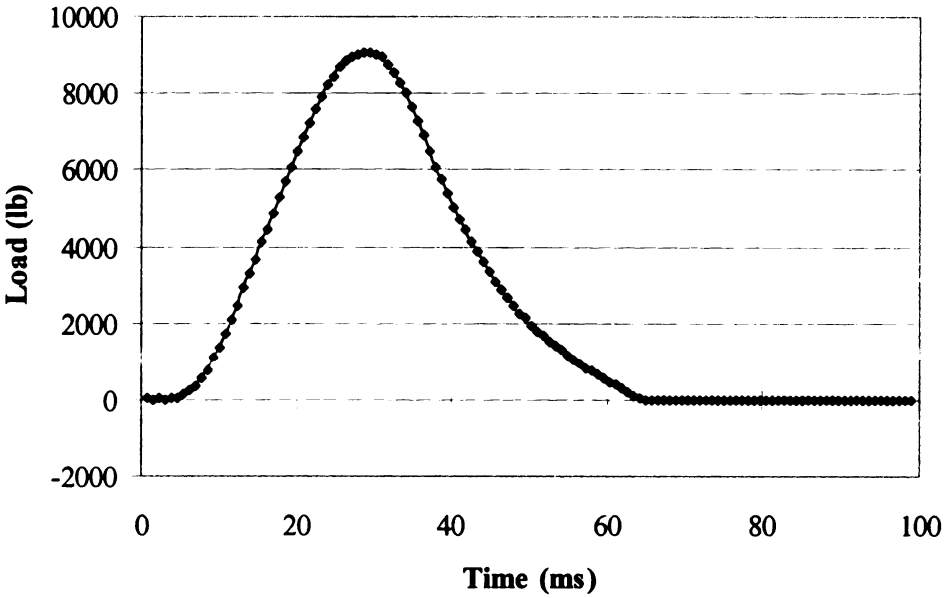

Figure 4.1 FWD load versus time

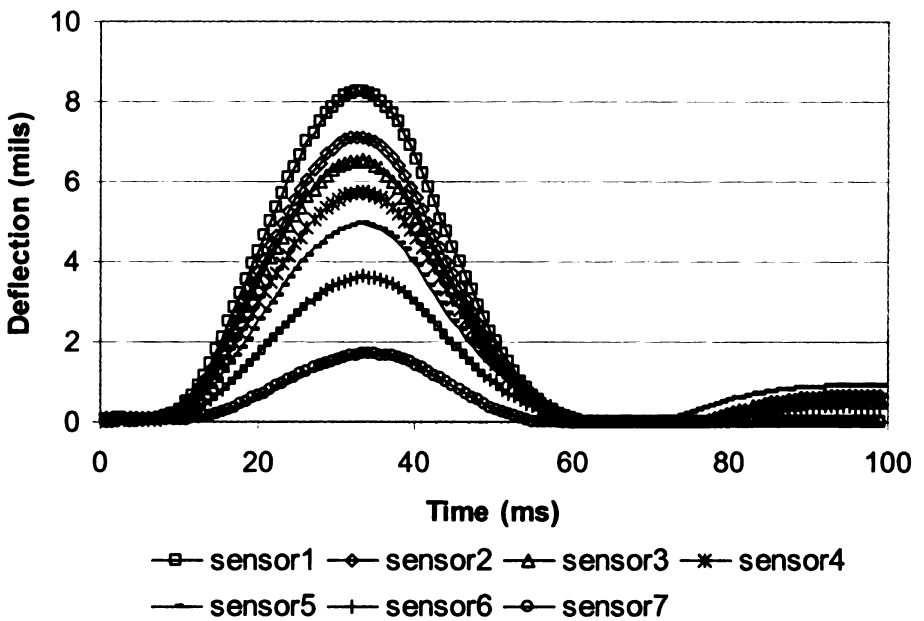

Figure 4.2 Deflections versus time

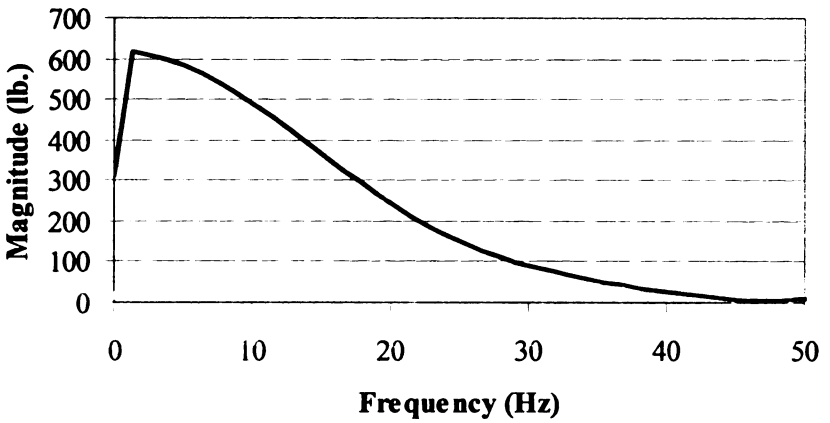

(a) Magnitude of Fast-Fourier Transform of load

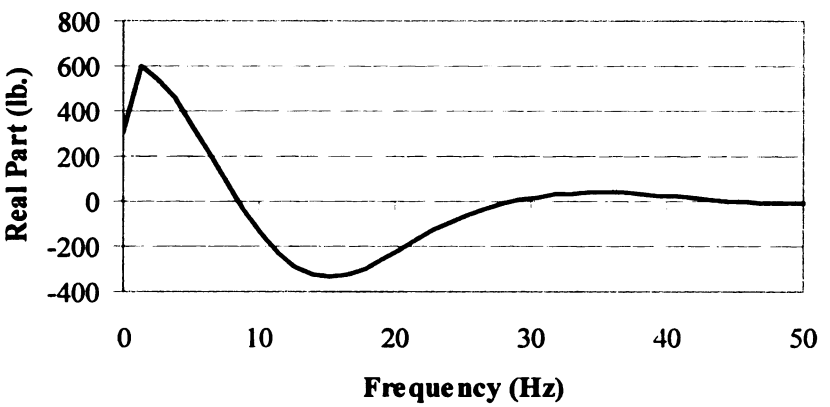

(b) Real part of Fast-Fourier Transform of load

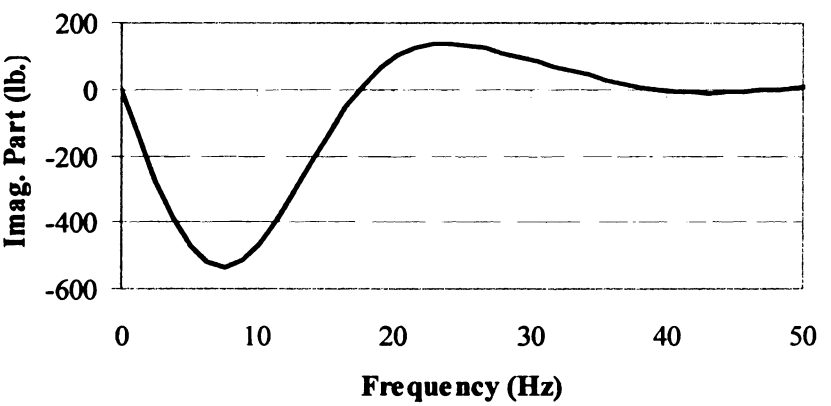

(c) Imaginary part of Fast-Fourier Transform of load

Figure 4.3 Fast-Fourier Transform of load-time history

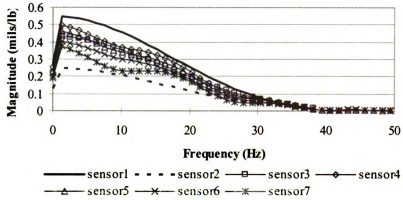

(a) Magnitude of Fast-Fourier Transform of deflection

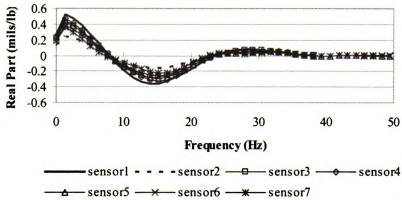

(b) Real part of Fast-Fourier Transform of deflection

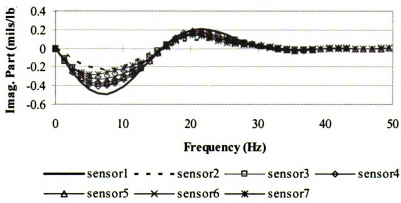

(c) Imaginary part of Fast- Fourier Transform of deflection

Figure 4.4 Fast- Fourier Transform of deflection

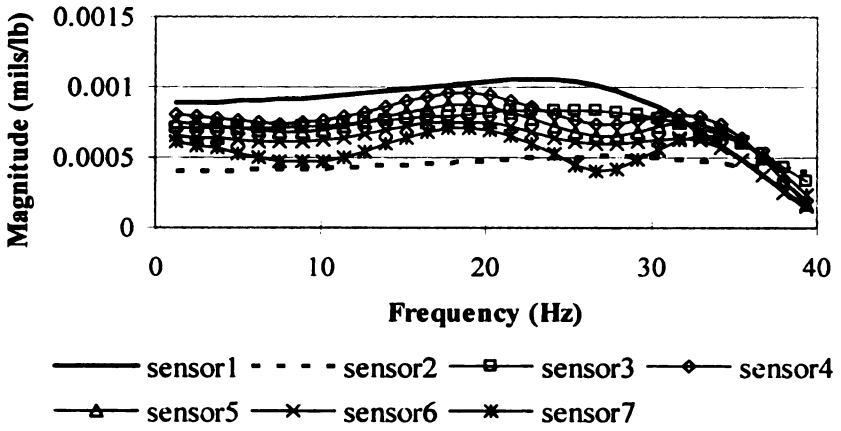

(a) Magnitude of transfer function

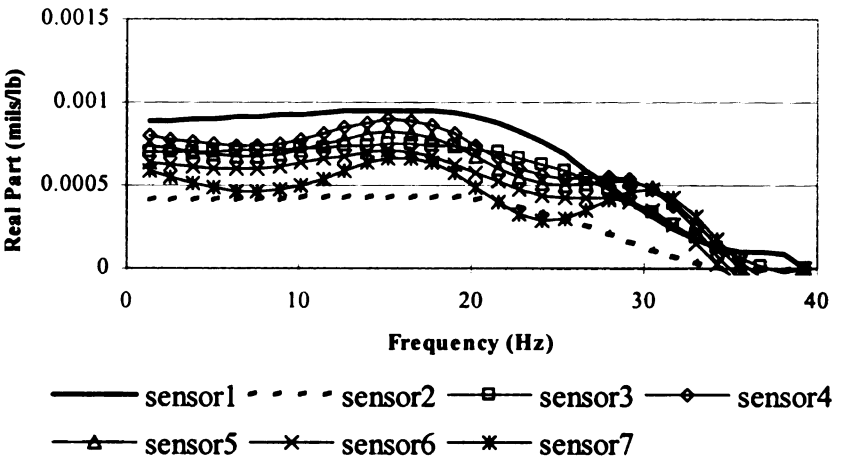

(b) Real part of transfer function

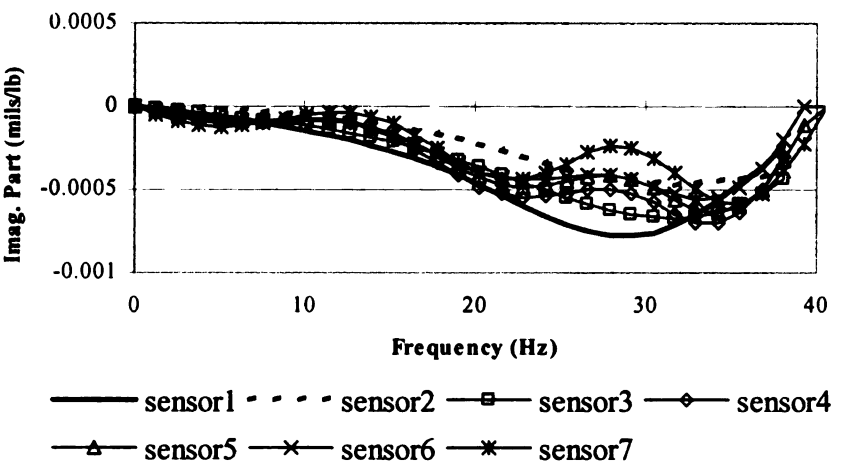

(c) Imaginary part of transfer function

Figure 4.5 Fast-Fourier Transform of transfer function

Because E is complex, the slope is evaluated for both the real and imaginary parts of the modulus. A similar approximation is used for the thickness using the increment ΔH_i. The expression for the slope of the curve relating deflection and thickness is the same as that for the real part of the modulus. Also, for both moduli and thickness, since the slope is not known analytically, it is obtained numerically by using the following equations:

$$\left.\frac{\partial \overline{w}}{\partial E}\right|_{E=\hat{E}^1} = \frac{W^1\left(\hat{E}^1(1+r)\right)-W^1\left(\hat{E}^1\right)}{r\hat{E}^1} + i\frac{W^2\left(\hat{E}^1(1+r)\right)-W^2\left(\hat{E}^1\right)}{r\hat{E}^1}$$

$$\left.\frac{\partial \overline{w}}{\partial E}\right|_{E=\hat{E}^2} = \frac{W^2\left(\hat{E}^2(1+r)\right)-W^2\left(\hat{E}_1^2\right)}{r\hat{E}^2} - i\frac{W^1\left(\hat{E}^2(1+r)\right)-W^1\left(\hat{E}^2\right)}{r\hat{E}^2} \qquad (4.1)$$

$$\left.\frac{\partial \overline{w}}{\partial H}\right|_{H=\hat{H}} = \frac{W^1\left(\hat{H}(1+r)\right)-W^1\left(\hat{H}\right)}{r\hat{H}} + i\frac{W^2\left(\hat{H}(1+r)\right)-W^2\left(\hat{H}\right)}{r\hat{H}}$$

in which r is sufficiently small. This requires additional deflections to be computed, arising from moduli and thickness values of $\hat{E}^{i+1}$ and $\hat{H}^{i+1}$, respectively.

For the described system of n identified parameters (I complex moduli and n-I layer thicknesses) and m sensors, the slope is represented by the gradient matrix

$$G^i = \left[\left.\frac{\partial \overline{w}}{\partial E}\right|_{E=E^1+iE^2} \quad \left.\frac{\partial \overline{w}}{\partial H}\right|_{H=H^1}\right] = \{[G_1][G_2][H]\} \qquad (4.2)$$

where

$$[G_1]=\begin{bmatrix} \frac{\partial \overline{w}_1}{\partial E_1^1} & \frac{\partial \overline{w}_1}{\partial E_2^1} & \cdots & \frac{\partial \overline{w}_1}{\partial E_l^1} \\ \vdots & & & \vdots \\ \frac{\partial \overline{w}_m}{\partial E_1^1} & \frac{\partial \overline{w}_m}{\partial E_2^1} & \cdots & \frac{\partial \overline{w}_m}{\partial E_l^1} \end{bmatrix} [G_2]=\begin{bmatrix} \frac{\partial \overline{w}_1}{\partial E_1^2} & \frac{\partial \overline{w}_1}{\partial E_2^2} & \cdots & \frac{\partial \overline{w}_1}{\partial E_l^2} \\ \vdots & & & \vdots \\ \frac{\partial \overline{w}_m}{\partial E_1^2} & \frac{\partial \overline{w}_m}{\partial E_2^2} & \cdots & \frac{\partial \overline{w}_m}{\partial E_l^2} \end{bmatrix}$$

$$[H]=\begin{bmatrix} \frac{\partial \overline{w}_1}{\partial H_1} & \frac{\partial \overline{w}_1}{\partial H_2} & \cdots & \frac{\partial \overline{w}_1}{\partial H_{n-l}} \\ \vdots & & & \vdots \\ \frac{\partial \overline{w}_m}{\partial H_1} & \frac{\partial \overline{w}_m}{\partial H_2} & \cdots & \frac{\partial \overline{w}_m}{\partial H_{n-l}} \end{bmatrix}$$

and

$$\frac{\partial \overline{w}_j}{\partial E_k^1}=\frac{W_j^1\left([R]E_k^1\right)-W_j^1\left(E_k^1\right)}{rE_k^1}+i\frac{W_j^2\left([R]E_k^1\right)-W_j^2\left(E_k^1\right)}{rE_k^1}$$

$$\frac{\partial \overline{w}_j}{\partial E_k^2}=\frac{W_j^2\left([R]E_k^2\right)-W_j^2\left(E_k^2\right)}{rE_k^2}-i\frac{W_j^1\left([R]E_k^2\right)-W_j^1\left(E_k^2\right)}{rE_k^2}$$

$$\frac{\partial \overline{w}_j}{\partial H_k}=\frac{W_j^1([R]H_k)-W_j^1(H_k)}{rH_k}+i\frac{W_j^2([R]H_k)-W_j^2(H_k)}{rH_k}$$

$[R]$ is a diagonal matrix with the k th diagonal element being (1+r) and all other elements being 1. Thus the partial derivative is estimated numerically by taking the difference in the jth deflection arising from the use of a set of moduli and thicknesses. The increments to the moduli and thicknesses, $\{\Delta E, \Delta H\}^i$ can then be obtained by solving the equations:

$$\{\hat{w}^i\} + [G^i]\{\Delta E, \Delta H\}^i = \{w\} \tag{4.3}$$

Because equations (4.3) are over determined with *m* equations and *n* unknowns, a least squared solution or SVD method are used to solve for $\{\Delta E, \Delta H\}^i$:

The revised moduli and thicknesses are obtained through:

$$\{E, H\}^{i+1} = \{E, H\}^i + \{\Delta E, \Delta H\}^i \tag{4.4}$$

The iteration is completed when the changes in layer moduli and thicknesses are smaller than a set of specified tolerances:

$$\frac{\hat{E}_{k,1}^{i+1} - \hat{E}_{k,1}^i}{\hat{E}_{k,1}^i} \le \varepsilon_1, \frac{\hat{E}_{k,2}^{i+1} - \hat{E}_{k,2}^i}{\hat{E}_{k,2}^i} \le \varepsilon_2, \frac{\hat{H}_k^{i+1} - \hat{H}_k^i}{\hat{E}_k^i} \le \varepsilon_1 \tag{4.5}$$

where k = 1, 2, …, n.

In addition, the computed and measured deflections must match closely, so that the root-mean-square error in real and imaginary deflections must be smaller than a given tolerance:

$$RMS_1 = \sqrt{\sum_{j=1}^{m} \left(\frac{\hat{w}_{j,1}^{i+1} - \hat{w}_{j,1}^i}{\hat{w}_{j,1}^i} \right)^2} \le \varepsilon_4, RMS_2 = \sqrt{\sum_{j=1}^{m} \left(\frac{\hat{w}_{j,2}^{i+1} - \hat{w}_{j,2}^i}{\hat{w}_{j,2}^i} \right)^2} \le \varepsilon_5 \tag{4.6}$$

4.5.2 Time-domain Backcalculation using Peak Deflection and Time Lag

In the FWD response time history, the peak deflection reflects the stiffness of the pavement, and the time lag between the peak of the applied FWD load and a sensor deflection reflects the effects of pavement inertia and damping. Only the peak deflections from each sensor and the time lags between the peak load and the peak deflections at each sensor are used in the backcalculation algorithm. The vector of measured responses is therefore $\{U\} = \left\{ w_1 \quad t_1 \quad \cdots \quad w_m \quad t_m \right\}^T$, where m is the number of sensors, w_i is the peak deflection at sensor i, and t_i is the time lag between the peak load and peak deflections.

The unknown properties of pavement layer i are taken to be the real and imaginary parts of the complex modulus, E_{1i} and E_{2i}, respectively, and the thickness H_i. The vector of unknowns becomes $\{x\} = \{[E_{11} \quad \cdots \quad E_{1l}] \quad [E_{2l} \quad \cdots \quad E_{2l}] \quad [H_1 \quad \cdots \quad H_l]\}^T$, where l is the total number of layers in the pavement.

Following the derivation by Harichandran et al. (1994), the increment to the unknown parameters in iteration i, $\{\Delta x\}_i$, is obtained by solving the linear set of equations

$$\{\hat{U}\}^i + [G]^i \{\Delta x\}^i = \{U\} \tag{4.7}$$

where $\{\hat{U}\}^i$ is the vector of peak deflections and time lags computed using the estimates of the pavement layer properties at iteration i, and $\{G\}^i$ is the gradient matrix at iteration i given by

$$[G]^i = \left[\frac{\partial\{U\}}{\partial\{x\}}\right]_{\{x\}=\{\hat{x}\}^i} = \left[[G_1]^i[G_2]^i[G_3]^i\right]_{\{x\}=\{\hat{x}\}^i} \tag{4.8}$$

where

$$[G_1]^i = \begin{bmatrix} \frac{\partial w_1}{\partial E_{11}} & \frac{\partial w_1}{\partial E_{12}} & \cdots & \frac{\partial w_1}{\partial E_{1l}} \\ \frac{\partial t_1}{\partial E_{11}} & \frac{\partial t_1}{\partial E_{12}} & \cdots & \frac{\partial t_1}{\partial E_{1l}} \\ \vdots & \vdots & \vdots & \vdots \\ \frac{\partial w_m}{\partial E_{11}} & \frac{\partial w_m}{\partial E_{12}} & \cdots & \frac{\partial w_m}{\partial E_{1l}} \\ \frac{\partial t_m}{\partial E_{11}} & \frac{\partial t_m}{\partial E_{12}} & \cdots & \frac{\partial t_m}{\partial E_{1l}} \end{bmatrix}_{\{x\}=\{\hat{x}\}^i} \qquad [G_2]^i = \begin{bmatrix} \frac{\partial w_1}{\partial E_{21}} & \frac{\partial w_1}{\partial E_{22}} & \cdots & \frac{\partial w_1}{\partial E_{2l}} \\ \frac{\partial t_1}{\partial E_{21}} & \frac{\partial t_1}{\partial E_{22}} & \cdots & \frac{\partial t_1}{\partial E_{2l}} \\ \vdots & \vdots & \vdots & \vdots \\ \frac{\partial w_m}{\partial E_{21}} & \frac{\partial w_m}{\partial E_{22}} & \cdots & \frac{\partial w_m}{\partial E_{2l}} \\ \frac{\partial t_m}{\partial E_{21}} & \frac{\partial t_m}{\partial E_{22}} & \cdots & \frac{\partial t_m}{\partial E_{2l}} \end{bmatrix}_{\{x\}=\{\hat{x}\}^i}$$

$$[G_3]^i = \begin{bmatrix} \frac{\partial w_1}{\partial H_1} & \frac{\partial w_1}{\partial H_2} & \cdots & \frac{\partial w_1}{\partial H_l} \\ \frac{\partial t_1}{\partial H_1} & \frac{\partial t_1}{\partial H_2} & \cdots & \frac{\partial t_1}{\partial H_l} \\ \vdots & \vdots & \vdots & \vdots \\ \frac{\partial w_m}{\partial H_1} & \frac{\partial w_m}{\partial H_2} & \cdots & \frac{\partial w_m}{\partial H_l} \\ \frac{\partial t_m}{\partial H_1} & \frac{\partial t_m}{\partial H_2} & \cdots & \frac{\partial t_m}{\partial H_l} \end{bmatrix}_{\{x\}=\{\hat{x}\}^i}$$

The partial derivatives in the gradient matrix must be evaluated numerically using

$$\left.\frac{\partial U_j}{\partial x_k}\right|_{\{x\}=\{\hat{x}\}^i} = \frac{U_j\left([R]\{\hat{x}\}^i\right) - U_j\left(\{\hat{x}\}^i\right)}{r\hat{x}_k^i}, \quad j = 1, 2\cdots, 2m \quad , k = 1, 2\cdots, 3l \tag{4.9}$$

where U can be the peak deflection or the corresponding time lag and x is the layer parameter (real or imaginary modulus, or thickness). [R] is a diagonal matrix with the k^{th} diagonal element being $(1 + r)$ and all other elements being 1. A separate call to the

forward calculation program is required to compute the partial derivatives in each column of the gradient matrix.

Equation (4.7) represents a set of $2m$ equations in $3l$ unknowns. Since there are more equations than unknowns, more robust method for solving the problem is to use the singular value decomposition (SVD). This algorithm has been implemented in the program.

After the increments $\{\Delta x\}^i$ are obtained by solving Equation 4.7, the revised moduli and thicknesses are obtained from:

$$\{x\}^{i+1} = \{x\}^i + \{\Delta x\}^i \tag{4.10}$$

The iteration is terminated when the changes in layer moduli and thicknesses are smaller than a set of specified tolerances:

$$\frac{\hat{E}_{1k}^{i+1} - \hat{E}_{1k}^{i}}{\hat{E}_{1k}^{i}} \le \varepsilon_1 \quad \frac{\hat{E}_{2k}^{i+1} - \hat{E}_{2k}^{i}}{\hat{E}_{2k}^{i}} \le \varepsilon_1 \quad \frac{\hat{H}_{k}^{i+1} - \hat{H}_{k}^{i}}{\hat{H}_{k}^{i}} \le \varepsilon_1 \quad k = 1,2,\cdots,l \tag{4.11}$$

4.5.3 Time Domain Backcalculation using traces of time histories

In this method, the deflection time histories are matched within a range of time near the peak responses. The backcalculation algorithm is similar to that described above, except that the gradient matrix is expanded to include deflection basins at individual time steps within the specified range in time. The vector of measured responses is:

$$\{U\} = \left\{ [w_1(t_s) \quad \cdots \quad w_m(t_s)] \quad \cdots \quad [w_1(t_f) \quad \cdots \quad w_m(t_f)] \right\}^T \tag{4.12}$$

where m is the number of sensors, $w_j(t_s)$ is the deflection of sensor j at the starting time and $w_j(t_f)$ is the deflection at the final time of the specified range. The vector of unknowns is described as $\left\{\begin{bmatrix} E_1^1 & \cdots & E_l^1 \end{bmatrix} \begin{bmatrix} E_1^2 & \cdots & E_l^2 \end{bmatrix} \begin{bmatrix} H_1 & \cdots & H_{l-1} \end{bmatrix}\right\}^T$. The increment to the unknown parameters in iteration n, $\{\Delta x\}n$, is obtained by solving Equation (4.10), where $\{\hat{U}\}^n$ is the vector of deflections at individual time steps, within the specified time range, computed using the estimates of the pavement layer properties at iteration n, and the gradient matrix $[G]^n$ at iteration n, in Equation (4.13), is composed of the following submatrices:

$$[G_1]=\begin{bmatrix} \frac{\partial w_1(t_s)}{\partial E_1^1} & \frac{\partial w_1(t_s)}{\partial E_2^1} & \cdots & \frac{\partial w_1(t_s)}{\partial E_l^1} \\ \vdots & \vdots & \vdots & \vdots \\ \frac{\partial w_m(t_s)}{\partial E_1^1} & \frac{\partial w_m(t_s)}{\partial E_2^1} & \cdots & \frac{\partial w_m(t_s)}{\partial E_l^1} \\ \vdots & \vdots & \vdots & \vdots \\ \frac{\partial w_1(t_f)}{\partial E_1^1} & \frac{\partial w_1(t_f)}{\partial E_2^1} & \cdots & \frac{\partial w_1(t_f)}{\partial E_l^1} \\ \vdots & \vdots & \vdots & \vdots \\ \frac{\partial w_m(t_f)}{\partial E_1^1} & \frac{\partial w_m(t_f)}{\partial E_2^1} & \cdots & \frac{\partial w_m(t_f)}{\partial E_l^1} \end{bmatrix}, [G_2]=\begin{bmatrix} \frac{\partial w_1(t_s)}{\partial E_1^2} & \frac{\partial w_1(t_s)}{\partial E_2^2} & \cdots & \frac{\partial w_1(t_s)}{\partial E_l^2} \\ \vdots & \vdots & \vdots & \vdots \\ \frac{\partial w_m(t_s)}{\partial E_1^2} & \frac{\partial w_m(t_s)}{\partial E_2^2} & \cdots & \frac{\partial w_m(t_s)}{\partial E_l^{21}} \\ \vdots & \vdots & \vdots & \vdots \\ \frac{\partial w_1(t_f)}{\partial E_1^2} & \frac{\partial w_1(t_f)}{\partial E_2^2} & \cdots & \frac{\partial w_1(t_f)}{\partial E_l^2} \\ \vdots & \vdots & \vdots & \vdots \\ \frac{\partial w_m(t_f)}{\partial E_1^2} & \frac{\partial w_m(t_f)}{\partial E_2^2} & \cdots & \frac{\partial w_m(t_f)}{\partial E_l^2} \end{bmatrix},$$

$$[G_3]=\begin{bmatrix} \frac{\partial w_1(t_s)}{\partial H_1} & \frac{\partial w_1(t_s)}{\partial H_2} & \cdots & \frac{\partial w_1(t_s)}{\partial H_l} \\ \vdots & \vdots & \vdots & \vdots \\ \frac{\partial w_m(t_s)}{\partial H_1} & \frac{\partial w_m(t_s)}{\partial H_2} & \cdots & \frac{\partial w_m(t_s)}{\partial H_l} \\ \vdots & \vdots & \vdots & \vdots \\ \frac{\partial w_1(t_f)}{\partial H_1} & \frac{\partial w_1(t_f)}{\partial H_2} & \cdots & \frac{\partial w_1(t_f)}{\partial H_l} \\ \vdots & \vdots & \vdots & \vdots \\ \frac{\partial w_m(t_f)}{\partial H_1} & \frac{\partial w_m(t_f)}{\partial H_2} & \cdots & \frac{\partial w_m(t_f)}{\partial H_l} \end{bmatrix} \tag{4.13}$$

The partial derivatives in the gradient matrix must be evaluated numerically using Equation (4.9) and the revised moduli and tolerances are obtained using Equations (4.10) and (4.11).

4.6 SVD method

SVD is a very powerful set of techniques for dealing with sets of equations or a matrix that are either singular or else numerically very close to singular. SVD methods are based on the following theorem of linear algebra, which is in the reference (Press et al, 1989): Any M×N matrix $[A]$whose number of rows M is greater than or equal to its number of columns N, can be written as the product of an M × N column-orthogonal matrix $[U]$, an N × N diagonal matrix $[\omega]$ with positive or zero elements (the singular values), and the transpose of an N × N orthogonal matrix $[V]$.

The matrix $[A]$ can be decomposed as three matrices as follows:

$$\begin{bmatrix} A \end{bmatrix} = \begin{bmatrix} U \end{bmatrix} \cdot \begin{bmatrix} \omega_1 & & & \\ & \omega_2 & & \\ & & \cdots & \\ & & & \omega_N \end{bmatrix} \cdot \begin{bmatrix} V \end{bmatrix}^T \tag{4.14}$$

Where, $U \cdot U^T = 1$, $V \cdot V^T = 1$, and $[\omega]$ is diagonal matrix.

For the following ill conditioned system of equations

$$\begin{bmatrix} A \end{bmatrix} \cdot \begin{bmatrix} X \end{bmatrix} = \begin{bmatrix} b \end{bmatrix} \tag{4.16}$$

Inversing $[A]$ by SVD, $[X]$ can be expressed as

$$\begin{bmatrix} X \end{bmatrix} = \begin{bmatrix} V \end{bmatrix} \cdot \begin{bmatrix} \frac{1}{\omega_1} & & & \\ & \frac{1}{\omega_2} & & \\ & & \cdots & \\ & & & \frac{1}{\omega_N} \end{bmatrix} \cdot \begin{bmatrix} U \end{bmatrix}^T \cdot \begin{bmatrix} b \end{bmatrix} \tag{4.17}$$

where, $U \cdot U^T = 1$, $V \cdot V^T = 1$, and $\left[\frac{1}{\omega}\right]$ is a diagonal matrix.

4.6.1 Truncating Singular Values

Reference (Press, 1989) defines the condition number of a matrix as a ratio of the largest of ω_j to the smallest ω_j.

$$\text{Condition number} = \frac{\omega \max}{\omega \min} \tag{4.18}$$

A matrix $[A]$ is singular or ill conditioned if its condition number is too large. Reference (Press, 1989) suggested this number should be adjusted according to the experiment with the specific problem.

Define the threshold of truncation as:

$$\omega_j < \omega_{\max} \cdot 10^{-Threshold} \tag{4.19}$$

where $j = 1,2,\cdots\cdots, N$

After selecting the threshold of a condition number, the SVD algorithm will simply replace $\frac{1}{\omega_j}$ with zero.

4.6.2 Scaling

The objective of scaling is to reduce the possibility of ill conditioning in the inverse problem. In this process, the nonlinear equation (4.3) including parameters of modulus, damping ratio, and thickness will be simultaneously identified. Since the absolute value among modulus, thickness, and damping ratio are not compatible, the elements of the

gradient matrix vary from a very small value to a large value. Therefore during SVD process, the value of ω_j varies from a very small number to large number correspondingly. The condition number can be determined using equation (4.18). A matrix is singular if its condition number is infinite, or if it is too large (Press, 1989). Take the example of Michigan US131 site. If no scaling is performed, the value of the condition number is within the order of 10^6 in all iterations, potentially causing ill-conditioning. Scaling will make all the elements in the gradient matrix compatible through dividing by a number compatible to the values of the modulus, damping ratio, and thickness, respectively. When scaling is performed in the Michigan US131 site, the condition numbers decreases to the order of 10^3 in all iterations, thus diminishing the possibilities of an ill-conditioned problem and increasing the likehood of getting a reasonable solution during the inversion process.

4.7 Modifications to the Solution

The MICHBACK backcalculation solution allows for modifying the Newton method algorithm such that the total number of calls to the forward calculation program can be reduced (Mahmood, 1993). In the modified method several iterations are performed with a gradient matrix before it is revised. Although, the convergence in the modified approach is slower than the normal method, the *n* forward calculations required for calculating the gradient matrix during each iteration can be reduced. This method was adopted in the current algorithm.

CHAPTER 5 - DYNABACK PROGRAM STRUCTURE AND FEATURES

5.1 General

The DYNABACK program has been written in Fortran 77 computer language and includes several source files. The source files are written using the Microsoft Fortran complier version 4.0. User-friendly features have been designed to facilitate the use of the program by any pavement engineers. The program can read the output files of KUAB Falling Weight Deflectometer (FWD) used by MDOT, and other FWDs such as Dynatest. The program provides a range of options to the user to view and process the deflection data before it is analyzed. In this chapter, the general structure and the features of the program are described. The function of each of the program subroutines is briefly introduced in Appendix A.

5.2 Data Input

Deflection data can be entered using the deflection output file format of KUAB used by MDOT; the file can be read and processed by the program automatically. The cross-sectional data, Poisson's ratios, type of the layers being analyzed, the desired convergence criteria, expected ranges of the layer parameters, the number of sampled points, the number of points in the FFT algorithm must be enter using the keyboard. Users are allowed to specify the layout of deflection sensors using the keyboard input. The default weighting factor (for matching deflections) allocated to each sensor is 1.0, but can be changed by the user if desired. The input information is stored in a data file, which can be edited on the interactive screen at any stage.

When processing the deflection data from a file, comprehensive keyboard input is required only at the start of the analysis. All the essential information required to operate the program is stored in easily accessible data files. The various options provided to view, process, and analyze the deflection data from FWD files are discussed in the next section.

5.3 Processing a FWD Deflection Data File

The DYNABACK program can read output files containing deflection data generated by the KUAB software. The system is also flexible for Dynatest software and only minor changes would be required. The programs provide features that make the pre-processing of the deflection data easy and efficient. The program allows for plotting the measured data so that the user may be able to identify and if necessary, remove any outlier indicative of unwanted sensor measurements. The program also plots the frequency content of the load and deflections in order for the user to decide on the range of frequencies to be used in the analysis. The highlights of the various features in the program are covered in the following sections.

5.3.1 Reviewing and Processing the Deflection Data

This feature is useful in checking for any anomalies in the measured load or sensor time histories. The user can view the peak deflection basin as well as the time lags corresponding to the peak response for each sensor. Figure 5.1 shows an example of these plots. The program can also plot the deflection and load time histories simultaneously so that the user can easily select the duration (length) of the record to be used in the analysis.

For example, according to Figure 5.1, the user may select 100 milliseconds as the duration for the analysis.

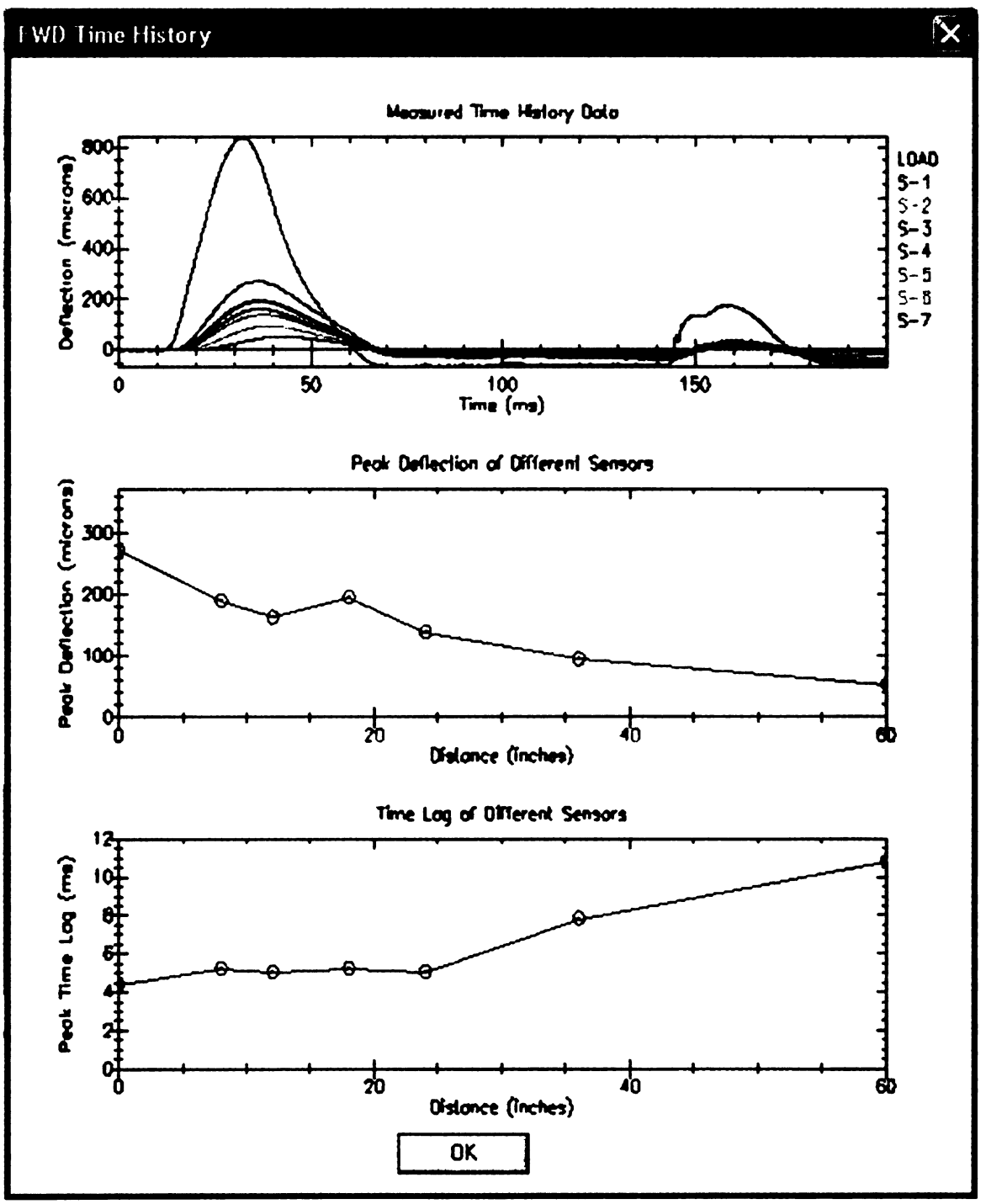

Figure 5.1 Typical plots for measured FWD load and deflection data

5.3.2 Data Analysis Options

DYNABACK allows for backcalculating layer parameters in either the frequency or time domain. The features highlighted in the previous section are designed to help the user decide on whether to use time-domain or frequency-domain solution. For example, if the deflection time histories are cutoff prematurely so that the free vibration response is not allowed to decay to zeros, the user may consider using the time-domain solution to avoid the problems associated with truncation for the frequency-domain solution. Conversely, if the curve of time lag versus sensor location is very irregular, then the user may want to try the frequency-domain solution. Furthermore, in the frequency-domain solution, the user can choose the frequencies at which the backcalculation is to be done. The results for the various frequencies are averaged by the program automatically. Naturally, the user may want to try both frequency and time domain solutions and compare the results from both analyses.

5.4 Presentation of Backcalculation Results

The backcalculated results are saved in a file, which can be printed, or can be viewed on the screen. In single frequency backcalculation, the results can be seen graphically to observe the variation of the backcalculation parameters with frequency. For cases where the backcalculated results have reached either the upper or lower bounds, as specified by the user, a warning message is posted in the output for the user to consider. The program also provides the measured and simulated deflections for a visual inspection of the match.

Typical results from frequency and time-domain backcalculation are shown in Figures 5.2 and 5.3, respectively.

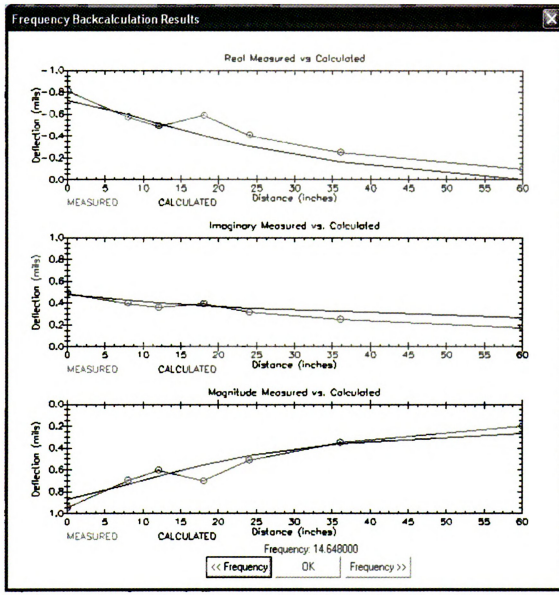

Figure 5.2 Typical output plots from frequency-domain backcalculation

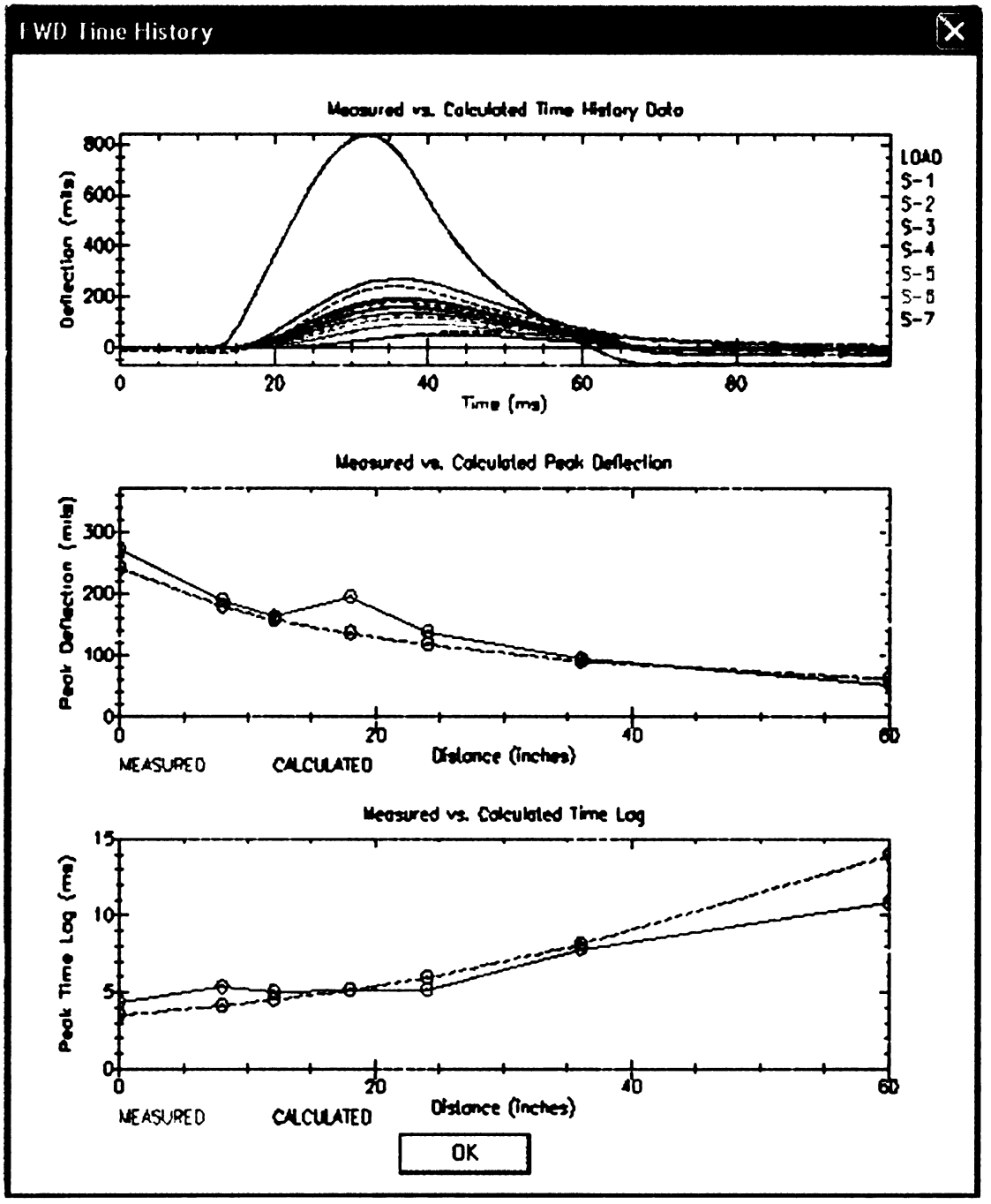

Figure 5.3 Typical output plots from time-domain backcalculation

5.5 Program Structure

The main flow chart of the program is presented in Figure 5.4. The program first reads the inventory data (layer thicknesses, assumed material properties, sensor configuration, etc.) and the load and deflection time histories. Seed values for the layer parameters that are to be backcalculated are also input at this point. The program also allows for the options of estimating the subgrade modulus and the depth-to-stiff layer (or ground water table). These values are obtained using the regression equations presented in Chapter 3. Once the input data are entered, the program allows the user to select the main backcalculation method; i.e., either frequency- or time-domain analysis. For each method, the user has the option to backcalculate layer thicknesses or to assume them to be fixed. If the layer thicknesses are fixed, the program will backcalculate the damping ratios for all layers; if layer thicknesses are backcalculated the program fixes the damping ratios of the unbound materials (which generally do not vary significantly) and allows for backcalculating only the damping ratios of the asphalt concrete layer. Once backcalculation is performed, the results can be viewed graphically and the results are saved in both summary and detailed formats in separate files which can be viewed or printed, as desired. The details of frequency- and time-domain backcalculation procedures are shown in Figure 5.5, Figure 5.6, and Figure 5.7, respectively.

In frequency-domain backcalculation (Figure 5.5) the load and deflection time histories are first corrected to the frequency domain using the FFT algorithm. The user selects the frequencies at which backcalculation is to be performed, and the program then calculates the steady-state (harmonic) response at these prescribed frequencies. For each frequency,

the program computes the gradient matrix according to the option chosen by the user (e.g., the matrix will be different depending on whether layer thicknesses are backcalculated or not). The program then revises the real moduli (Cases A and B), imaginary moduli of specified layers (all layers for Case A; AC layer only for Case B) and thickness (Case B). Then the program calculates the real and imaginary deflections as well as the corresponding RMS errors. The procedure is repeated until the convergence criteria are met or the maximum number of iterations is reached. Once the analysis is completed, the results can be plotted and printed in either a summary or detailed format.

In time-domain backcalculation (Figure 5.6 or Figure 5.7) the program first determines the peak deflections and corresponding time lags from the measured sensor records or traces of time histories. The user can view the frequency contents of the measured load and deflection, and select the frequencies at which the steady-state response is to be calculated for determining the transient response (to save on computational time, the forward solution allows for calculating the response at a limited number of frequencies and interpolating the response at the remaining frequencies). The program then calculated the transient deflections and determines the peak values and the corresponding time lags (or traces of time histories) from the calculated responses. Next, the program computes the gradient matrix according to the option chosen by the user (either with or without thickness backcalculation). The program then revises the real moduli for all layers (Cases C, D, E, and F), imaginary moduli of the specified layers (Case C and E) and layer thicknesses (Case D and F), and calculates the transient deflections as well as the corresponding peak values and time lags, together with their respective RMS errors. The procedure is repeated until the convergence criteria are met or the maximum number of

iterations is reached. Once the analysis is completed, the results can be plotted and printed in either a summary or detailed format.

5.6 Backcalculation of Layer Properties

For each method of analysis (i.e., frequency- and time-domain backcalculation) the backcalculation tasks performed by the program can be divided in to two major groups:

1. Backcalculation of all layer moduli and damping ratios without thickness backcalculation (Cases A, C, and D for frequency- and time-domain method, respectively)

2. Backcalculation of all layer moduli, AC damping ratio and layer thicknesses (Cases B, D , and F for frequency- and time-domain methods, respectively)

5.6.1 Cases A, C, and E

For these cases, layer thicknesses are fixed and the program backcalculates the moduli and damping ratios of all layers. The user may choose to use the estimated depth-to-stiff layer if the program detects the presence of a stiff layer from the free vibration response. In that case, the program will use the estimated depth-to-stiff layer.

5.6.2 Cases B, D, and F

For these cases, in addition to layer moduli, the layer thicknesses (including the depth-to-stiff layer) are allowed to be backcalculated. The program also allows for backcalculating the AC damping ratio; however the damping ratios of the remaining layer are fixed.

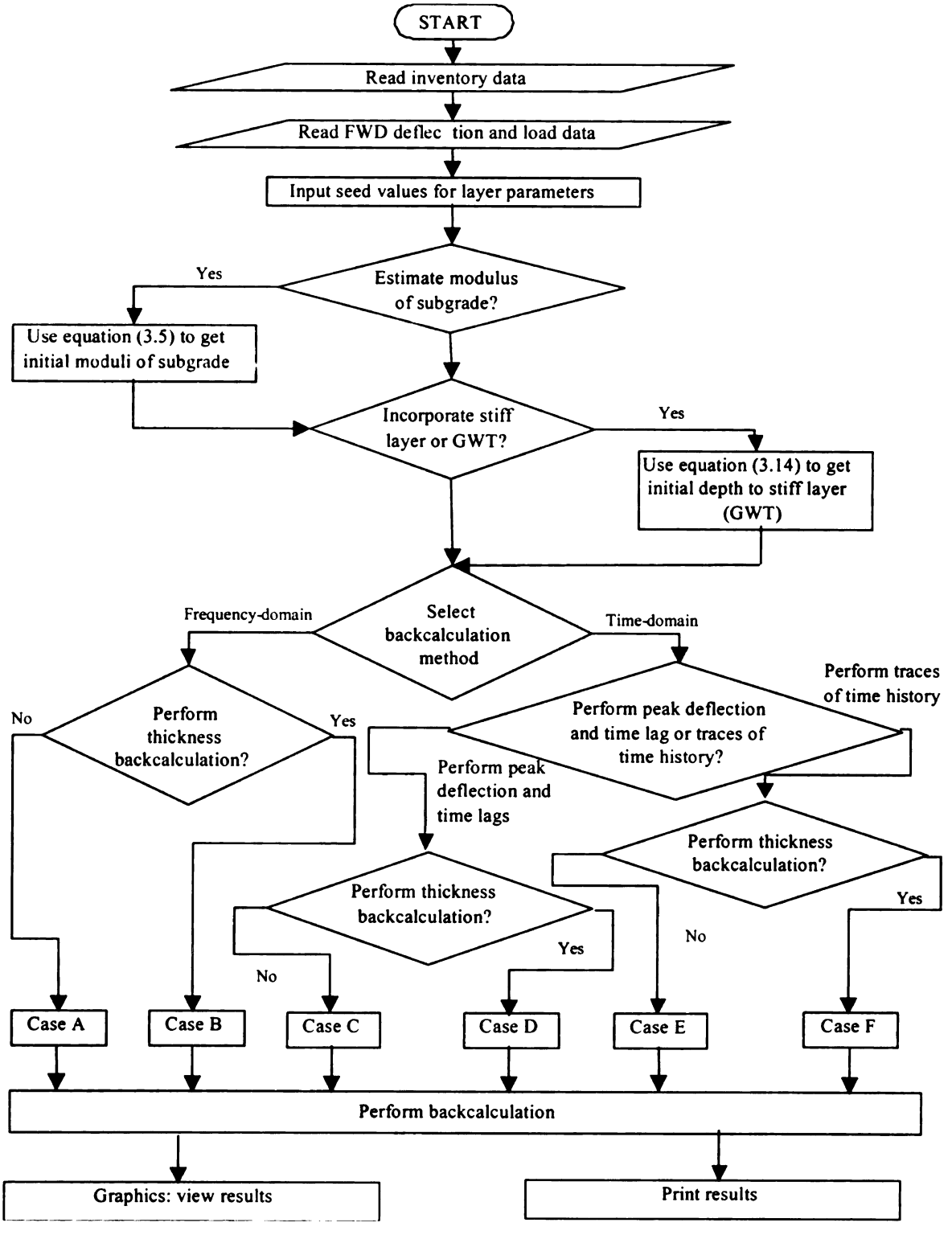

Figure 5.4 Main Flow chart for DYNABACK

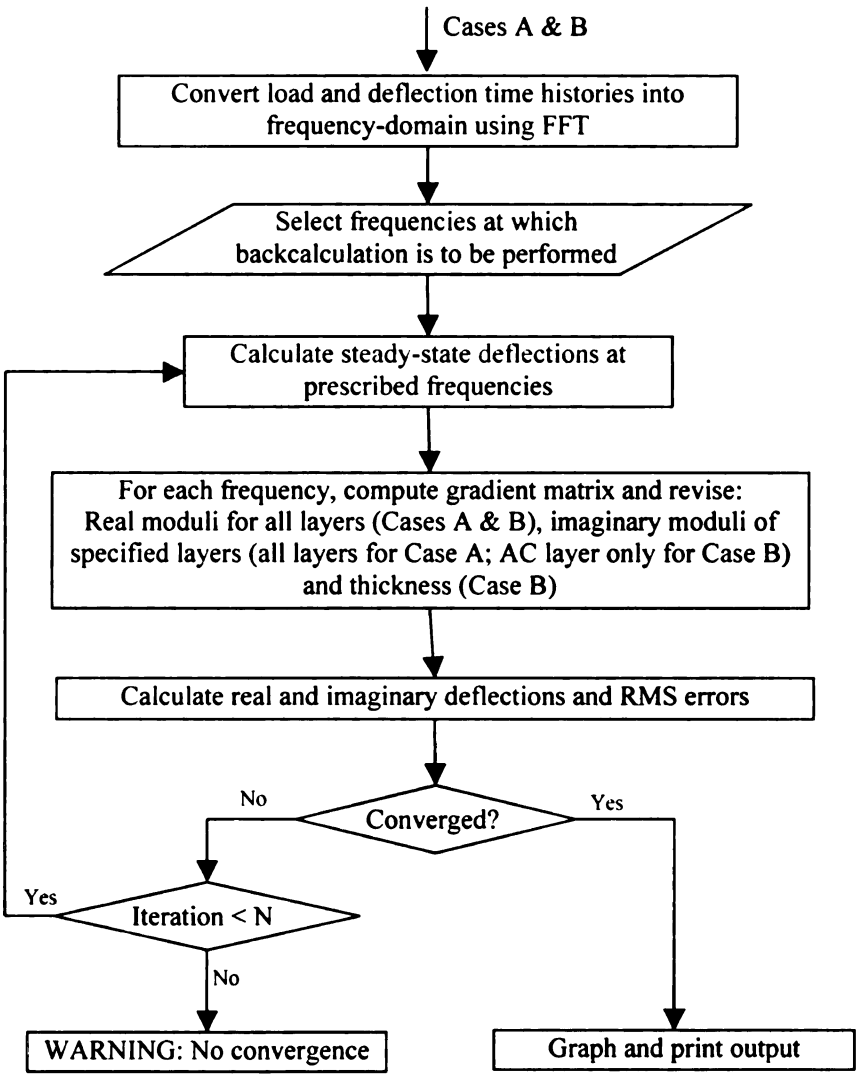

Figure 5.5 Details of frequency-domain backcalculation procedure (Cases A & B)

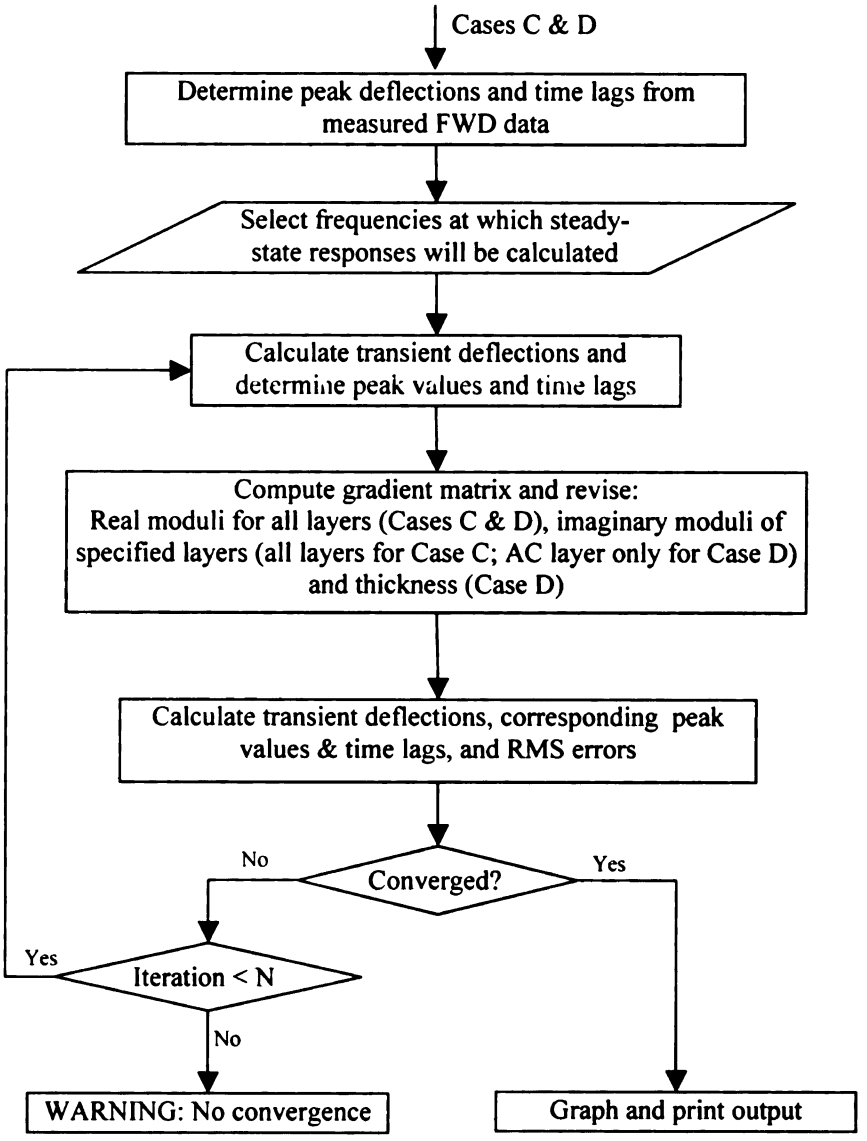

Figure 5.6 Details of time-domain backcalculation procedure using peak time and time lag (Cases C & D)

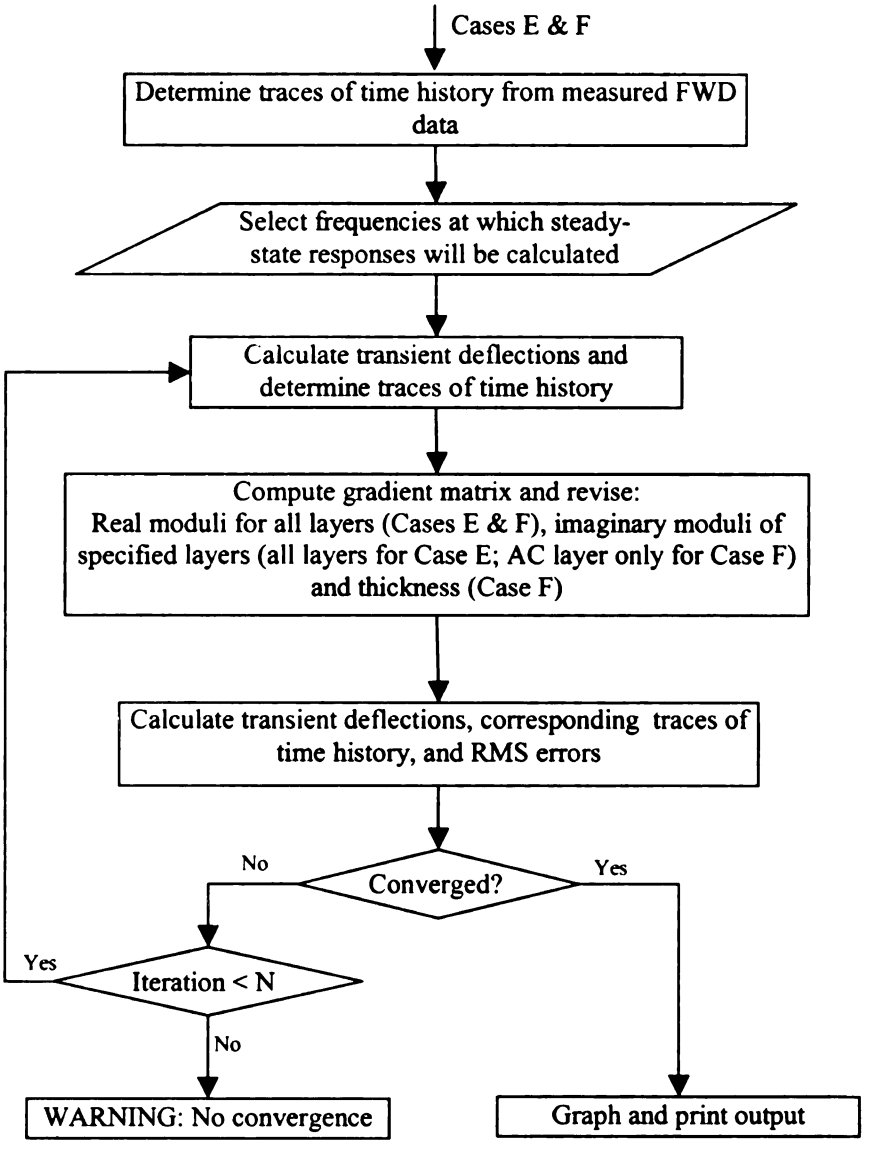

Figure 5.7 Details of time-domain backcalculation procedure using traces of time history (Cases E & F)

CHAPTER 6 - THEORETICAL VERIFICATION

6.1 Introduction

In this chapter, the theoretical aspects of the backcalculation program are validated using theoretical deflection basins generated by SAPSI. Numerical examples have been included to highlight various aspects of the program using both frequency and time-domain backcalculations, including the ability to backcalculate layer moduli and damping, layer thicknesses, the depth-to-stiff layer, as well as the possibility of backcalculating these parameters for profiles with different stiffness and thickness characteristics with a larger number of layers. In addition, the effects of deflection measurement accuracy and signal truncation in time on backcalculation results are investigated. Finally, convergence characteristics and the uniqueness of backcalculation results are investigated. Sensitivity analysis of the backcalculated results to the various layer parameters is conducted.

6.2 Theoretical Frequency-Domain Backcalculation using Steady-State Response

The usefulness and robustness of the new backcalculation solution was verified through a large number of backcalculation examples with theoretical deflection basins. It should be noted that this option is not currently available in the latest version of DYNABACK because of implementation problems with field data. The effects of layer thickness (i.e., thin/thick layers), layer stiffness (stiff/soft layer combinations), and multiple frequencies (low, medium, and high frequency combinations) were investigated. For each pavement section, layer thicknesses and properties were input into SAPSI and the theoretical

complex deflections at lateral distances of 0, 8, 12, 18, 24, 36, and 60 inches from the center of the loaded area were generated. The load magnitude was 10,000 lb, and a circular contact area was used with a radius of 5.91 inches.

6.2.1 Effect of Modulus, Thickness and Frequency Combinations

The purpose of this exercise is to insure that the backcalculation algorithm works for a variety of profiles and frequency combinations. Nine different profiles and twenty-seven frequency combinations were used, for a total of 243 runs. The list of frequency combinations is presented in Table 6.1. The profiles used and the backcalculation results are shown in Table 6.2. The errors in backcalculated results are summarized in Figure 6.1 through Figure 6.9. The results indicate excellent agreement between backcalculated and actual parameters for more than 90 percent of the cases.

Table 6.1 List of frequency combinations

Frequency Combination	Low	Medium	High	Frequency Combination	Low	Medium	High
1	0.63	6.34	15.85	15	2.53	10.14	25.36
2	0.63	6.34	20.29	16	2.53	13.95	15.85
3	0.63	6.34	25.36	17	2.53	13.95	20.29
4	0.63	10.14	15.85	18	2.53	13.95	25.36
5	0.63	10.14	20.29	19	3.8	6.34	15.85
6	0.63	10.14	25.36	20	3.8	6.34	20.29
7	0.63	13.95	15.85	21	3.8	6.34	25.36
8	0.63	13.95	20.29	22	3.8	10.14	15.85
9	0.63	13.95	25.36	23	3.8	10.14	20.29
10	2.53	6.34	15.85	24	3.8	10.14	25.36
11	2.53	6.34	20.29	25	3.8	13.95	15.85
12	2.53	6.34	25.36	26	3.8	13.95	20.29
13	2.53	10.14	15.85	27	3.8	13.95	25.36
14	2.53	10.14	20.29				

Table 6.2 Profiles used

Profile No.	Layer	Thickness (in)	Damping Ratio	Modulus (ksi)
1	AC	3	0.08	250
	Base	12	0.03	30
	Subbase	12	0.03	15
	Subgrade	∞	0.02	10
2	AC	3	0.08	250
	Base	6	0.03	30
	Subbase	24	0.03	15
	Subgrade	∞	0.02	5
3	AC	6	0.08	500
	Base	6	0.03	30
	Subbase	24	0.03	15
	Subgrade	∞	0.02	5
4	AC	6	0.08	500
	Base	6	0.03	50
	Subbase	12	0.03	15
	Subgrade	∞	0.02	10
5	AC	6	0.08	500
	Base	12	0.03	30
	Subbase	12	0.03	15
	Subgrade	∞	0.02	5
6	AC	6	0.08	500
	Base	12	0.03	30
	Subbase	12	0.03	15
	Subgrade	∞	0.02	10
7	AC	6	0.08	500
	Base	12	0.03	30
	Subbase	12	0.03	15
	Subgrade	∞	0.02	15
8	AC	9	0.08	750
	Base	6	0.03	30
	Subbase	12	0.03	15
	Subgrade	∞	0.02	5
9	AC	9	0.08	1000
	Base	6	0.03	30
	Subbase	12	0.03	15
	Subgrade	∞	0.02	5

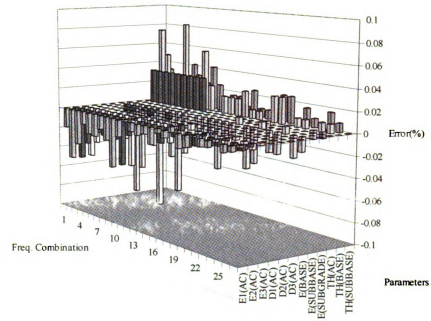

Figure 6.1 Percent error in backcalculated results – profile 1

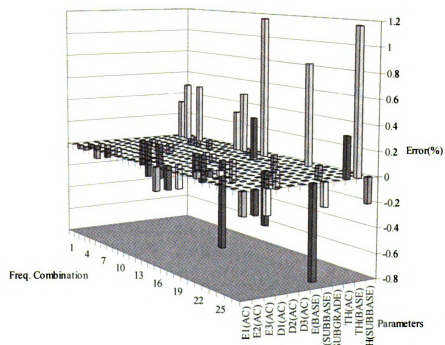

Figure 6.2 Percent error in backcalculated results – profile 2

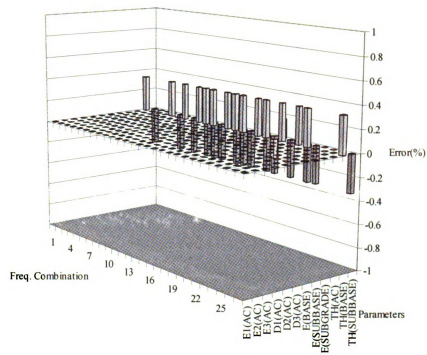

Figure 6.3 Percent error in backcalculated results – profile 3

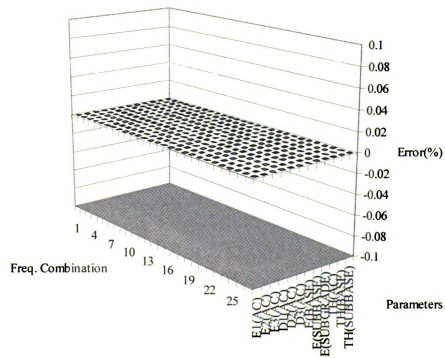

Figure 6.4 Percent error in backcalculated results – profile 4

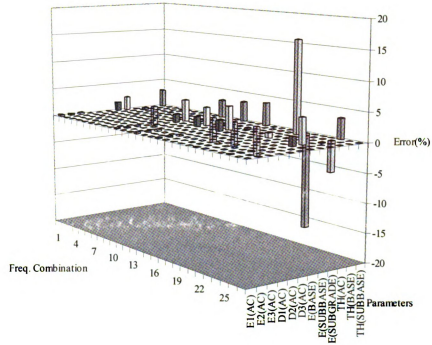

Figure 6.5 Percent error in backcalculated results – profile 5

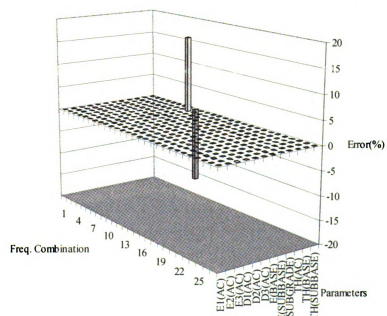

Figure 6.6 Percent error in backcalculated results – profile 6

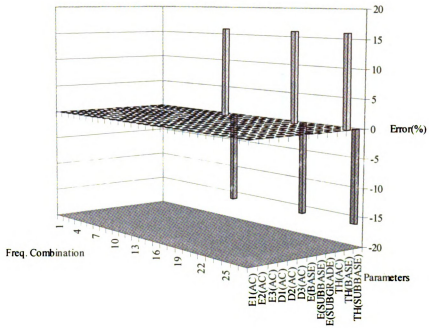

Figure 6.7 Percent error in backcalculated results – profile 7

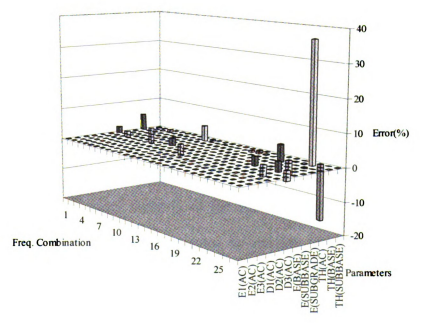

Figure 6.8 Percent error in backcalculated results – profile 8

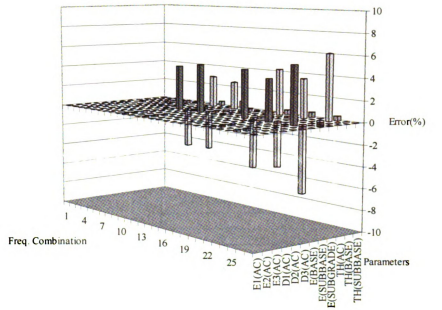

Figure 6.9 Percent error in backcalculated results – profile 9

6.2.2 Effect of Sub-Layering on Backcalculation Results

SAPSI uses the finite layer method to calculate pavement response. It models the pavement system using the finite element method with each layer representing an element of finite thickness in the vertical direction and infinite extent in the horizontal direction. Each pavement layer must be subdivided into several sublayers to insure accuracy of the results. Therefore its accuracy depends on the sublayer thicknesses. The effect of the fineness in the sub-layering was investigated by running the backcalculation program using coarse and fine sublayers. Table 6.3 and Table 6.4 show the coarse and fine layered profiles, respectively. The analysis was performed on profile 5, with the frequency combination of 3.8, 6.3, and 25.4 Hz.

Table 6.5 shows the results from the coarse and fine layers, respectively. It can be seen that the relative error is high when the coarse layers are used. Using the finer layers improved the solution significantly.

Table 6.3 Profile with coarse sub-layering

Pavement Layer	Sublayer Number	Thickness (in)
AC	1	0.25
	2	0.25
	3	0.5
	4	1.0
	5	2.0
	6	2.0
Base	7	4.0
	8	8.0
Subbase	9	12.0
Subgrade	10	12.0

Table 6.4 Profile with fine sub-layering

Pavement Layer	Sublayer Number	Thickness (in)
AC	1	0.25
	2	0.25
	3	0.312
	4	0.391
	5	0.488
	6	0.610
	7	0.763
	8	0.789
	9	0.954
	10	1.19
Base	11	1.49
	12	1.86
	13	2.33
	14	2.91
	15	3.41
Subbase	16	4.26
	17	7.74
Subgrade	18	12.0

Table 6.5 Backcalculation results using coarse sub-layering

Layer Name	True value			Backcalculated Parameters					
				Coarse Sublayering			Fine Sublayering		
	Modulus (ksi) Damping	Ratio Thickness	(in)	Modulus (psi)	Damping Ratio	Thickness (in)	Modulus (psi)	Damping Ratio	Thickness (in)
AC (2Hz)	500	0.08		500261	0.08		500023	0.08	
AC(12Hz)	500	0.08	6	500246	0.08	6.00	500045	0.08	6.00
AC(24Hz)	500	0.08		500316	0.08		500036	0.08	
Base	30	0.03	12	29983	---	13.92	29994	---	12.04
Subbase	15	0.02	12	15125	---	10.03	14980	---	11.93
Subgrade	5	0.02	∞	4999	---	---	5001	---	---

6.2.3 Dynamic Backcalculation of Additional Layers

The program has been expanded to backcalculate the complex moduli and thicknesses for pavement systems with up to six layers and four frequencies. For 5- and 6-layer systems, the backcalculation has to be done at four frequencies. The results for 5-layer and 6-layer systems are shown in Table 6.6 and Table 6.7, respectively. The results indicate that the program is able to backcalculate layer parameters of pavements with up to six layers.

Table 6.6 Theoretical backcalculation of a five-layer pavement system

Layer Name	True value			Backcalculated Parameters		
	Modulus (psi)	Damping Ratio	Thickness (in)	Modulus (psi)	Damping Ratio	Thickness (in)
AC(2Hz)	500000	0.05		500000	0.05	
AC(12Hz)	500000	0.05	6	500000	0.05	6
AC(22Hz)	500000	0.05		500000	0.05	
AC(28Hz)	500000	0.05		500000	0.05	
Base 1	25000	0.03	10	25000	---	10
Base 2	20000	0.03	10	20000	---	9.999
Subbase 1	17000		12	17000		12.001
Subgrade	15000	0.02		15000	---	---

Table 6.7 Theoretical backcalculation of a six-layer pavement system

Layer Name	True value			Backcalculated Parameters		
	Modulus (psi)	Damping Ratio	Thickness (in)	Modulus (psi)	Damping Ratio	Thickness (in)
AC(2Hz)	500000	0.05		500000	0.05	
AC(12Hz)	500000	0.05		500000	0.05	
AC(22Hz)	500000	0.05	6	500000	0.05	6
AC(28Hz)	500000	0.05		500000	0.05	
Base 1	25000	0.03	10	25000	---	10
Base 2	20000	0.03	10	20000	---	10
Subbase 1	17000		12	17000		12.037
Subbase 2	16000	0.03	12	16000	---	11.963
Subgrade	15000	0.02		15000	---	---

6.2.4 Backcalculation of the Depth-to-Stiff Layer (DSL)

In a layered pavement system, the stiff layer can be incorporated by assigning a high modulus to the bottom layer. However, the depth to this layer may or may not be known. Previous work by Roesset (1995) presented a set of regression equations to estimate the depth-to-stiff layer for different conditions (saturated subgrade, unsaturated subgrade, etc.). However, the estimation of depth-to-stiff layer based solely on regression equations can give rise to significant errors in the backcalculated moduli. Therefore, it is necessary to develop an iterative process to improve the estimation. The iterative process for estimating the depth-to-stiff layer in the new program is similar to that of backcalculating the layer thickness. Also, when the modulus of the bedrock is greater than 500,000 psi, it becomes very difficult for the backcalculation routine to identify the modulus. This difficulty arises because the deflection basin is not sensitive to the modulus of the stiff layer beyond this value. Consequently, for the case of a pavement profile with stiff layer, the stiff layer modulus is fixed at 1,000,000 psi. An example illustrating the ability of the backcalculation program to backcalculate the depth-to-stiff layer using the main routine for modulus and thickness backcalculation is presented herein.

Table 6.8 through Table 6.10 show the results of backcalculation with three different DSL values (10, 20 and 30 ft). The asphalt properties were assumed as frequency independent, as shown in the table. The results show that the program backcalculates the DSL very accurately. Note that these results are based on the steady-state solution in SAPSI.

Table 6.8 Comparison of theoretical and backcalculated layer parameters – DSL=10 ft

Layer Name	True value			Backcalculated Results		
	Modulus (psi)	Damping Ratio	Thickness (in)	Modulus (psi)	Damping Ratio	Thickness (in)
AC(3.8 Hz)	500000	0.05		500001	0.05	
AC(7.6 Hz)	500000	0.05	6	500001	0.05	6
AC(12.0 Hz)	500000	0.05		500001	0.05	
Base	35000	0.03	10	35000	---	10
Subgrade	15000	0.02	120	15000	---	120
Bedrock	100000	0.05	∞	---	---	---

Table 6.9 Comparison of theoretical and backcalculated layer parameters – DSL=20 ft

Layer Name	True value			Backcalculated Results		
	Modulus (psi)	Damping Ratio	Thickness (in)	Modulus (psi)	Damping Ratio	Thickness (in)
AC(3.8 Hz)	500000	0.05		500007	0.05	
AC(7.6 Hz)	500000	0.05	6	500007	0.05	6
AC(12.0 Hz)	500000	0.05		500007	0.05	
Base	35000	0.03	10	35000	---	10
Subgrade	15000	0.02	240	15000	---	240
Bedrock	100000	0.05	∞	---	---	---

Table 6.10 Comparison of theoretical and backcalculated layer parameters – DSL=30 ft

Layer Name	True value			Backcalculated Results		
	Modulus (psi)	Damping Ratio	Thickness (in)	Modulus (psi)	Damping Ratio	Thickness (in)
AC(3.8 Hz)	500000	0.05		500000	0.05	
AC(7.6 Hz)	500000	0.05	6	500000	0.05	6
AC(12.0 Hz)	500000	0.05		500000	0.05	
Base	35000	0.03	10	35000	---	10
Subgrade	15000	0.02	360	15000	---	360
Bedrock	100000	0.05	∞	---	---	---

6.3 Theoretical Frequency-Domain Backcalculation using Transient Response

The preceding sections dealt with backcalculation results using steady-state (harmonic) deflection basins at different frequencies. In this section, transient deflection time histories were generated artificially using SAPSI. The backcalculation program converts these time histories into the frequency-domain, then backcalculates the layer parameters at different frequencies. The results presented herein are based on backcalculation at either a single frequency or multiple frequencies. However, note that the backcalculation at multiple frequencies is not implemented in the software.

6.3.1 Comparison of Single and Multiple Frequency Backcalculation Results

The results using single and multiple frequency backcalculation are shown in Figure 6.10 through Figure 6.15 for the AC modulus, damping ratio and thickness, base modulus and thickness, and subgrade modulus, respectively.

Examination of the results indicates that both single frequency and multiple frequency backcalculation algorithms produce very good results, including backcalculation of layer thicknesses. One exception is when the base thickness is backcalculated using the

combination of frequencies (19.5, 22 and 24.4 Hz). This implies that single frequency backcalculation can produce similar results to those from multiple frequency backcalculation when the number of pavement layers is limited to three.

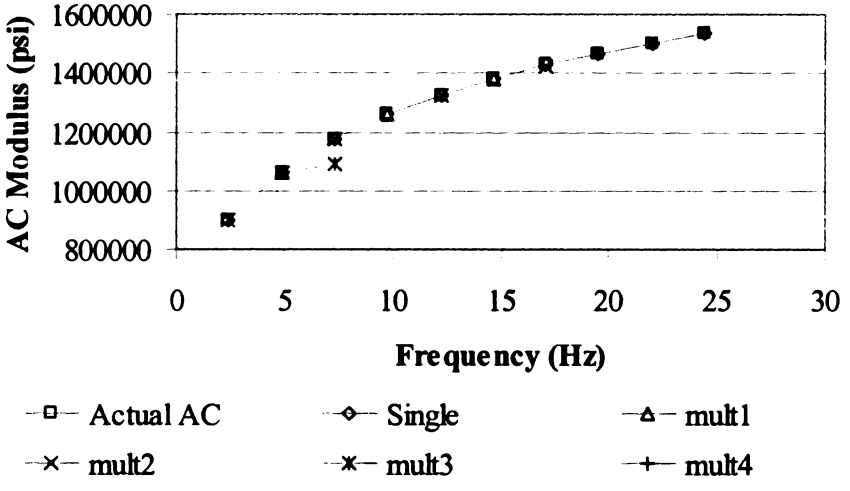

Figure 6.10 Comparison of AC modulus using single and multiple frequency backcalculation

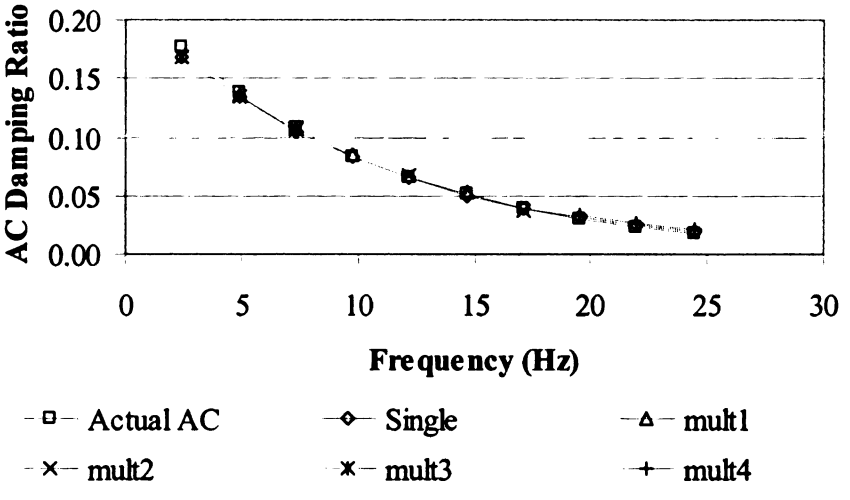

Figure 6.11 Comparison of AC damping ratio using single and multiple frequency backcalculation

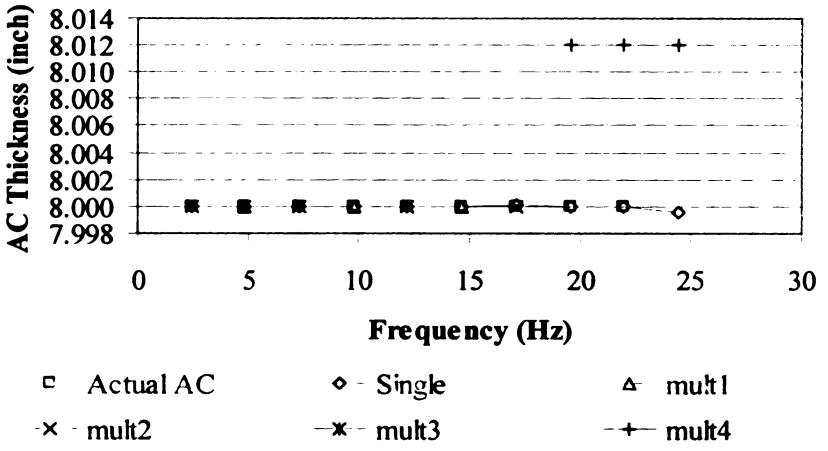

Figure 6.12 Comparison of AC thickness using single and multiple frequency backcalculation

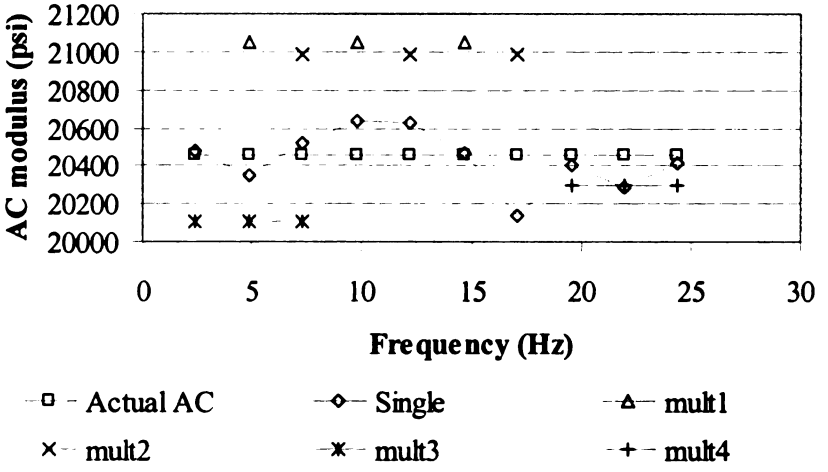

Figure 6.13 Comparison of base modulus using single and multiple frequency backcalculation

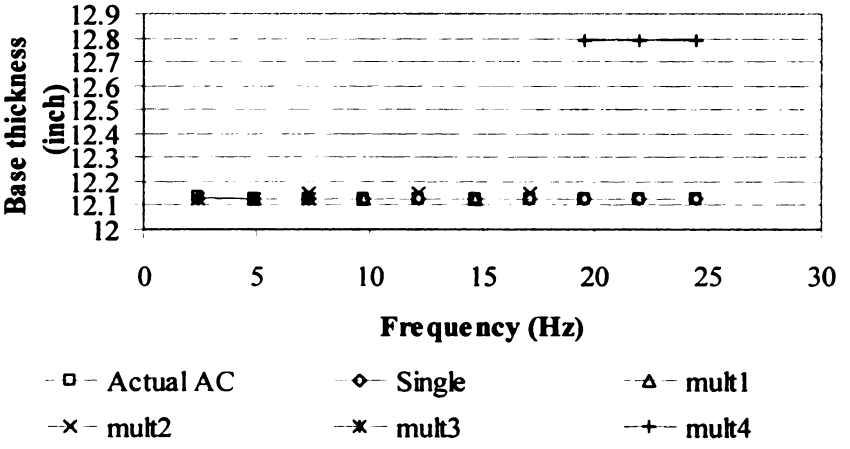

Figure 6.14 Comparison of base thickness using single and multiple frequency backcalculation

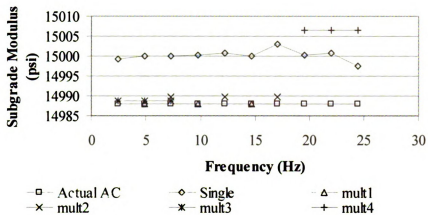

Figure 6.15 Comparison of subgrade modulus using single and multiple frequency backcalculation

6.3.2 Backcalculation of Damping Ratio for Unbound Layers

In this section, the program capability to backcalculate the damping ratios of the unbound pavement layers (in addition to the AC layer) is investigated. Figure 6.16 through Figure 6.21 show backcalculated results for the modulus and damping ratio of the AC, base and subgrade layers, respectively, using single frequency backcalculation with known layer thicknesses. The backcalculated values show very good agreement with the actual values.

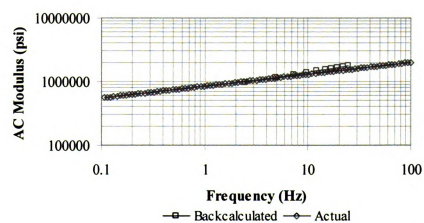

Figure 6.16 Comparison of backcalculated and actual AC modulus without thickness backcalculation

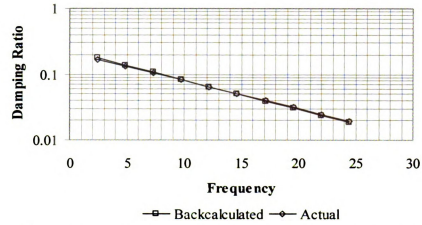

Figure 6.17 Comparison of backcalculated and actual AC damping ratios without thickness backcalculation

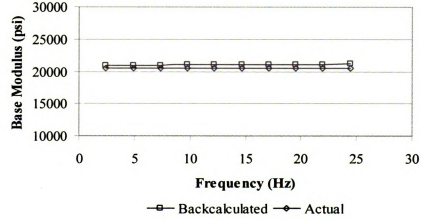

Figure 6.18 Comparison of backcalculated and actual base modulus without thickness backcalculation

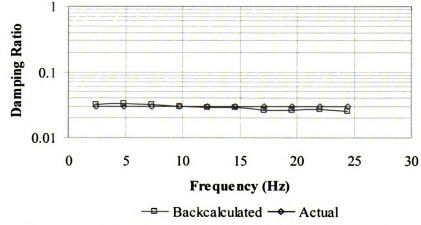

Figure 6.19 Comparison of backcalculated and actual base damping ratios without thickness backcalculation

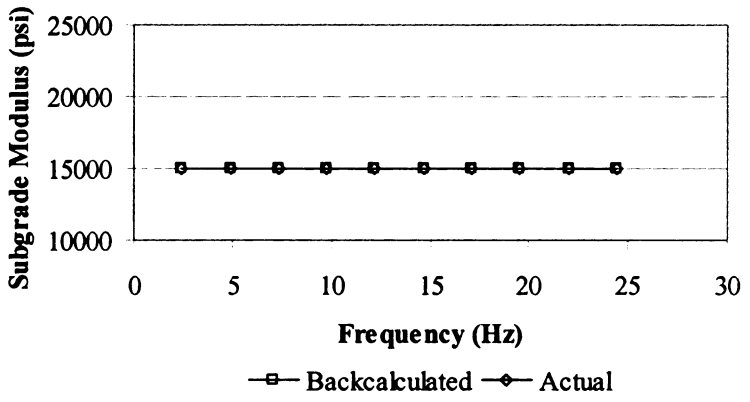

Figure 6.20 Comparison of backcalculated and actual subgrade modulus without thickness backcalculation

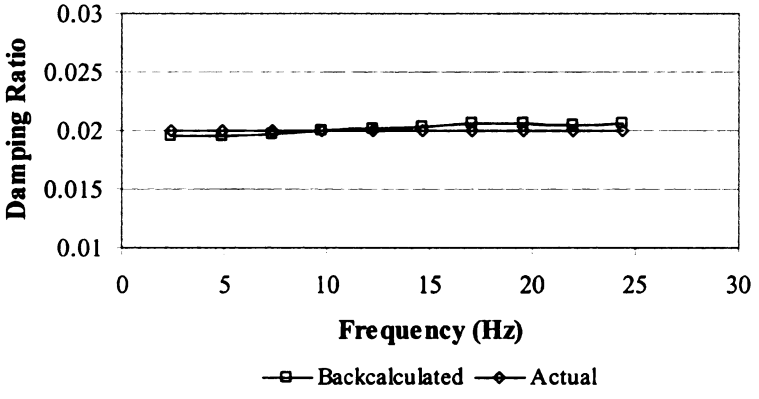

Figure 6.21 Comparison of backcalculated and actual subgrade damping ratios without thickness backcalculation

6.3.3 Uniqueness of Backcalculated Results

Many backcalculation programs suffer from the disadvantage that the backcalculated results are highly dependent on the seed modulus values provided by the user. The farther the guess is from the true values, the higher are the chances of converging to a wrong solution. The convergence of Newton's method is, in general, problem dependent. However, backcalculation of layer properties from FWD deflection data appears to be a well behaved problem (Mahmood, 1993). For static backcalculation of flexible

pavements, the results obtained using Newton's method seem to be independent of the starting value (Mahmood, 1993). In the following subsections, the sensitivity of the backcalculated results obtained by the frequency-domain solution to the seed values is investigated. The effect of layer thickness and moduli as well as the number of pavement layers on the uniqueness of backcalculation results are also considered.

6.3.3.1 Profiles with Different AC Layer Moduli

The uniqueness of backcalculation results are considered for pavement profiles with different AC layer moduli. The properties of the three layer flexible pavements used in the analysis are listed in Table 6.11. The seed moduli values are listed in Table 6.12. The results are shown in Figure 6.22 through Figure. The Figures show that the results are generally good for all three cases, although they tend to be slightly better at lower frequencies. Also, the results from the frequency-domain solution are not affected by the seed moduli. The only difference is in the number of iterations required to meet the given convergence criteria.

Table 6.11 Profiles used for verifying uniqueness of solution (varying layer moduli)

Layer Name	Actual Modulus (ksi)						Thickness (inch)
	Low		Medium		High		
	E1	E2	E1	E2	E1	E2	
AC	300	30	500	50	800	80	9
Base	45	2.70	75	4.5	45	2.7	8
Subgrade	7.5	0.30	15	0.6	7.5	0.3	∞

Table 6.12 Seed modulus values used for verifying uniqueness of solution with three-layer pavement system

Case number	AC		base		Subgrade	
	E1(ksi)	E2(ksi)	E1(ksi)	E2(ksi)	E1(ksi)	E2(ksi)
Case 1	1000	100	1000	100	1000	100
Case 2	1	0.1	1	0.06	1	0.04

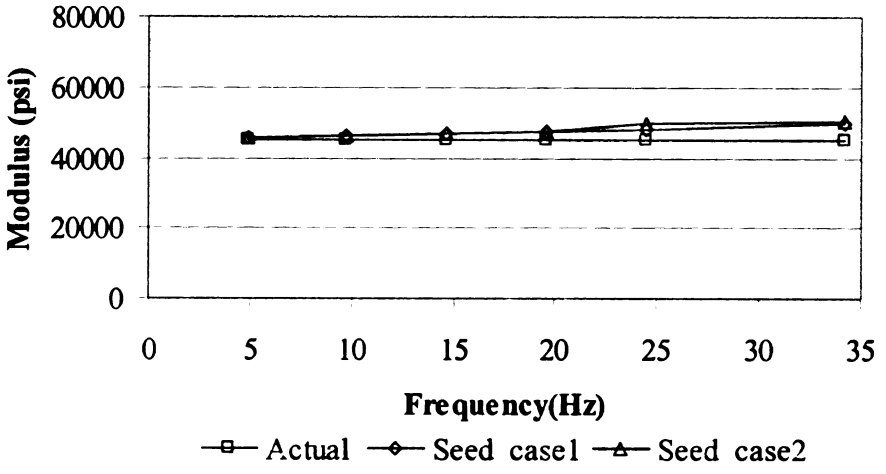

(a) AC

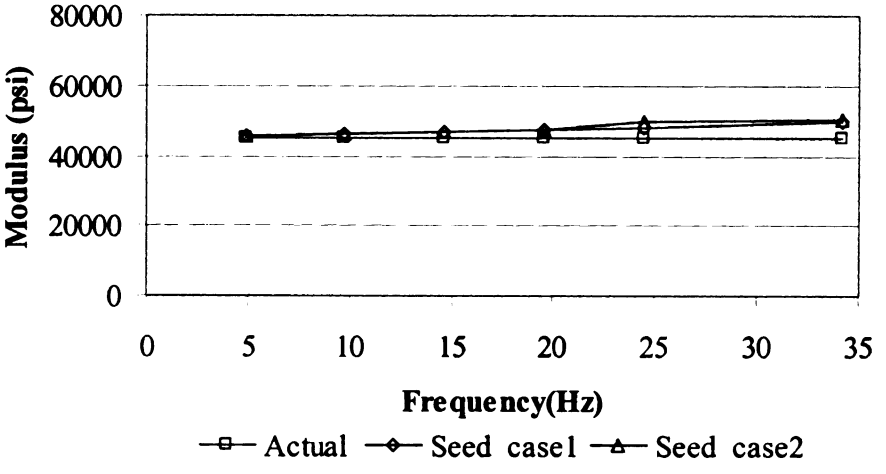

(b) Base

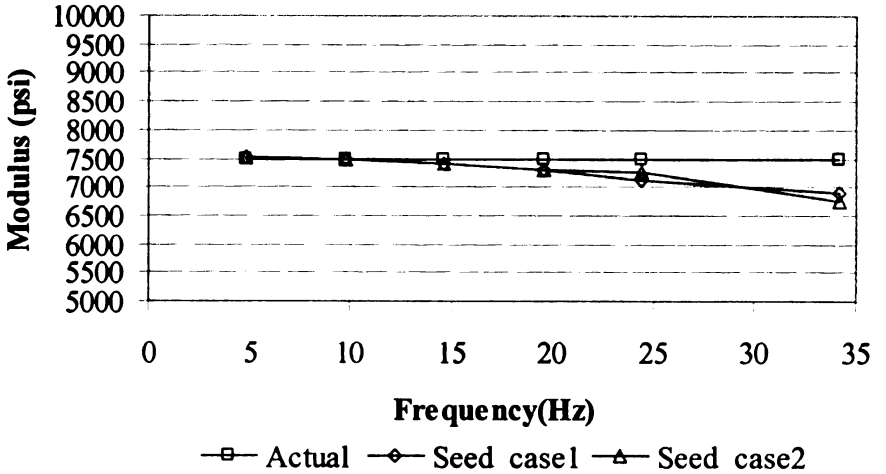

(c) Subgrade

Figure 6.22 Effect of seed moduli on backcalculation results - low AC modulus

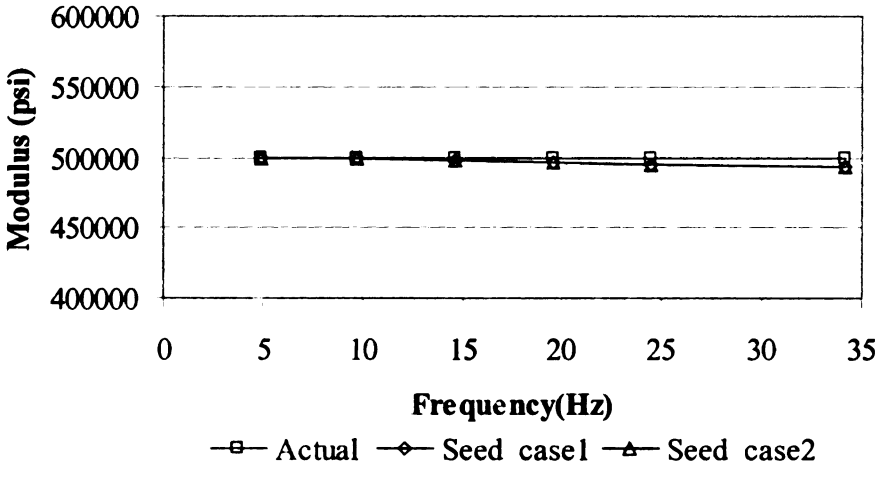

(a) AC

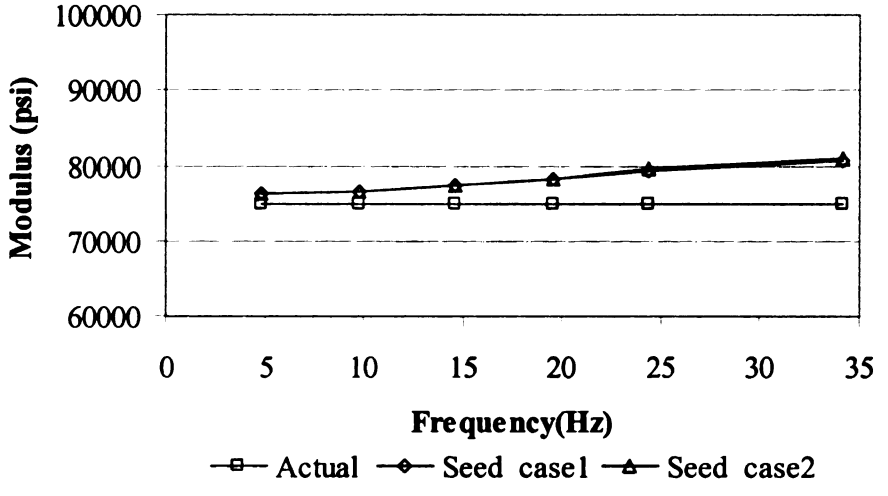

(b) Base

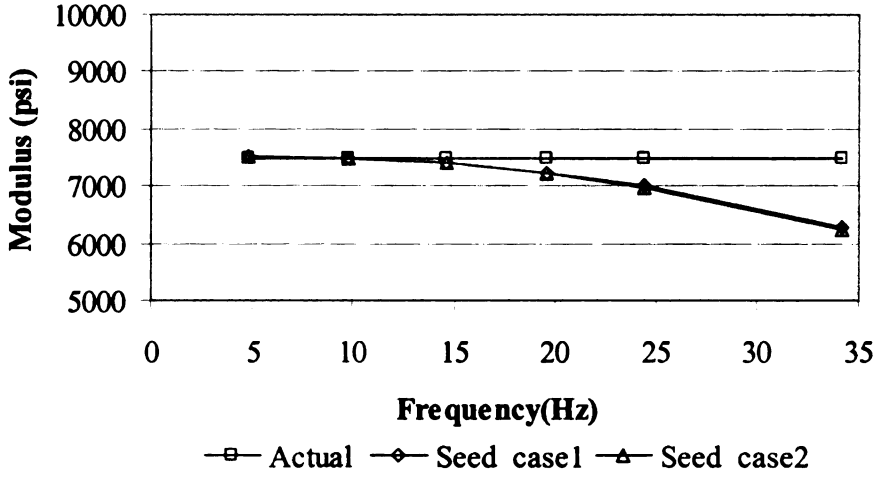

(c) Subgrade

Figure 6.23 Effect of seed moduli on backcalculation results - medium AC modulus

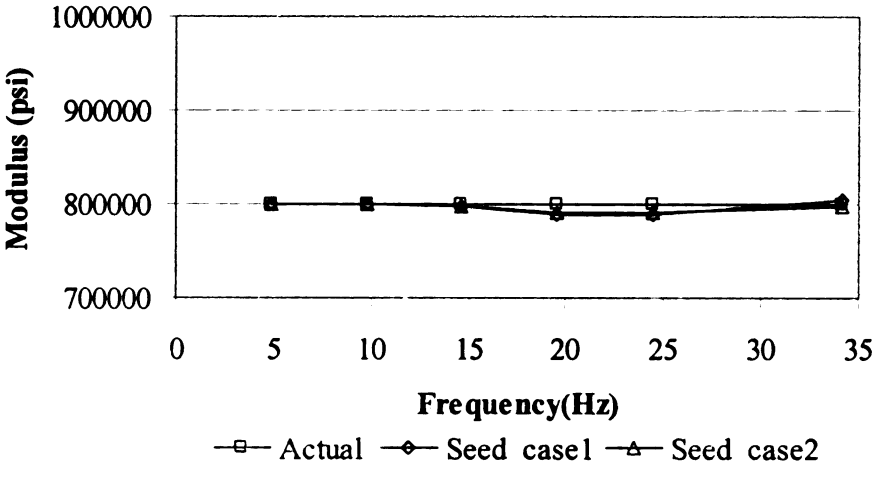

(a) AC

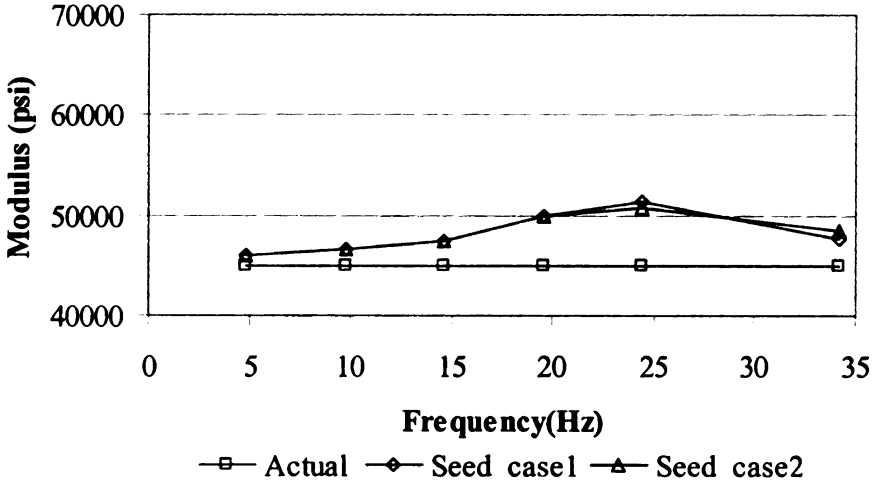

(b) Base

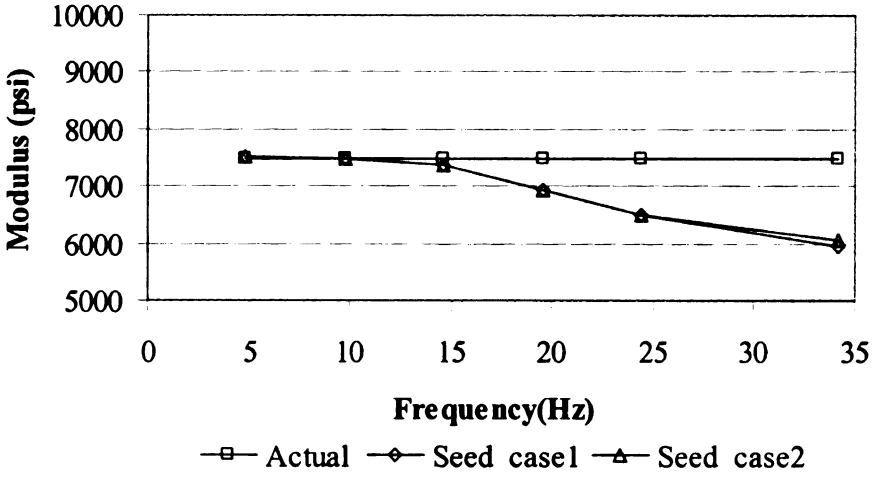

(c) Subgrade

Figure 6.24 Effect of seed moduli on backcalculation results - high AC modulus

6.3.3.2 Profiles with Different AC Layer Thicknesses

The uniqueness of the solution was investigated for pavement profiles with different AC layer thicknesses. The properties of the three layer flexible pavements used in the analysis are listed in Table 6.13. The same seed moduli values that were listed in Table 6.12 above were used. The results are shown in Figure 6.25 through Figure 6.27. The Figures show that the results are generally good for all three cases, although they tend to be slightly better at the lower frequencies. Again, the results from the frequency-domain solution are not affected by the seed moduli. The only difference is in the number of iterations required to meet the given convergence criteria.

Table 6.13 Profiles used for verifying uniqueness of solution
(varying AC layer thickness)

Layer name	Modulus (ksi)		Thickness (in)		
	E1	E2	Thin	Medium	Thick
AC	600	30	5	9	14
Base	45	2.7	8		
Subgrade	7.5	0.3	∞		

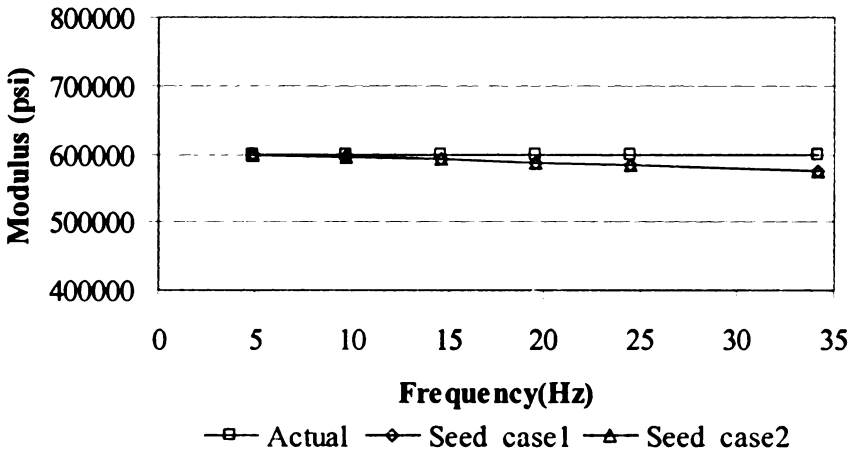

(a) AC

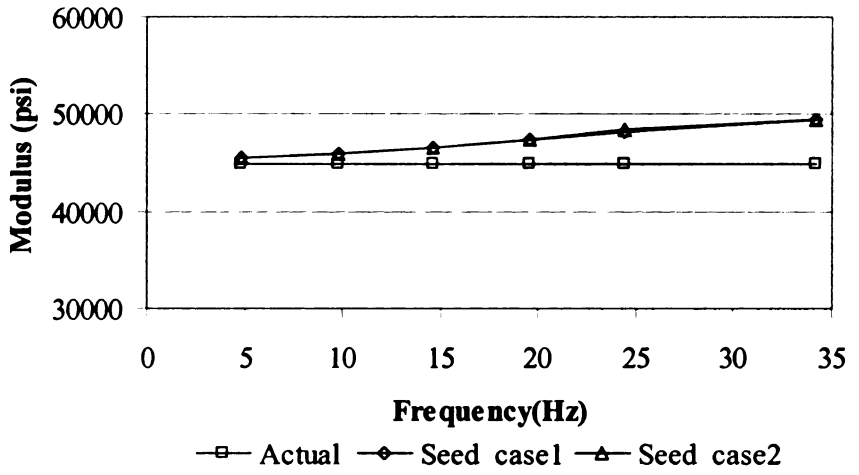

(b) Base

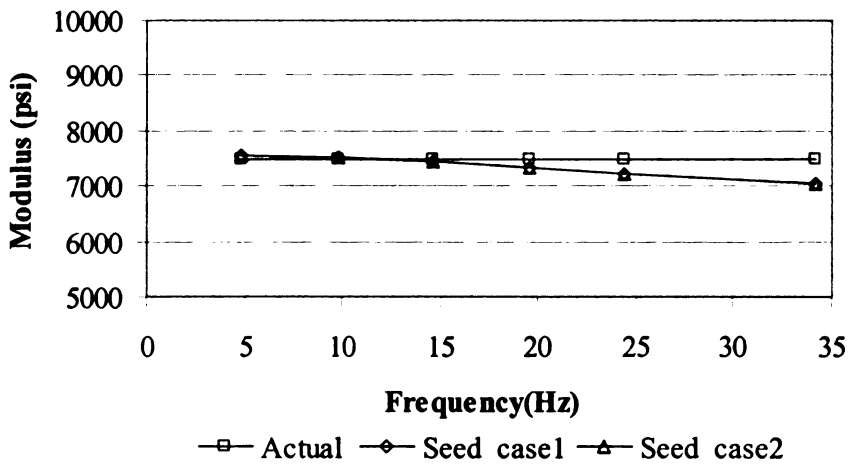

(c) Subgrade

Figure 6.25 Effect of seed moduli on backcalculation results –thin AC layer

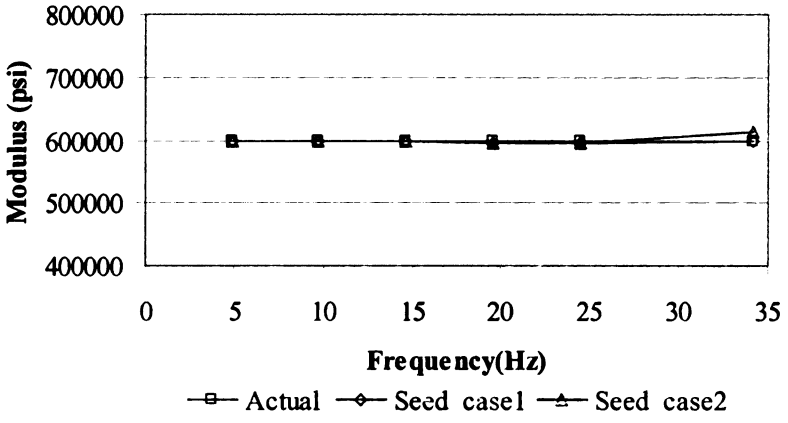

(a) AC

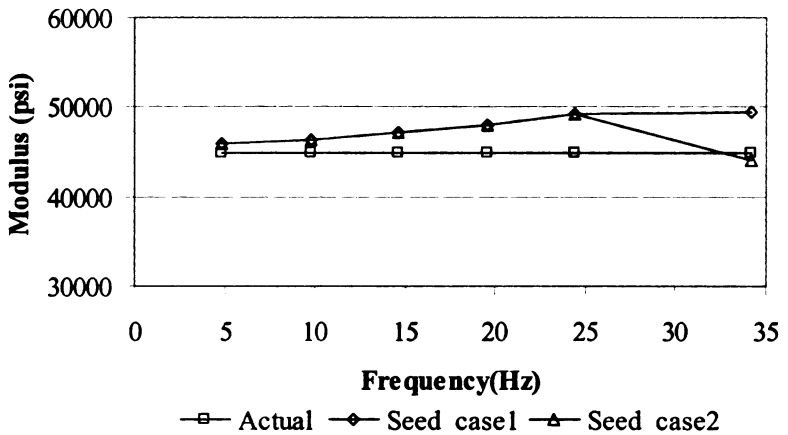

(b) Base

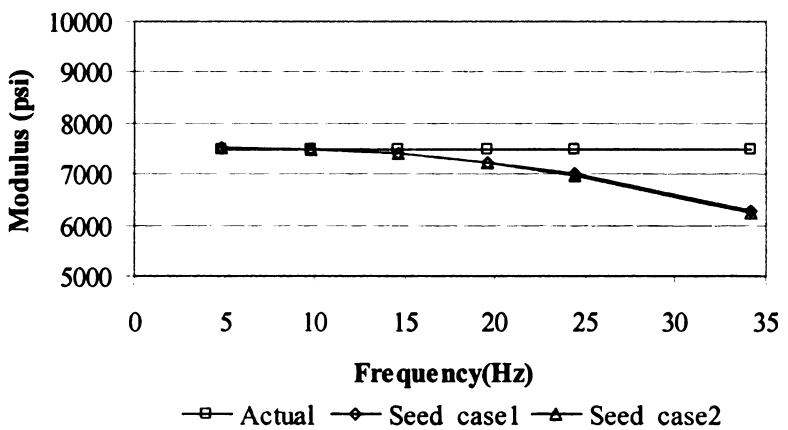

(c) Subgrade

Figure 6.26 Effect of seed moduli on backcalculation results –medium thick AC layer

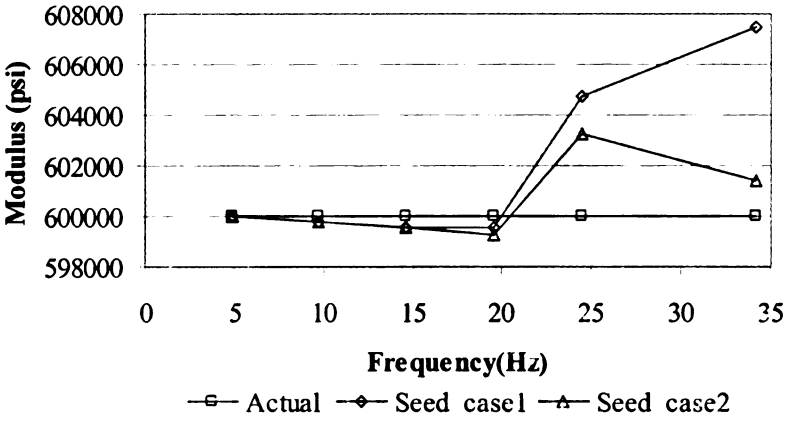

(a) AC

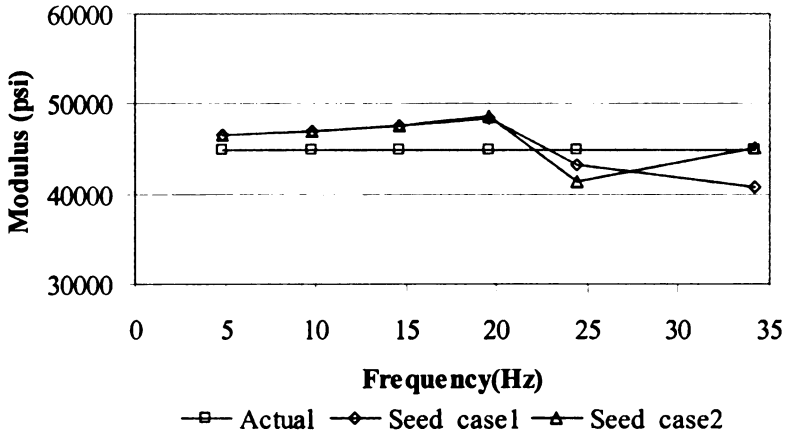

(b) Base

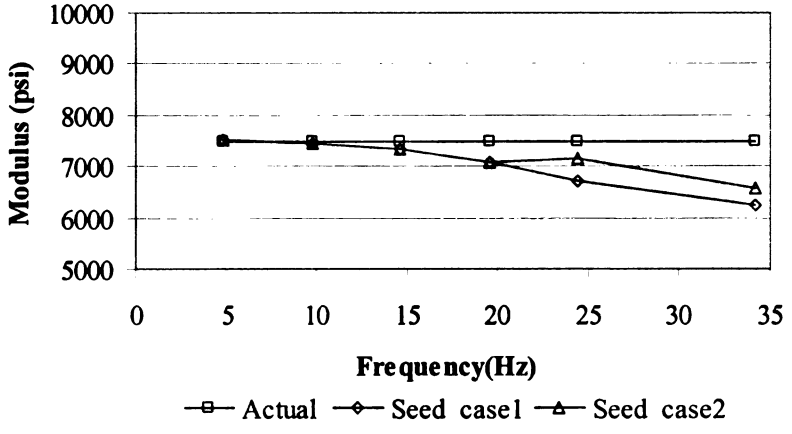

(c) Subgrade

Figure 6.27 Effect of seed moduli on backcalculation results –thick AC layer

6.3.3.3 Four-Layer Pavement Profile

A four layer pavement system was analyzed, for the cases of medium stiff and stiff AC moduli. The properties of the four layer flexible pavements used in the analysis are listed in Table 6.14. The seed moduli values are listed in Table 6.15. The results are shown in Figure 6.28 and Figure 6.29. The Figures show that, for both cases, the results are generally good and are not affected by seed moduli at frequencies below 25 Hz. The solution diverges at higher frequencies.

Table 6.14 Four-layer profile used for verifying uniqueness of solution

Layer name	Modulus (ksi)				Thickness (in)
	Medium-high		High		
	E1	E2	E1	E2	
AC	500	50	800	80	9
Base	45	2.7	75	4.5	8
Subbase	15	0.9	25	1.5	8
Subgrade	7.5	0.3	15	0.6	∞

Table 6.15 Seed modulus values for verifying uniqueness of solution with four-layer pavement system

Case number	AC		Base		Subbase		Subgrade	
	E1(ksi)	E2(ksi)	E1(ksi)	E2(ksi)	E1(ksi)	E2(ksi)	E1(ksi)	E2(ksi)
Case 1	1000	100	1000	100	1000	100	1000	100
Case 2	1	0.1	1	0.06	1	0.06	1	0.04

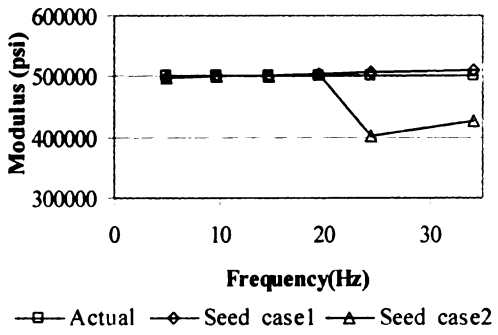

(a) AC

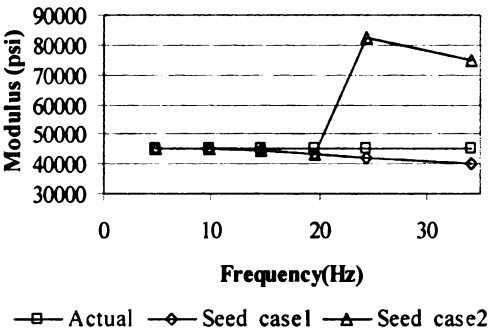

(b) Base

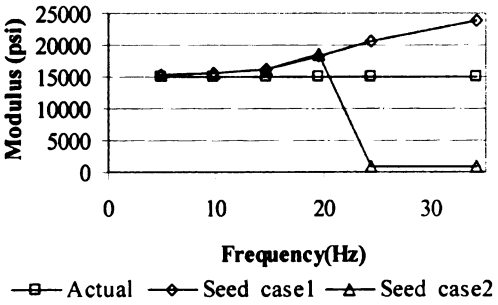

(c) Subbase

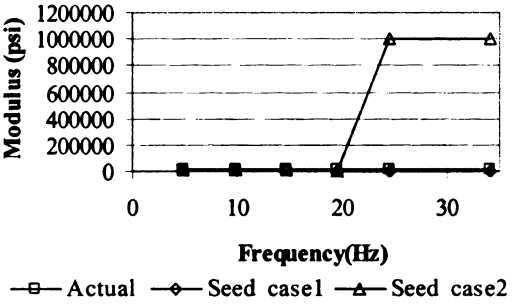

(d) Subgrade

Figure 6.28 Effect of seed moduli on backcalculation results – four-layer profile with medium-stiff AC layer

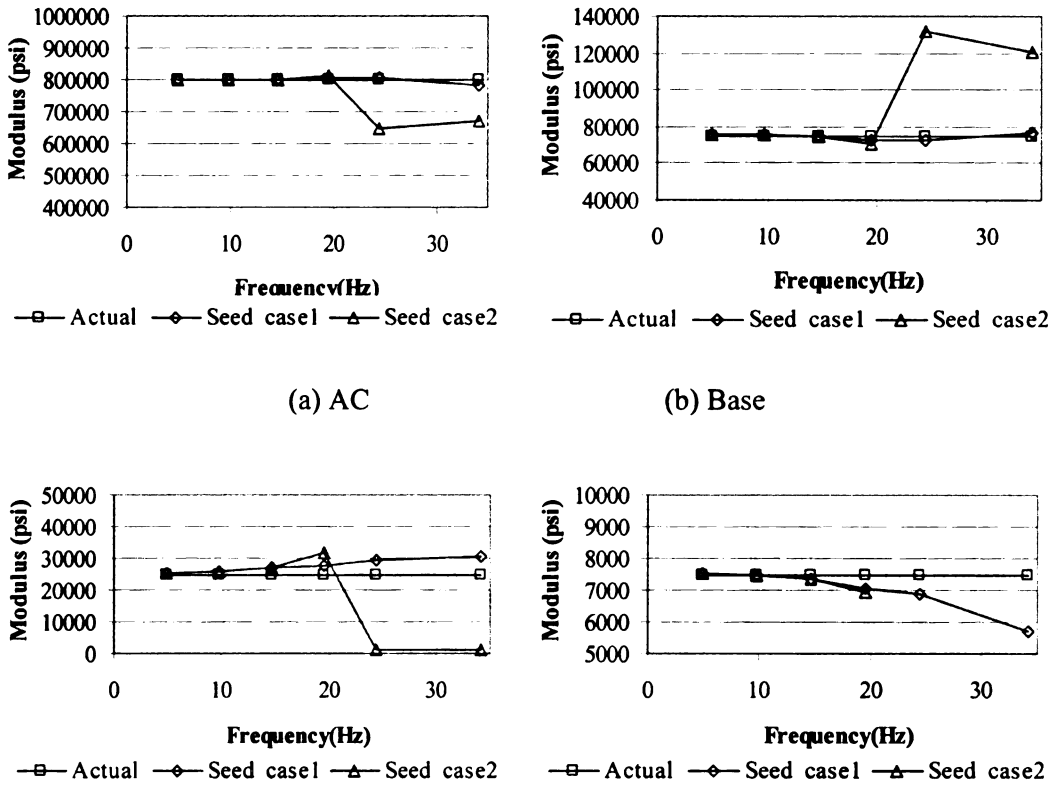

Figure 6.29 Effect of seed moduli on backcalculation results – four-layer profile with stiff AC layer

6.3.4 Convergence Characteristics

Newton's method is, in general, a rapidly converging and accurate optimization technique. The convergence characteristics have been tested in this section using the deflection data generated by SAPSI. The results for a three layer pavement with thin and medium-thick AC layer (see Table 6.13 for the profiles) are shown in Figure 6.30 through Figure 6.32, and Figure 6.33 through Figure 6.35, respectively. The results show that the solution converged within 10 iterations irrespective of the seed values. For the profile with medium-thick AC layer, the solution converges after 12 iterations. These results

indicate that the frequency-domain solution has very good convergence characteristics when using synthetic data, suggesting the theoretical algorithm for backcalculation in the frequency-domain is satisfactory.

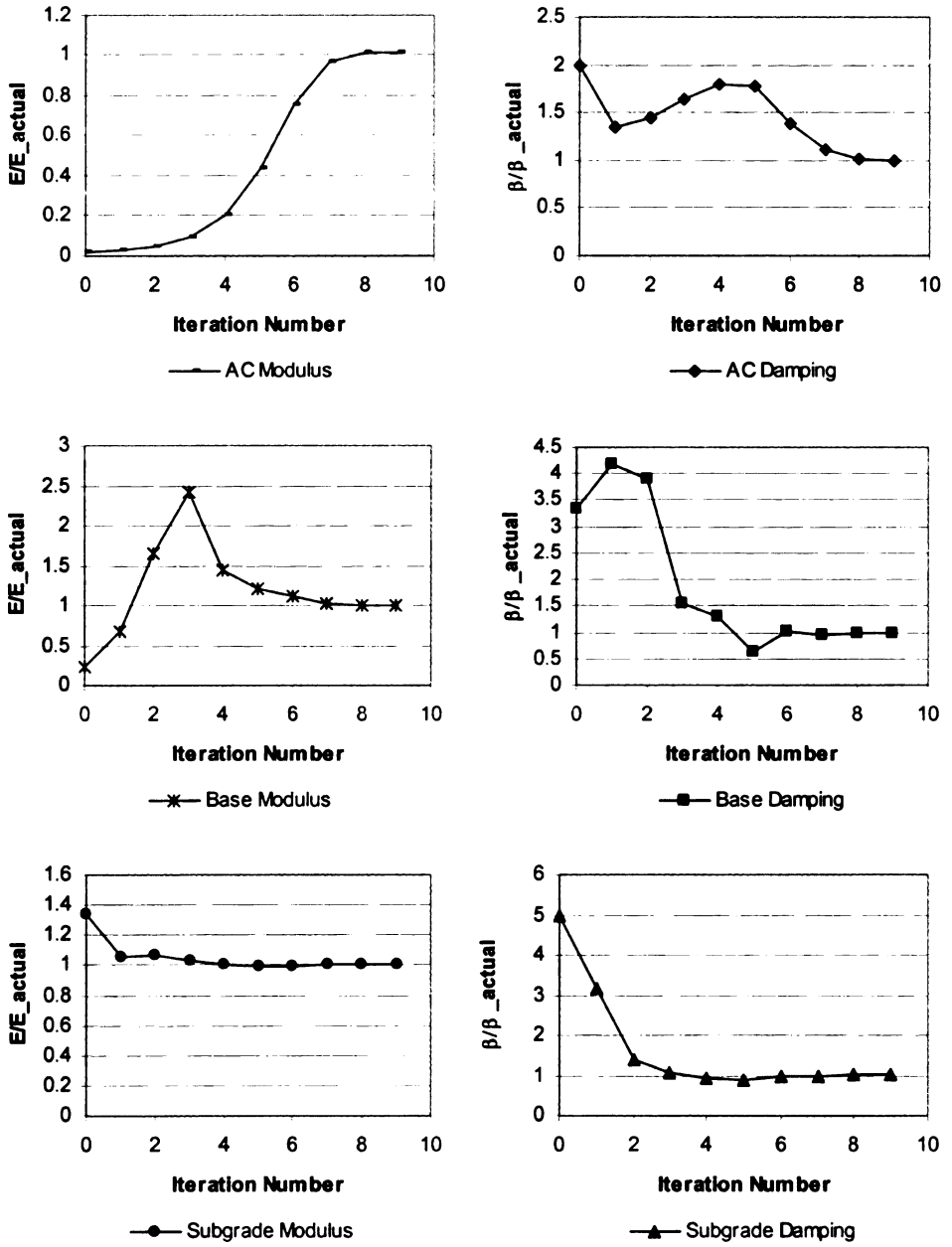

Figure 6.30 Convergence of layer parameters for a three-layer pavement with thin AC layer – 4.88 Hz

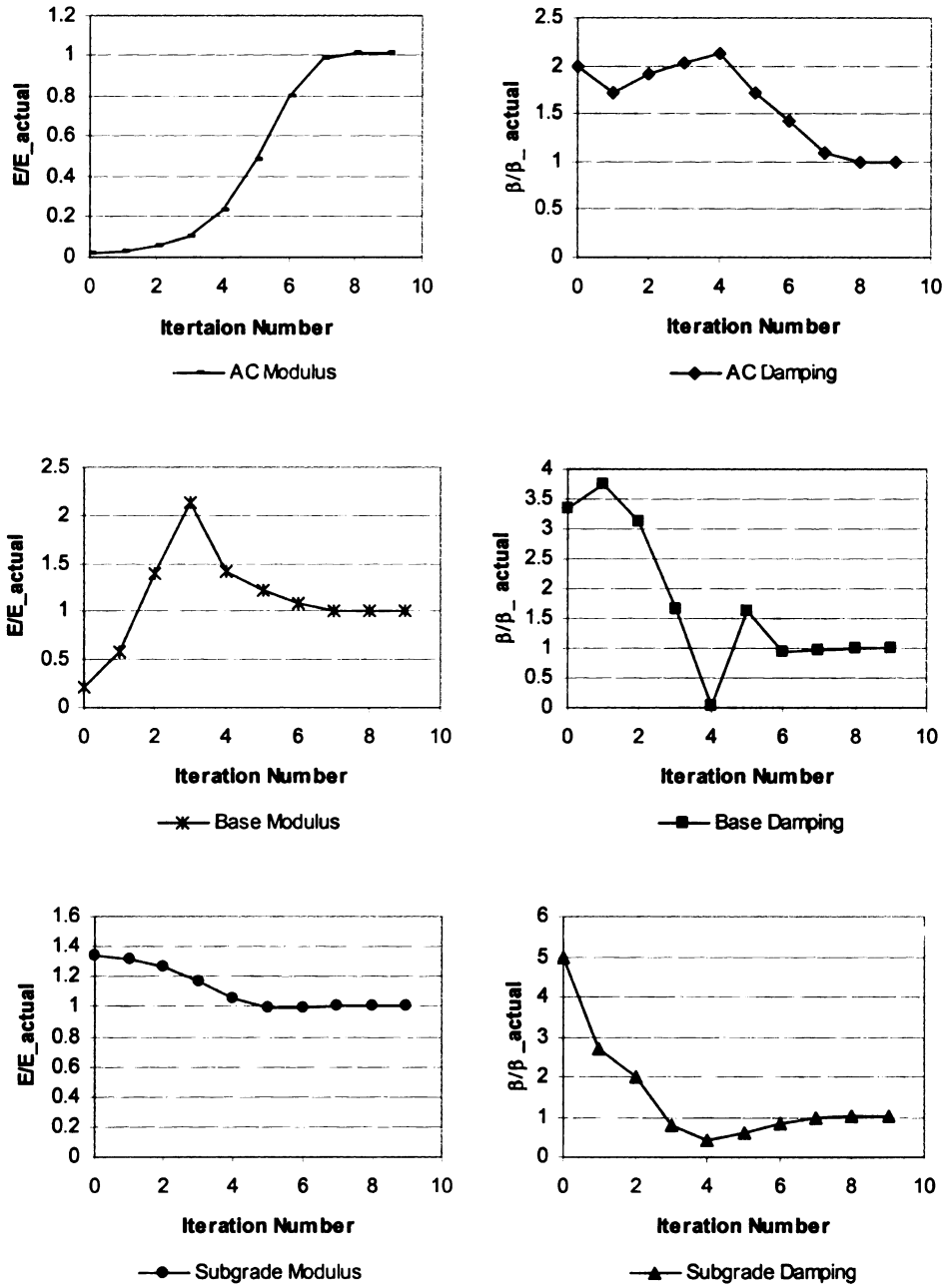

Figure 6.31 Convergence of layer parameters for a three-layer pavement with thin AC layer – 24.4 Hz

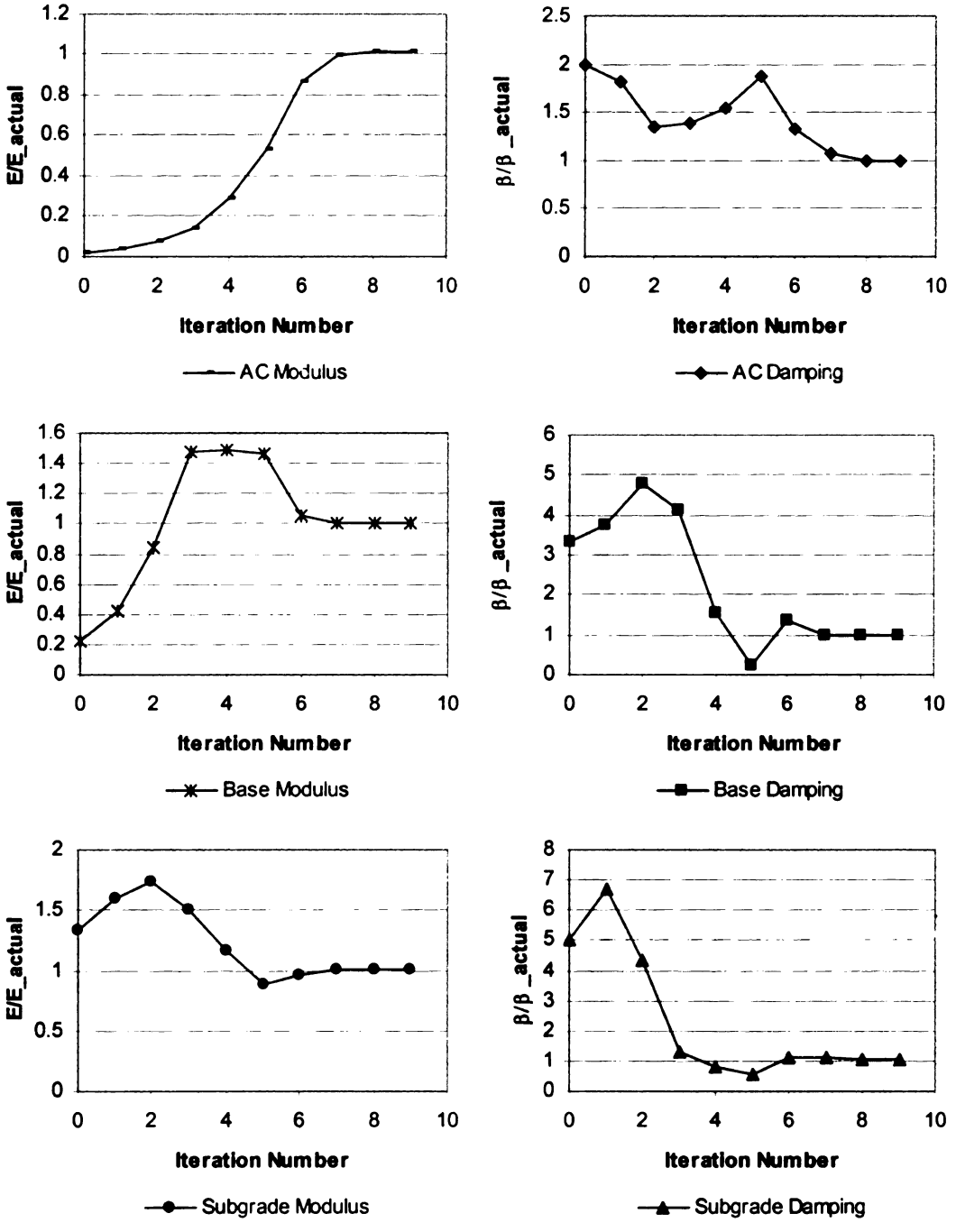

Figure 6.32 Convergence of layer parameters for a three-layer pavement with thin AC layer – 48.8 Hz

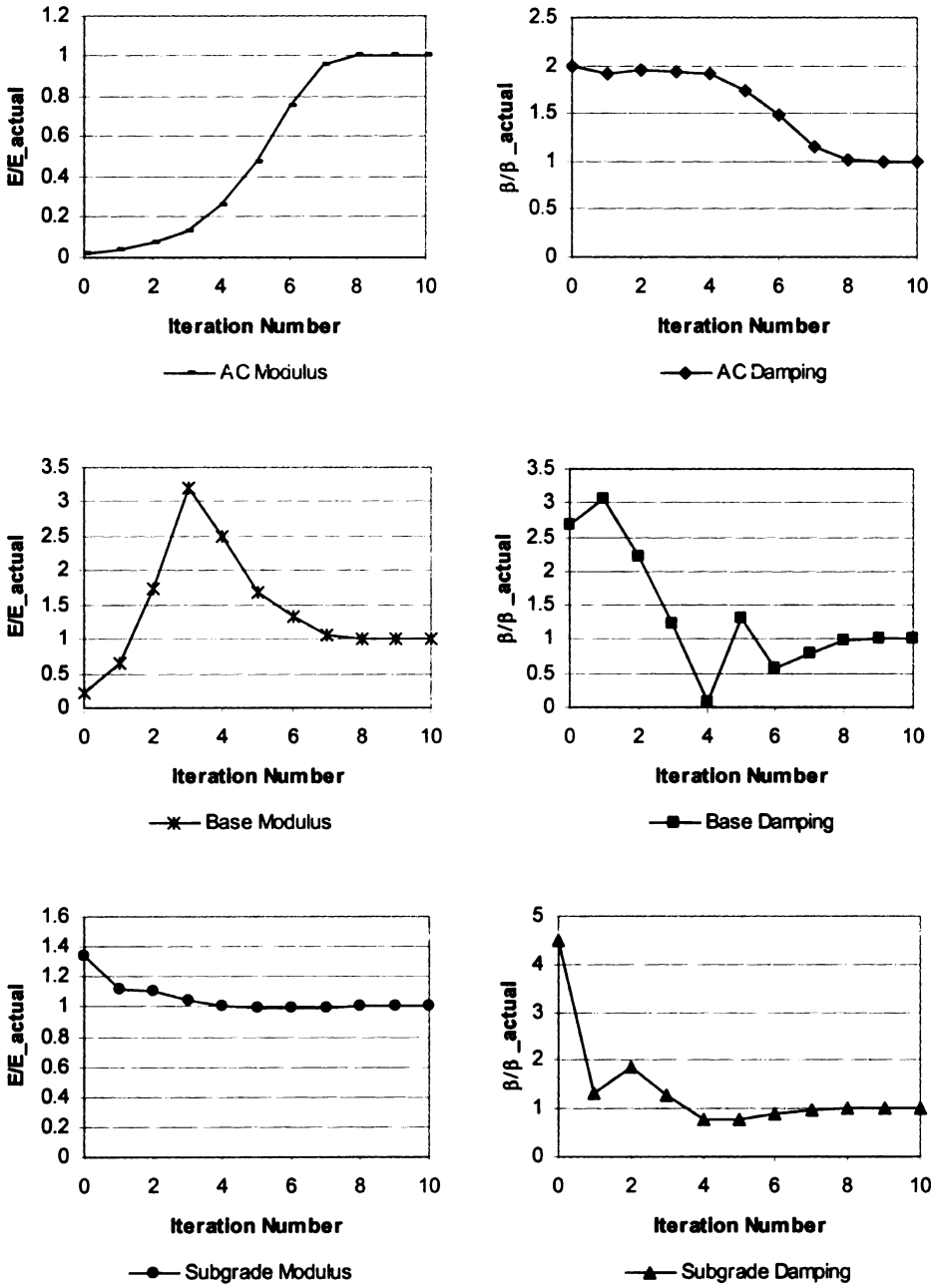

Figure 6.33 Convergence of layer parameters for a three-layer pavement with medium-thick AC layer – 4.48 Hz

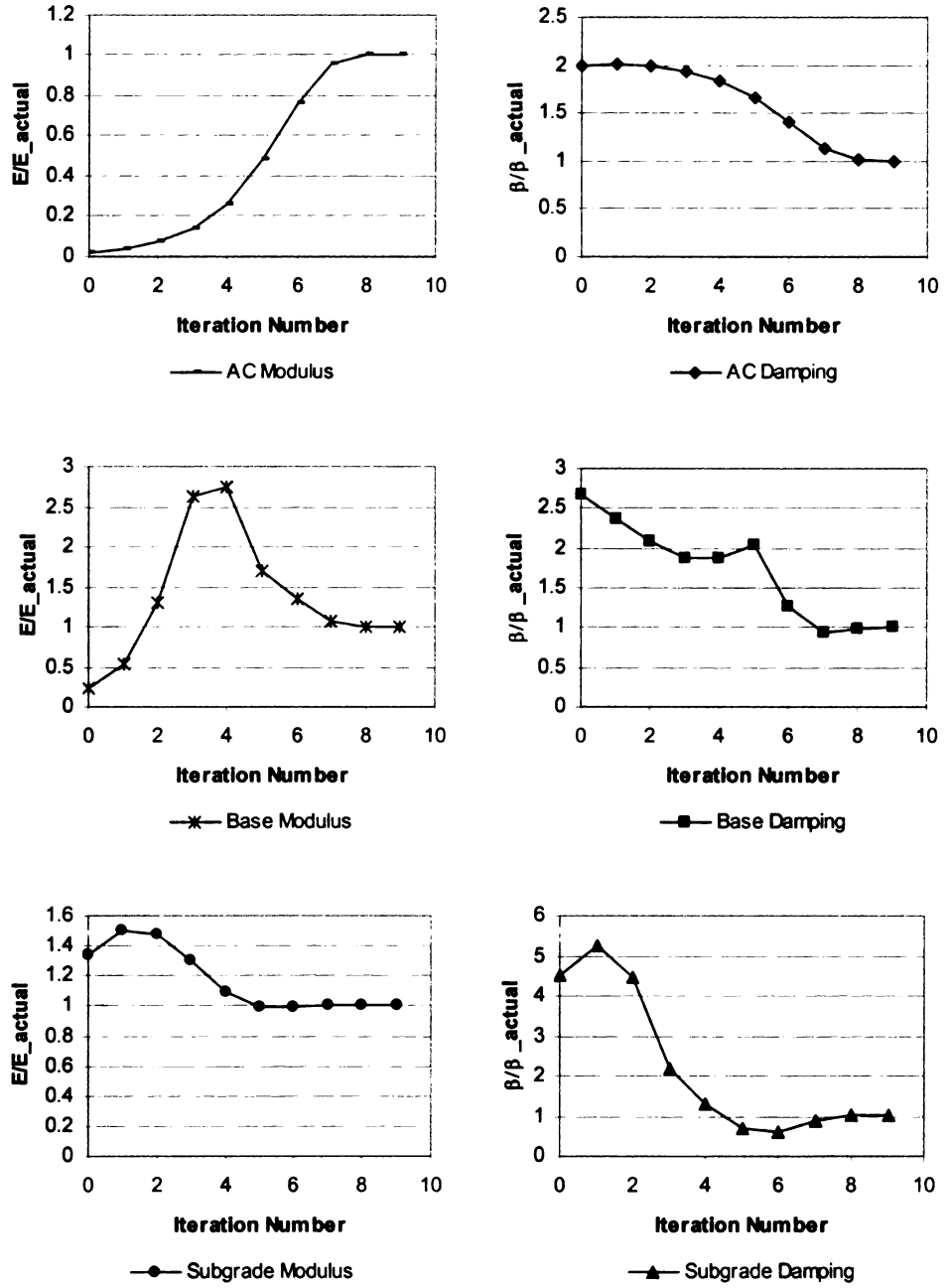

Figure 6.34 Convergence of layer parameters for a three-layer pavement with medium-thick AC layer – 24.4 Hz

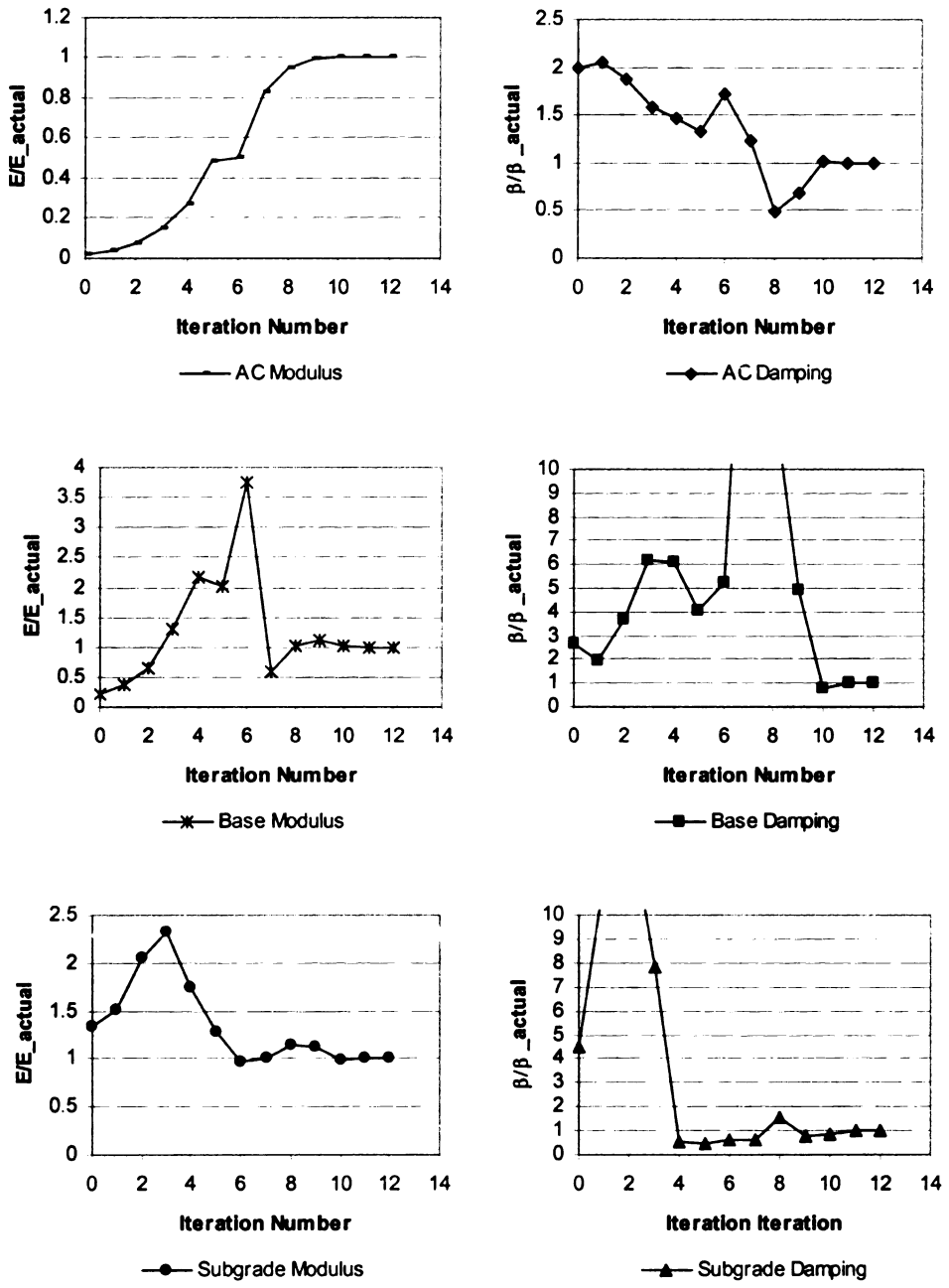

Figure 6.35 Convergence of layer parameters for a three-layer pavement with medium-thick AC layer – 48.8 Hz

6.3.5 Effect of Poisson's Ratio on Backcalculated Layer Parameters

Several studies were conducted to assess the effect of Poisson's ratios of the various layers on calculated deflections. Using static analysis Pichmani (1972) concluded that only Poisson's ratio of the roadbed soil has some appreciable effect on the surface deflections. Variations in the Poisson's ratios of the other layers were found to have little effect on the surface deflections. This and other similar findings have led to a general consensus that since Poisson's ratios of the pavement layers have little influence on the surface deflections, their effect on the backcalculated layer moduli may be neglected. No study appears to have investigated the direct effect of Poisson's ratios on the dynamic backcalculation layer moduli. In this study, this issue was investigated and results are presented in this section.

First an attempt was made to backcalculate the modulus, thickness, and Poisson's ratio of the AC layer for a simple profile. The profile with a 9 inch AC layer in Table 6.13 was used for this example. The results shown in Figure 6.36 indicate that the Poisson's ratio of the AC layer cannot be backcalculated since it reaches either the upper or the lower boundary.

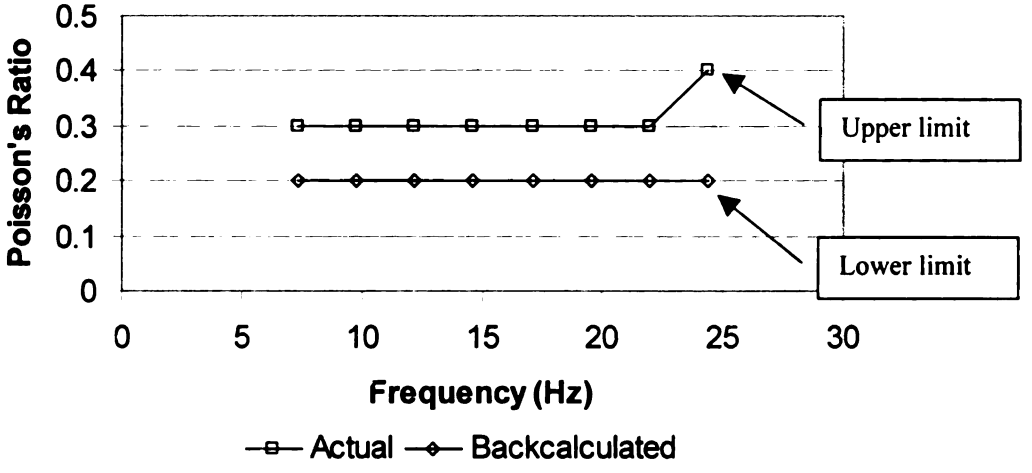

Figure 6.36 Backcalculated Poisson's ratio at various frequencies

In light of these results, it was decided to look at the effect of Poisson's ratio on the backcalculated results. The deflection basins used in the previous sections were generated by using constant Poisson's ratios of 0.35, 0.40 and 0.45 for the AC, base and the roadbed soil, respectively. To assess the effect of Poisson's ratio on the backcalculated layer moduli, the value of Poisson's ratio was varied by 0.05 from the true value for one layer at a time. The results of this analysis for the same 9 inch AC pavement are shown in Figure 6.37 through Figure 6.39. The results indicate that for frequencies below 20 Hz, the effects of variations in Poisson's ratios on the backcalculated moduli are negligible, with the error being within 2%, 5% and 6% for the AC, base and subgrade modulus, respectively. The error is higher at higher frequencies, reaching 4%, 20% and 27% for the AC, base and subgrade modulus, respectively, at 44 Hz. Based on these results, it appears that it would be prudent to limit backcalculation to frequencies lower than about 20 Hz in order to minimize the errors caused by the variation in Poisson's ratio.

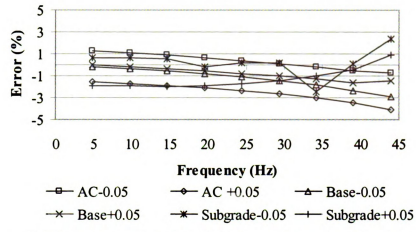

Figure 6.37 Percent error in AC moduli due to change in Poisson's ratio

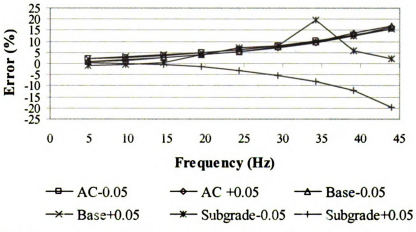

Figure 6.38 Percent error in base modulus due to change in Poisson's ratio

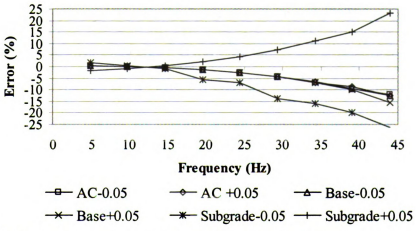

Figure 6.39 Percent error in subgrade modulus due to change in Poisson's ratio

6.3.6 Simulation of Measurement Errors

To investigate the possible reasons for the erratic behavior of the backcalculated layer parameters with frequency observed using measured FWD data from the field, synthetic deflection time histories were generated using SAPSI with different precision levels and durations.

One source of error is the precision of the deflection measurements. The precision of the sensor readings in Dynatest and KUAB FWD machines is about ± 0.1 and ± 1 micrometer, respectively. It is generally believed that since the deflections at the outer sensors are comparatively smaller, imprecision at these sensors have a large contribution towards the overall error especially for the lower layer. In this section, the effects of imprecision in deflections at different sensor locations on the backcalculated layer parameters are examined. For simplicity the maximum error of ±1 micrometer is used.

Another source of error for frequency-domain analysis is the truncation in the duration of the load and deflection time histories. Note that the fluctuation of the backcalculated parameters along frequency is basically due to the truncated FWD sensor records. The Fourier spectrum of the truncated signal is not the same as the original signal, leading to a different deflection basin at a given frequency, and hence resulting in poor backcalculation results. Taking an average value across the frequency-domain, while technically incorrect, may lead to more reasonable estimates of the backcalculated parameters. To investigate the effect of signal truncation, dynamic backcalculation was conducted using both truncated (60 ms) and longer (200 ms) load and deflection time

histories. An alternative solution to this problem is to perform the time-domain backcalculation.

The combination of these two sources of error can lead to very large errors in sensor deflections, as shown in Figure 6.40. Such errors will inevitably lead to erroneous backcalculation results.

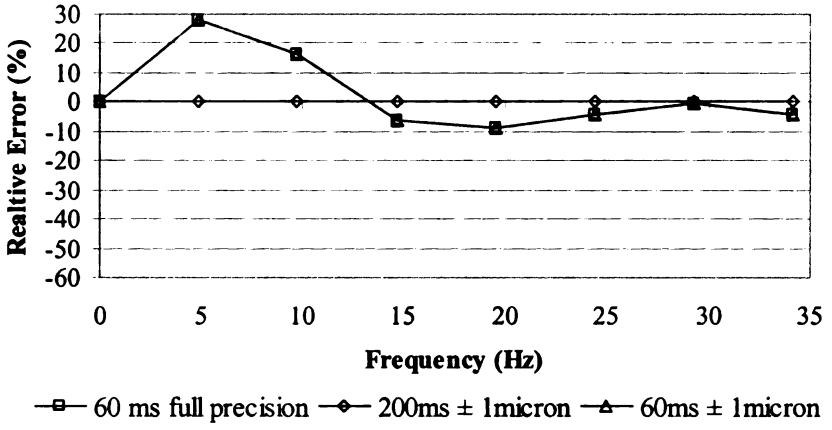

(a) Sensor 1

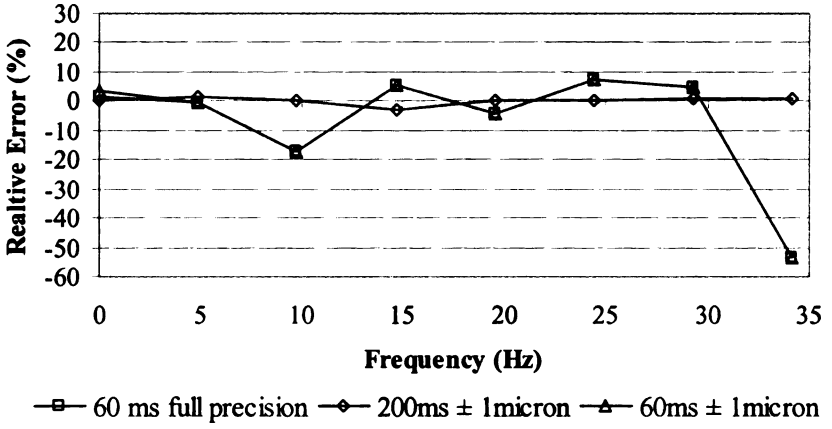

(b) Sensor 6

Figure 6.40 Effect of deflection imprecision and signal truncation on deflection basin errors

6.3.6.1 Effect of Deflection Imprecision on Backcalculated Results

The effect of deflection imprecision on backcalculation results was investigated for two cases: (i) when moduli and layer thicknesses are backcalculated, and (ii) when layer moduli and damping ratios are backcalculated. The pavement structure used in this analysis is shown in Table 6.16.

Table 6.16 Pavement structure used to study the effects of deflection imprecision on backcalculated results

Layer Name	Thickness (inch)	Modulus (ksi)	Damping Ratio	Unit Weight (pcf)	Poisson Ratio
AC	8	400 to 700 (from 5 to 25 Hz)	0.135 to 0.02 (from 5 to 25 Hz)	145	0.3
Base	12.13	20.4	0.03	135	0.35
Subgrade	54.69	15	0.02	125	0.4
Stiff layer	∞	100	0.05	145	0.15

Case (I) – Backcalculation of Layer Moduli and Thicknesses

In this case, layer moduli and thicknesses were backcalculated while the damping ratios of the unbound layers were assumed. Figure 6.41 through Figure 6.47 show the backcalculated parameters using surface deflections with full precision and ± 1 micron precision. The error in backcalculated layer thicknesses varies with the layer type and the frequency at which the backcalculation was performed. The maximum error in the backcalculated AC thickness was 2.5%, which is very reasonable. For the base layer, the errors in thickness varied from 7.5% to 16%, which is relatively large. For the subgrade depth (or depth-to-stiff layer,) the maximum error was 5.5%. Therefore, it appears that base thickness is the most affected by deflection imprecision. In terms of modulus backcalculation (for the case when layer thicknesses are also backcalculated,) the error in AC modulus (and damping ratio) was negligible. For the base modulus, the error is

within 5% except for one case (15 Hz) where the error is 20%. For the subgrade modulus, the maximum error was close to 7%.

Case (II) – Backcalculation of Layer Moduli and Damping Ratios

In this case, layer thicknesses are assumed while the moduli and damping ratios of all layers are backcalculated. Figure 6.48 through Figure 6.53 show the backcalculated parameters using surface deflections with full precision and ± 1 micron precision. The errors in backcalculated layer moduli (Figure 6.48 through Figure 6.50) are significantly lower than when layer thicknesses were backcalculated, with the error being within 1% for the AC and subgrade layers, and the maximum error being short of 4% for the base layer. The errors in backcalculated damping ratios (Figure 6.51 through Figure 6.53) are insignificant except for one case (15 Hz) where the backcalculated base damping ratio was 2.3% as compared to the actual value of 3%.

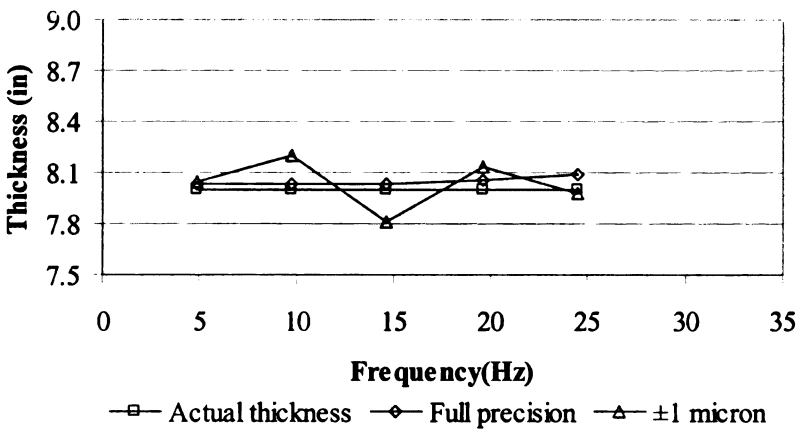

Figure 6.41 Effect of deflection precision on AC thickness backcalculation (thickness backcalculation enabled)

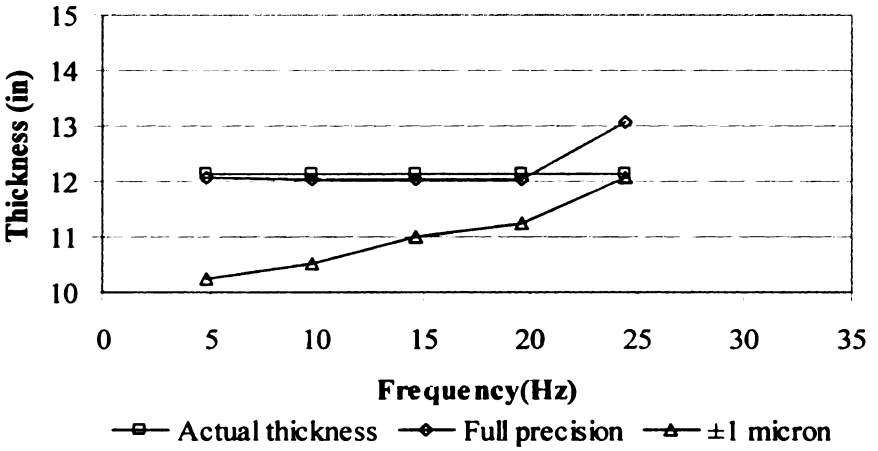

Figure 6.42 Effect of deflection precision on base thickness backcalculation (thickness backcalculation enabled)

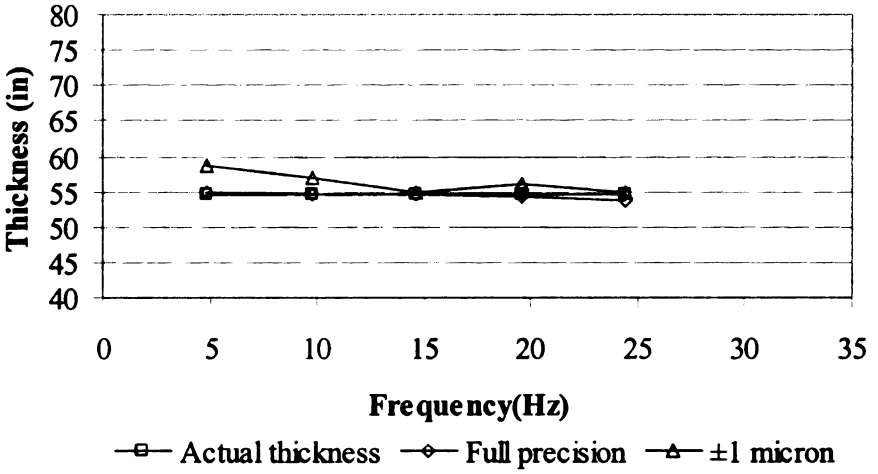

Figure 6.43 Effect of deflection precision on depth-to-stiff layer backcalculation (thickness backcalculation enabled)

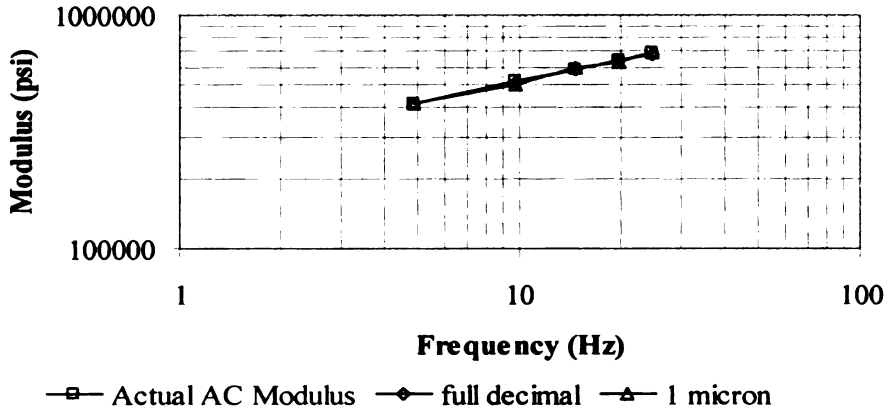

Figure 6.44 Effect of deflection precision on ac modulus backcalculation (thickness backcalculation enabled)

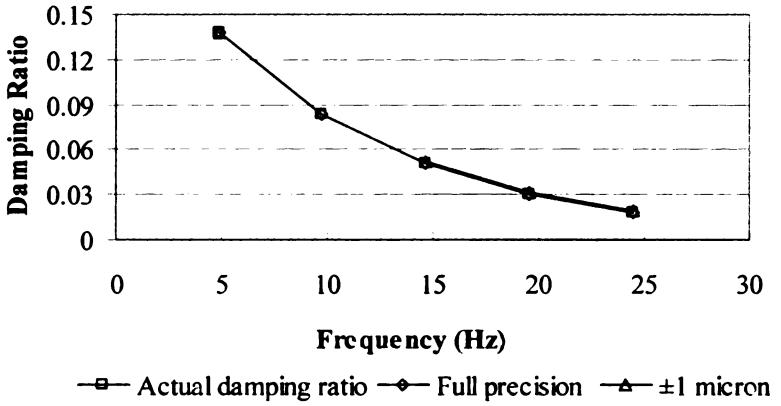

Figure 6.45 Effect of deflection precision on AC damping ratio backcalculation (thickness backcalculation enabled)

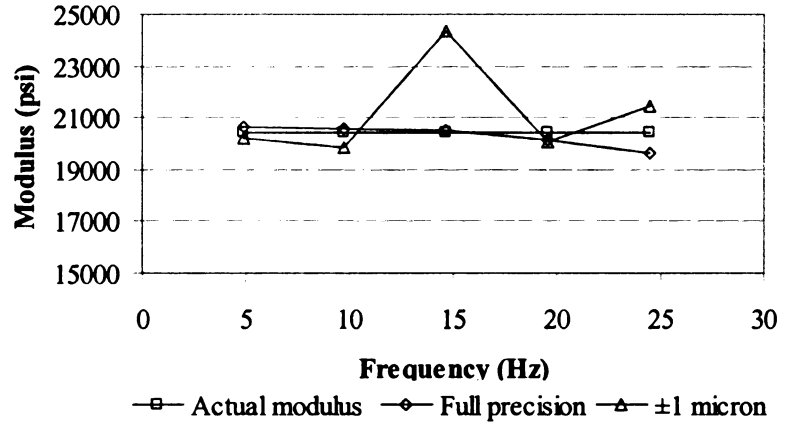

Figure 6.46 Effect of deflection precision on base modulus backcalculation (thickness backcalculation enabled)

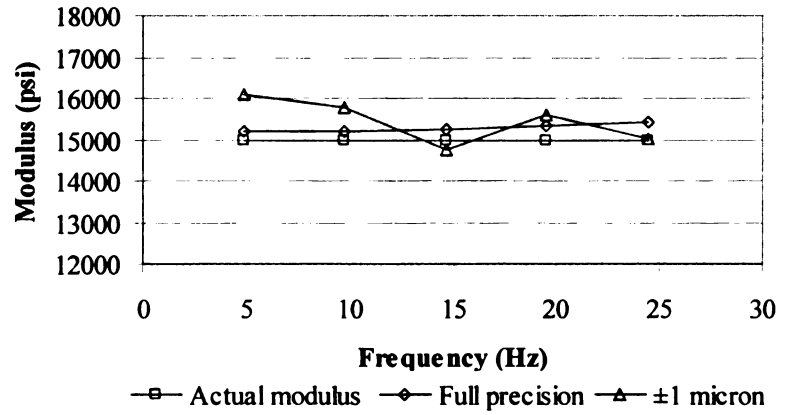

Figure 6.47 Effect of deflection precision on subgrade modulus backcalculation (thickness backcalculation enabled)

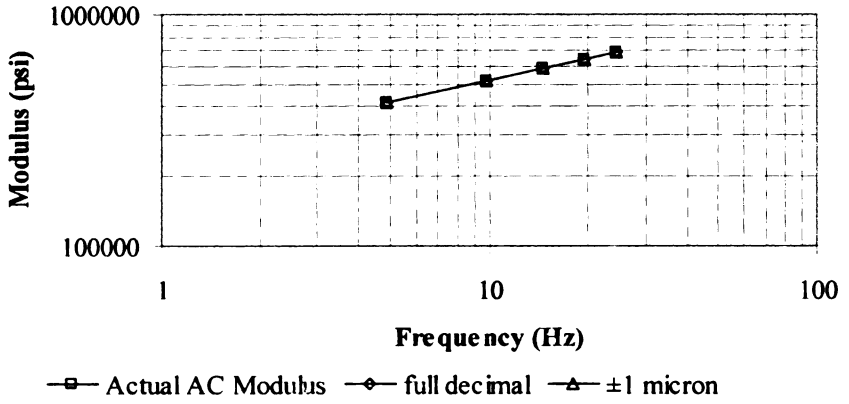

Figure 6.48 Effect of deflection precision on AC modulus backcalculation (layer thicknesses assumed)

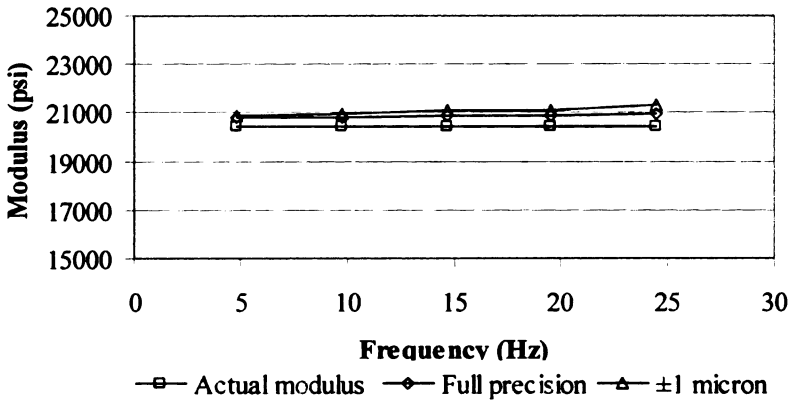

Figure 6.49 Effect of deflection precision on base modulus backcalculation (layer thicknesses assumed)

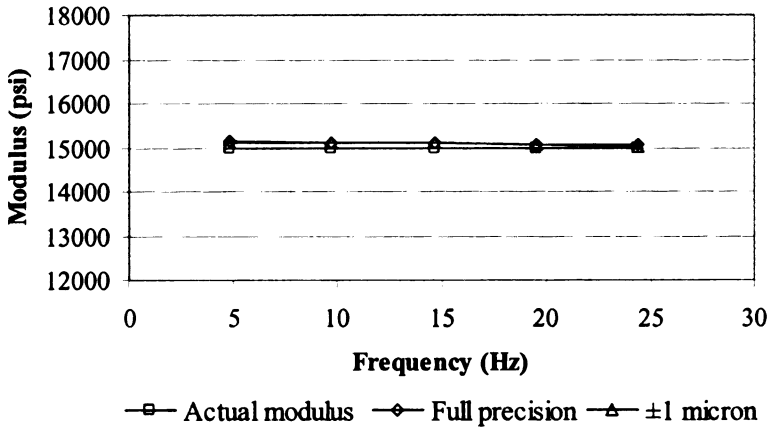

Figure 6.50 Effect of deflection precision on subgrade modulus backcalculation (layer thicknesses assumed)

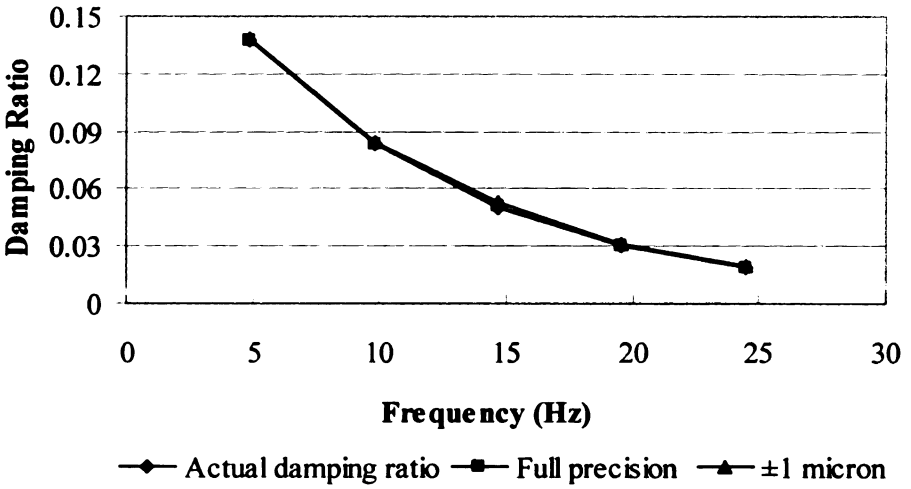

Figure 6.51 Effect of deflection precision on AC damping ratio backcalculation (layer thicknesses assumed)

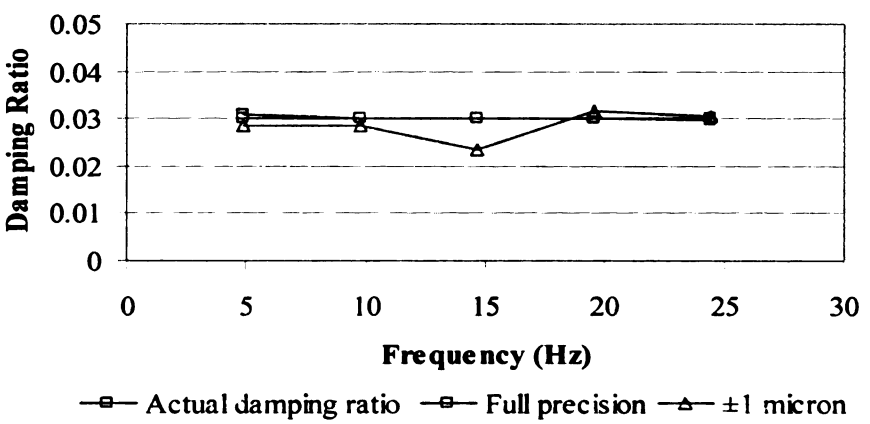

Figure 6.52 Effect of deflection precision on base damping ratio backcalculation (layer thicknesses assumed)

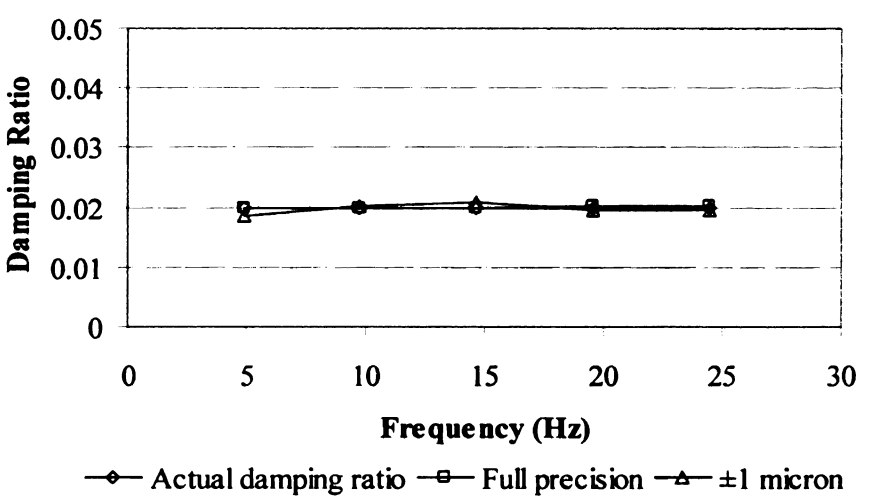

Figure 6.53 Effect of deflection precision on subgrade damping ratio backcalculation (layer thicknesses assumed)

6.3.6.2 Effect of Signal Truncation on Backcalculated Results

The effect of signal truncation on backcalculation results was investigated for two cases: (i) deflections matched within ±1 micron and (ii) deflections matched with full precision. The program was not able to backcalculate layer thicknesses when the deflection records were truncated, so only the results without thickness backcalculation are shown. The pavement structure used in this analysis is shown in Table 6.17.

Table 6.17 Pavement structure used to study the effects of signal truncation on backcalculated results

Layer Name	Thickness (inch)	Modulus (ksi)	Damping Ratio	Unit Weight (pcf)	Poisson Ratio
AC	8	210	0.30	145	0.3
Base	12.13	18	0.15	135	0.35
Subgrade	54.69	24.1	0.06	125	0.4
Stiff layer	∞	100	0.07	145	0.15

Case (I) – Backcalculation with ±1 Micron Precision

Figure 6.54 through Figure 6.61 show the backcalculated parameters using 200 ms and 60 ms (truncated) records. The results clearly show that there are errors associated with the truncation of the load and deflection time histories. Using the longer (200 ms) records, DYNABACK was able to backcalculate layer moduli and damping ratios correctly. However, when the truncated (60 ms) records were used, backcalculated parameters showed an erratic behavior with frequency. Basically, the frequency content of the motion is modified when the response is truncated before it fully decays. This will result in deflection basins that are different enough to change the backcalculation results. Figure 6.62 shows examples of deflection basins using the truncated and full time histories, while Table 6.18 shows the corresponding RMS values at different frequencies.

The table shows that these values can be very high at certain frequencies. The lowest RMS values occur at the frequencies where the response is maximal. For the real part of the deflection basin, this occurs at 0 Hz; while for the imaginary part of the deflection basin, it occurs at about 10 Hz for this profile. This suggests that if the truncation problem cannot be avoided in FWD measurements, deflection matching should be done at these frequencies, for the real and imaginary parts separately.

The error in the AC modulus varies from -8% to + 17% (Figure 6.54). For the base layer, the error varies from -10% to +12% (Figure 7.50), and for the subgrade layer, the error varies from -4% to +22% (Figure 6.56). The error for the stiff layer modulus varies from -19% to + 32% (Figure 6.57). More importantly, the erratic behavior with frequency that was observed in the backcalculated parameters from field FWD records is similar to that shown in the above figures (see Chapter 7). Therefore, it can be safely stated that this erratic behavior is indeed caused by the truncation in time.

The percent errors in backcalculated damping ratios are larger than those for moduli. The error in the AC damping ratio varies from -50% to + 30% (Figure 6.58). For the base layer, the error varies from -47% to +73% (Figure 6.59), and for the subgrade layer, the error varies from -48% to +60% (Figure 6.60). The error for the stiff layer modulus varies from -71% to + 128% (Figure 6.61).

Case (II) – Backcalculation with Full Precision

Figure 6.63 through Figure 6.70 show the backcalculated parameters using 200 ms and 60 ms (truncated) records with full precision deflection matching. Comparison of these results with those from case (i) shows practically no difference. This means that the

errors caused by truncation outweigh those that may be caused by sensor deflection imprecision.

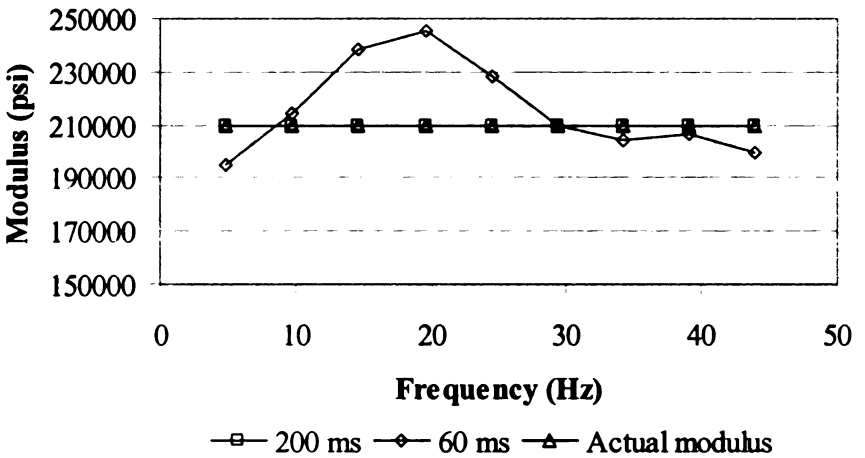

Figure 6.54 Effect of signal truncation on AC modulus backcalculation (thicknesses known with ±1 micron precision)

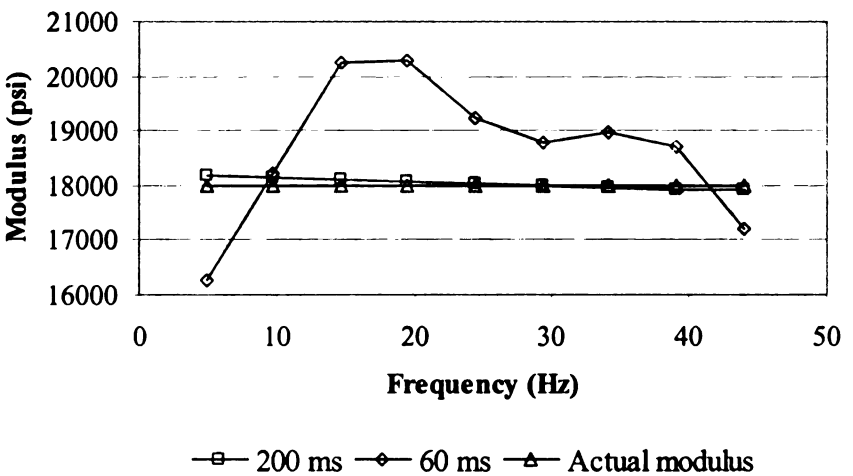

Figure 6.55 Effect of signal truncation on base modulus backcalculation (thicknesses known with ±1 micron precision)

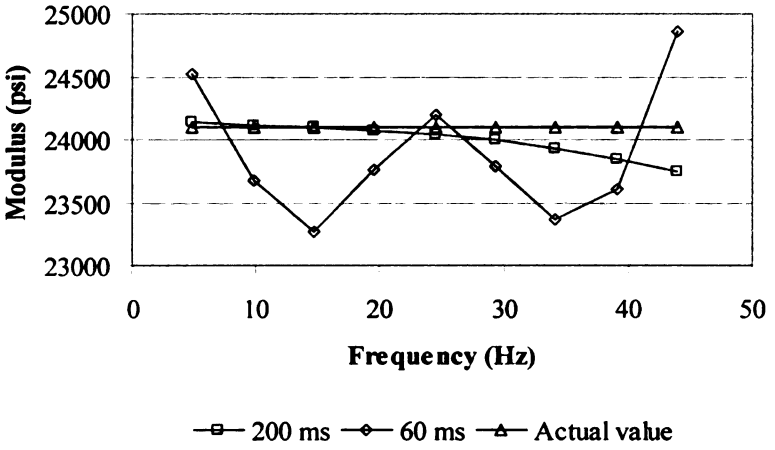

Figure 6.56 Effect of signal truncation on subgrade modulus backcalculation (thicknesses known with ±1 micron precision)

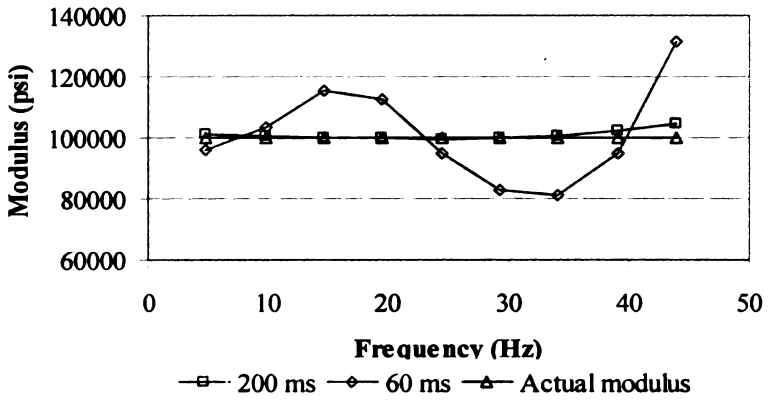

Figure 6.57 Effect of signal truncation on stiff layer modulus backcalculation (thicknesses known with ±1 micron precision)

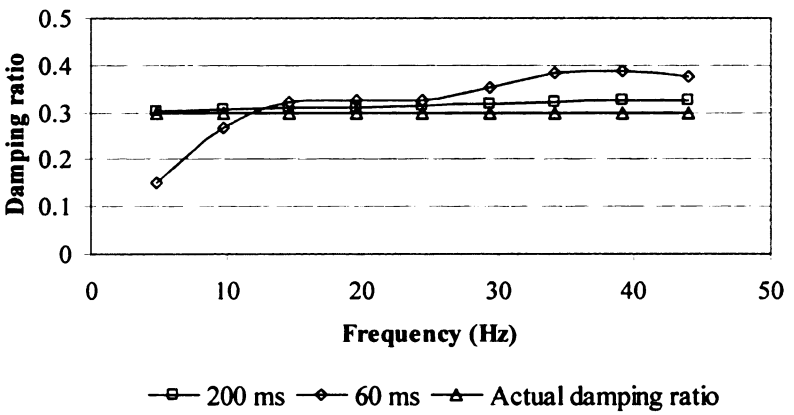

Figure 6.58 Effect of signal truncation on AC damping ratio backcalculation (thicknesses known with ±1 micron precision)

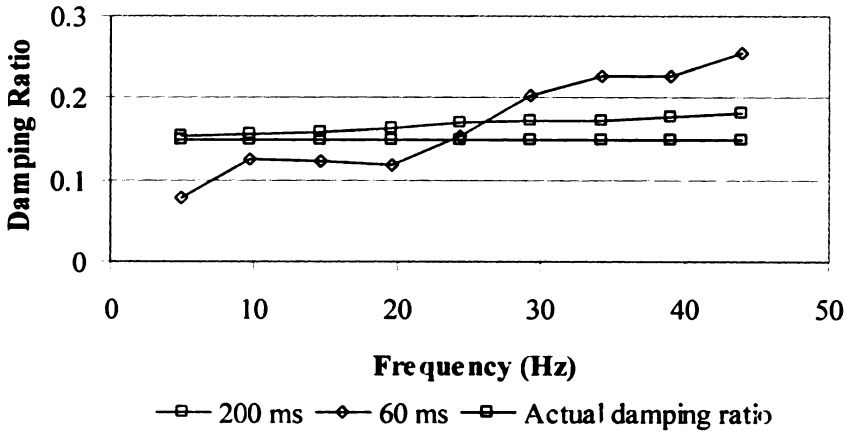

Figure 6.59 Effect of signal truncation on base damping ratio backcalculation (thicknesses known with ±1 micron precision)

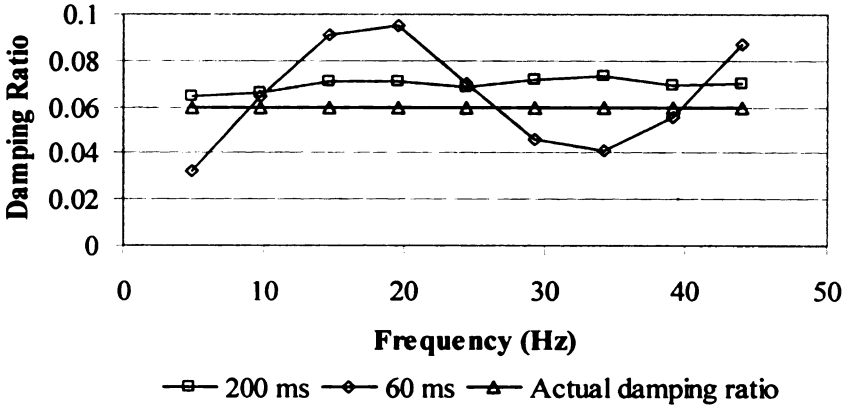

Figure 6.60 Effect of signal truncation on subgrade damping ratio backcalculation (thicknesses known with ±1 micron precision)

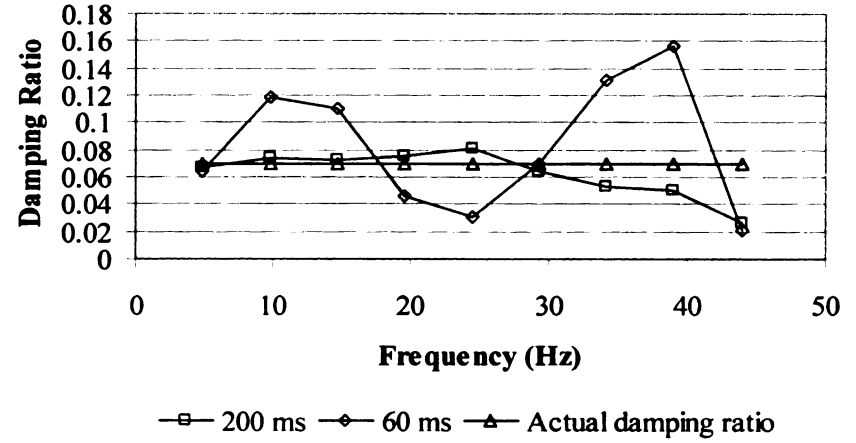

Figure 6.61 Effect of signal truncation on stiff layer damping ratio backcalculation (thicknesses known with ±1 micron precision)

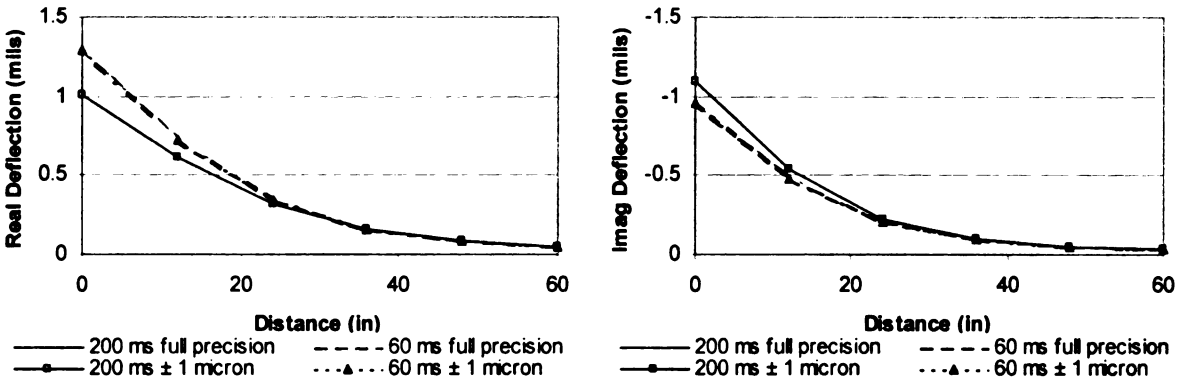

(a) 4.88 Hz

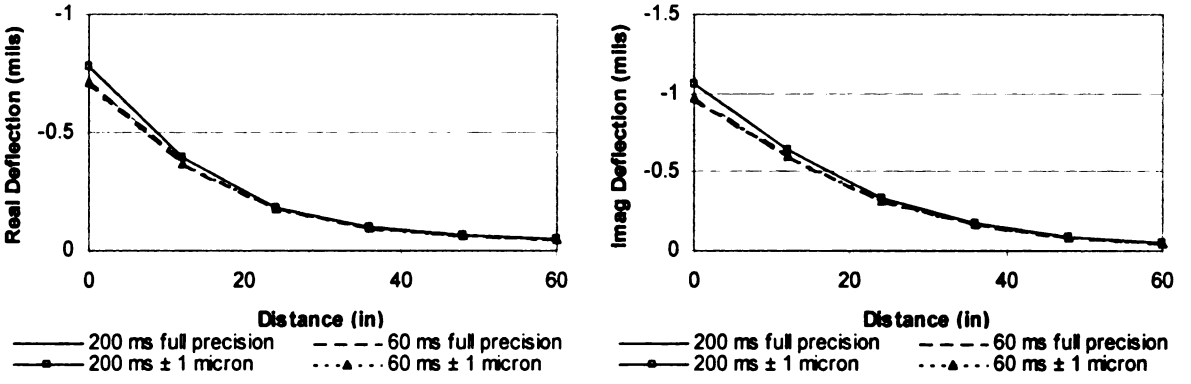

(b) 19.53 Hz

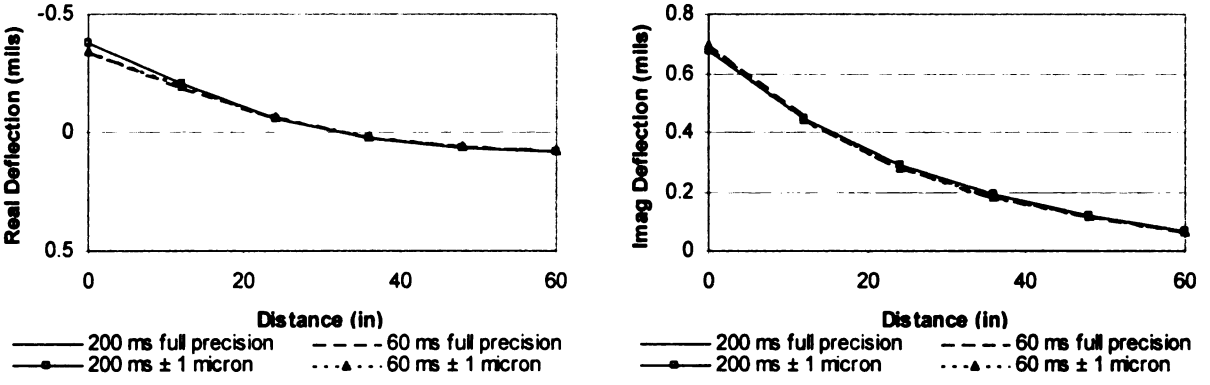

(c) 39.06 Hz

Figure 6.62 Effect of signal truncation on deflection basins

Table 6.18 RMS values for deflection basins corresponding to truncated versus untruncated sensor signals

	RMS(%)	
Frequency (Hz)	Real Part	Imag. Part
0	3%	N/A
4.88	34%	18%
9.77	28%	3%
14.65	N/A	11%
19.53	12%	10%
24.41	9%	51%
29.3	9%	297%
34.18	56%	12%
39.06	46%	7%
43.95	751%	39%
48.83	40%	204%

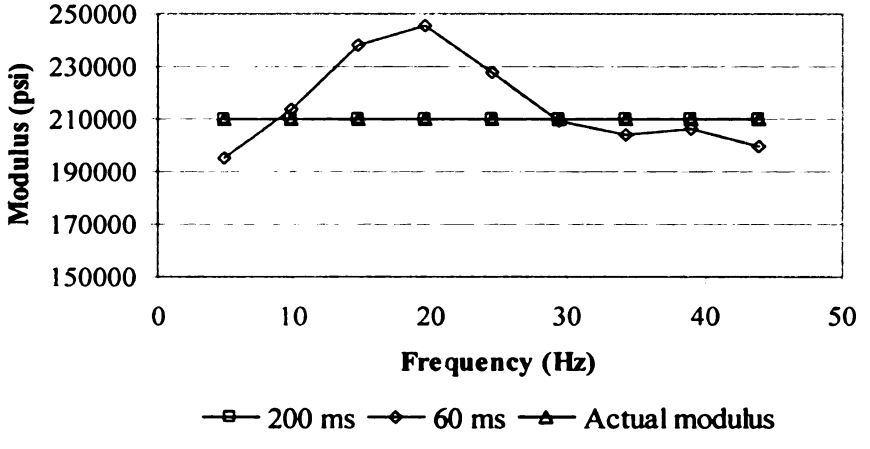

Figure 6.63 Effect of signal truncation on AC modulus backcalculation (thicknesses known with full precision)

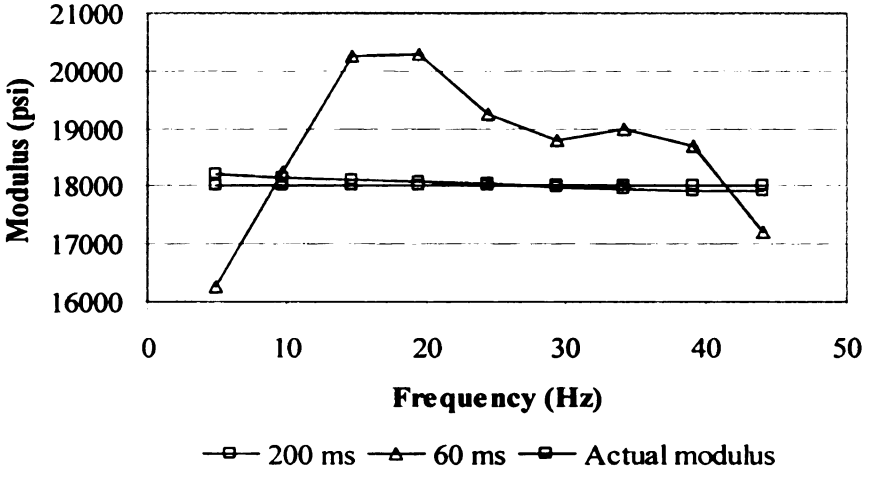

Figure 6.64 Effect of signal truncation on base modulus backcalculation (thicknesses known with full precision)

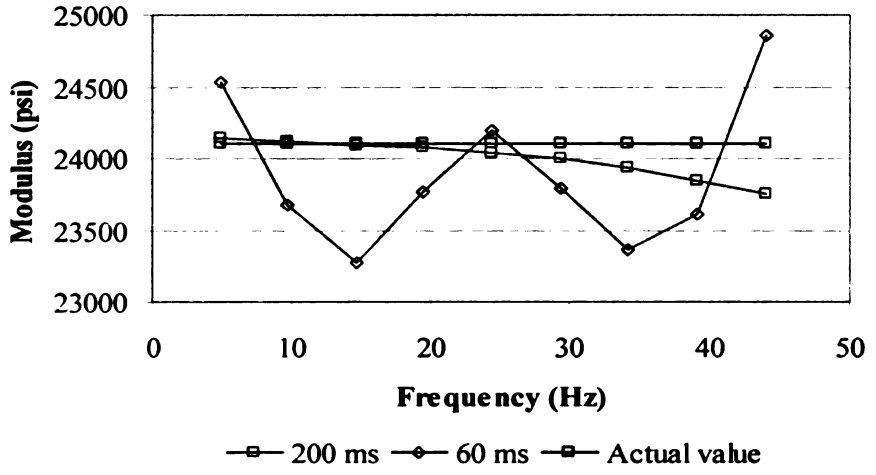

Figure 6.65 Effect of signal truncation on subgrade modulus backcalculation (thicknesses known with full precision)

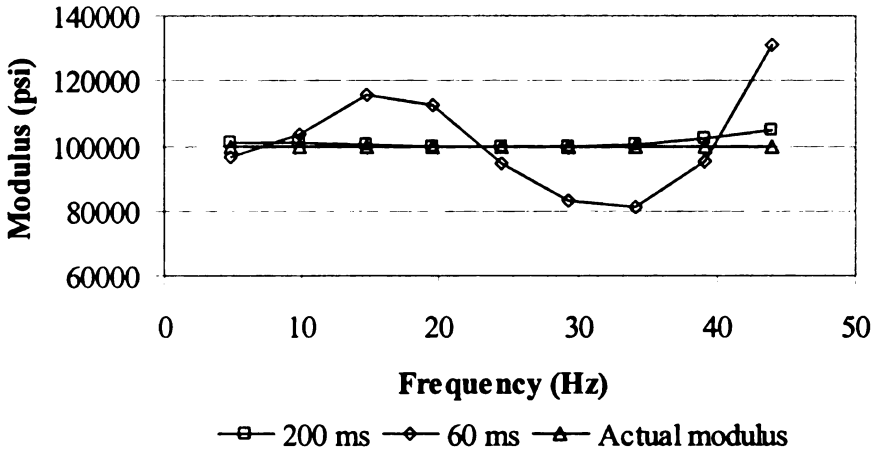

Figure 6.66 Effect of signal truncation on stiff layer modulus backcalculation (thicknesses known with full precision)

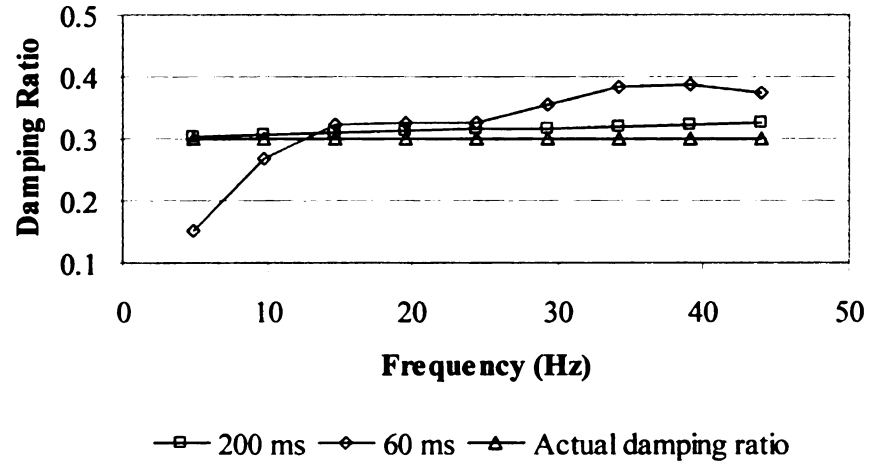

Figure 6.67 Effect of signal truncation on AC damping ratio backcalculation (thicknesses known with full precision)

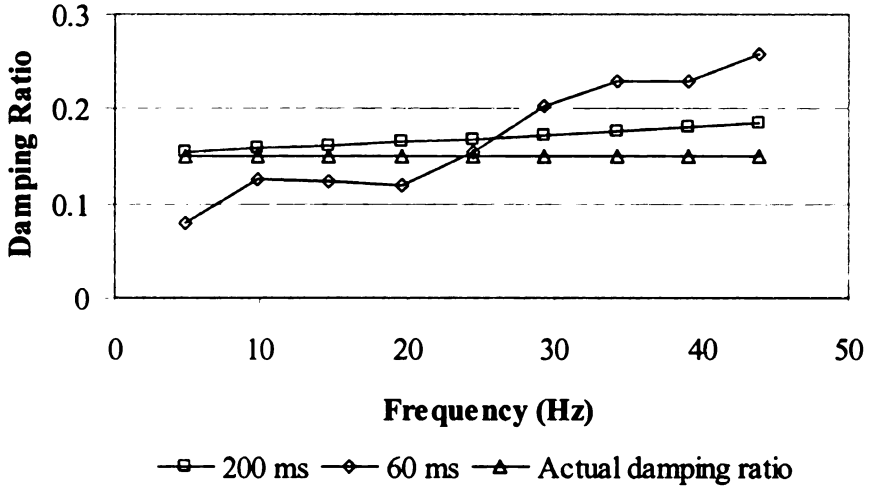

Figure 6.68 Effect of signal truncation on base damping ratio backcalculation (thicknesses known with full precision)

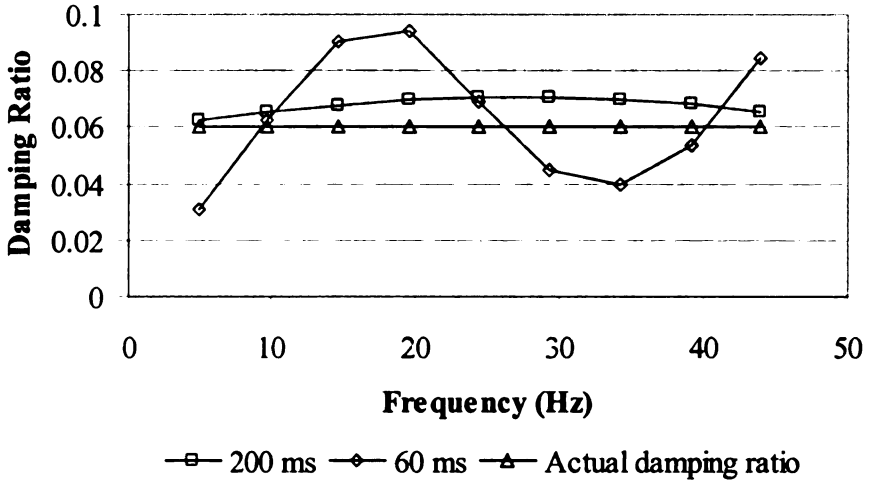

Figure 6.69 Effect of signal truncation on subgrade damping ratio backcalculation (thicknesses known with full precision)

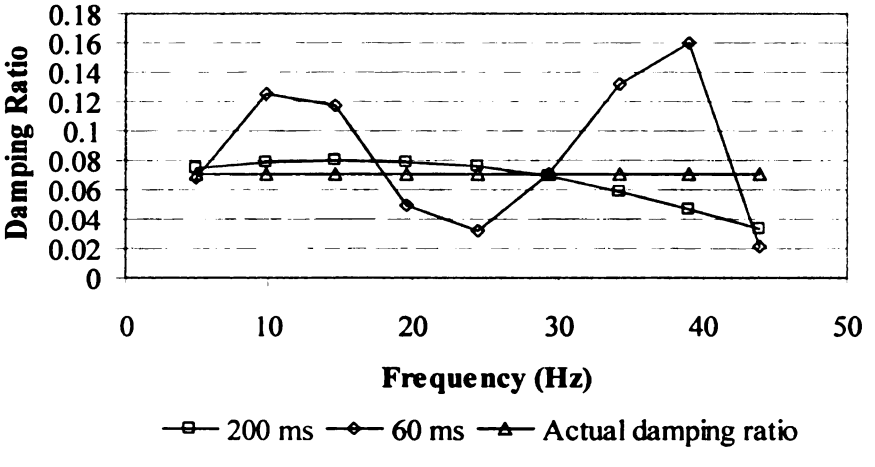

Figure 6.70 Effect of signal truncation on stiff layer damping ratio backcalculation (thicknesses known with full precision)

6.3.6.3 Extrapolation

In frequency-domain backcalculation, the FWD load and deflection time histories are transformed to the frequency domain using the Fast Fourier Transform (FFT) algorithm. The FFT works on a digitized signal which is a series of discrete values sampled at fixed intervals of time. The FFT sample size must be a power of two. Therefore, the process which is called zero-packing is used to obtain this sampling size. Since the sampling time is limited, sensor deflection time histories are truncated before they die out. Because the discrete Fourier Transform assumes periodicity, the truncated signal is converted to periodic signal with a discontinuity at the point of truncation. It was shown that the pulse discontinuity produces an undesirable effect on the FFT of the pulse (Chatti et al, 2003, Uzan, 1994 and Magnuson, 1988).

Extrapolation is used to predict the future of a time history from a record of its past. The extrapolation equation using linear prediction is expressed as (Press, 1989):

$$y_n = \sum_{j=1}^{N} d_j y_{n-j} + x_n \qquad (1)$$

where, x_n is the discrepancy of the prediction at time step n, and d_j are the linear prediction (LP) coefficients. These coefficients characterize the known signal in terms of a finite number of poles that best represent its spectrum in the complex z-plane.

The equation can predict the next value y_n of a time series from the previous N values y_{n-j}, $j = 1 \cdots N$. N should be chosen as a small number (Press, 1989). In this section, the extrapolation is conducted for different sensors using different N-values for the different sensors. Figure 6.71 through Figure 6.76 show extrapolations of FWD time histories with different N-values for the different sensors. The following conclusions can be made from the figures:

1. The value of N will affect the extrapolated portion of the record. The smallest value of N will lead to a line with no decay. Increasing N will cause the extrapolated portion to become non-linear, with fluctuations that decay with time.

2. For the different FWD sensors, different N-values may need to be selected to match the different time histories. In this analysis, N-values of 2, 3, 4, 5, 6, and 7 were used.

Based on the above results, two cases of tail extrapolation corrections were used: Case 1 with N_1= 5, N_2= 4, N_3= 4, N_4= 4, N_5= 4, and N_6= 3 corresponding to sensor1 through sensor 6, respectively; and case 2 with N_1= 7, N_2= 4, N_3= 4, N_4= 3, N_5= 2, and N_6= 2. The frequency-based backcalculation is then performed using the corrected time histories. Figure 6.77 through Figure 6.84 show the backcalculation results for the various parameters. According to these results, the following conclusions can be made:

1. Backcalculation results obtained using the extrapolated ("corrected") time histories are still different from the true values. Therefore extrapolation can not

solve the truncation problem, and it is necessary for frequency-based backcalculation to use the full time history if it does not decay to zero.

2. The choice of N is key in the extrapolation correction; a different choice of extrapolation order (N) will cause different backcalculation results.

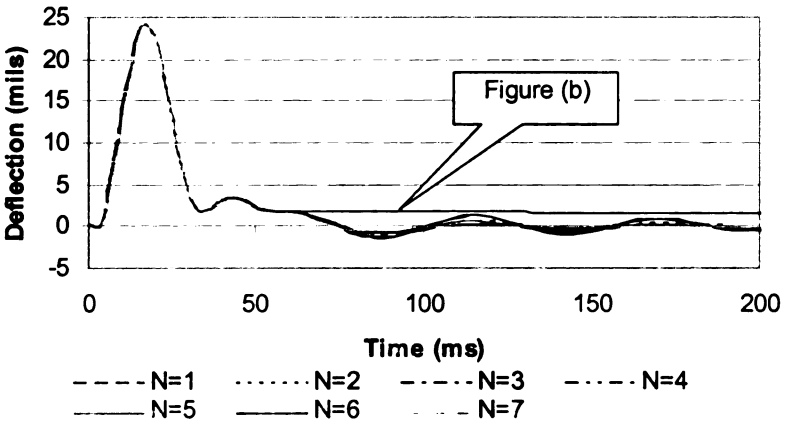

(a)

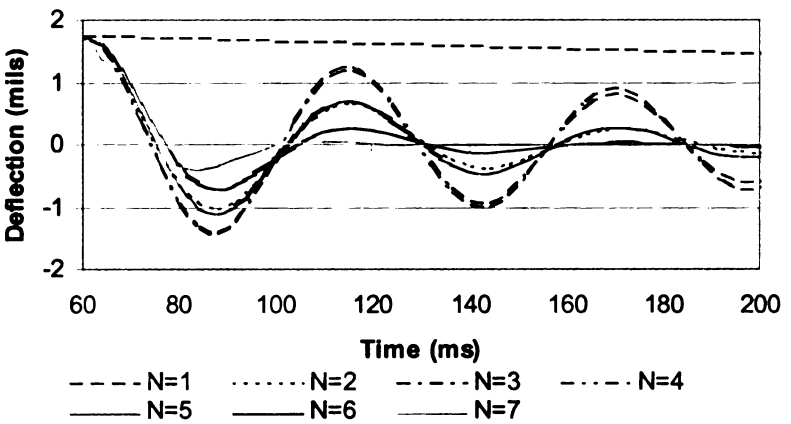

(b)

Figure 6.71 Comparison of different order extrapolations for sensor 1

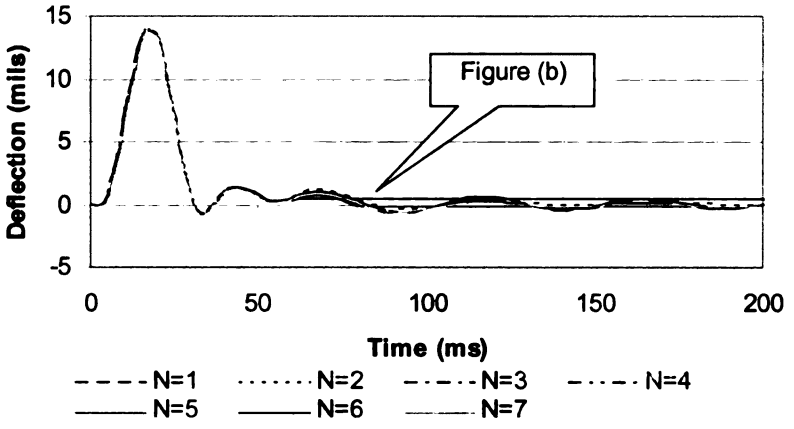

(a)

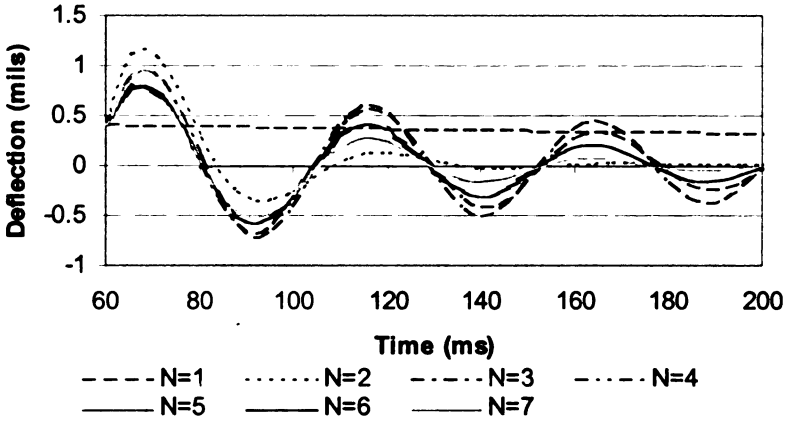

(b)

Figure 6.72 Comparison of different order extrapolations for sensor 2

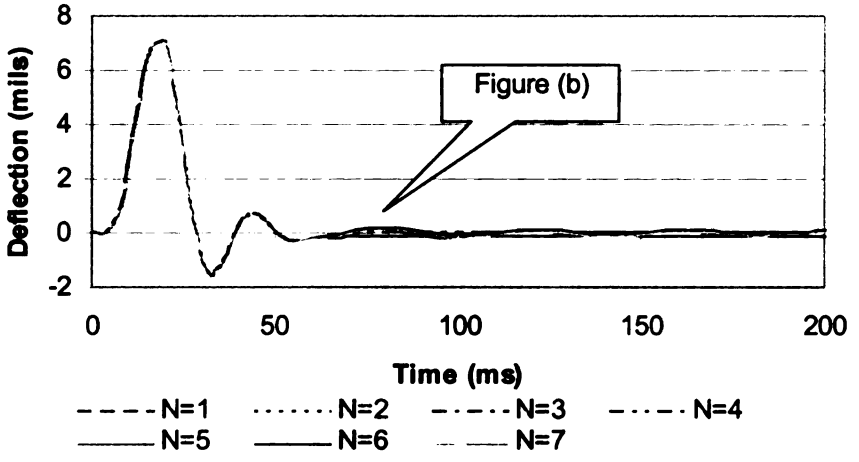

(a)

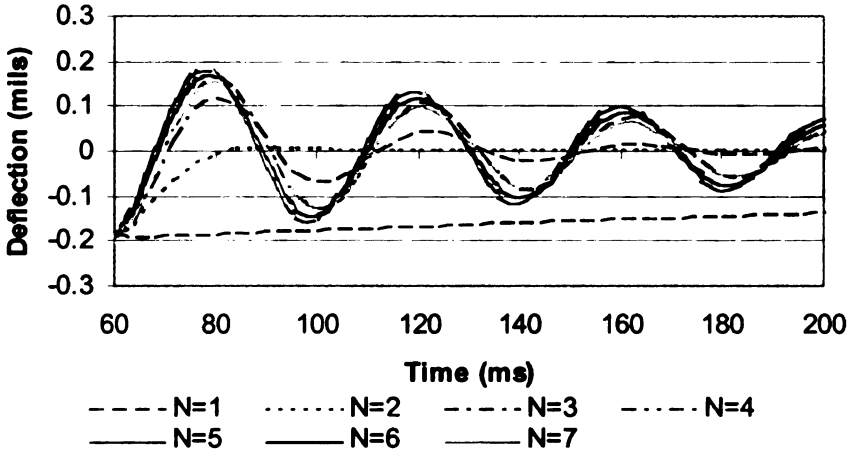

(b)

Figure 6.73 Comparison of different order extrapolations for sensor 3

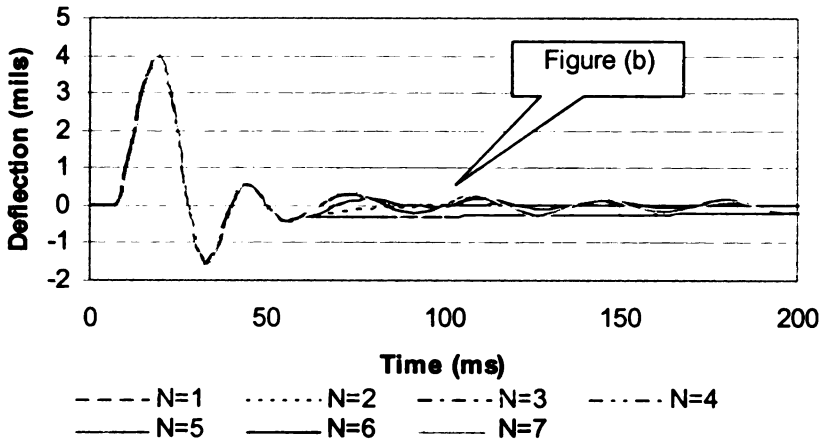

(a)

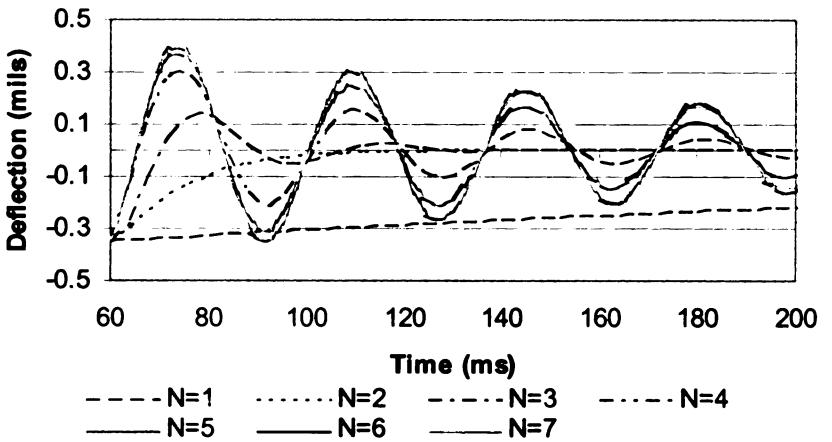

(b)

Figure 6.74 Comparison of different order extrapolations for sensor 4

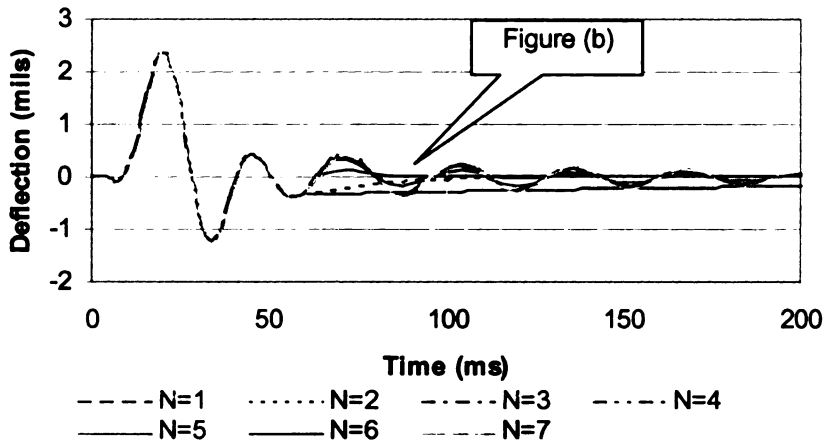

(a)

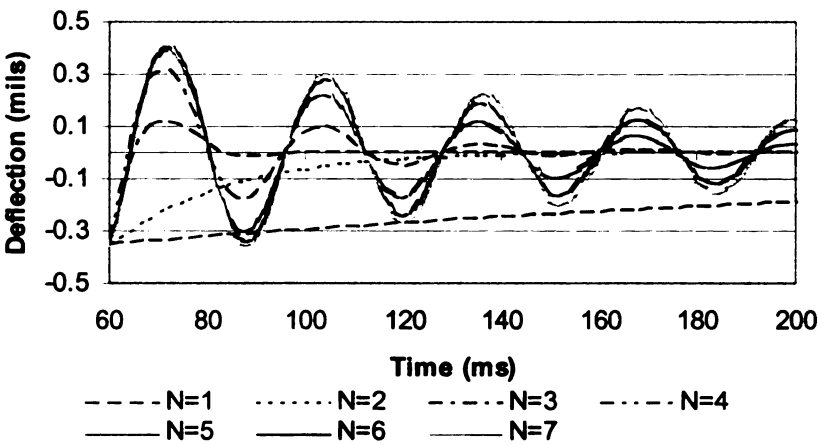

(b)

Figure 6.75 Comparison of different order extrapolations for sensor 5

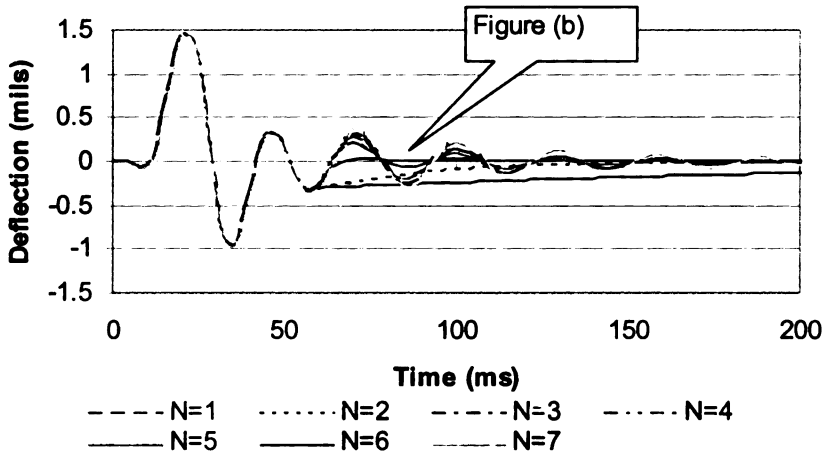

(a)

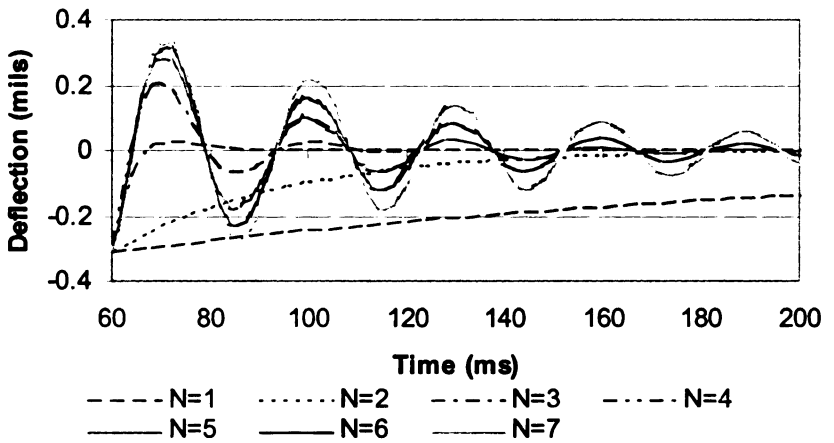

(b)

Figure 6.76 Comparison of different order extrapolations for sensor 6

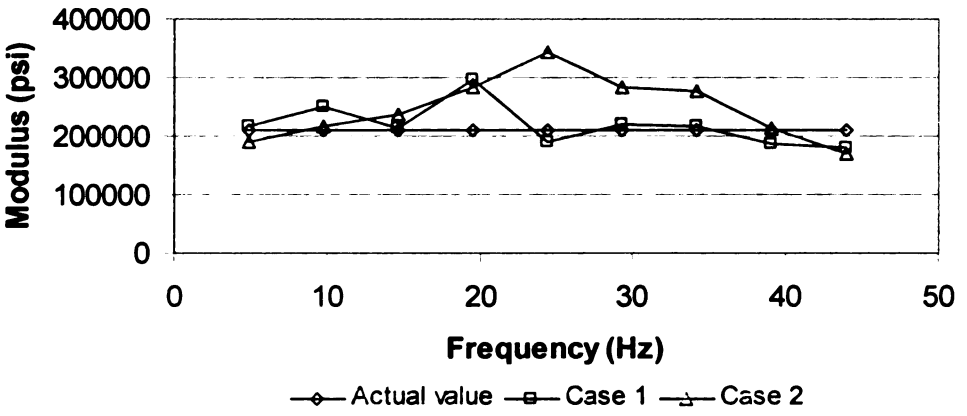

Figure 6.77 Effect of extrapolation on AC modulus backcalculation

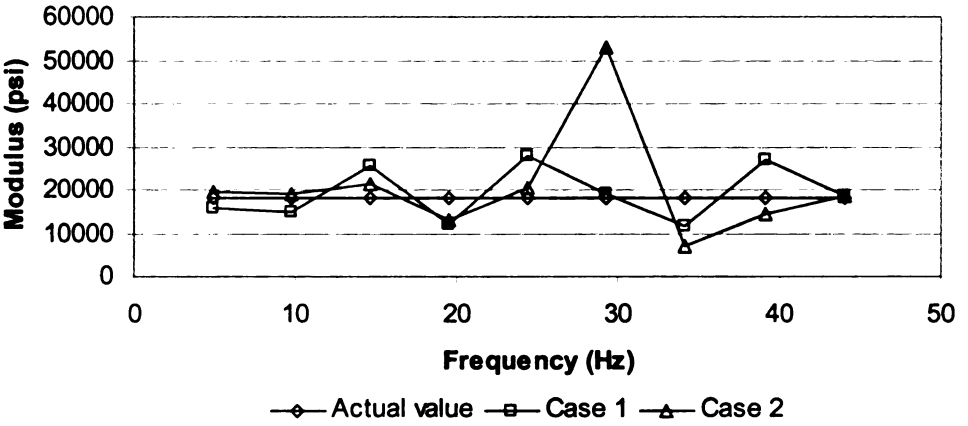

Figure 6.78 Effect of extrapolation on base modulus backcalculation

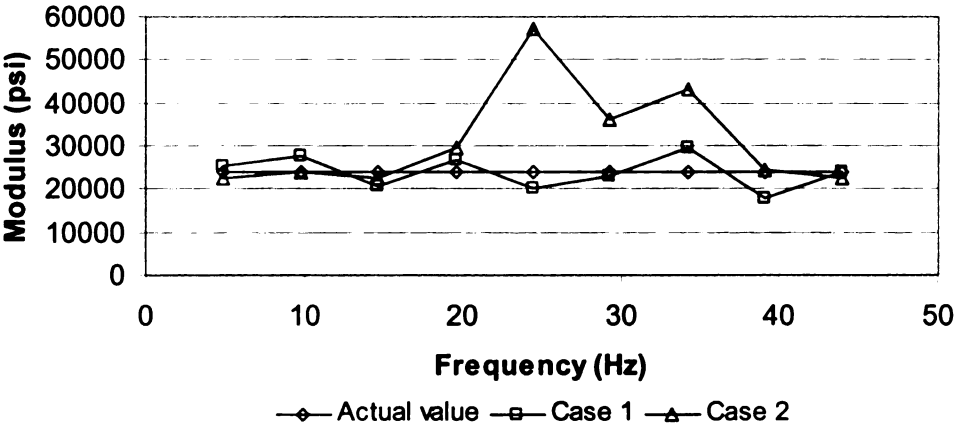

Figure 6.79 Effect of extrapolation on subgrade modulus backcalculation

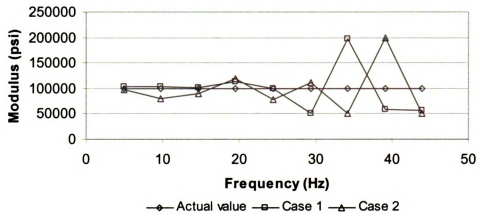

Figure 6.80 Effect of extrapolation on stiff layer modulus backcalculation

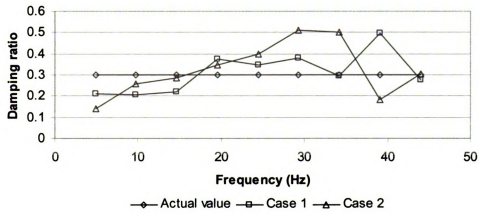

Figure 6.81 Effect of extrapolation on AC damping ratio backcalculation

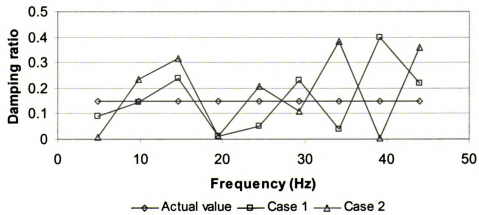

Figure 6.82 Effect of extrapolation on base damping ratio backcalculation

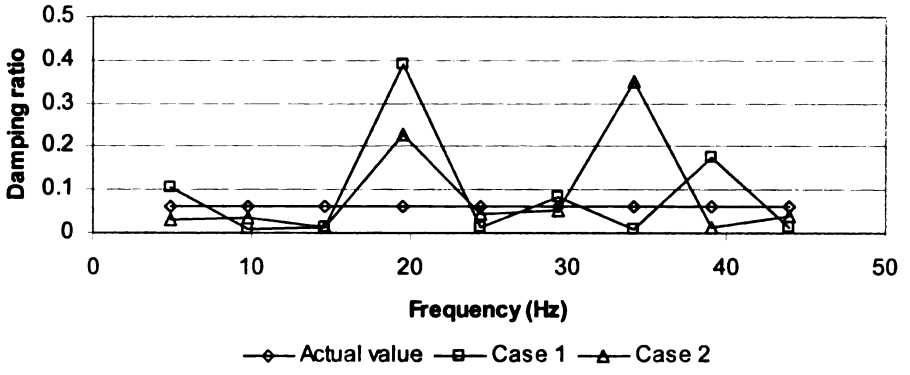

Figure 6.83 Effect of extrapolation on subgrade damping ratio backcalculation

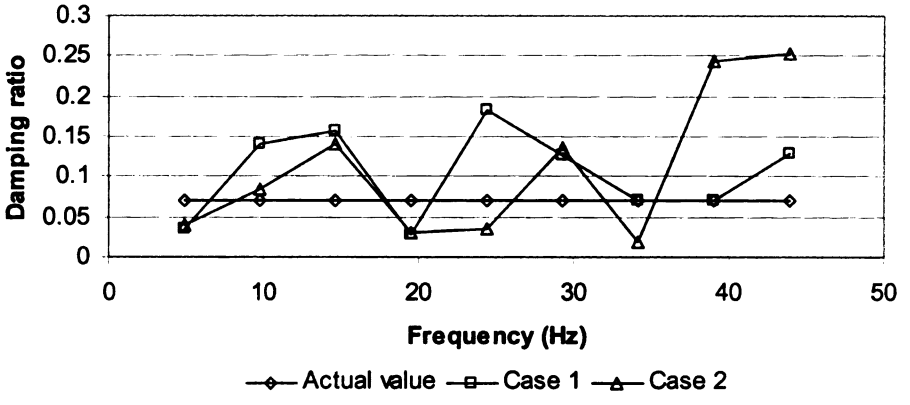

Figure 6.84 Effect of extrapolation on stiff layer damping ratio backcalculation

6.3.7 Comparison of Dynamic and Static Backcalculation Results

Although dynamic backcalculation of layer moduli from deflection time histories should be more realistic in identifying pavement moduli, deflection data collected from the FWD have mostly been analyzed by using the static layered analysis methods. In this section, the backcalculation results from static and dynamic backcalculation are compared. Time histories of surface deflections were generated using SAPSI. The peak load and deflection values were input in the MICHBACK program for static backcalculation. The pavement profiles used are those described above (see Table 6.11 and Table 6.13). The

results are shown in Table 6.19 and Table 6.20 for three-layer and four-layer pavement systems, respectively. The results indicate large differences in the static and dynamic backcalculated results. For the three-layer pavement system, MICHBACK overestimates the AC modulus by 4 to 29% and the subgrade modulus by 24% to 89%. The percent error for the base modulus varies from -42% to +33%. For the four-layer pavement system, the results from MICHBACK are not reliable, especially for the base and subbase layer moduli, where the base modulus is underestimated by a factor of 4 to 6, and the subbase modulus is overestimated by a factor of 2 to 9. It should be noted, however, that the forward solution in MICHBACK is the CHEVRONX static layered elastic program, which may produce very different results from those from SAPSI.

Table 6.19 Comparison of static and dynamic backcalculation results for three-layer pavement systems

Case	DYNABACK			MICHBACK		
	AC (ksi)	Base (ksi)	Subgrade (ksi)	AC (ksi)	Base (ksi)	Subgrade (ksi)
Soft AC modulus	300	45	7.5	342.8	59.7	10.6
Medium-stiff AC modulus	500	75	15	519.3	85.3	18.6
Stiff AC modulus	800	45	7.5	1034.9	35.2	11.8
Thin AC layer	600	45	7.5	563.9	59.4	9.6
Medium-thick AC layer	600	45	7.5	747.3	48.4	11.4
Thick AC layer	600	45	7.5	747.3	26.1	14.2

Table 6.20 Comparison of static and dynamic backcalculation results for four-layer pavement systems

Case	DYNABACK				MICHBACK			
	AC (ksi)	Base (ksi)	Subbase (ksi)	Subgrade (ksi)	AC (ksi)	Base (ksi)	Subbase (ksi)	Subgrade (ksi)
Med-stiff AC modulus	500	45	115	7.5	375.0	7.5	100.0	9.9
Stiff AC modulus	800	75	25	15	613.8	16.6	54.1	11.3

6.4 Time-domain Backcalculation using Peak Deflection and Time Lag

As mentioned above, FWD response time histories are often truncated in time and do not tend to zero at the end of the time window due to drifts in the measurement system. These inaccuracies can yield significant errors when transforming the measured data to the frequency-domain, and subsequently difficulties are encountered in the backcalculation. Time-domain backcalculation is more attractive than frequency-domain backcalculation because the inaccurate regions of the FWD response time histories can be ignored.

In order to minimize computational effort, only two pieces of information from the deflection time histories at each sensor are used: (a) the peak deflection, and (b) the time delay between the peak of the load and the peak of the deflection.

6.4.1 Sensitivity Analysis

The peak deflections are influenced by the layer stiffnesses and the time lags are influenced by the pavement inertia and damping characteristics. The profile used for this study is shown in Table 6.21. In order to investigate the relationship between the response characteristics (deflections and time lag) and layer properties (moduli, damping and thickness), a sensitivity analysis was conducted. The layer moduli of a four-layer flexible pavement section of medium AC thickness were varied and their effects on the calculated surface deflections and time lags were studied by plotting them against the layer moduli, damping ratio, and thickness (see Figure 6.85 through Figure 6.95). Six time histories were computed at the locations r = 0, 12, 24, 36, 48 and 60 inches from the load.

Table 6.21 Profiles used for the sensitivity analysis

Layer	Thickness (in)	Damping Ratio	Modulus (ksi)
AC	8	0.05	400
Base	12	0.03	40
Subgrade	55	0.02	30
Bedrock	∞	0.02	400

The following observations can be made:

1. For the AC layer, thickness has greater effect on deflection and time lag than modulus, and damping ratio. As thickness increased, the deflection decreased; however, the time lag may or may not increase for different sensors. As modulus increased, the deflection decreased, and the time lag may or may not increase for different sensors. As the damping ratio increased, the deflection increased.

2. For the base and subbase layers, the results are similar to those for the AC layer. Thickness has greater effect on deflection and time lag than modulus and damping ratio. Increasing the thickness or modulus resulted in decrease of the deflection, and the time lag either increased or decreased depending on the sensor. Increasing damping ratio resulted in an increase of the deflections as well as the time lags.

3. For subgrade layer, as modulus increased, the deflection and the time lag decreased. As damping ratio increased, the deflection and the time lag increased.

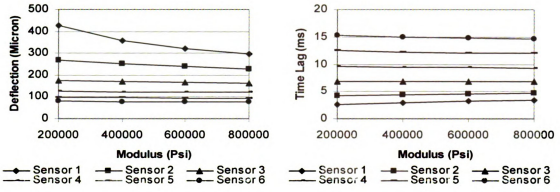

Figure 6.85 Effect of AC modulus on pavement deflection and time lag

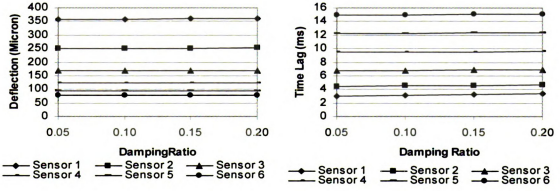

Figure 6.86 Effect of AC damping on pavement deflection and time lag

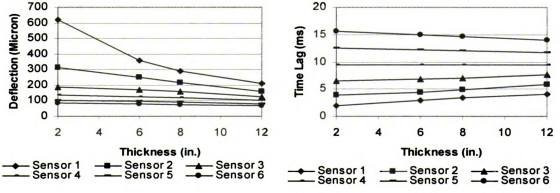

Figure 6.87 Effect of AC thickness on pavement deflection and time lag

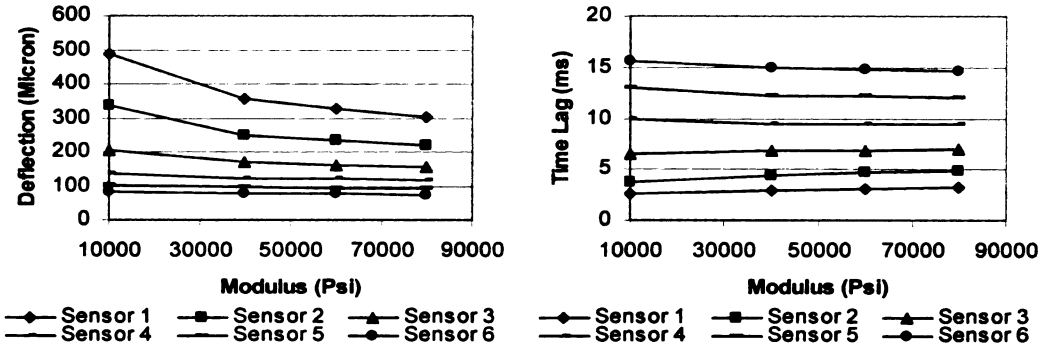

Figure 6.88 Effect of base modulus on pavement deflection and time lag

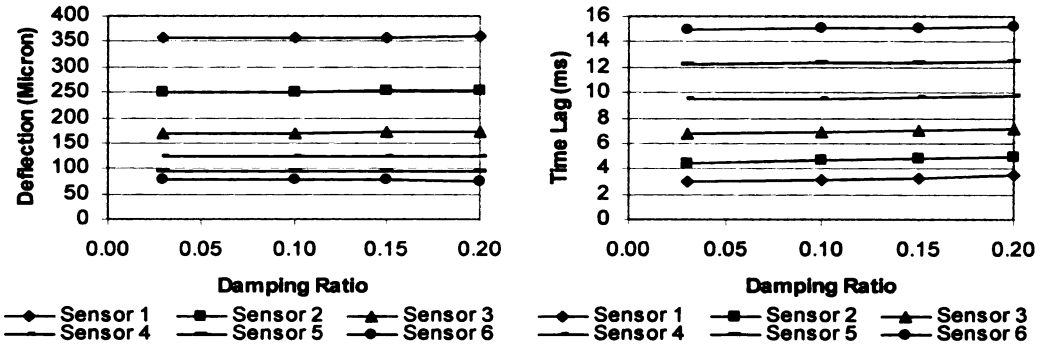

Figure 6.89 Effect of base damping on pavement deflection and time lag

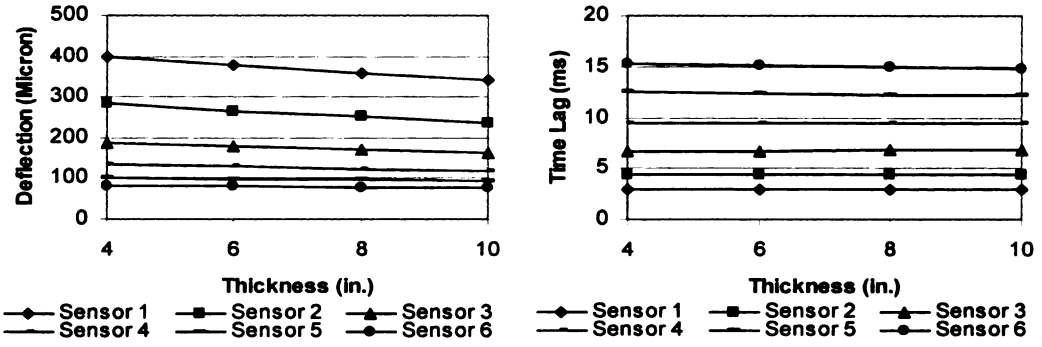

Figure 6.90 Effect of base thickness on pavement deflection and time lag

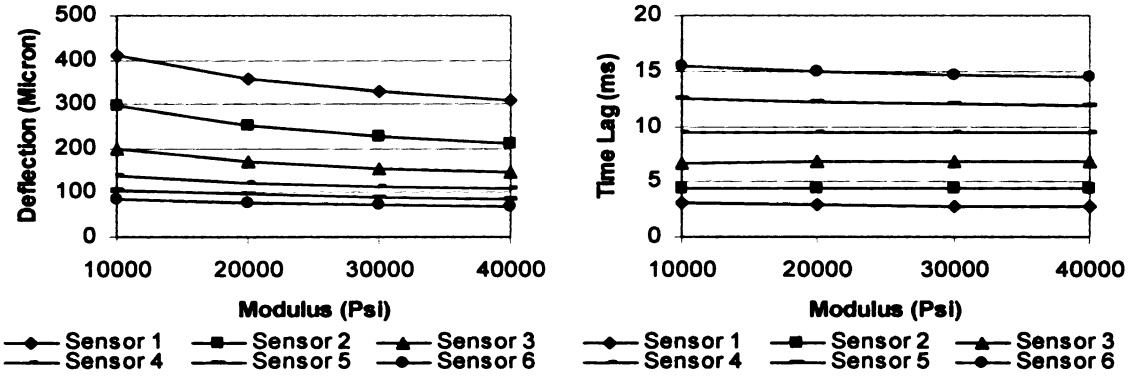

Figure 6.91 Effect of subbase modulus on pavement deflection and time lag

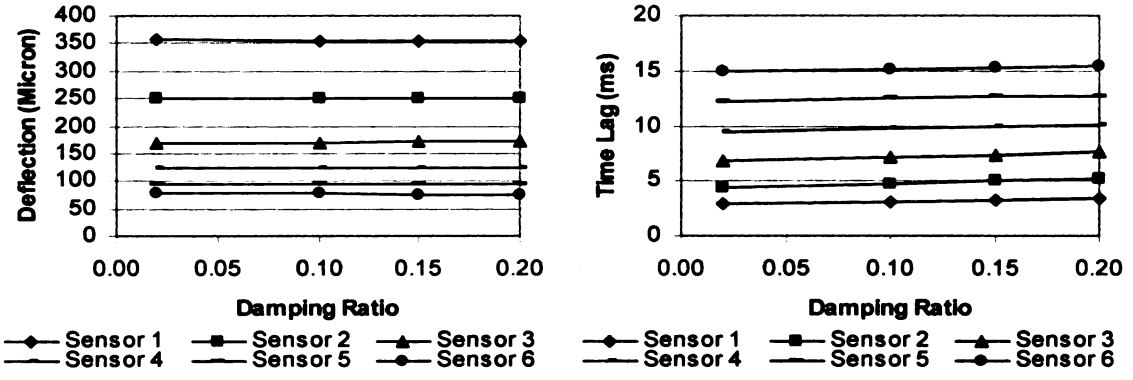

Figure 6.92 Effect of subbase damping on pavement deflection and time lag

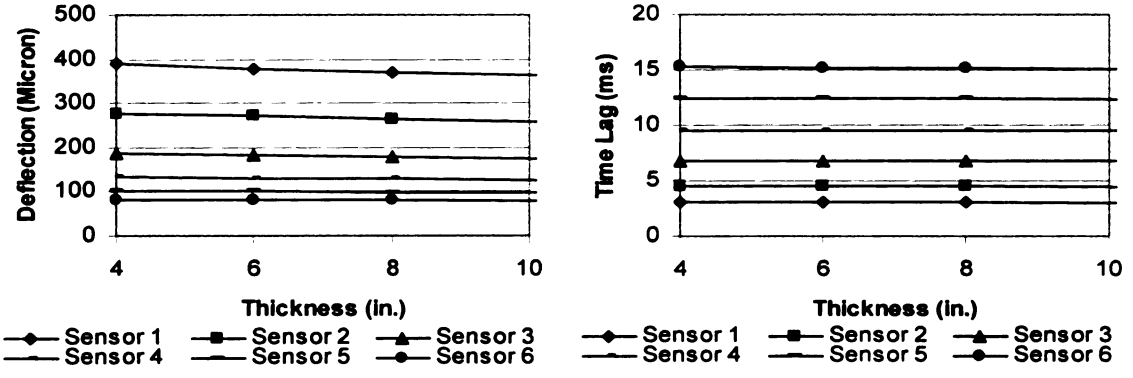

Figure 6.93 Effect of subbase thickness on pavement deflection and time lag

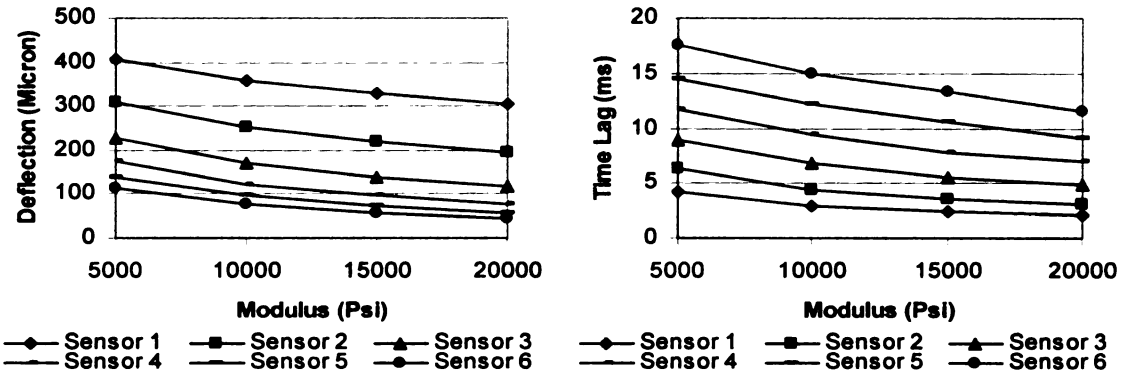

Figure 6.94 Effect of subgrade modulus on pavement deflection and time lag

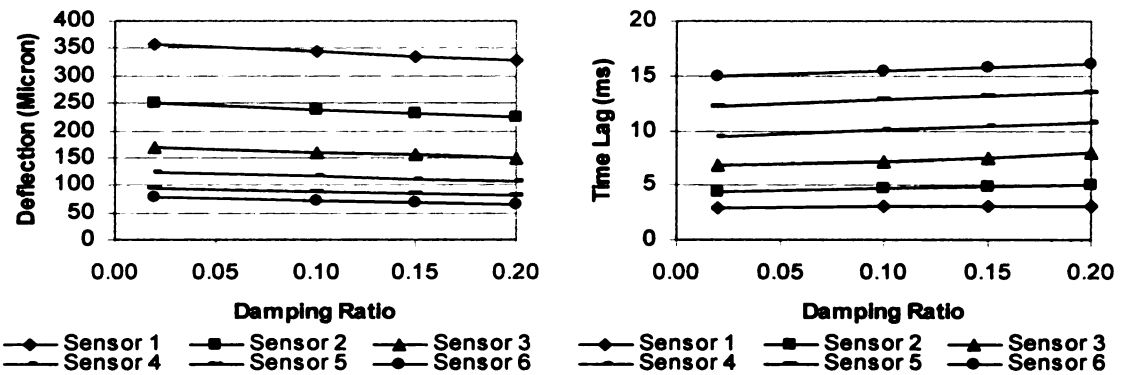

Figure 6.95 Effect of subgrade damping on pavement deflection and time lag

6.4.2 Theoretical Verification

Synthetic FWD data were generated for several pavement structures consisting of asphalt, base and subgrade layers using the SAPSI computer program. The pavement profiles are given in Table 6.22. The computed vertical displacement time histories obtained from the SAPSI program were used as input for the backcalculation. Seven time histories were computed at the locations r = 0, 8, 12, 18, 24, 36, and 60 inches from the load.

Table 6.22 Pavement profiles for synthetic data

Profile	Layer Name	Thickness (in.)	Modulus (ksi)	Damping Ratio	Unit Weight (pcf)	Poisson's Ratio
Profile 1	AC	7.2	250	.10	145	0.3
	Base	10	30	.03	135	0.35
	Subgrade	∞	10	.02	125	0.45
Profile 2	AC	4	250	.10	145	0.35
	Base	36	20	.03	135	0.35
	Subgrade	∞	10	.03	125	0.4
Profile 3	AC	8	400	.075	145	0.35
	Base	12	30	.02	135	0.35
	Subgrade	∞	5	.05	125	0.45
Profile 4	AC	12	600	.05	145	0.35
	Subgrade	60	10	.03	135	0.4
	Stiff layer	∞	500	.01	125	0.2
Profile 5	AC	12	500	.05	145	0.35
	Base	30	10	.03	135	0.4
	Sat. subgrade	∞	44.1	.01	125	0.48

Two types of dynamic backcalculation were performed: (a) Estimation of the layer moduli and damping ratios using the correct thicknesses, and (b) estimation of the layer moduli, damping ratios and thicknesses. Static backcalculation using MICHBACK (10) was also per-formed using the peak deflections from the synthetic time histories of Profile 1. Table 6.23 shows the static and dynamic backcalculation results for Profile 1. The percentage errors for each back-calculated parameter are shown within parentheses. Using dynamic analysis, the backcalculated layer moduli and damping ratios are essentially exact if the thicknesses are assumed to be known. Errors occur if the thicknesses are also backcalculated, but the impact of these errors is small. For the latter case, the errors in the backcalculated moduli and thicknesses are within 2%. The errors in the backcalculated damping ratios are as high as 33%, but the impact of this on the time histories is negligible since the damping ratios are small to begin with. Also, since the damping ratios are not used at present in pavement rehabilitation decisions, these errors are not significant in practice.

Table 6.23 Comparison of dynamic and static backcalculation results using synthetic data for profile 1

	True Value	Seed Value	Dynamic Backcalculation				Static Backcalculation (MICHBACK)	
			Known Layer Thicknesses Case (a)		Unkown Layer Thicknesses Case (b)			
AC modulus (ksi)	250	450	250.0	(0%)	250.8	(0.3%)	207.7	(-16.9%)
AC damping ratio	0.1	0.3	0.099	(0%)	0.10	(0.0%)	—*	
AC thickness (in.)	7.2	12	—		7.23	(0.4%)	—	
Base modulus (ksi)	30	70	29.99	(0%)	29.43	(-1.9%)	39.50	(31.7%)
Base damping ratio	0.03	0.1	0.03	(0%)	0.02	(-33%)	—	
Base thickness (in.)	10	15	—		10.10	(-1.1%)	—	
Subgrade modulus (ksi)	10	70	10.0	(0%)	10.0	(0%)	10.15	(1.5%)
Subgr. damping ratio	0.02	0.1	0.02	(0%)	0.022	(10.0%)	—	

* Results are not applicable

A sensitivity analysis (not shown here for brevity) revealed that peak deflections and time lags were least sensitive to damping ratios. Deflections were more sensitive to modulus than to thickness, and time lags were mostly sensitive to AC thickness and subgrade moduli.

The static backcalculation (from MICHBACK) underestimates the AC modulus by 16.9% and compensates for this by overestimating the base modulus by 31.7%. These errors are partly due to the fact that the forward analysis routine in MICHBACK is the CHEVRONX pro-gram, which produces slightly different results than those from SAPSI.

Table 6.24 shows dynamically backcalculated pavement layer parameters for profiles 2 through 5, when layer thicknesses are known. The percentage errors for each backcalculated parameter are shown within parentheses. The backcalculated layer moduli and damping ratios are essentially exact for three of the four profiles. For profile 4, where there is a stiff layer with a modulus of 500 ksi, there are large errors in the backcalculated damping ratios as well as in the modulus of the stiff layer. The errors are not of practical

significance, though, since damping ratios are very small and the stiff layer modulus is high. More importantly, the errors in backcalculated AC, base and subgrade moduli are within 2%. The RMS errors for all cases are very low, and the convergence rate was good except for profile 4. Table 6.25 shows dynamically backcalculated pavement layer parameters for profiles 2 through 5, when layer thicknesses are unknown. The backcalculated layer moduli, damping ratios and thicknesses are essentially exact for profiles 2 and 3. However, large errors occur for profiles 4 and 5. The highest errors observed are for profile 4, which has a stiff layer condition with unknown modulus value. Note that if this value is given, then the solution converges with very accurate results. For profile 5, which has a saturated subgrade (simulating a ground water table condition), the results are not as good as those for profiles 2 and 3, but much better than those for profile 5. This is because while a ground water table does present a stiff layer condition, the stiff layer modulus is not nearly as high as that of profile 5. Finally, as expected, the RMS errors are somewhat higher when layer thicknesses are backcalculated; however, all cases except for profile 4 converged.

Table 6.24 Dynamic backcalculation results (known thickness) using synthetic data for profiles 2 through 5

	Profile 2		Profile 3		Profile 4		Profile 5	
	True values	Results	True values	Results	True values	Results	True values	Results
AC modulus (ksi)	250	250 (0.0%)	400	399 (-0.2%)	600	608 (1.4%)	500	500 (0.0%)
AC damping ratio	0.1	0.10 (0.0%)	0.075	0.07 (-6.7%)	0.05	0.03 (-40%)	0.05	0.05 (0.0%)
Base modulus (ksi)	20	20.0 (0.0%)	30	30.0 (0.0%)	10	9.8 (-2%)	10	10.0 (0.0%)
Base damping ratio	0.03	0.03 (0.0%)	0.02	0.02 (0.0%)	0.03	0.05 (67%)	0.03	0.03 (0.0%)
Subgrade modulus (ksi)	10	10.0 (0.0%)	5	5.0 (0.0%)	500	661.7 (32%)	44.1	44.0 (-0.2%)
Subgrade damping ratio	0.03	0.03 (0.0%)	0.05	0.05 (0.0%)	0.01	0.04 (300%)	0.01	0.01 (0.0%)
No. of iterations	10		8		30		11	
RMS	0.02%		0.17%		0.8%		0.09%	

Table 6.25 Dynamic backcalculation results (unknown thickness) using synthetic data for profiles 2 through 5

	Profile 2		Profile 3		Profile 4		Profile 5	
	True values	Results	True values	Results	True values	Results	True values	Results
AC modulus (ksi)	250	243 (-2.8%)	400	400 (0.0%)	600	568 (-5%)	500	501 (0.2%)
AC damping	0.1	0.1 (0.0%)	0.075	0.072 (-4%)	0.05	0.01 (-80%)	0.05	0.06 (20%)
AC Thickness	4	4.0 (0.0%)	8	8.0 (0.0%)	12	12.8 (6.7%)	12	12.0 (0.0%)
Base modulus (ksi)	20	20.0 (0.0%)	30	30.0 (0.0%)	10	6.0 (-40%)	10	10.7 (7%)
Base damping	0.03	0.03 (0.0%)	0.02	0.02 (0.0%)	0.03	0.11 (266%)	0.03	0.01 (-66%)
Base Thickness	36	35.9 (-0.3%)	12	12.0 (0.0%)	60	42.4 (-29%)	30	32.0 (6%)
Subgrade modulus (ksi)	10	10.0 (0.0%)	5	5.0 (0.0%)	500	2015 (303%)	44.1	44.0 (-0.2%)
Subgrade damping	0.03	0.03 (0.0%)	0.05	0.05 (0.0%)	0.01	0.10 (900%)	0.01	0.02 (100%)
No. of iterations	13		19		30		13	
RMS	0.77%		0.02%		1.9%		0.79%	

6.4.3 Uniqueness

Synthetic FWD data were generated for a pavement structure consisting of asphalt, base and subgrade layers using SAPSI. The profile 1 provided in Table 6.22 was used. The computed vertical displacement time histories obtained from SAPSI were used as input for the backcalculation process. Seven time histories were computed at the locations r = 0, 8, 12, 18, 24, 36, and 60 inches from the load. Table 6.26 and Table 6.27 summarize the results with and without thickness backcalculation using different seed values. The results show that the backcalculated moduli and thicknesses are independent of seed values, proving the uniqueness of the solution. For damping, the differences covered by

varying the seed values are higher, although they are not of practical significance since the damping ratios vary between 1% and 3% and their effect in the response is negligible.

Table 6.26 Uniqueness of results without thickness backcalculation

	Case 1		Case 2		Case 3	
	Seed value	Results	Seed value	Results	Seed value	Results
AC modulus	450	250.0 (0%)	80	247.2 (-1.12%)	350	248.0 (-0.8%)
AC damping	0.3	0.099 (-1.0%)	0.01	0.101 (1.0%)	0.2	0.099 (-0.1%)
Base modulus	70	29.99 (-0.03%)	10	29.97 (-0.1%)	20	30.05 (0.17%)
Base damping	0.1	0.030 (0.0%)	0.01	0.028 (6.67%)	0.01	0.031 (3.33%)
Subgrade modulus	70	10.00 (0.0%)	4	9.97 (-0.3%)	20	9.97 (-0.3%)
Subgrade damping	0.1	0.020 (0.0%)	0.01	0.020 (0.0%)	0.01	0.019 (5.0%)

Table 6.27 Uniqueness of results when thickness backcalculation is enabled

	Case 1		Case 2		Case 3	
	Seed value	Results	Seed value	Results	Seed value	Results
AC modulus	450	250.5 (0.2%)	80	250.4 (0.2%)	350	250.2 (0.1%)
AC damping	0.3	0.11 (10%)	0.01	0.15 (50%)	0.2	0.11 (10%)
AC Thickness	12	7.23 (0.4%)	4	7.34 (1.9%)	8.0	7.2 (0.0%)
Base modulus	70	29.66 (1.1%)	10	28.9 (-3.7%)	20	30.0 (0.0%)
Base damping	0.1	0.02 (-33.3%)	0.01	0.01 (-66.7%)	0.01	0.02 (-33.3%)
Base Thickness	15	9.82 (-1.8%)	5	10.0 (0.0%)	7.0	9.9 (1.0%)
Subgrade modulus	70	10.00 (0%)	4	10.0 (0.0%)	20	10.0 (0.0%)
Subgrade damping	0.1	0.027 (35%)	0.01	0.01 (50%)	0.01	0.017 (-15.0%)

6.4.4 Convergence Characteristics

The convergence characteristics were studied using synthetic data. Figure 6.96 through Figure 6.101 show convergence plots for layer moduli, damping ratios and thicknesses with and without thickness backcalculation when using different seed values. When the layer thicknesses are fixed, the solution converges within 10 iterations. When including thickness backcalculation, the solution converges within 10 to 20 iterations. These results show excellent convergence characteristics even when layer thicknesses are backcalculated, with the convergence rate being slightly faster for the cases when layer thicknesses are not backcalculated.

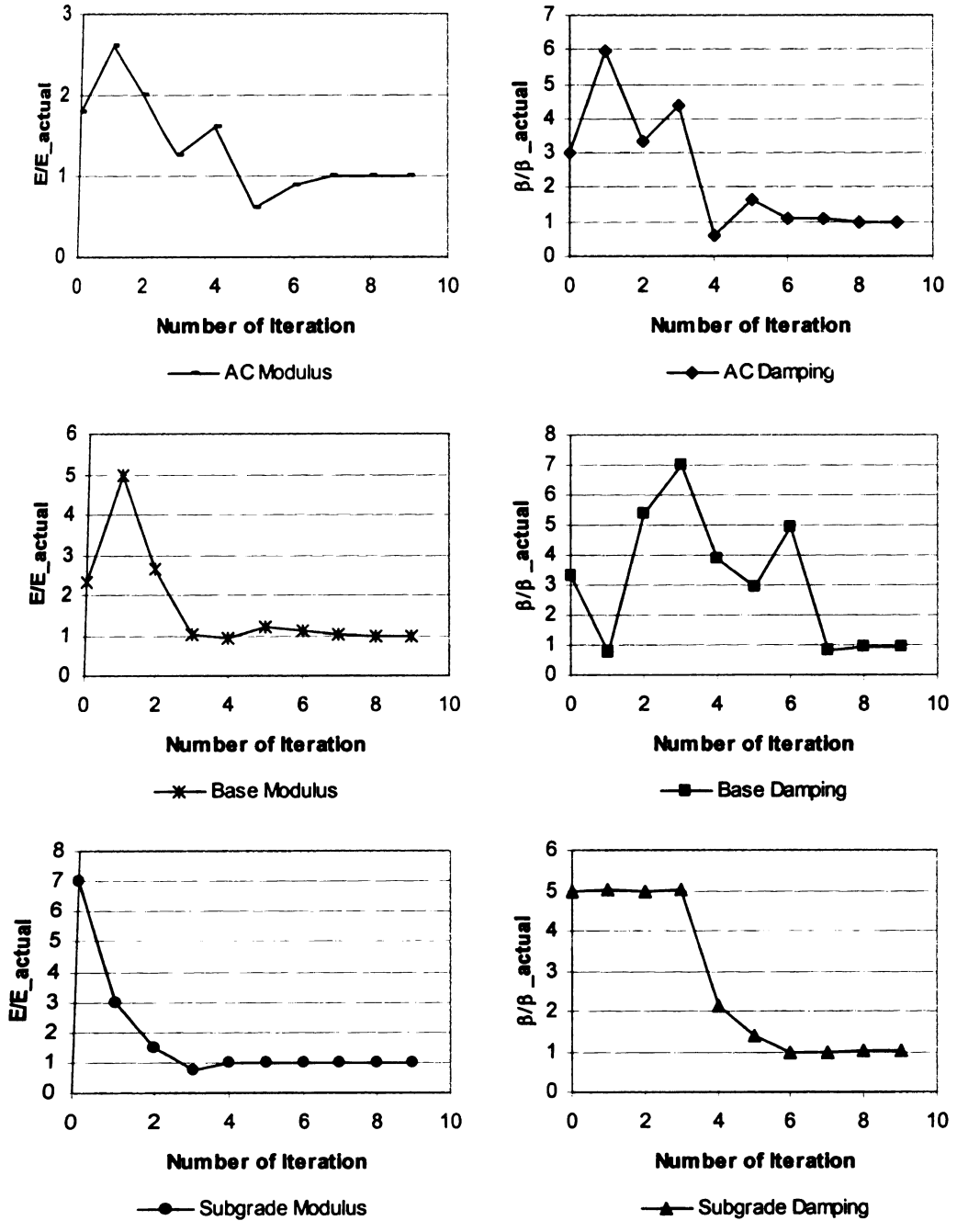

Figure 6.96 Convergence of layer parameters for case 1 (no-thickness backcalculation)

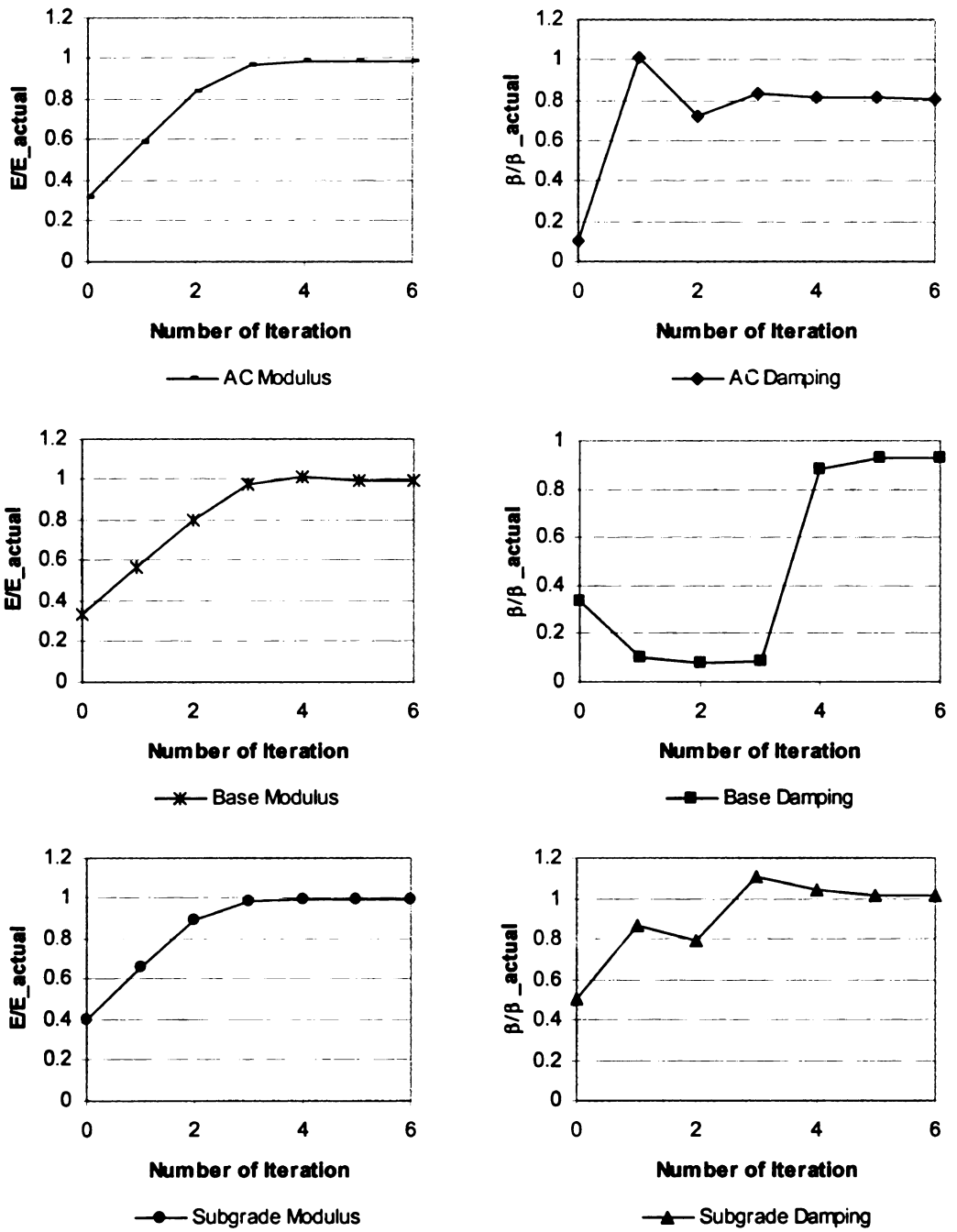

Figure 6.97 Convergence of layer parameters for case 2 (no-thickness backcalculation)

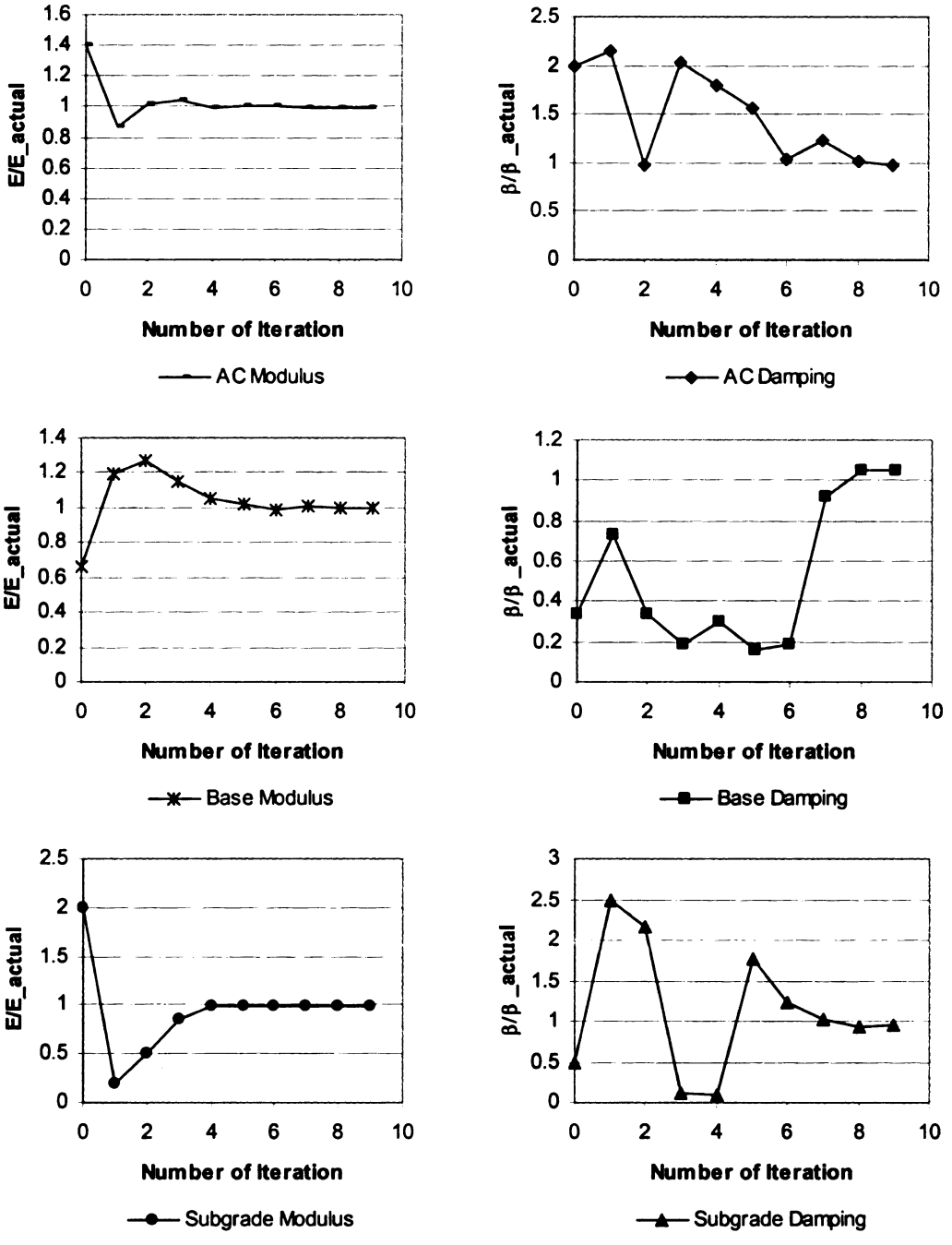

Figure 6.98 Convergence of layer parameters for case 3 (no-thickness backcalculation)

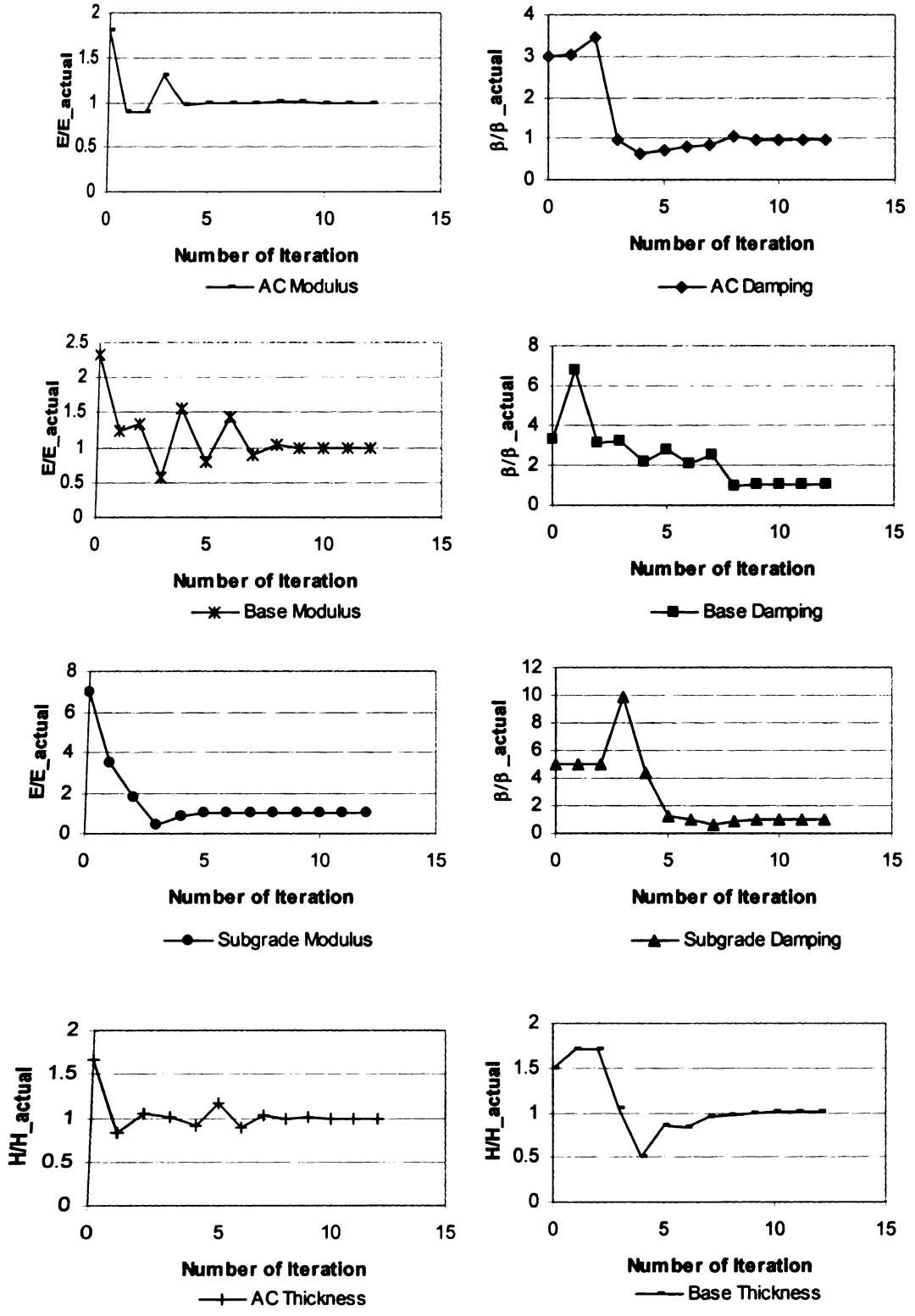

Figure 6.99 Convergence of layer parameters for case 1 (thickness backcalculation)

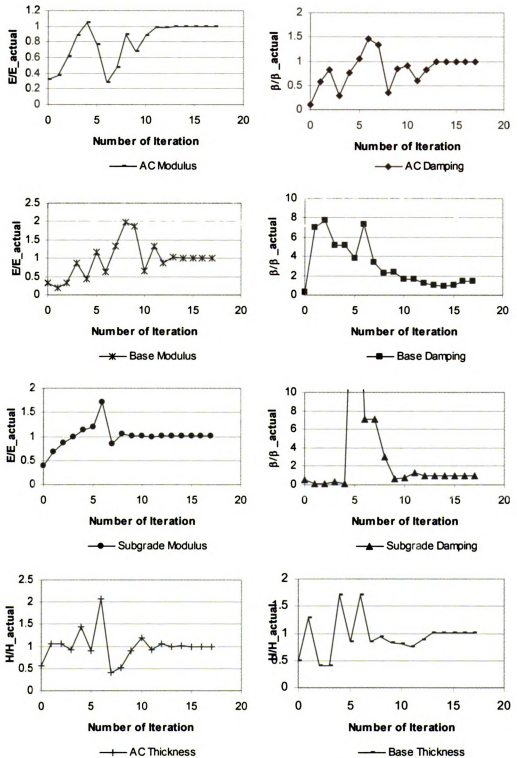

Figure 6.100 Convergence of layer parameters for case 2 (thickness backcalculation)

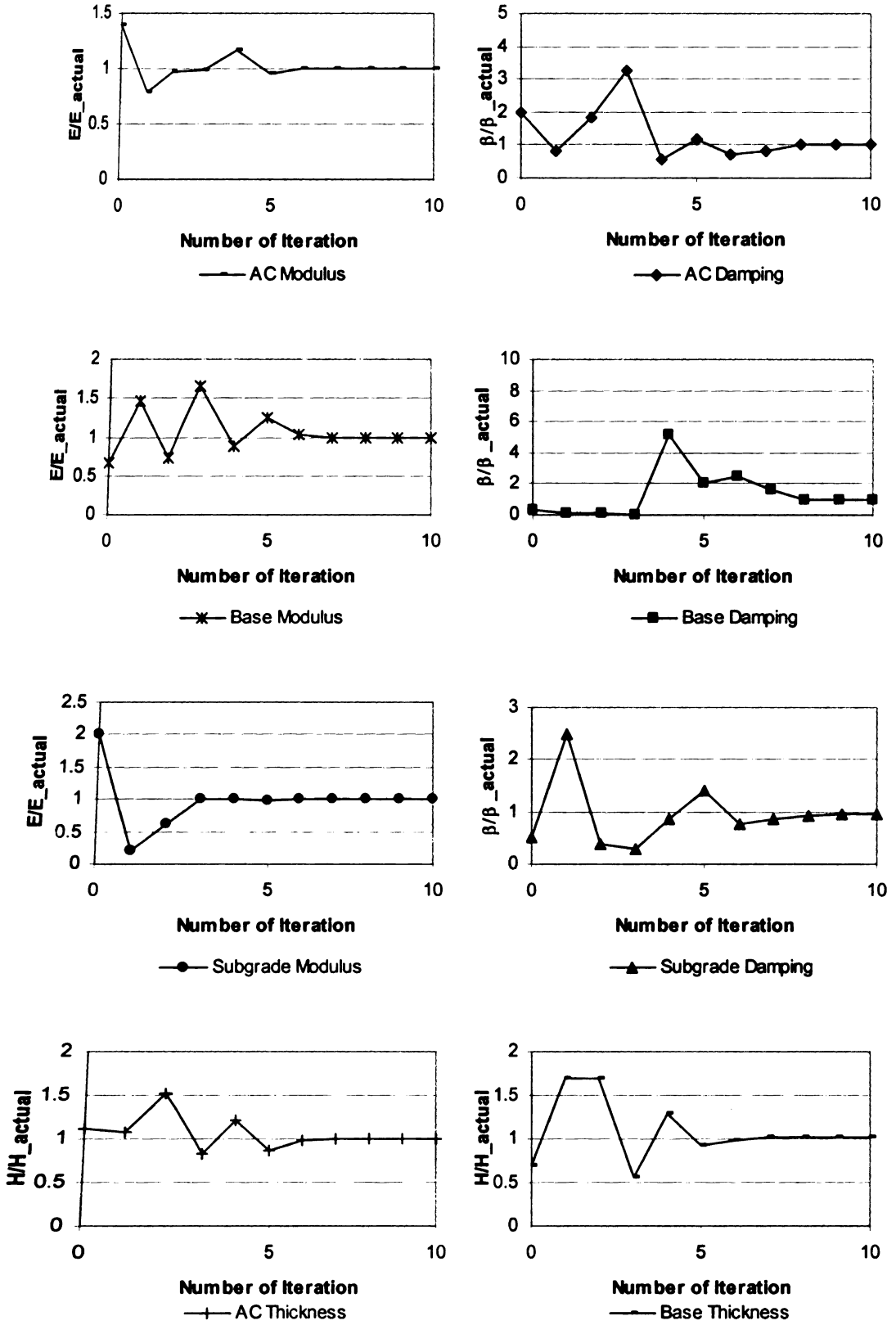

Figure 6.101 Convergence of layer parameters for case 3 (thickness backcalculation)

6.5 Time Domain Backcalculation using Traces of Time History

6.5.1 Theoretical Verification

Synthetic FWD data from pavement profiles in Table 6.22 were used in this section for theoretical verification. Table 6.28 shows the pavement layer parameters for profiles 2 through 5, when layer thicknesses are known. The percentage errors for each back-calculated parameter are shown within parentheses. The backcalculated layer moduli and damping ratios are excellent for all cases. It is noted that profile 4, which has a stiff layer condition, has the largest error (5%), and the corresponding RMS is 0.06%.Table 6.29 shows dynamically backcalculated pavement layer parameters for profiles 2 through 5, when layer thicknesses are unknown. It shows that all cases except profile 4 are excellent in identifying the parameters. Case 4 has a stiff layer condition, which makes it harder to backcalculate the parameters. However, all cases converged.

Table 6.28 Dynamic backcalculation results (known thickness) using synthetic data for profiles 2 through 5

	Profile 2		Profile 3		Profile 4		Profile 5	
	True values	Results	True values	Results	True values	Results	True values	Results
AC modulus (ksi)	250	250 (0.0%)	400	400 (0.0%)	600	600.2 (0.0%)	500	500 (0.0%)
AC damping ratio	0.1	0.10 (0.0%)	0.075	0.075 (0.0%)	0.05	0.05 (0.0%)	0.05	0.05 (0.0%)
Base modulus (ksi)	20	20.0 (0.0%)	30	30.0 (0.0%)	10	10 (0.0%)	10	10.0 (0.0%)
Base damping ratio	0.03	0.03 (0.0%)	0.02	0.02 (0.0%)	0.03	0.032 (6.7%)	0.03	0.03 (0.0%)
Subgrade modulus (ksi)	10	10.0 (0.0%)	5	5.0 (0.0%)	500	523 (5%)	44.1	44.1 (0.0%)
Subgrade damping ratio	0.03	0.03 (0.0%)	0.05	0.05 (0.0%)	0.01	0.01 (0.0%)	0.01	0.01 (0.0%)
No. of iterations	10		9		15		10	
RMS	0.00%		0.00%		0.06%		0.00%	

Table 6.29 Dynamic backcalculation results (unknown thickness) using synthetic data for profiles 2 through 5

	Profile 2		Profile 3		Profile 4		Profile 5	
	True values	Results	True values	Results	True values	Results	True values	Results
AC modulus (ksi)	250	250 (0.0%)	400	400 (0.0%)	600	500 (0.0%)	500	500 (0.0%)
AC damping	0.1	0.1 (0.0%)	0.075	0.072 (-4%)	0.05	0.005 (0.0%)	0.05	0.05 (0.0%)
AC Thickness	4	4.0 (0.0%)	8	8.0 (0.0%)	12	12.8 (0.0%)	12	12.0 (0.0%)
Base modulus (ksi)	20	20.0 (0.0%)	30	30.0 (0.0%)	10	6.0 (0.0%)	10	10.0 (0.0%)
Base damping	0.03	0.03 (0.0%)	0.02	0.02 (0.0%)	0.03	0.03 (0.0%)	0.03	0.03 (0.0%)
Base Thickness	36	36 (0.0%)	12	12.0 (0.0%)	60	60 (0.0%)	30	30.0 (0%)
Subgrade modulus (ksi)	10	10.0 (0.0%)	5	5.0 (0.0%)	500	466.1 (6.8%)	44.1	44.1 (-0.0%)
Subgrade damping	0.03	0.03 (0.0%)	0.05	0.05 (0.0%)	0.01	0.01 (0.0%)	0.01	0.01 (0.0%)
No. of iterations	12		11		19		16	
RMS	0.00%		0.00%		0.07%		0.00%	

6.5.2 Uniqueness

In this subsection, profile 1 provided in Table 6.22 was used for checking the uniqueness of the backcalculated parameters, Table 6.28 and Table 6.29 show that the method using traces of time histories can coverage to the true value successfully, and has more accurate results than that using peak deflection and time lag. Therefore, it is believed that backcalculation using traces of time histories is superior to other methods.

Table 6.30 Uniqueness of results without thickness backcalculation using traces of time histories

	Seed value	Results	Seed value	Results	Seed value	Results
AC modulus	450	250.0 (0.0%)	80	250.0 (0.0%)	350	250.0 (0.0%)
AC damping	0.3	0.1 (0.0%)	0.01	0.1 (0.0%)	0.2	0.1 (0.0%)
Base modulus	70	30.00 (0.0%)	10	300.0 (0.0%)	20	300.0 (0.0%)
Base damping	0.1	0.030 (0.0%)	0.01	0.030 (0.0%)	0.01	0.030 (0.0%)
Subgrade modulus	70	10.00 (0.0%)	4	10.00 (0.0%)	20	10.00 (0.0%)
Subgrade damping	0.1	0.020 (0.0%)	0.01	0.020 (0.0%)	0.01	0.020 (0.0%)

Table 6.31 Uniqueness of results when thickness backcalculation is enabled using traces of time histories

	Seed value	Results	Seed value	Results	Seed value	Results
AC modulus	450	250.0 (0.0%)	80	250.0 (0.0%)	350	250.0 (0.0%)
AC damping	0.3	0.1 (0.0%)	0.01	0.1 (0.0%)	0.2	0.1 (0.0%)
AC Thickness	12	7.20 (0.0%)	4	7.20 (0.0%)	8.0	7.20 (0.0%)
Base modulus	70	30.00 (0.0%)	10	30.00 (0.0%)	20	30.00 (0.0%)
Base damping	0.1	0.030 (0.0%)	0.01	0.030 (0.0%)	0.01	0.030 (0.0%)
Base Thickness	15	10.00 (0.0%)	5	10.00 (0.0%)	7.0	10.00 (0.0%)
Subgrade modulus	70	10.00 (0.0%)	4	10.00 (0.0%)	20	10.00 (0.0%)
Subgrade damping	0.1	0.02 (0.0%)	0.01	0.02 (0.0%)	0.01	0.02 (0.0%)

6.5.3 Convergence Characteristics

The convergence characteristics of time domain solution are studied in this section using the pavement profile listed in Table 6.22. Figure 6.102 through Figure 6.110 show the convergence plots for layer moduli, damping ratios and thickness with and without

thickness backcalculation when using different seed values. It shows that the backcalculated parameters can converge to the true value within a few iterations, and that the number of iterations when layer thicknesses are known is less than cases for unknown layer. This conclusion is similar to that made for the method using peak deflection and time lag.

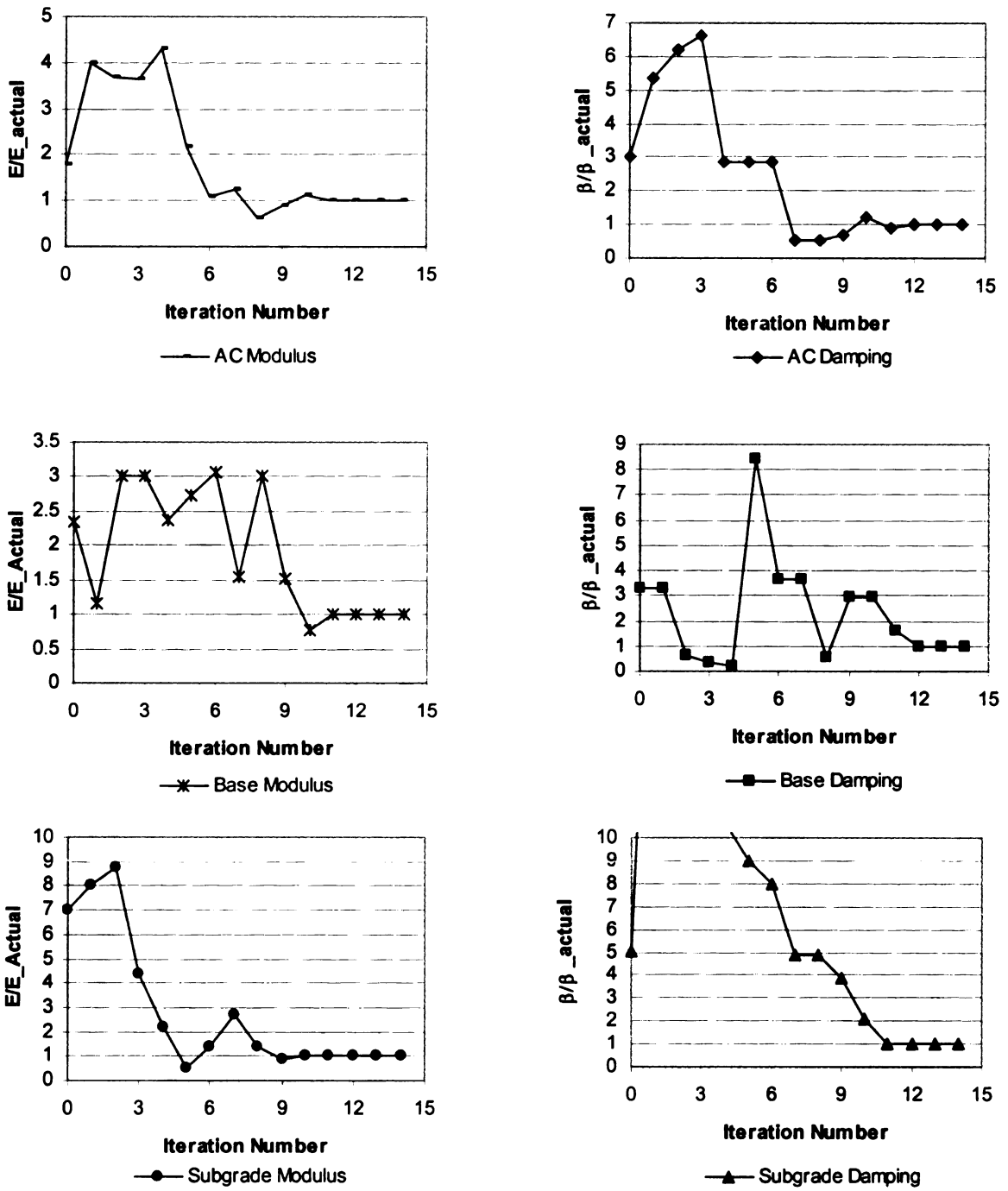

Figure 6.102 Convergence of layer parameters for case 1 (no-thickness backcalculation)

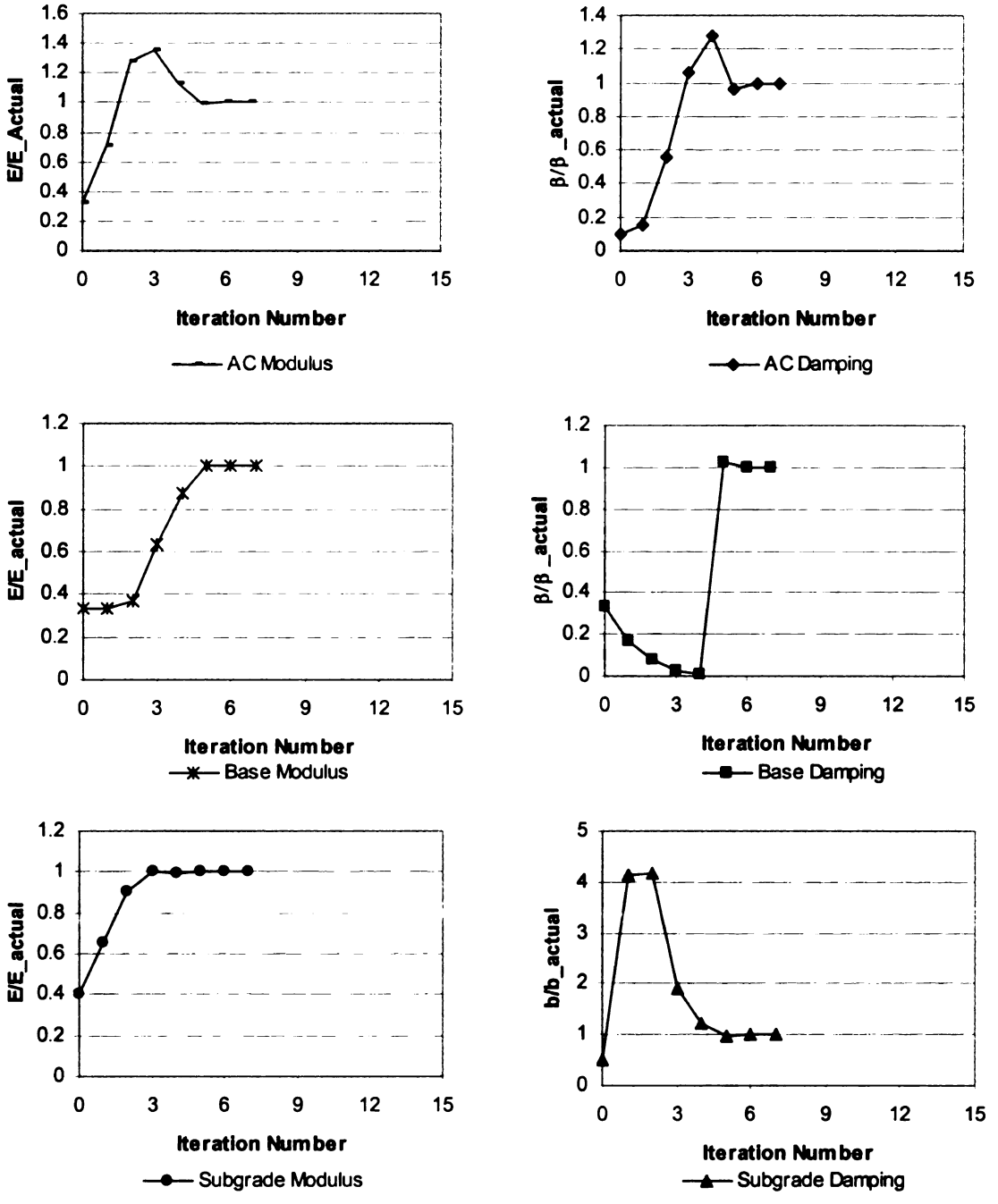

Figure 6.103 Convergence of layer parameters for case 2 (no-thickness backcalculation)

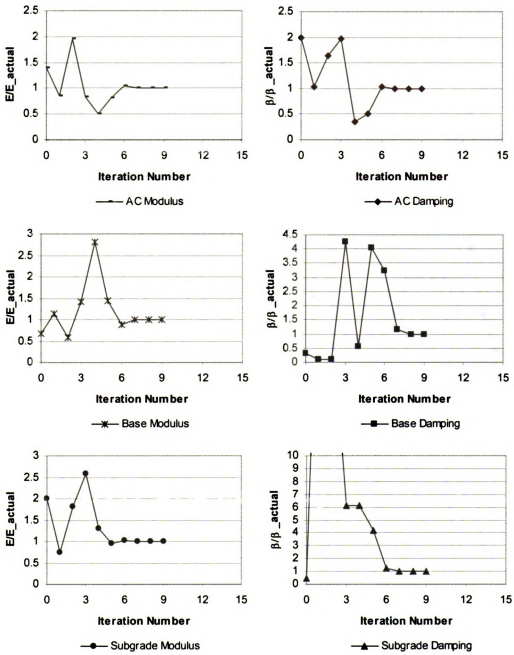

Figure 6.104 Convergence of layer parameters for case 3 (no-thickness backcalculation)

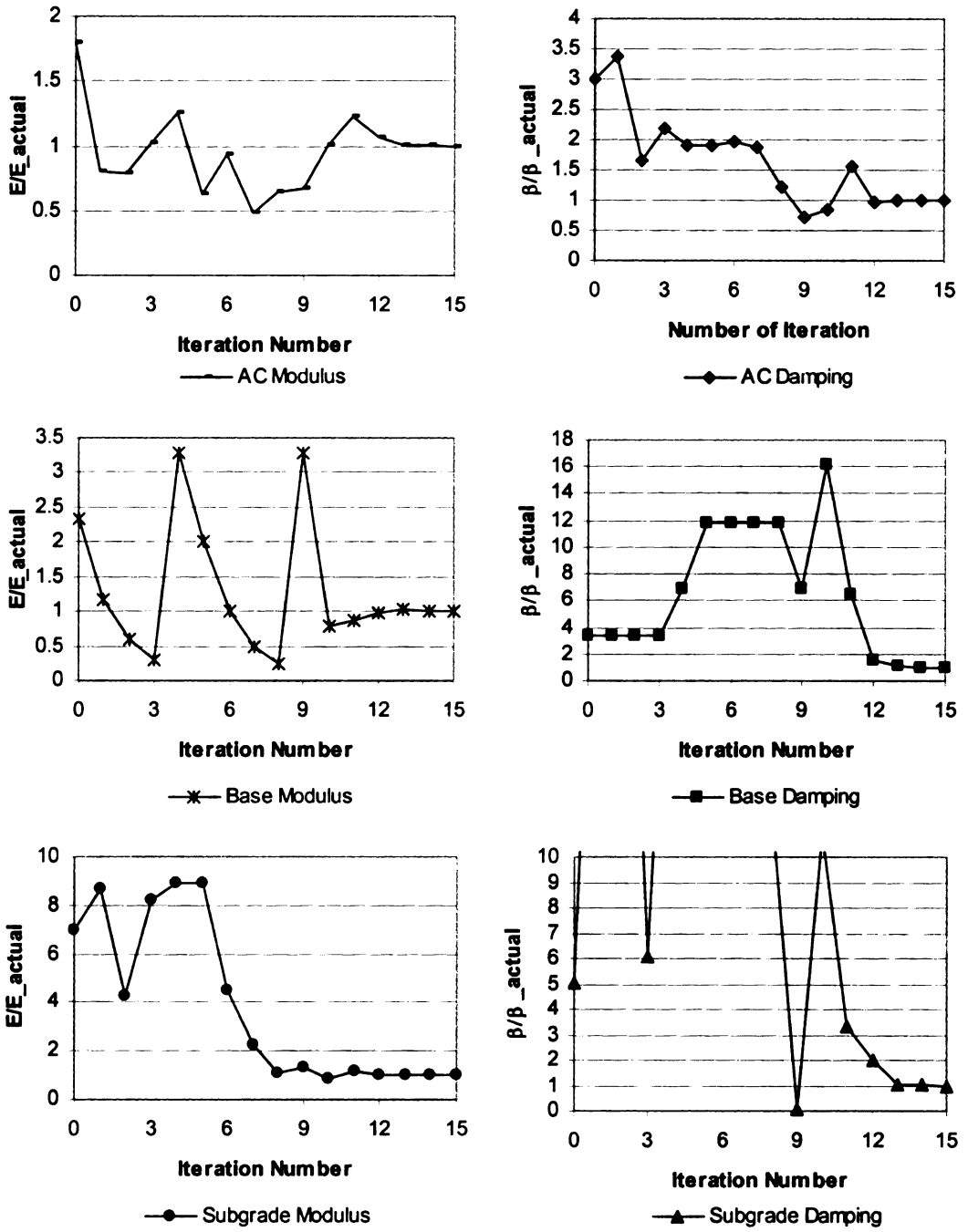

Figure 6.105 Convergence of layer parameters for case 1 (thickness backcalculation)

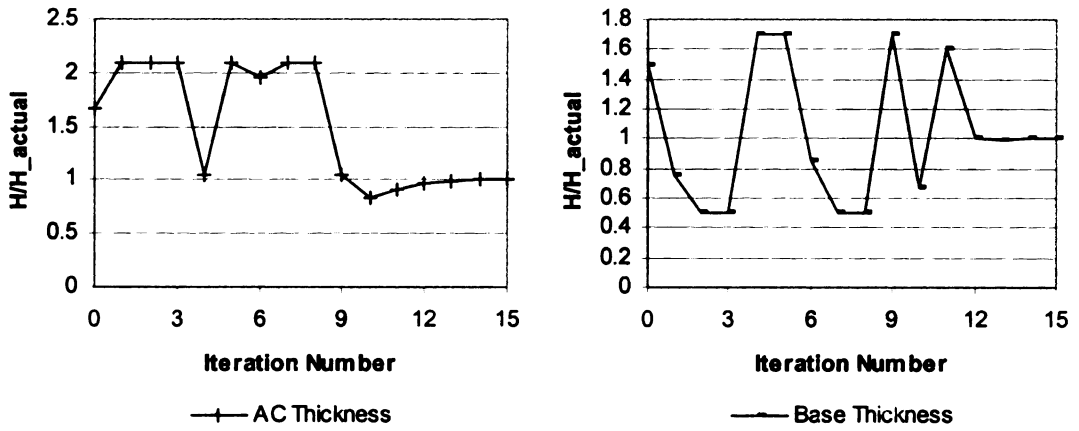

Figure 6.106 Convergence of layer thickness for case 1 (thickness backcalculation)

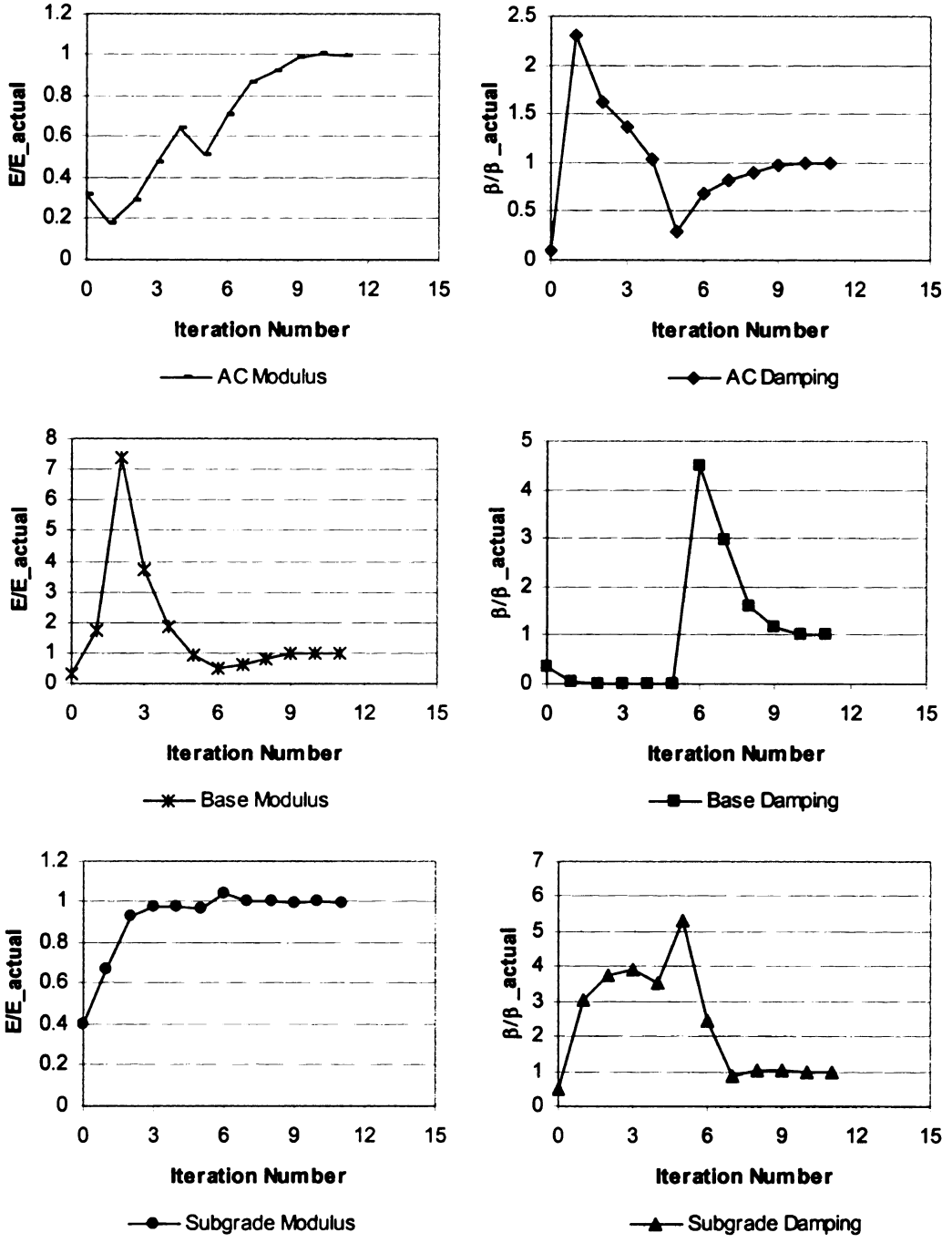

Figure 6.107 Convergence of layer parameters for case 2 (thickness backcalculation)

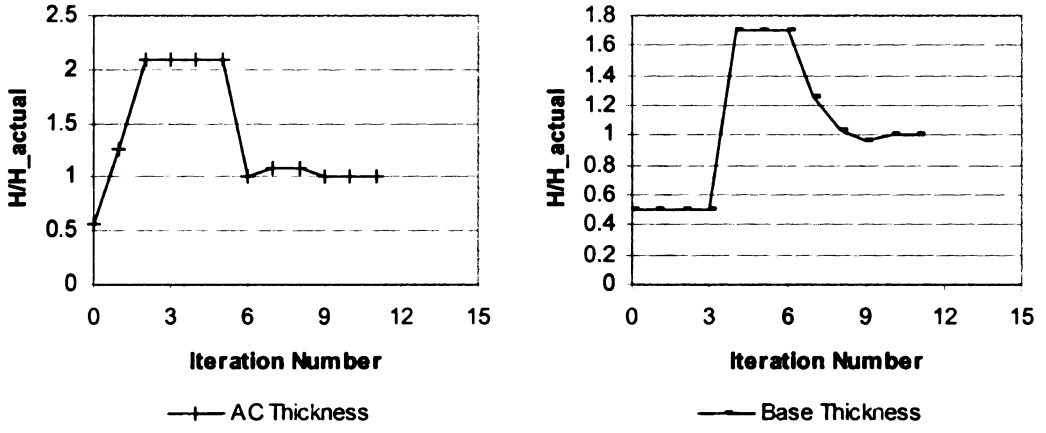

Figure 6.108 Convergence of layer thickness for case 2 (thickness backcalculation)

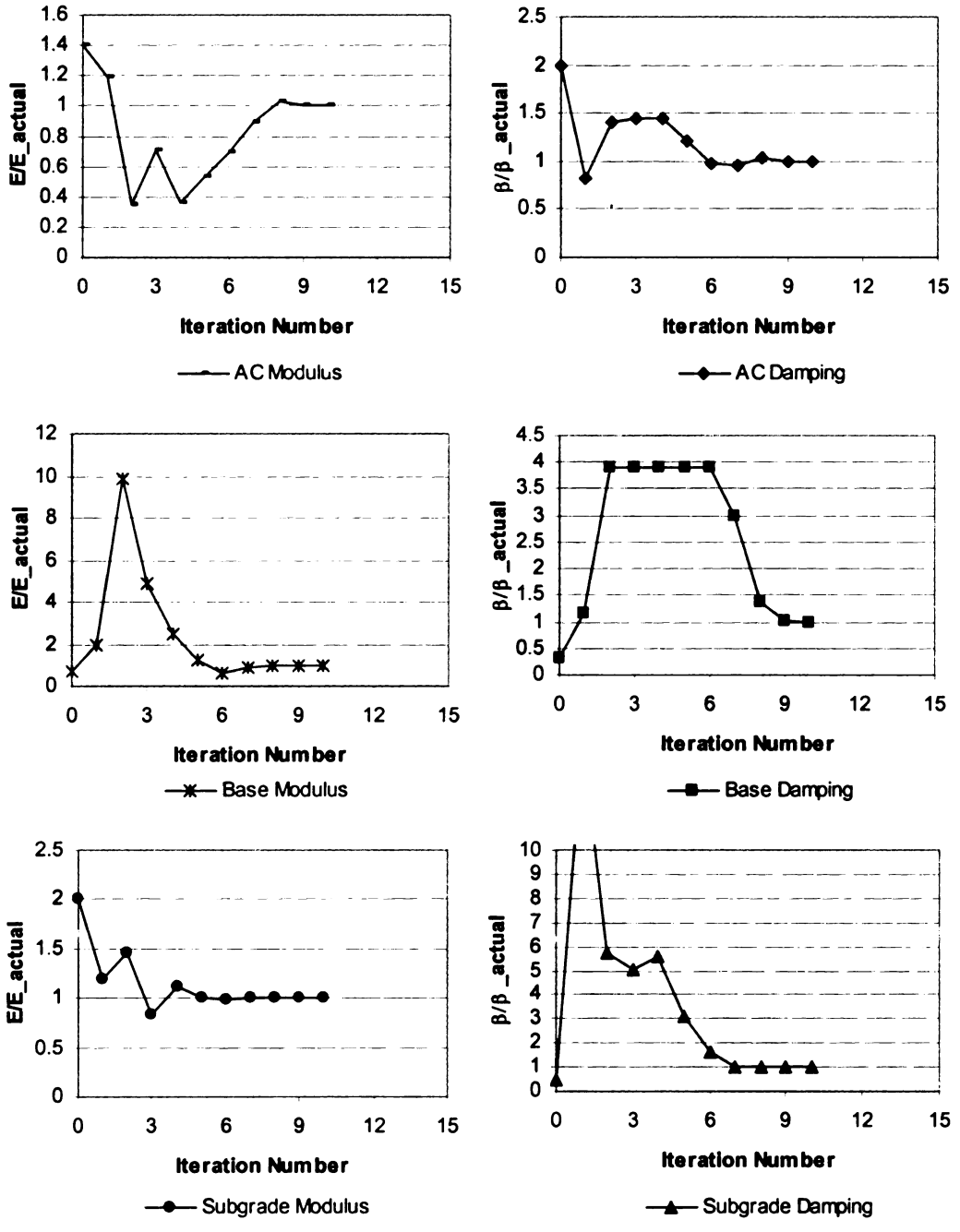

Figure 6.109 Convergence of layer parameters for case 3 (thickness backcalculation)

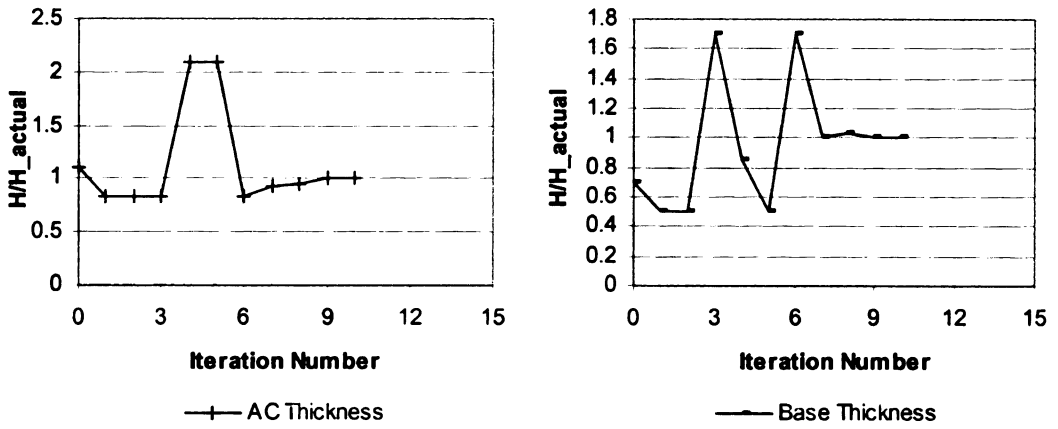

Figure 6.110 Convergence of layer thickness for case 3 (thickness backcalculation)

6.5.4 Effect of Incorrect Damping Ratio Specification on Backcalculation Results

The effect of incorrectly specifying the damping ratio of the base and subgrade on backcalculated moduli and layer thicknesses was investigated for the three layer pavement having the properties shown in profile 1 of Table 6.22. The actual base and subgrade damping ratio are 3% and 2%, respectively. Either the base damping or subgrade damping was specified with the error ranging from -50% to 50%. Table 6.32 shows all nine combination of damping ratio and case 5 corresponds to when the true value for the base and subgrade layers are used; i.e., reference case. The ratios of backcalculated to actual values are shown in Figure 6.111 through Figure 6.115. The results show that the effect of incorrectly specifying the subgrade damping ratio can lead to relatively large errors in larger moduli and thicknesses, except for the subgrade layer. The most predictions are for case 9, 6 and 3, respectively. These correspond to an assumed subgrade damping ratio that is higher (by 50%) than the actual value. Case 2 and 8 correspond to using the correct subgrade damping ratio and an incorrect base damping ratio. The errors in backcalculated parameters are much less significant in these two

cases, suggesting that the effect of base damping ratio is not as important. Case 1, 4, and 7 correspond to an assigned subgrade damping ratio that is lower (by 50%) than the actual value. The errors in backcalculated parameters are not as severe as those in those in case 3, 6, and 9, suggesting that underestimating the damping ratio of the subgrade is not as risky as overestimating it. For case1, while the error in backcalculated AC damping ratio is high (about 70%), its practical significant is low. Finally, the backcalculated subgrade modulus is not affected by any of the incorrectly specified damping ratio values.

Table 6.32 List of damping ratio combination for base and subgrade

Damping Ratio Combination	Base	Subgrade
1	0.015	0.01
2	0.015	0.02
3	0.015	0.03
4	0.03	0.01
5	0.03	0.02
6	0.03	0.03
7	0.045	0.01
8	0.045	0.02
9	0.045	0.03

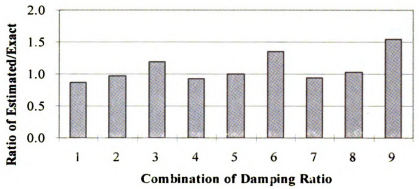

Figure 6.111 Error in backcalculated AC modulus due to different damping ratio combination from base and subgrade

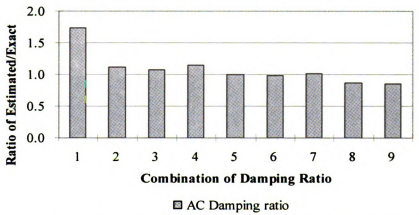

Figure 6.112 Error in backcalculated AC damping ratio due to different damping ratio combination from base and subgrade

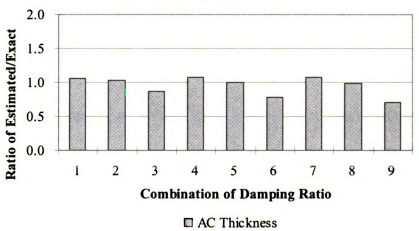

Figure 6.113 Error in backcalculated AC thickness due to different damping ratio combination from base and subgrade

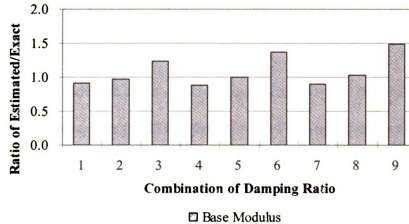

Figure 6.114 Error in backcalculated base modulus due to different damping ratio combination from base and subgrade

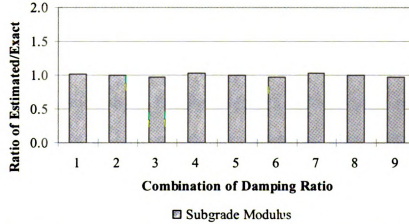

Figure 6.115 Error in backcalculated subgrade modulus due to different damping ratio combination from base and subgrade

6.6 Summary

In this chapter, time histories of FWD surface deflections generated theoretically were used to verify the capabilities of the newly developed dynamic backcalculation program. In general, it was found that the frequency response-based backcalculation method can lead to large errors in deflection basins if the FWD records are truncated before the motions fully decay in time. The errors due to sensor imprecision were found to be less significant.

Based on the analysis, the following conclusions were drawn for frequency-domain backcalculation:

The backcalculation results are all in excellent agreement with the true values. Both the average root mean square error (RMS) on the calculated and actual deflection basins and the relative errors on layer moduli and thicknesses are practically zero, indicating that the program has the ability of backcalculate the moduli and thicknesses accurately.

Theoretical backcalculation shows that among the modulus, damping ratio, thickness and Poisson's ratio, the modulus is the easiest to backcalculate followed by damping ratio, thickness and Poisson's ratio.

Theoretical backcalculation shows that the frequency backcalculation program gives satisfactory convergence of layer moduli and thicknesses when using untruncated deflection time histories. However backcalculation results at higher frequencies are less accurate than those obtained at low frequencies.

Although Poisson's ratio of the AC layer is frequency-dependent, assuming a constant value for it will not affect the results significantly because the backcalculated results are not sensitive to reasonable variations in this parameter.

The following conclusions were drawn for time-domain backcalculation:

Backcalculation based on synthetic time histories generated by SAPSI shows excellent stability and accuracy for both methods (peak deflection and traces). However, since the traces of time history uses more information than the peak deflection, it is recommended that the backcalculation using traces of time history be used for field application.

The time-domain approach can match selected features of the measured time histories directly, while ignoring the inaccurate measurement regions in time. Therefore, from this point of view, the time-domain backcalculation is better than the frequency-domain backcalculation.

Numerical examples illustrate that the method is able to backcalculate layer moduli and thicknesses accurately from synthetically generated FWD data for a three layer pavement system. Backcalculation of layer damping ratios is less accurate, but the influence of this error on the pavement response is insignificant.

CHAPTER 7 - FIELD VALIDATION OF DYNABACK

7.1 General

Measured deflection time history data from several FWD tests conducted in Michigan and elsewhere were analyzed to evaluate the applicability of the DYNABACK to interpret field tests. The analyses include the comparison of backcalculated layer moduli and damping ratios with MICHBACK results for various pavement sections and load levels. The backcalculation was done in both frequency and time-domains, where the time-domain backcalculation included backcalculation of thickness and modulus. The data were obtained from tests involving KUAB and Dynatest FWDs. Most pavement sections were analyzed as four-layer systems with some sections involving a stiff layer at shallow depth.

7.2 Backcalculation of Layer Parameters for Selected Pavement Sections

The selected pavement test sections include sites in Texas, Cornell University, Florence (Italy), Michigan and Kansas (LTPP study). The data were analyzed using DYNABACK and MICHBACK. For the frequency-domain solution, the results shown in this chapter are from single frequency backcalculation with the average values at the different frequencies reported. For the Texas site, different load levels were considered. The following describes the various test sites analyzed and the results of the backcalculation analyses.

7.2.1 Michigan Sites

The selection of the pavement test sections was accomplished in consultation with technical advisory group from the Michigan Department of Transportation (MDOT). The main criterion used in the selection is that the pavement sections be representative of the spectrum of pavement cross-sections, paving materials used in the state of Michigan and that the cross-section information be available. While dynamic FWD test data were available for three different projects, only the US131 project had complete coring data available. Therefore, only the results for this project are presented and discussed herein.

Layer thicknesses were obtained by coring, which was done at several locations. The cores were obtained by using a power auger equipped with a 6-inch coring bit. FWD tests were conducted at several locations along the road.

The data were sampled every 0.1 ms. and sampling time was 100 ms. The sensor spacings are shown in Table 7.1.

Table 7.1 Sensor layout (distances are in inches) – Michigan data

D1	D2	D3	D4	D5	D6	D7
0	8	12	18	24	36	60

A significant feature in the FWD records is the truncation of the pulses at the end of the 100 ms sample times. Ideally, the pulses should die out or go to zero at the end of the sample period. Instead, the deflection pulses usually cross the time axis and become negative before they are truncated. An effort was made to get longer deflection records; however, it appears that the accuracy of the sensor measurements after unloading is not acceptable, as the free vibrations show unrealistic trends in time. Figure 7.1 shows an

example of an "acceptable" time history from the KUAB FWD system, and Figure shows the filtered time history. Tables 7.15 and 7.16 show the pavement profiles for two control sections along US131

Table 7.2 Profile used for US131 site (section 50699)

Bore hole Number	AC Thickness (in)	Base Thickness (in)	Subbase Thickness (in)
15	7.2	6	46.8
20	7.2	4.8	48
30	7.0	4.8	42

Table 7.3 Profile used for US131 site (section 67015)

Bore hole Number	AC Thickness (in)	Base Thickness (in)	Subbase Thickness (in)
13	6	9.6	44.4

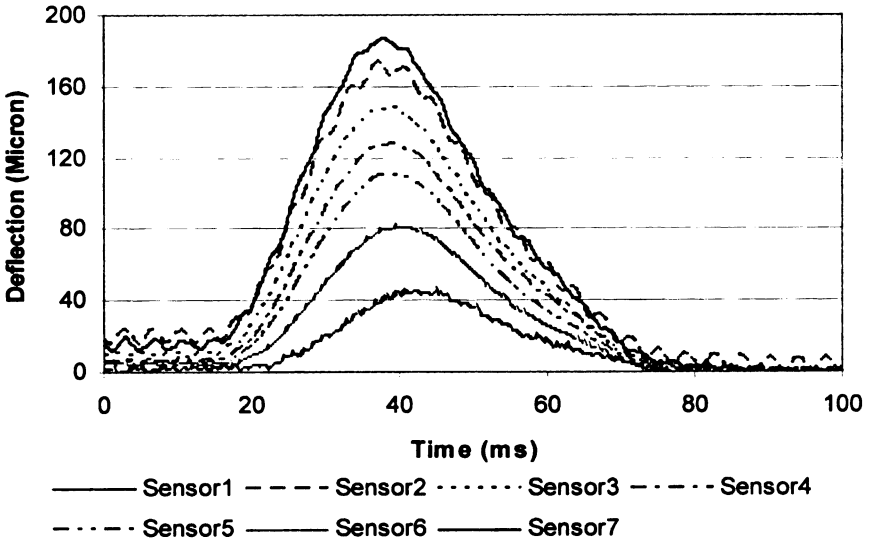

Figure 7.1 Time history from KUAB FWD

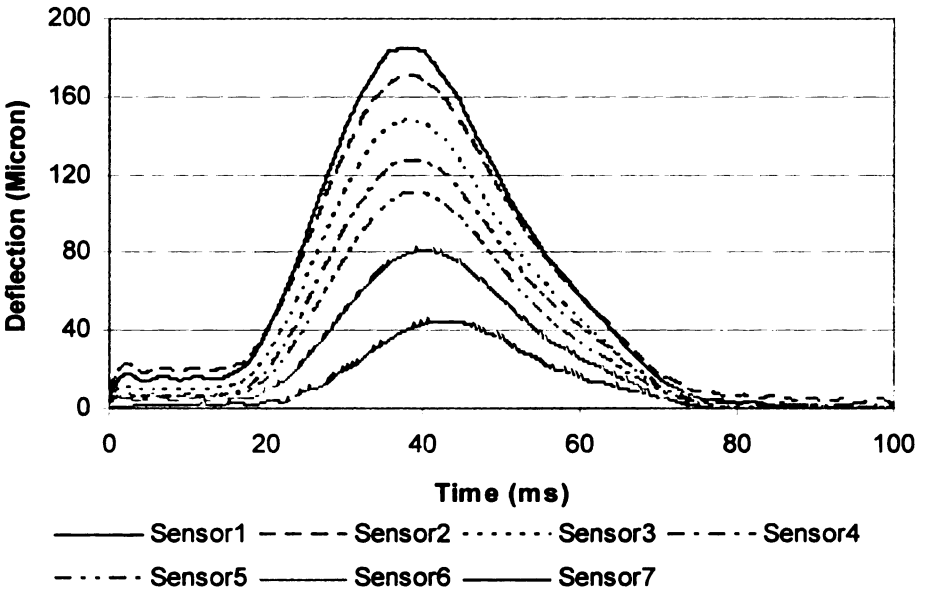

Figure 7.2 Filtered time history from KUAB FWD

7.2.1.1 Comparison of Dynamic and Static Backcalculation for Four layer System

Table 7.4 summarizes the backcalculation results when the profiles are characterized by a 4-layer system and layer thicknesses are known. The backcalculated moduli are generally high for all stations; however the time-domain backcalculation results seem to give unreasonable results. Note that the backcalculated damping ratios for both dynamic solutions are not reasonable. The static and dynamic backcalculation solutions give similar values for the AC, subbase and subgrade moduli, but different values for the base layer modulus.

Table 7.4 Comparison of frequency and time-domain backcalculation results with those from MICHBACK – US131 site

Test Site	Layer	Frequency-domain Dynamic Backcalculation		Time-domain Dynamic Backcalculation		Static Backcalculation
		Modulus (ksi)	Damping	Modulus (ksi)	Damping	Modulus (ksi)
15	AC	1953	0.08	2231	.04	2257
	Base	272	0.12	42	.16	99
	Subbase	34	0.18	32	.26	36
	Subgrade	39	0.07	60	.05	38
20	AC	1146	0.01	981	.08	1065
	Base	150	0.12	42	.05	75
	Subbase	46	0.15	31	.28	43
	Subgrade	18	0.15	27	.02	28
30	AC	697	0.13	838	.12	834
	Base	228	0.02	57	.11	89
	Subbase	27	0.16	27	.31	27
	Subgrade	39	0.08	48	.01	45
13	AC	1334	0.13	1444	0.14	1443
	Base	60	0.11	18	0.21	22
	Subbase	53	0.12	69	0.08	63
	Subgrade	29	0.18	28	0.02	32

Figure 7.3 through Figure 7.6 show the measured and predicted deflection basins at low, intermediate and high frequencies for the different sites. The comparisons are fair to poor, with the measured deflection basins showing irregular patterns for some test sensors and at certain frequencies. Figure 7.7 through Figure 7.10 show the measured and predicted peak deflections and time lags. The agreement is fair for peak deflections and poor for time lags, with the measured time lag curves showing irregular patterns. These irregularities could be caused by errors in sensor locations and/or synchronization problems in the time readings from different sensors.

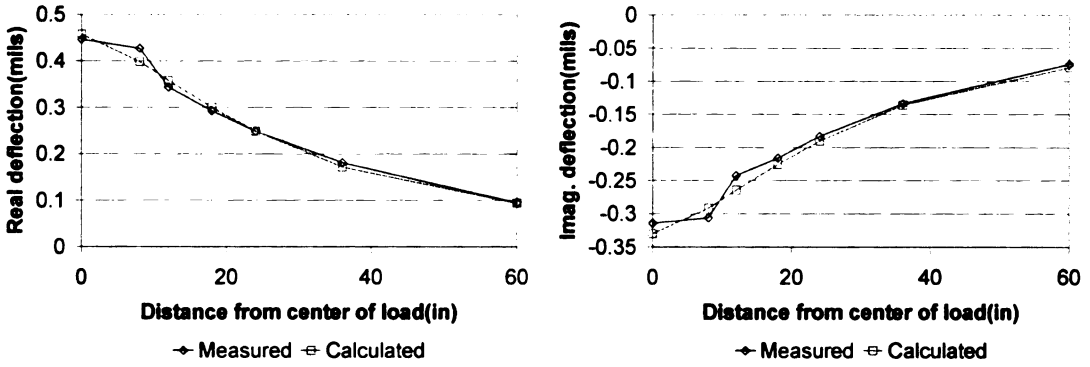

(a) Real and imaginary deflection basins at 2.44 Hz

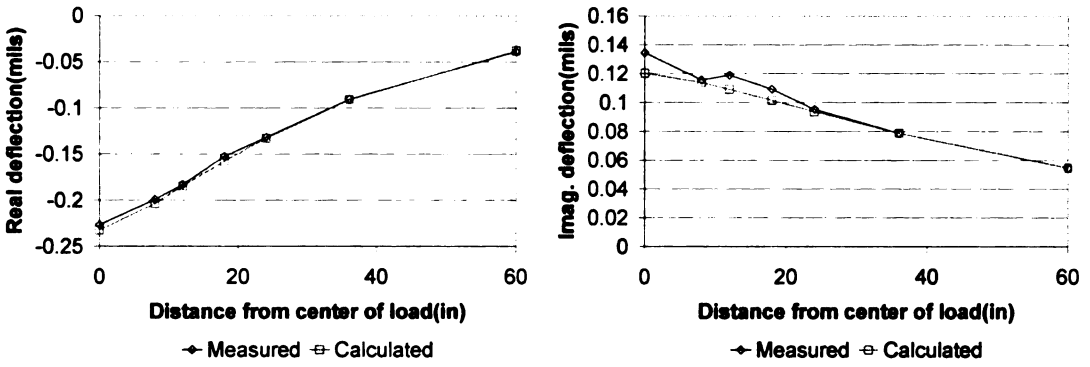

(b) Real and imaginary deflection basins at 14.65 Hz

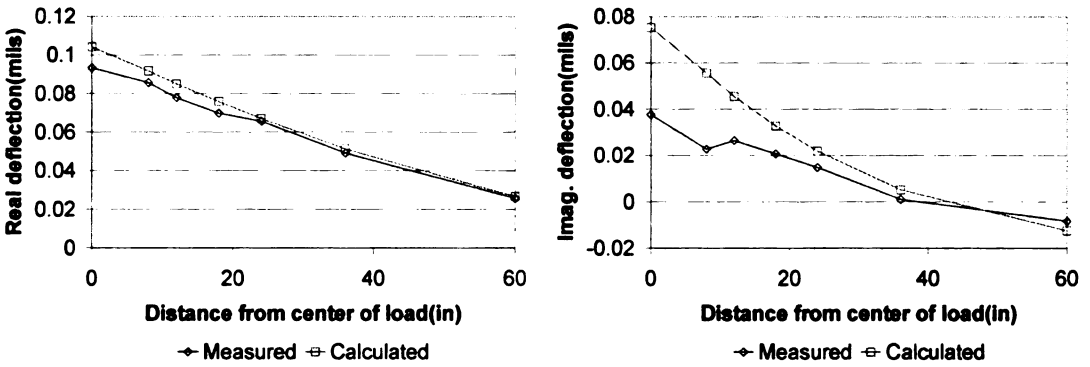

(c) Real and imaginary deflection basins at 24.41 Hz

Figure 7.3 Comparison of measured and predicted deflection basins for US131 (50699-15)

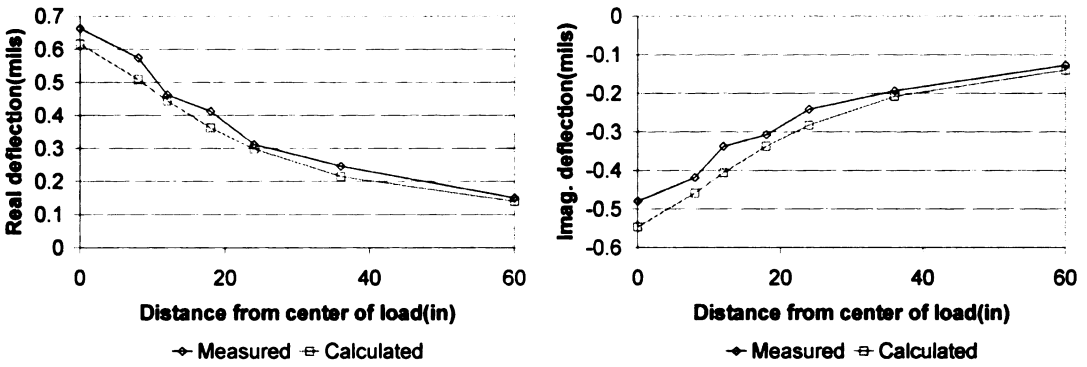

(a) Real and imaginary deflection basins at 2.44 Hz

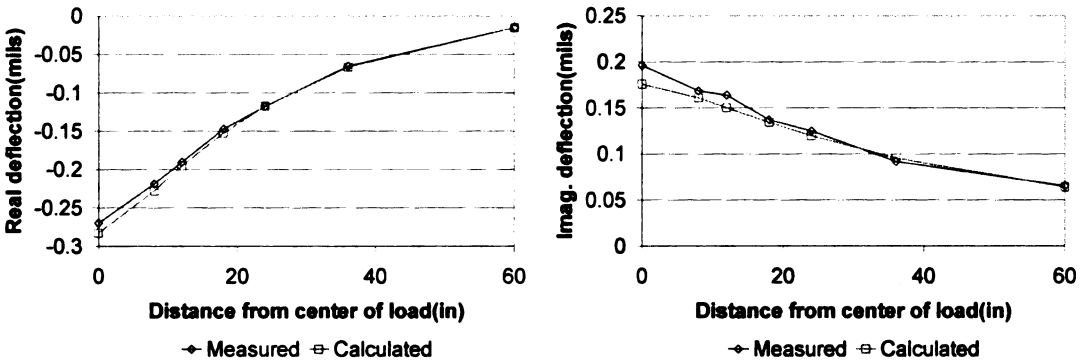

(b) Real and imaginary deflection basins at 14.65 Hz

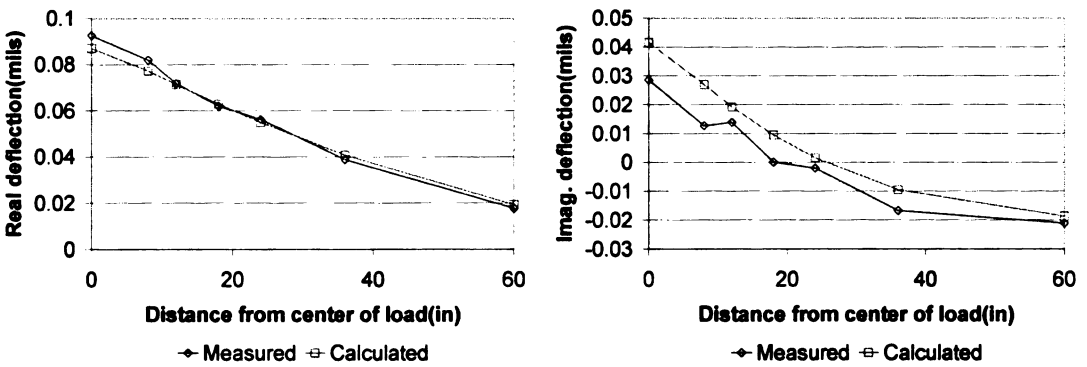

(c) Real and imaginary deflection basins at 24.41 Hz

Figure 7.4 Comparison of measured and predicted deflection basins for US131 (50699-20)

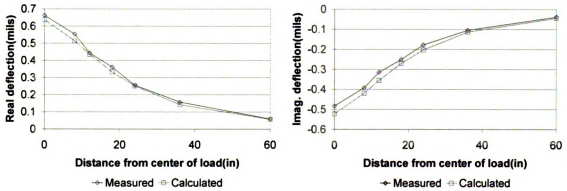

(a) Real and imaginary deflection basins at 2.44 Hz

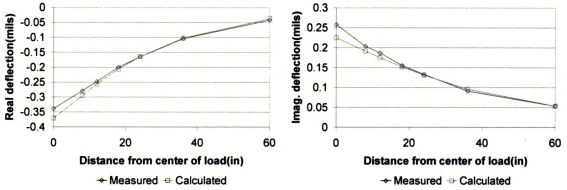

(b) Real and imaginary deflection basins at 14.65 Hz

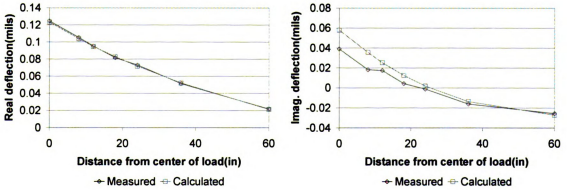

(c) Real and imaginary deflection basins at 24.41 Hz

Figure 7.5 Comparison of measured and predicted deflection basins for US131 (50699-30)

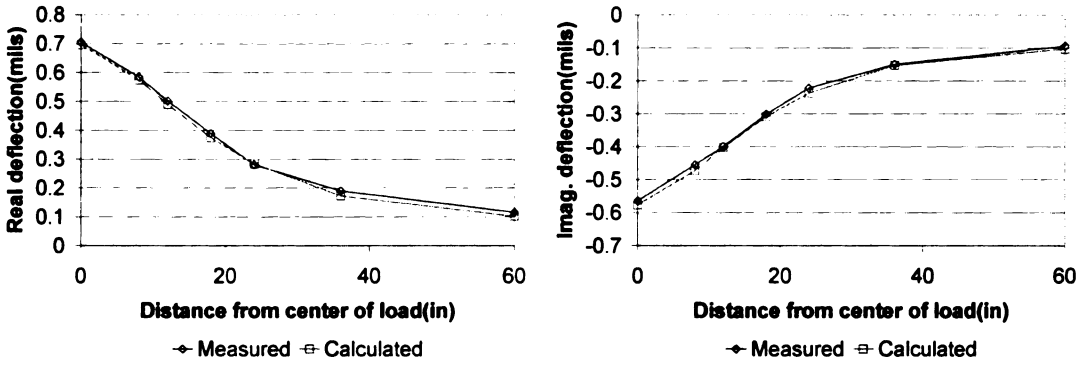

(a) Real and imaginary deflection basins at 2.44 Hz

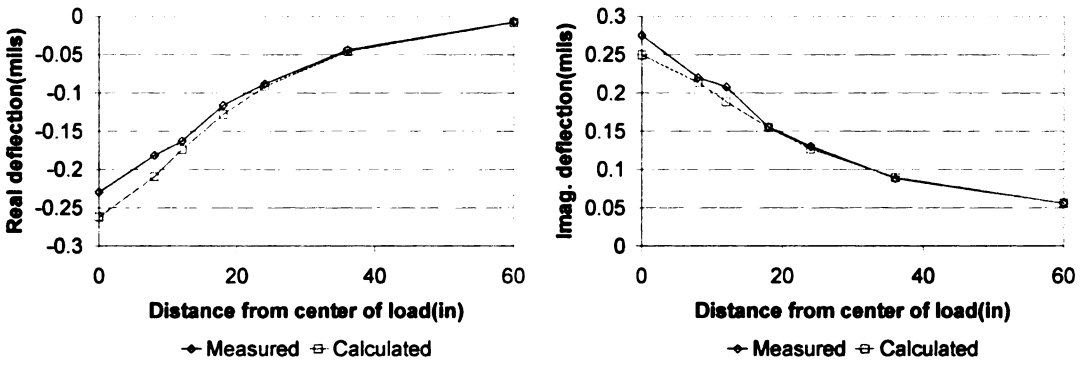

(b) Real and imaginary deflection basins at 14.65 Hz

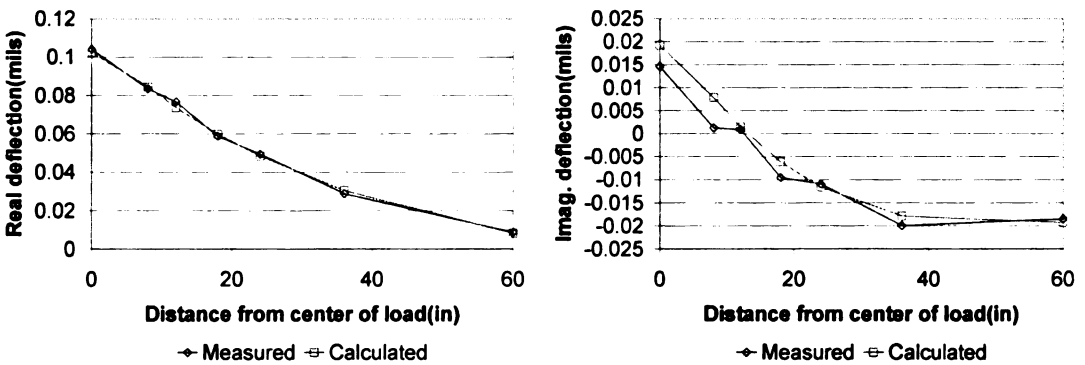

(c) Real and imaginary deflection basins at 24.41 Hz

Figure 7.6 Comparison of measured and predicted deflection basins for US131 (50157-13)

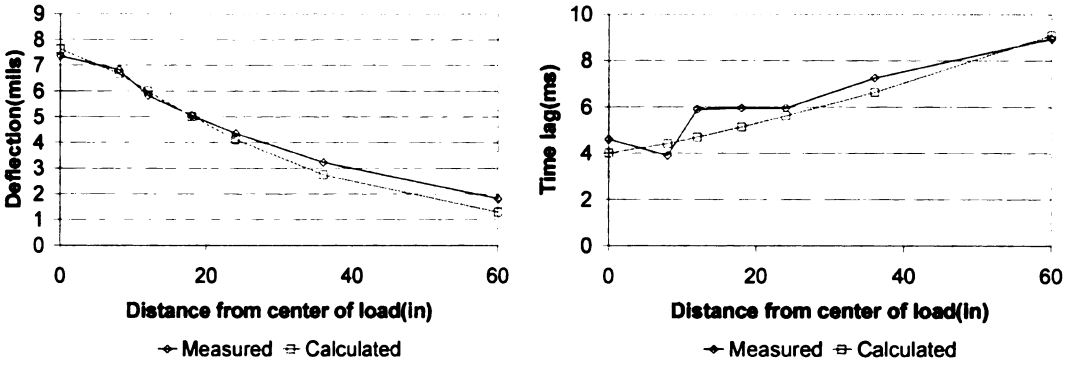

Figure 7.7 Comparison of measured and calculated peak deflections and time lags for US131 (50699-15)

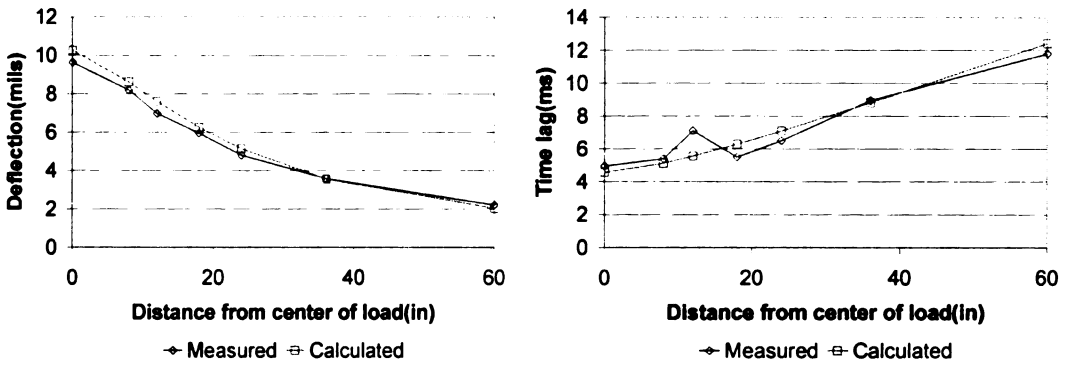

Figure 7.8 Comparison of measured and calculated peak deflections and time lags for US131 (50699-20)

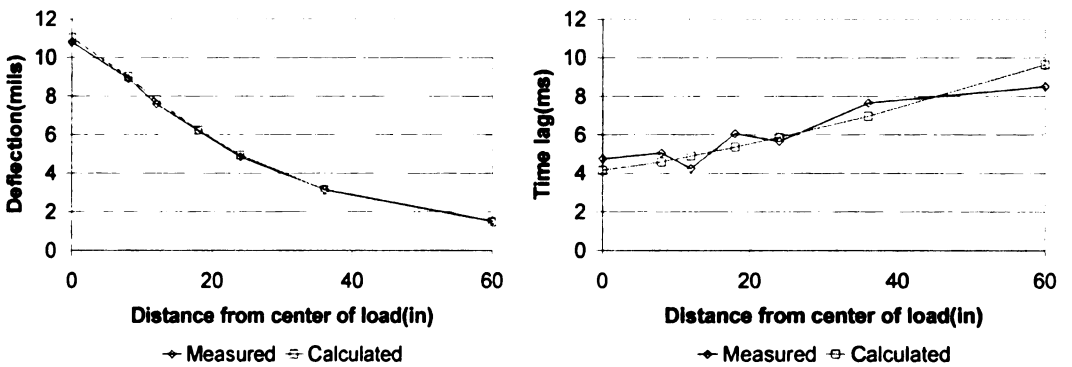

Figure 7.9 Comparison of measured and calculated peak deflections and time lags for US131 (50699-30)

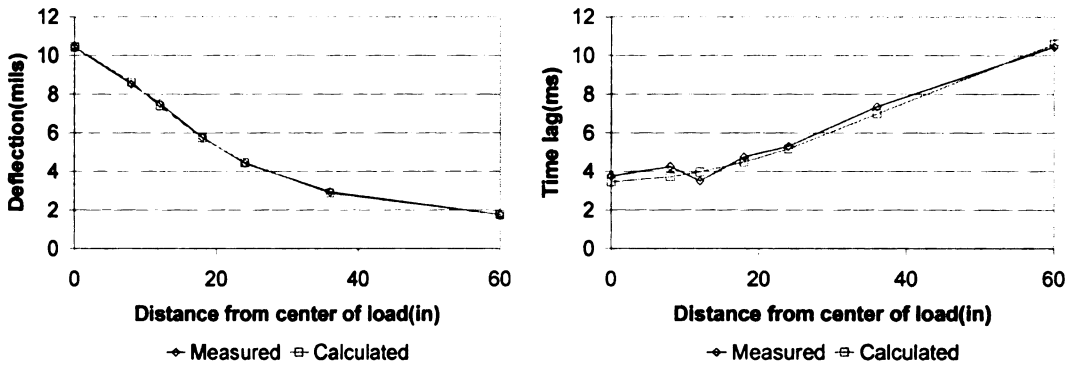

Figure 7.10 Comparison of measured and calculated peak deflections and time lags for US131 (50157-13)

7.2.1.2 Dynamic Time-domain Backcalculation Using Peak Deflections for Three layer System

In this analysis, the base and subbase layers were combined, and the program was allowed to backcalculate layer thicknesses. Table 7.5 shows the backcalculation results from time-domain analysis. The error in the backcalculated AC thickness varies from -17% to 39%. For the combined base and subbase layers, the errors in the backcalculated thickness are very large, with the value reaching the boundary in 3 out of 4 cases. The effect of thickness backcalculation on layer moduli is more pronounced for the AC layer, and the backcalculated damping ratios are erratic.

Figure 7.11 through Figure 7.18 show the surface deflection and time lag in different sites. The figures show fair to poor agreement between measured and predicted response, with the measured time lags showing irregular patterns. These irregularities could be caused by errors in sensor locations and/or synchronization problems in the time readings from different sensors.

Table 7.5 Backcalculation results from time-domain analysis – US131 site

Test Site	Layer	Without thickness Backcalculation		With Thickness Backcalculation		
		Modulus (ksi)	Damping	Modulus (ksi)	Damping	Thickness (in.)
15	AC	2350	0.05	1473	0.01	6.7
	Base	42	0.27	74	0.30	25.0
	Subgrade	37	0.01	41	0.05	---
20	AC	1038	0.07	1424	0.01	4.3
	Base	43	0.24	73	0.30	20.5
	Subgrade	28	0.01	27	0.12	---
30	AC	905	0.08	958	0.03	6.3
	Base	31	0.30	61	0.37	10.0
	Subgrade	47	0.01	36	0.13	---
13	AC	726	0.03	742	0.33	10.0
	Base	47	0.18	40	0.07	35.8
	Subgrade	31	0.01	31	0.12	---

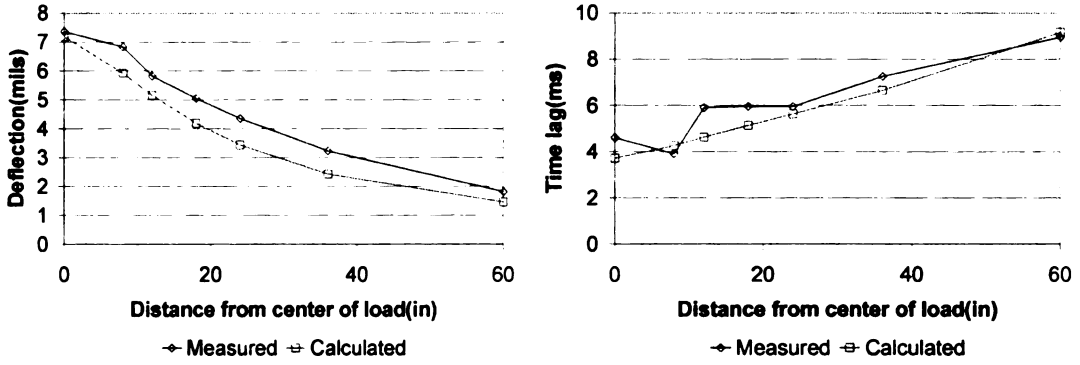

Figure 7.11 Comparison of measured and calculated peak deflections and time lags for US131 (50699-15) with thickness backcalculation

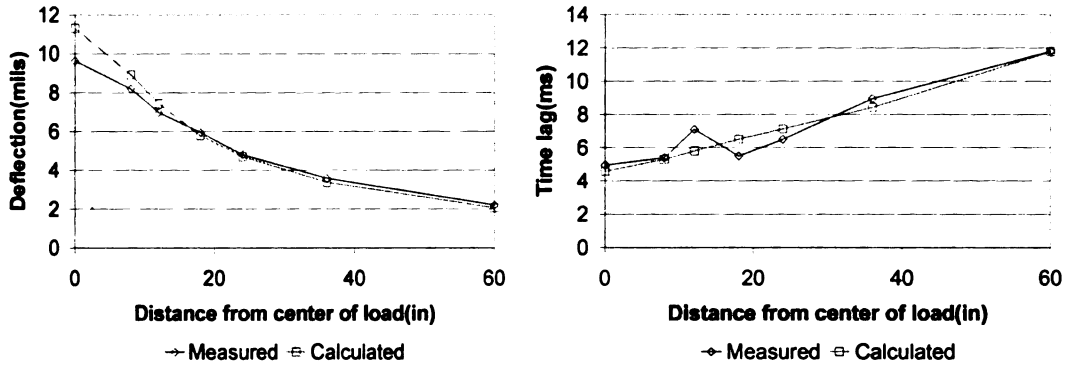

Figure 7.12 Comparison of measured and calculated peak deflections and time lags for US131 (50699-20) with thickness backcalculation

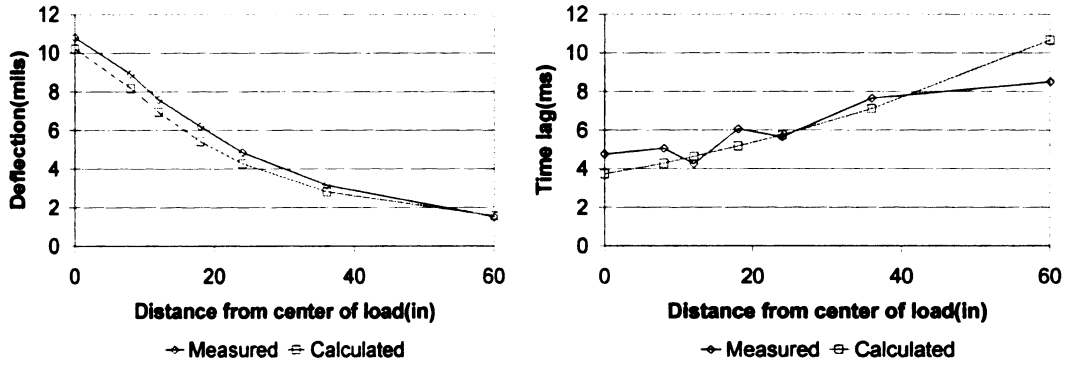

Figure 7.13 Comparison of measured and calculated peak deflections and time lags for US131 (50699-30) with thickness backcalculation

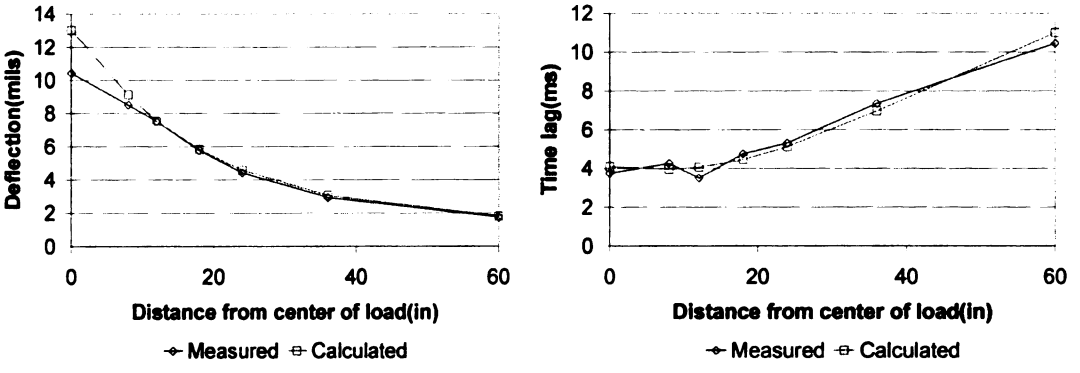

Figure 7.14 Comparison of measured and calculated peak deflections and time lags for US131 (50699-13) with thickness backcalculation

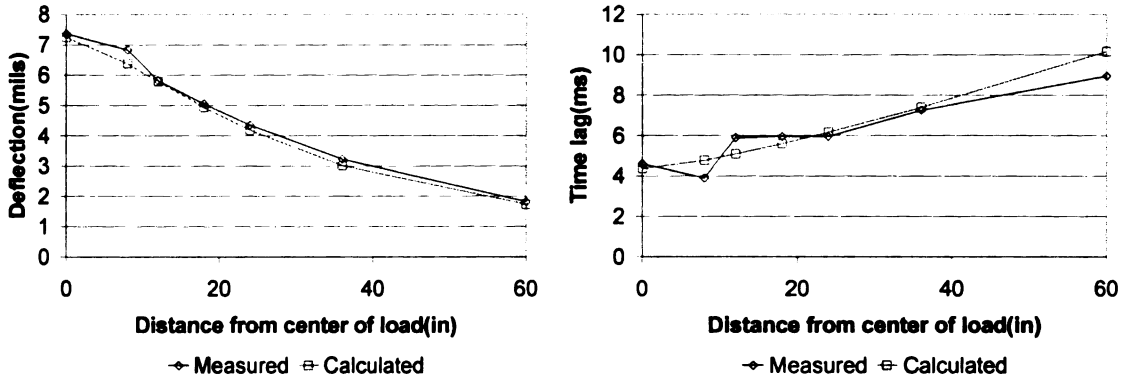

Figure 7.15 Comparison of measured and calculated peak deflections and time lags for US131 (50699-15) without thickness backcalculation

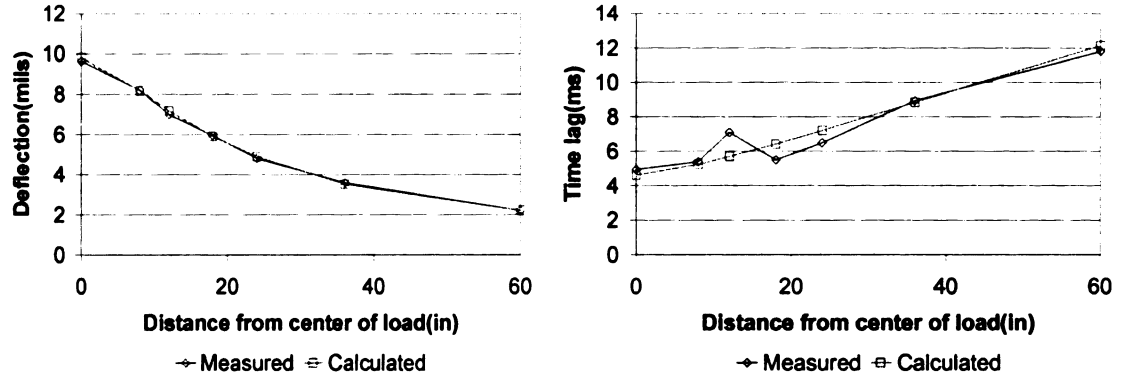

Figure 7.16 Comparison of measured and calculated peak deflections and time lags for US131 (50699-20) without thickness backcalculation

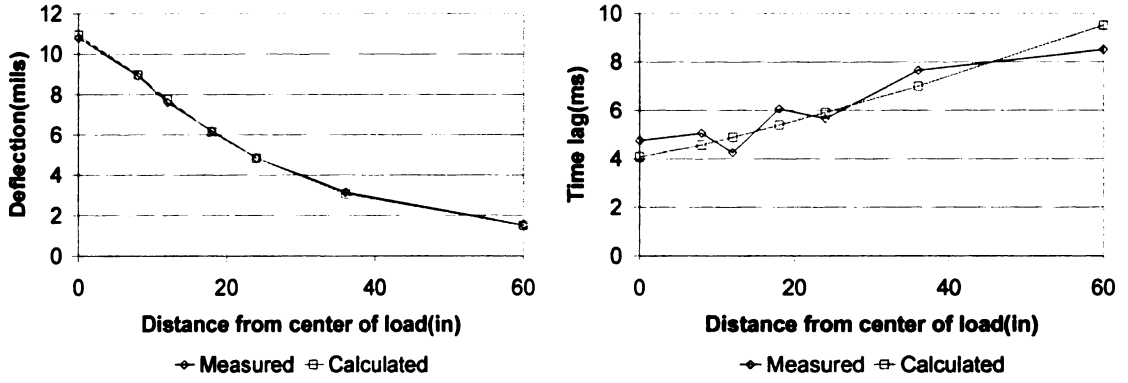

Figure 7.17 Comparison of measured and calculated peak deflections and time lags for US131 (50699-30) without thickness backcalculation

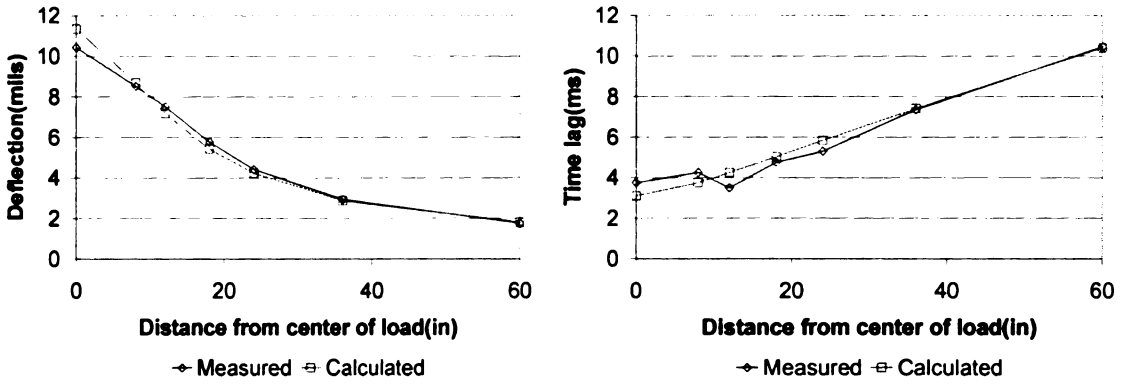

Figure 7.18 Comparison of measured and calculated peak deflections and time lags for US131 (50699-13) without thickness backcalculation

7.2.1.3 Dynamic Time-domain Backcalculation using Traces of Time History

In chapter 4, the need for truncating the singular value that are smaller than the critical allowable error in order to insure convergence was discussed in the context of the SVD method. Recall the equation (4.16)

$$\omega_j < \omega_{\max} \cdot 10^{-\alpha} \tag{4.16}$$

If a singular value is smaller than the $\omega_{\max} \cdot 10^{-\alpha}$, the rank of the gradient matrix is reduced, then reducing the ill-conditioning problem and insure converge. An appropriate threshold value for α needs to be selected carefully. In this section, backcalculation analysis is conducted for various sites using different α-value to investigate the convergence process.

Figure 7.19 shows that the iteration number until convergence is a function of α in US131 field data. The results indicate that the threshold value for α of 3 or 4 is appropriate for dynamic back calculation. Using an α value greater than 4 will lead to no

convergence, while an α value less than 3 lead to inaccuracy in the solution to the inverse problem.

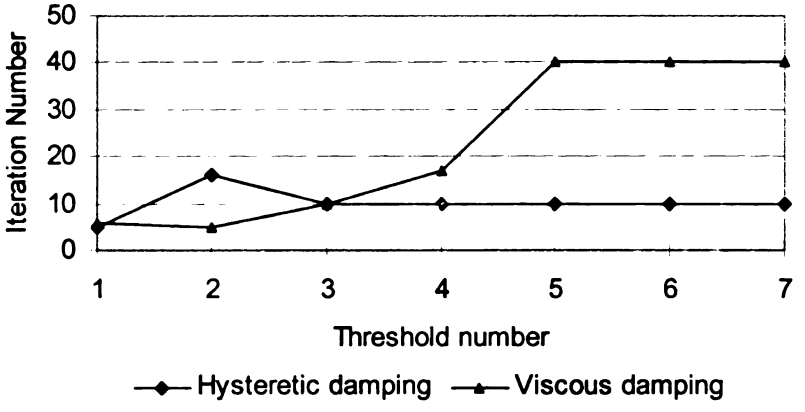

Figure 7.19 Iteration number to convergence versus α for US131 site

In this part, the same profile listed in Table 7.2 is used for the four-layer system in US131 site (section 50699_30). The backcalculation result from three different models including DYNABACK with hysteretic and viscous damping models and an exiting FEM method, which was developed by Matsui (1998) are shown in Figure 7.20 through Figure 7.26. It can be seen that the match from DYNBACK is slightly between that from the FEM model. Figure 7.27 shows the comparison of backcalculated layer moduli from the three models. The relative difference in layer moduli between hysteretic damping model and the viscous damping model is 16% for AC, 1% for base, -15% for subbase, and 13% for subgrade. The difference between the results from the FEM model and DYNABACK are large, especially for the base layer modulus (92%). This may be because of the difference of assumptions in the forward models.

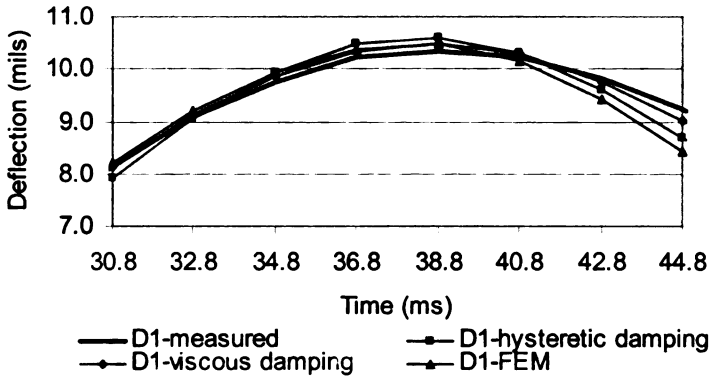

Figure 7.20 Comparison of measured and predicted deflection time histories for sensor 1

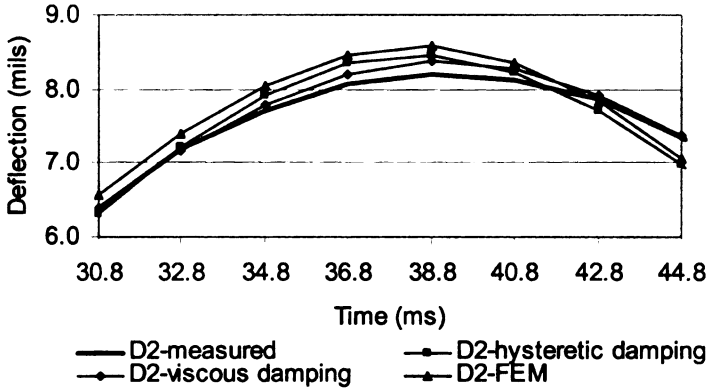

Figure 7.21 Comparison of measured and predicted deflection time histories for sensor 2

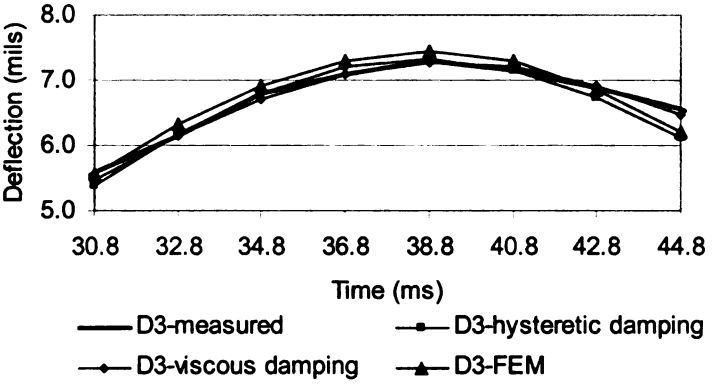

Figure 7.22 Comparison of measured and predicted deflection time histories for sensor 3

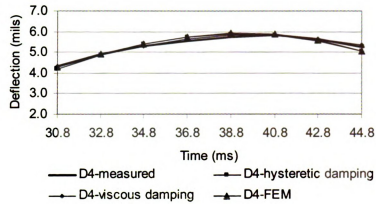

Figure 7.23 Comparison of measured and predicted deflection time histories for sensor 4

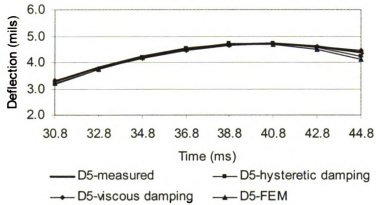

Figure 7.24 Comparison of measured and predicted deflection time histories for sensor 5

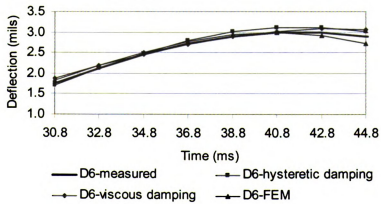

Figure 7.25 Comparison of measured and predicted deflection time histories for sensor 6

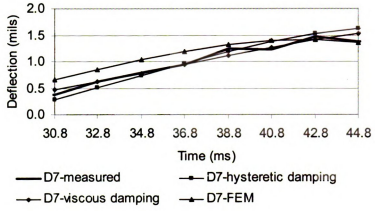

Figure 7.26 Comparison of measured and predicted deflection time histories for sensor7

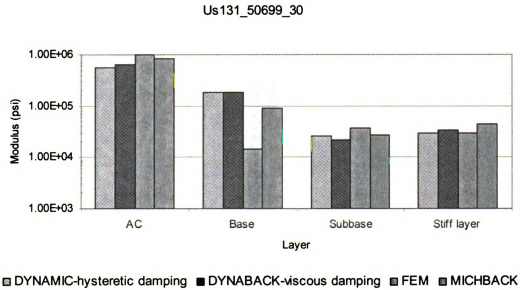

Figure 7.27 Comparison of backcalculated layer moduli from different models

The viscous damping model did not necessarily improve the backcalculation results in the backcalculation of the field FWD data; therefore the hysteretic damping is employed in the uniqueness analysis. The three different values of the seed moduli used in the program are provided in Table 7.6. The backcalculated results are shown in Figure 7.28.

The results show that the backcalculation program can yield excellent uniqueness results for different layers.

Table 7.6 Seed values used for backcalculation of Michigan data

Layer	Case 1		Case 2		Case 3	
Layer	Seed Modulus (ksi)	Seed Damping	Seed Modulus (ksi)	Seed Damping	Seed Modulus (ksi)	Seed Damping
AC	450	0.1	300	0.2	680	0.2
Base	70	0.08	45	0.05	105	0.05
Subbase	70	0.05	40	0.04	85	0.05
Subgrade	70	0.03	30	0.03	75	0.05

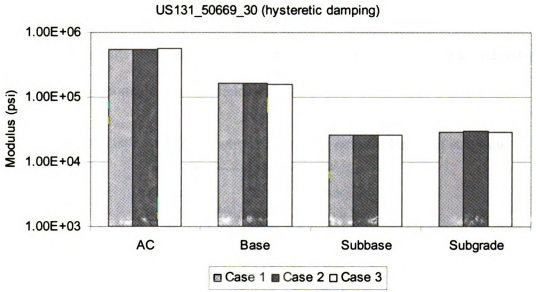

Figure 7.28 Comparison of backcalculated layer moduli using different seed values

Thickness backcalculation is considered next using the hysteretic damping model, since the viscous damping model did not necessarily improve the backcalculation results, and the interpretation of damping is easier. In general, simultaneous backcalculation of layer moduli and thicknesses is difficult. Therefore only the AC layer thickness is backcalculated along with AC, base, and subgrade layer moduli and AC damping ratio.

Damping ratio for base and subgrade are fixed in the backcalculation analysis. The various combinations of damping ratios for base and subgrade layer are listed in Table 7.7. The backcalculated results as shown in Figure 7.29 through Figure 7.33. The results indicate that the combination of damping ratio only significantly affect the AC damping ratio, which decreases with the combination number, (increasing damping ratios of base and subgrade layers). This can be expected because of compensation in the damping ratio of different layers. The AC thickness can also be affected varying by 13% to 21% from the true value. The effect of assuming different base and subgrade damping ratio on the backcalculated layer moduli is negligible. The implication of this finding is that, the backcalculated results deduced using the wrong damping ratios for base and subgrade layer should be reasonable even for field evaluation.

Table 7.7 List of the combination of damping ratio for base and subgrade

Damping Ratio Combination	Base	Subgrade
1	0.05	0.03
2	0.05	0.07
3	0.05	0.10
4	0.10	0.03
5	0.10	0.07
6	0.10	0.10
7	0.15	0.03
8	0.15	0.07
9	0.15	0.10

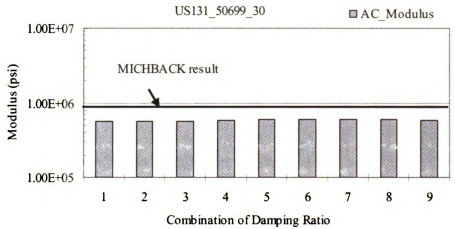

Figure 7.29 Comparison of backcalculated AC modulus for different damping ratio combinations for base and subgrade layers

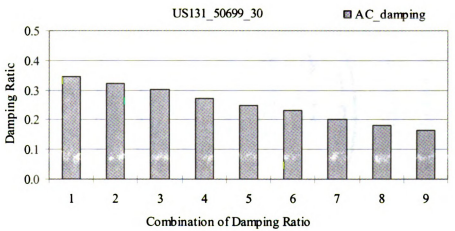

Figure 7.30 Comparison of backcalculated AC damping ratio for different damping ratio combinations for base and subgrade layers

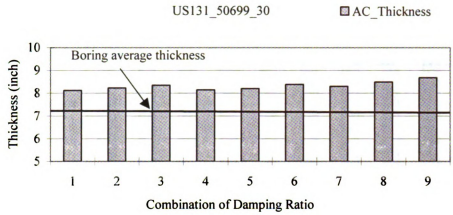

Figure 7.31 Comparison of backcalculated AC thickness for different damping ratio combinations for base and subgrade layers

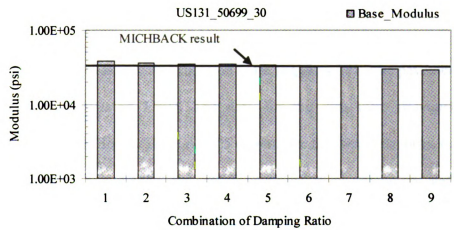

Figure 7.32 Comparison of backcalculated base modulus for different damping ratio combinations for base and subgrade layers

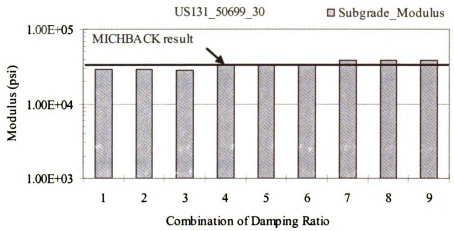

Figure 7.33 Comparison of backcalculated subgarde modulus for different damping ratio combinations for base and subgrade layers

7.2.2 Texas Site

This site is located in Texas near Jacksboro on State Highway 281. The pavement section was tested using a Dynatest FWD. The data for this site were provided by the Transportation Research Board (TRB) A2B05 committee. Surface deflections for various load levels (6000, 9000, 12000 and 16000 pounds) were measured and vertical displacements were recorded simultaneously with a Multi-Depth Deflectometer (MDD) at three depths (3.7, 12.4 and 23.4 in). The pavement's surface deflections were recorded at six points, 12 inches apart, starting at the center of the FWD load plate. The applied loads and deflections were recorded at 0.2 ms interval for 60 ms. The MDDs have anchors deep in the subgrade or bedrock, and the movement of these anchors during typical FWD-MDD tests has been recorded. The bedrock depth is approximately 6.2 ft below the surface. Figure 7.34 shows the test setup and pavement profile. The pavement is made up of an 8 in. asphalt concrete surface and a 12 in. flexible base layer on top of the subgrade.

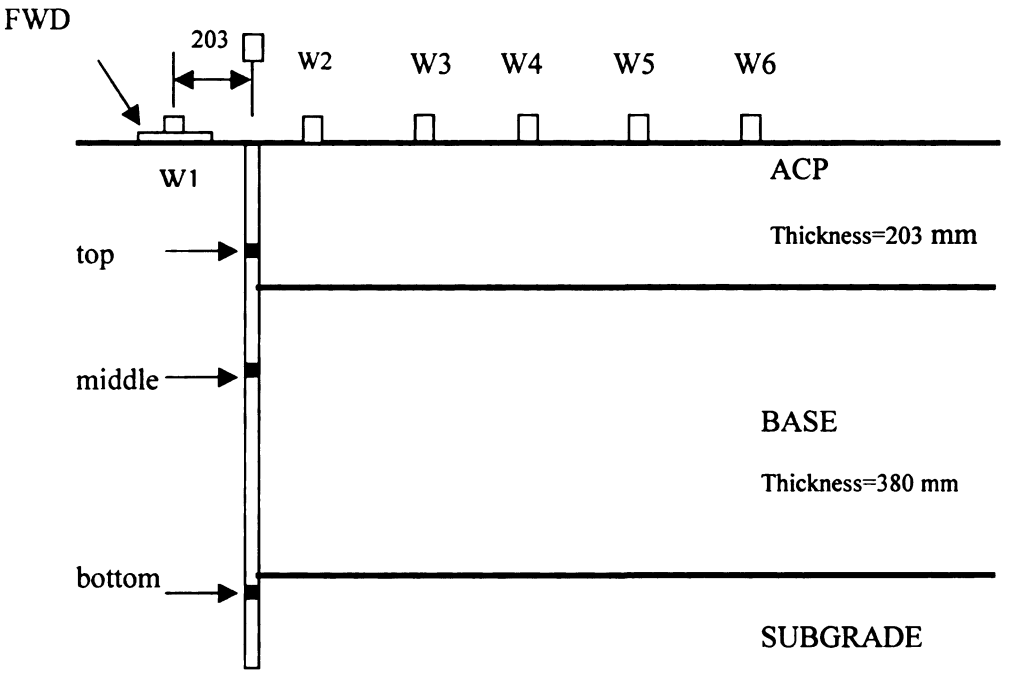

Figure 7.34 Pavement profile and test setup for Texas site

Figure shows the peak deflections versus peak load, normalized to the lowest load level values for the six sensors. The curves show higher than 1:1 ratios, indicating that the pavement system exhibits some nonlinear behavior. The nonlinearity is lowest for the first sensor, and generally increases for the farther sensors.

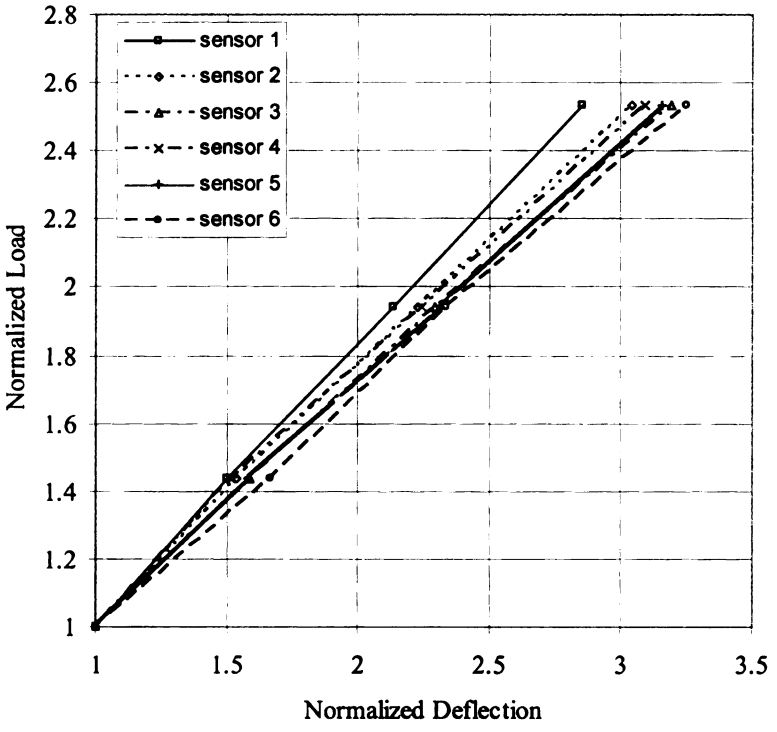

Figure 7.35 Normalized deflection versus FWD load

Figure 7.36 through Figure 7.39 show the time histories of the FWD load and measured sensor deflections for the four different load levels.

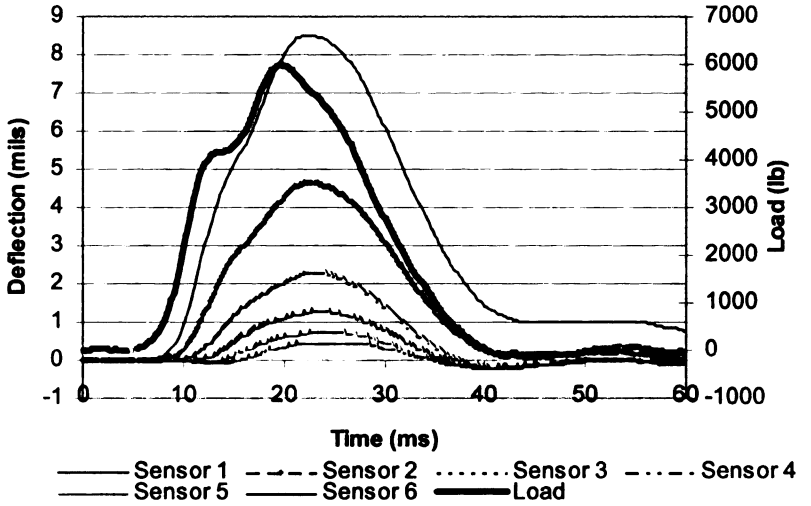

Figure 7.36 FWD load and deflection time histories (load level 1 – 6000 lb) – Texas site

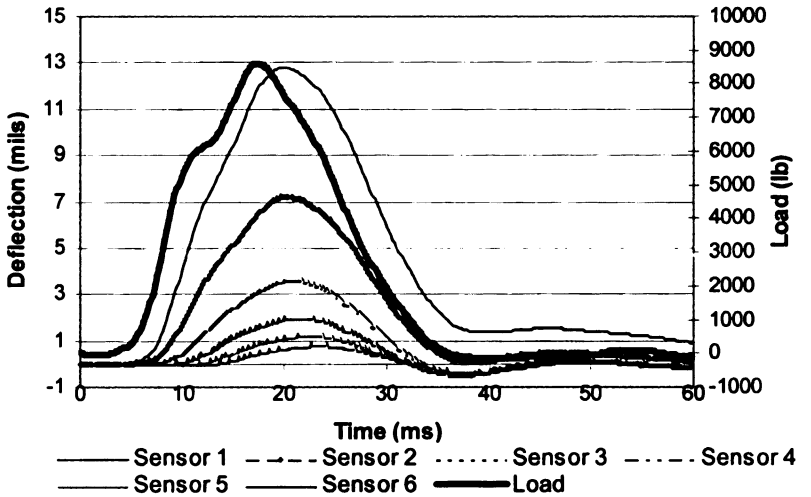

Figure 7.37 FWD load and deflection time histories (load level 2 – 9000 lb) – Texas site

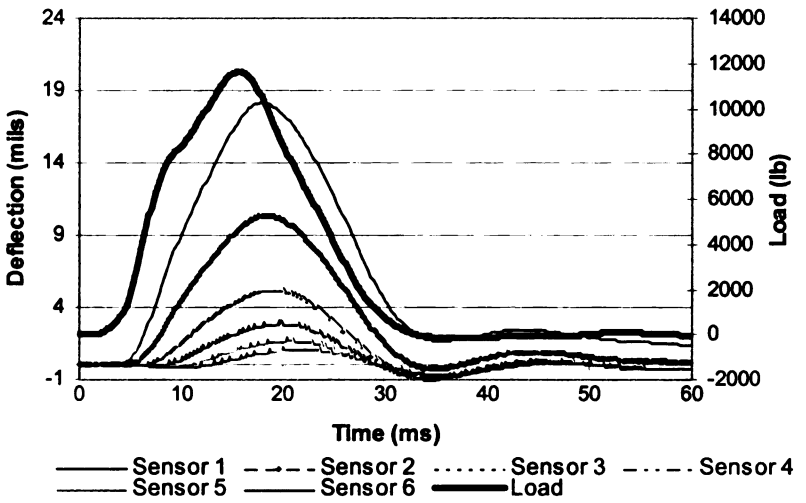

Figure 7.38 FWD load and deflection time histories (load level 3 – 12000 lb) – Texas site

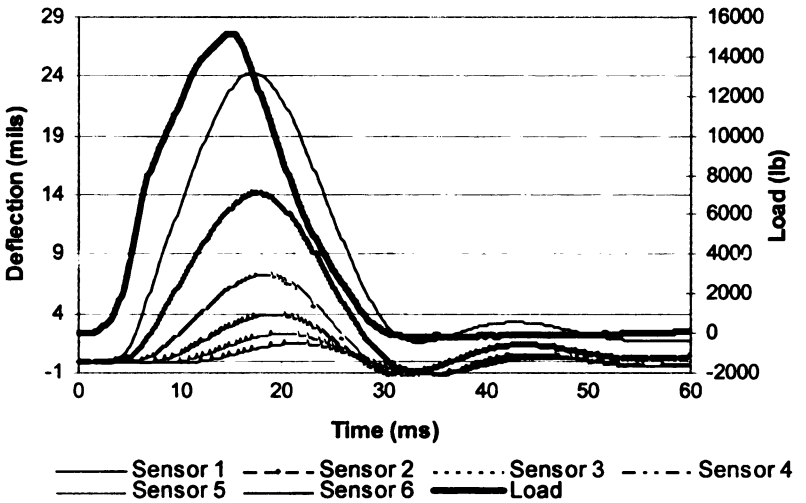

Figure 7.39 FWD load and deflection time histories (load level 4 – 15000 lb) – Texas site

The fluctuations in the free vibration response confirm the presence of a stiff layer at shallow depth, which traps the energy from the FWD load within the pavement system, thus causing the propagating waves to reflect back and forth. The fact that the response of the first and second sensors exhibit less vibrations, with the first sensor deflection

remaining positive even after the load reaches zero indicates high damping in the pavement system. This can be attributed to nonlinear material behavior in some of the pavement layers. The combination of stiff layer and material nonlinearity makes this site particularly challenging for backcalculation.

Table 7.8 and Table 7.9 show the profile used in the backcalculation exercise and the sensor layout, respectively.

Table 7.8 Profile used for Texas site

Layer Name	Thickness (in)	Unit Weight (pcf)	Poisson Ratio
AC	8	145	0.35
Base	12	135	0.40
Subgrade	55	120	0.45
Stiff layer	∞	145	0.25

Table 7.9 Sensor layout (distances are in inches)

D1	D2	D3	D4	D5	D6
0	12	24	36	48	60

7.2.2.1 Comparison of Dynamic and Static Backcalculation for Four-layer System

Normal practice for static analysis is to take the peaks of each of the deflection pulses from different sensors and form a deflection basin. The static force is taken as the peak of the corresponding force pulse. MICHBACK was used for the static backcalculation in order to investigate the difference between dynamic and static backcalculation result

Table 7.10 shows the results from frequency-domain, time-domain and static backcalculations. The backcalculated moduli from time and frequency-domain analyses agree with those from static analysis except for the stiff layer. However, the backcalculated damping from both dynamic solution are not consistent.

Table 7.10 Comparison of frequency and time-domain backcalculation results with those from MICHBACK – Texas site

Load Level	Layer	Frequency-domain Backcalculation		Time-domain Backcalculation		Static Backcalculation Modulus (ksi)
		Modulus (ksi)	Damping	Modulus (ksi)	Damping	
6000 lb	AC	208	0.23	195	0.12	191
	Base	23	0.15	22	0.06	29
	Subbase	29	0.08	26	0.11	22
	Stiff Layer	119	0.04	97	0.01	66
9000 lb	AC	216	0.20	197	0.02	214
	Base	20	0.16	20	0.337	21
	Subbase	28	0.06	26	0.03	23
	Stiff Layer	95	0.02	87	0.01	51
12000 lb	AC	212	0.22	163	0.522	203
	Base	19	0.17	27	0.01	22
	Subbase	26	0.07	20	0.10	20
	Stiff Layer	98	0.01	160	0.01	52
16000 lb	AC	228	0.25	167	0.55	214
	Base	18	0.17	27	0.04	20
	Subbase	26	0.07	19	0.01	19
	Stiff Layer	125	0.01	202	0.01	48

Figure 7.40 through Figure 7.43 show the match between measured and predicted deflection basins from frequency backcalculation. The match between measured and predicted deflection basins is better at low and high frequencies for real deflections. For intermediate frequencies, the match is better for imaginary deflections.

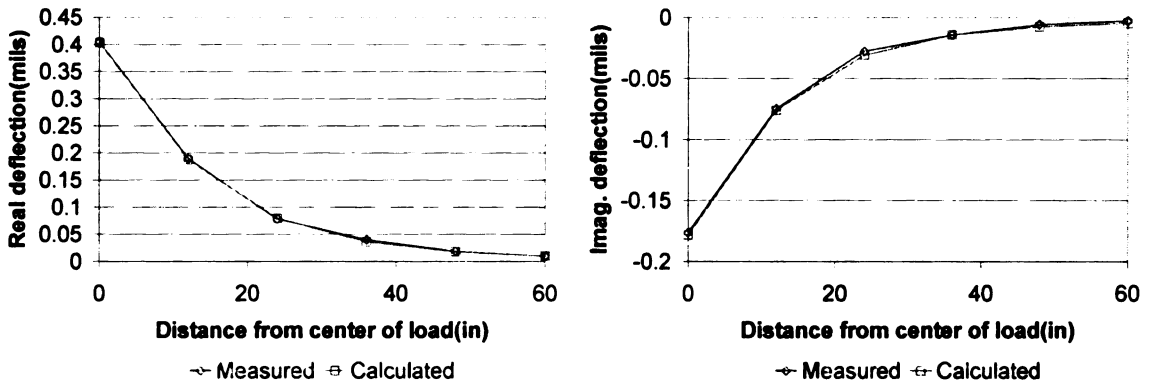

(a) Real and imaginary deflection basins at 2.44 Hz

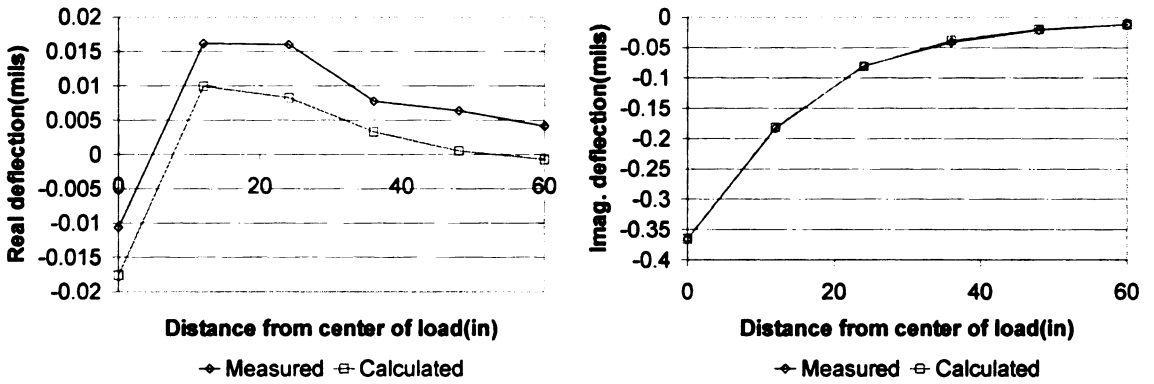

(b) Real and imaginary deflection basins at 9.77 Hz

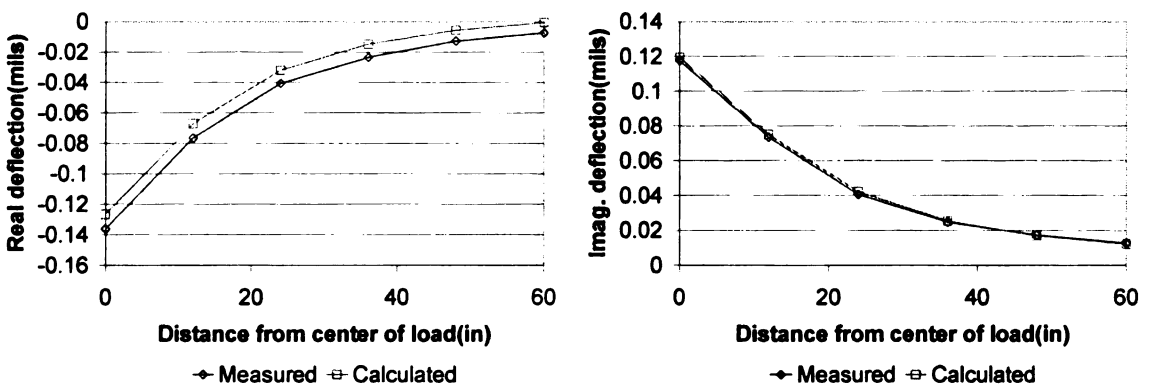

(c) Real and imaginary deflection basins at 26.86 Hz

Figure 7.40 Comparison of measured and predicted deflection basins for load level 1 – Texas site

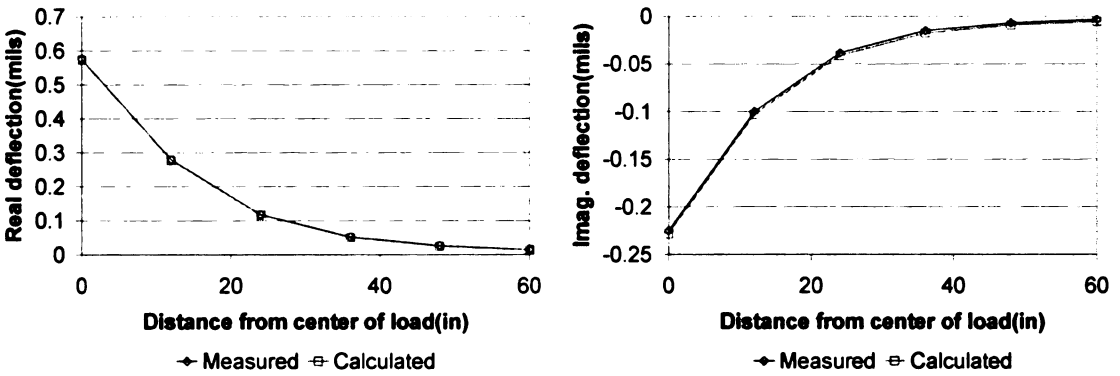

(a) Real and imaginary deflection basins at 2.44 Hz

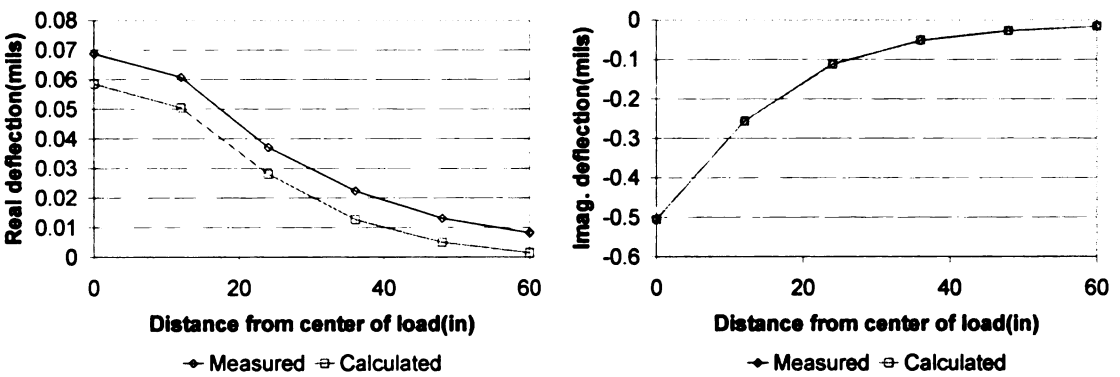

(b) Real and imaginary deflection basins at 9.77 Hz

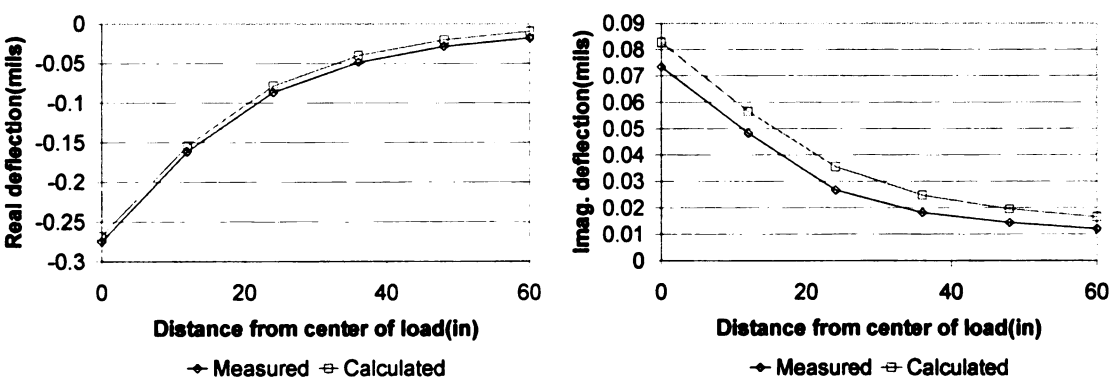

(c) Real and imaginary deflection basins at 26.86 Hz

Figure 7.41 Comparison of measured and predicted deflection basins for load level 2 – Texas site

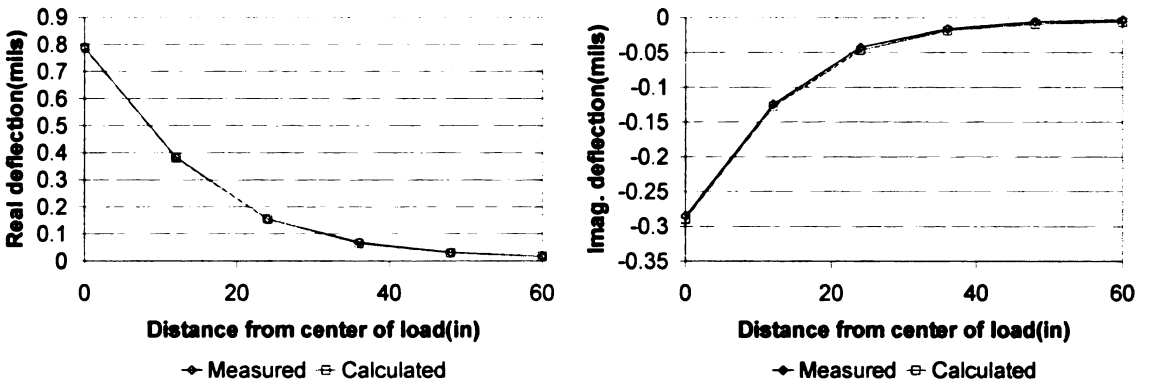

(a) Real and imaginary deflection basins at 2.44 Hz

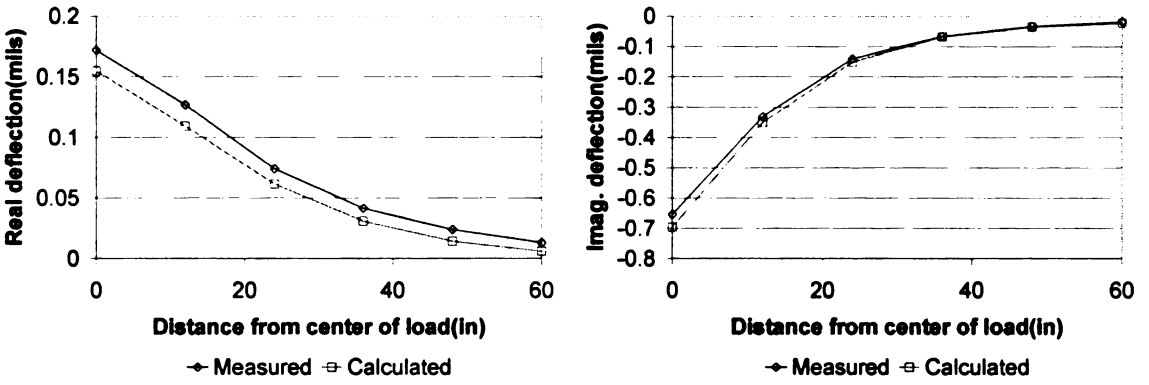

(b) Real and imaginary deflection basins at 9.77 Hz

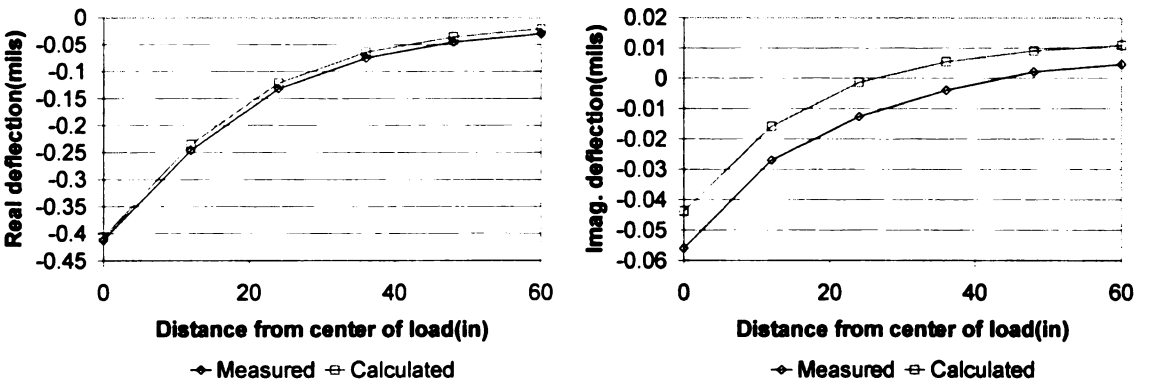

(c) Real and imaginary deflection basins at 26.86 Hz

Figure 7.42 Comparison of measured and predicted deflection basins for load level 3 – Texas site

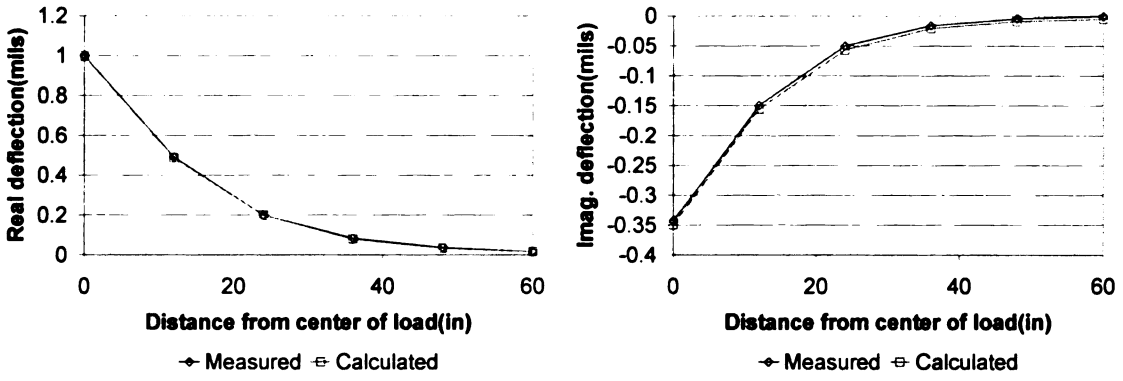

(a) Real and imaginary deflection basins at 2.44 Hz

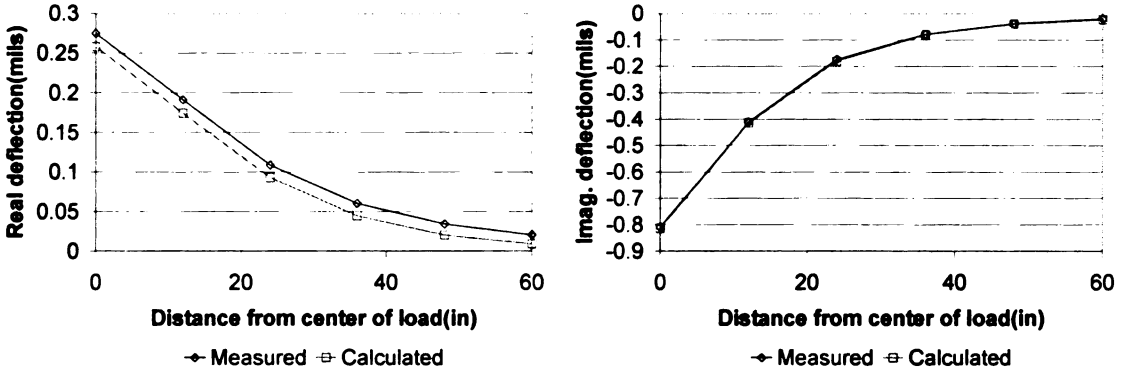

(b) Real and imaginary deflection basins at 9.77 Hz

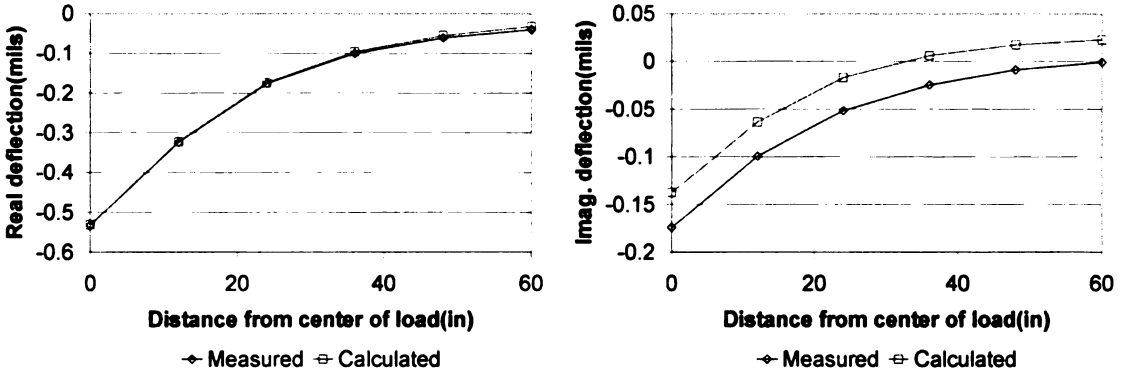

(c) Real and imaginary deflection basins at 26.86 Hz

Figure 7.43 Comparison of measured and predicted deflection basins for load level 4 – Texas site

Figure 7.44 through Figure 7.47 show matched deflection from time-domain backcalculation. The match for peak deflections is better than that for time lags. This could be due to errors in sensor locations or in time synchronization of the data acquisition system.

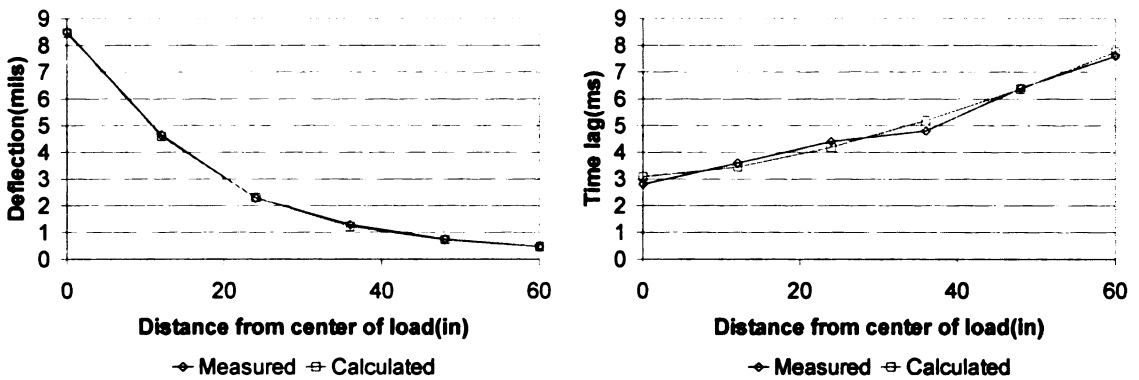

Figure 7.44 Comparison of measured and predicted deflection basins and time lags for load level 1 – Texas site

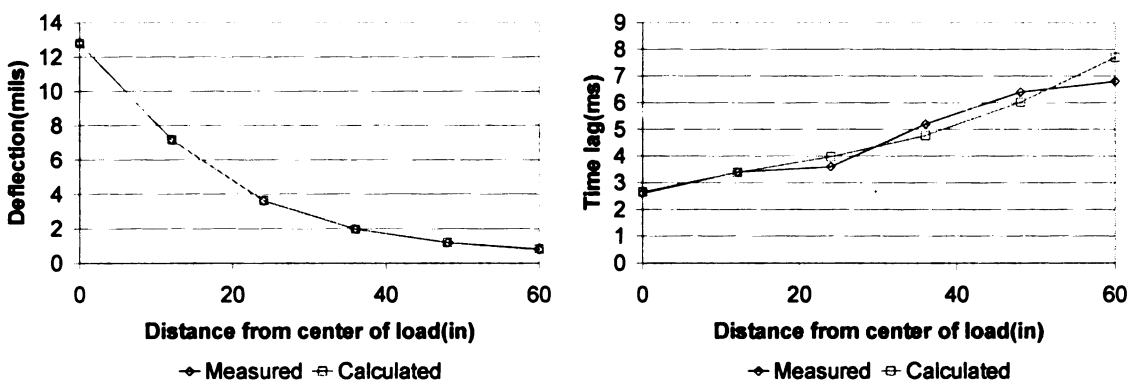

Figure 7.45 Comparison of measured and predicted deflection basins and time lags for load level 2 – Texas site

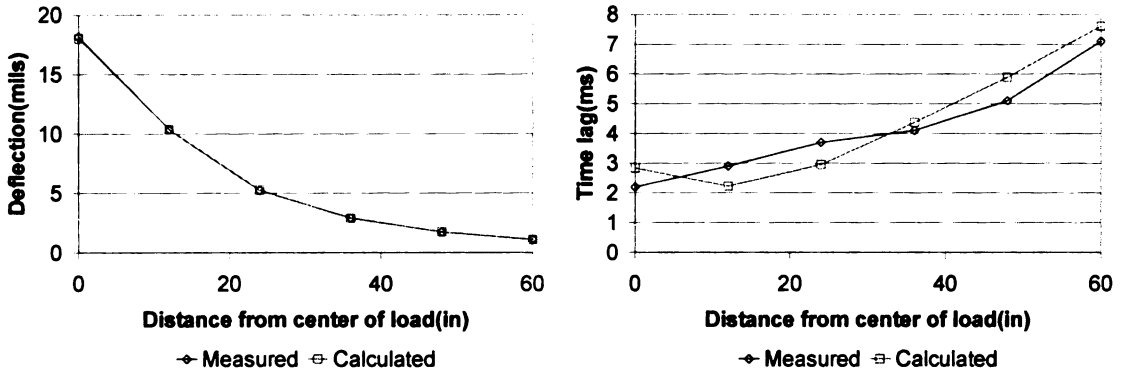

Figure 7.46 Comparison of measured and predicted deflection basins and time lags for load level 3 – Texas site

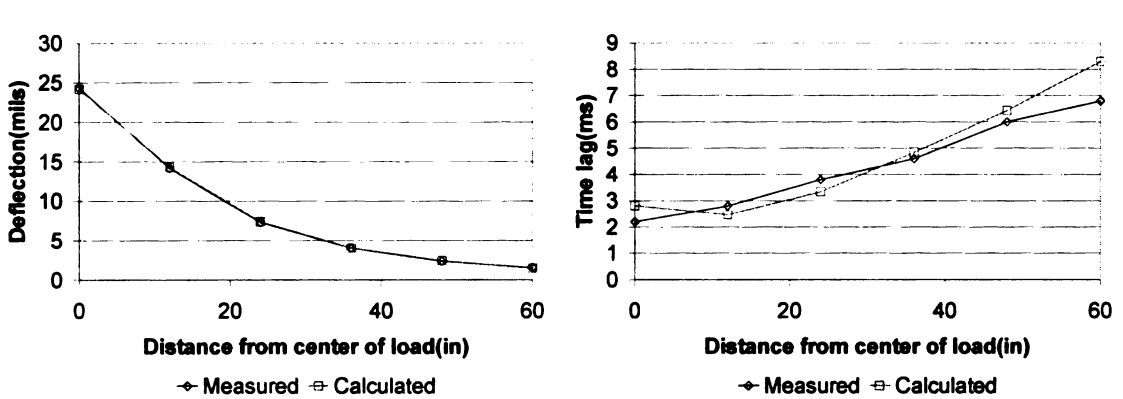

Figure 7.47 Comparison of measured and predicted deflection basins and time lags for load level 4 – Texas site

7.2.2.2 Dynamic Time-domain Backcalculation for Three- layer System

Due to the limited number of sensors, only 8 parameters including layer moduli, damping ratios and thicknesses can be backcalculated. The results are listed in Table 7.11. The results indicate that the error in backcalculated AC layer thickness varies between -25% and 4% while that in depth-to-stiff layer varies between 23% and 41%.

The effect of thickness backcalculation on backcalculated layer moduli is significant for the stiff layer, in unreasonablely high modulus value. On the other hand, thickness

backcalculation has not affected while it is not significant for the base layer. The effect on backcalculated AC layer modulus is variable. For both options, the backcalculated damping ratios are not reasonable.

Table 7.11 Backcalculation results for time-domain analysis – Texas site

Load Level	Layer	Dynamic Backcalculation Without Thickness		Dynamic Backcalculation With Thickness		
		Modulus (ksi)	Damping	Modulus (ksi)	Damping	Thickness (in.)
6000 lb	AC	192	0.11	300	0.73	6.0
	Base	23	0.12	27.3	0.09	94.8
	Stiff layer	125	0.58	3996	0.01	---
9000 lb	AC	154	0.49	172	0.29	8.3
	Base	25	0.04	25	0.10	82.3
	Stiff layer	67	0.45	3382	0.02	---
12000 lb	AC	151	0.53	230	0.35	6.8
	Base	25	0.08	24	0.12	84.0
	Stiff layer	201	0.02	4000	0.02	---
15000 lb	AC	182	0.42	366	0.49	7.5
	Base	21	0.14	21	0.10	92.8
	Stiff layer	104	0.46	306	0.27	---

Comparisons of measured and simulated deflection time histories are shown in Figure 7.48 through Figure 7.55. The match for peak deflections is significantly better than that for time lags. Again, this could be due to errors in sensor location or in time synchronization of the data acquisition system. Also, the effect of thickness backcalculation on matching the peak deflection and time lags is not visible.

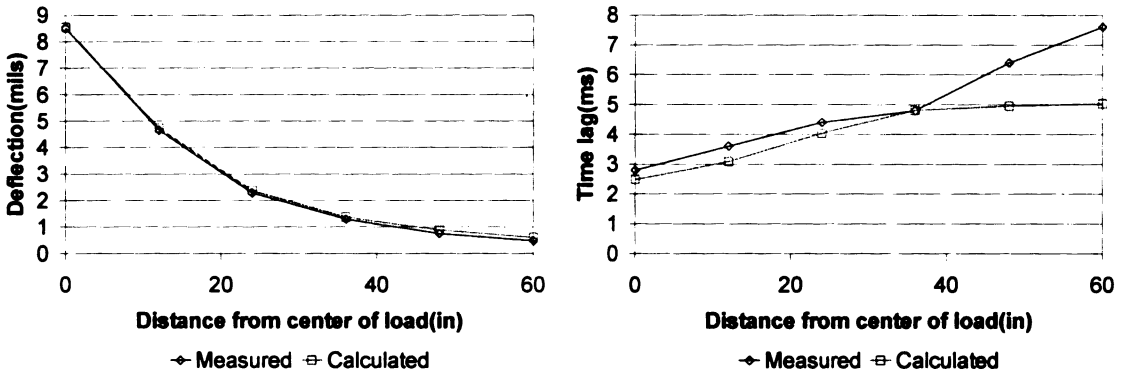

Figure 7.48 Comparison of measured and predicted deflection basins and time lags for load level 1 (with thickness) – Texas site

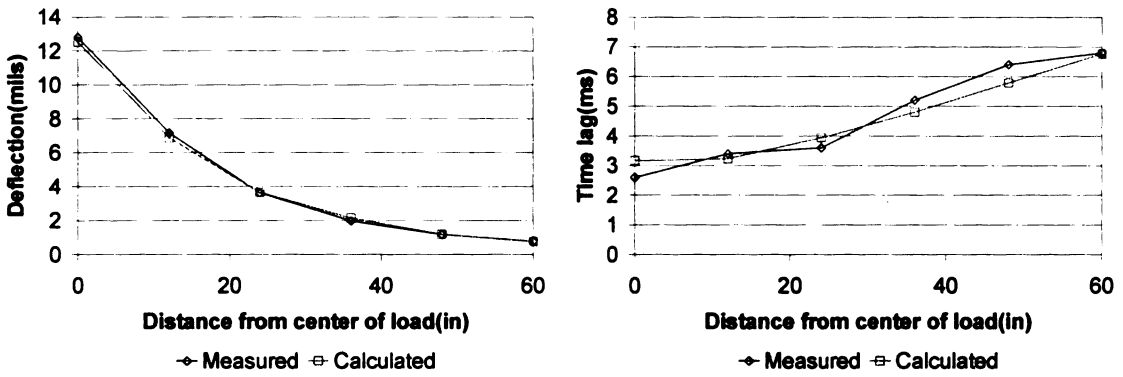

Figure 7.49 Comparison of measured and predicted deflection basins and time lags for load level 2 (with thickness) – Texas site

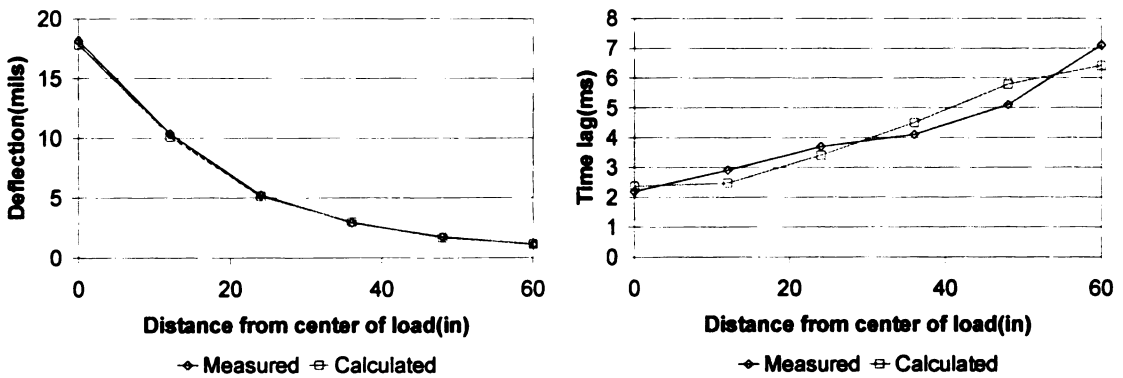

Figure 7.50 Comparison of measured and predicted deflection basins and time lags for load level 3 (with thickness) – Texas site

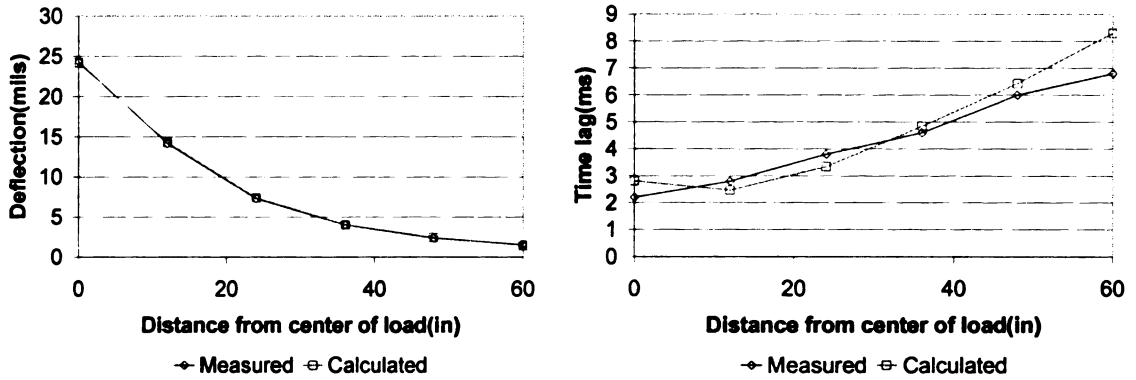

Figure 7.51 Comparison of measured and predicted deflection basins and time lags for load level 4 (with thickness) – Texas site

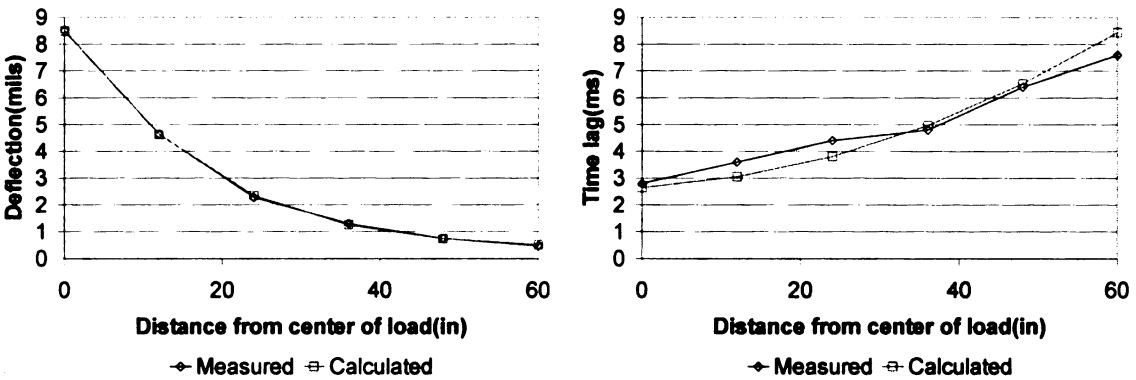

Figure 7.52 Comparison of measured and predicted deflection basins and time lags for load level 1 (without thickness) – Texas site

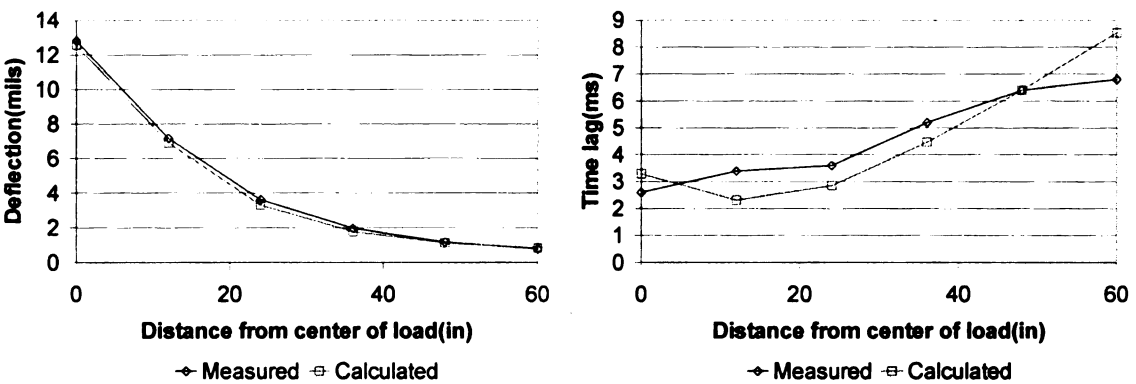

Figure 7.53 Comparison of measured and predicted deflection basins and time lags for load level 2 (without thickness) – Texas site

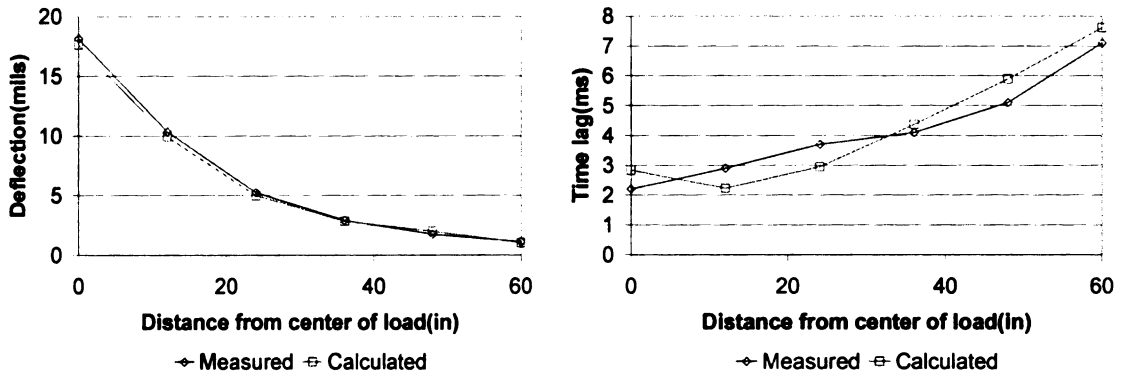

Figure 7.54 Comparison of measured and predicted deflection basins and time lags for load level 3 (without thickness) – Texas site

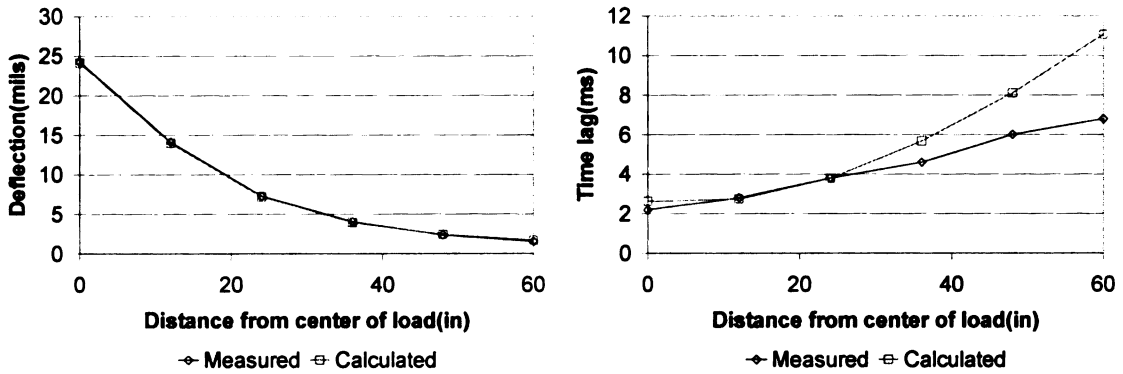

Figure 7.55 Comparison of measured and predicted deflection basins and time lags for load level 4 (without thickness) – Texas site

7.2.2.3 Dynamic Time-domain Backcalculation using Traces of Time History

In the first part, the relation between convergence and threshold (α) is investigated. Figure 7.56 shows the number of iterations until convergence as a function of α, The appropriate value for α is 3 or 4 in this site.

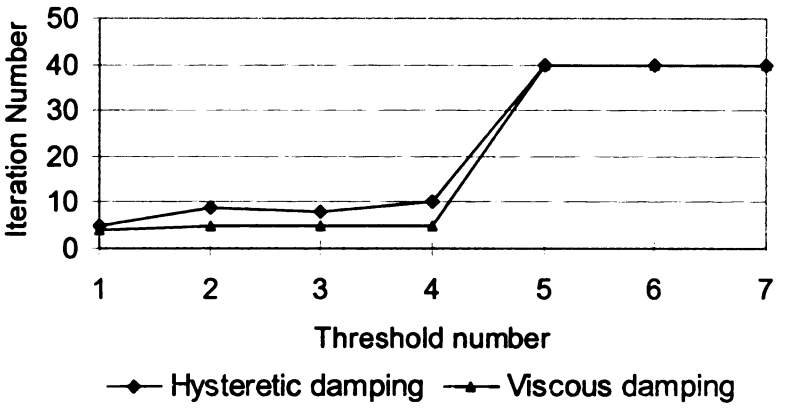

Figure 7.56 Iteration number to convergence versus α for Texas site

In the second part of the analysis, a three-layer pavement system with known thickness is used for backcalculation. The pavement profile is listed in Table 7.8. Since there is a present in this site a modulus of 500,000 psi was assumed for it, The FWD test result for a load level of 9000 lb was used for backcalculation. Figure 7.57 though Figure 7.62 show the traces of time history from both measurement and calculation. It can be seen that the program can provide a good match between the calculated and measured response. It is also noted that the matches in the last two sensors have large differences. This may be caused by the assumption of an arbitrary value for the stiff layer modulus, which will affect the propagation of the wave trapped above the stiff layer.

Figure 7.63 summarizes the backcalculation results in terms of modulus values. The backcalculation results indicate that the relative difference in layer moduli using hysteretic and viscous damping models can be relatively large (18% for AC, –48% for the base, and 43% for the subgrade layer) The difference between backcalculated moduli from the FEM model (Massui, 1998) and DYNABACK with hysteretic damping are 2%, 7% and 13 for the AC, base and subgrade layer, respectively.

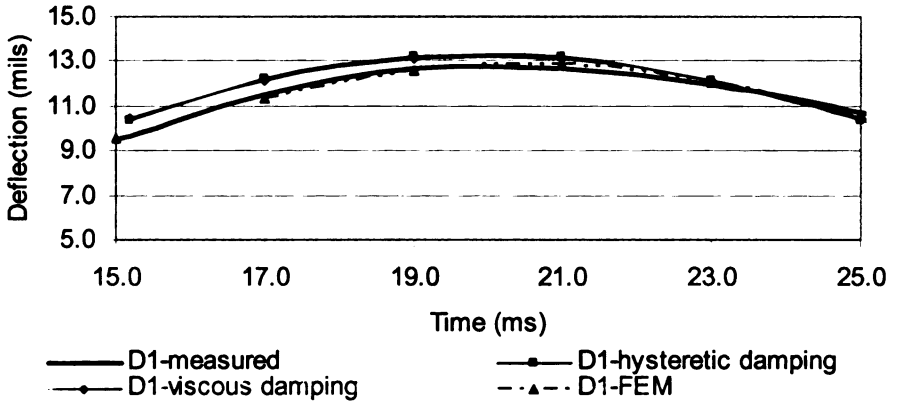

Figure 7.57 Comparison of measured and predicted deflection time histories for sensor 1

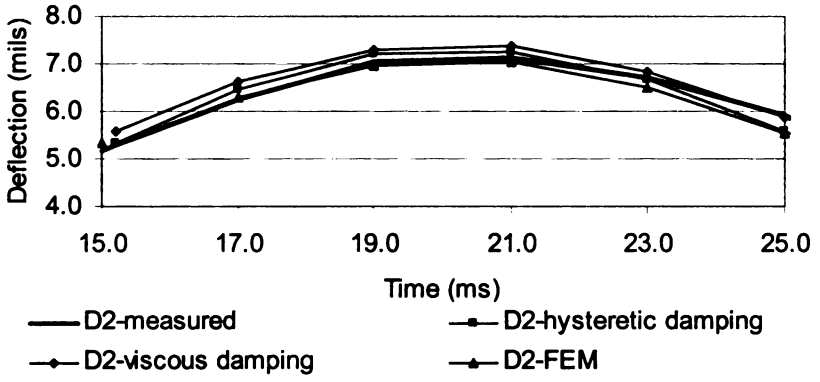

Figure 7.58 Comparison of measured and predicted deflection time histories for sensor 2

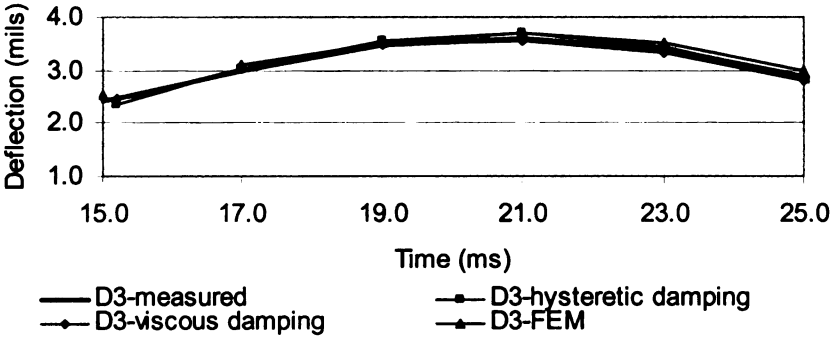

Figure 7.59 Comparison of measured and predicted deflection time histories for sensor 3

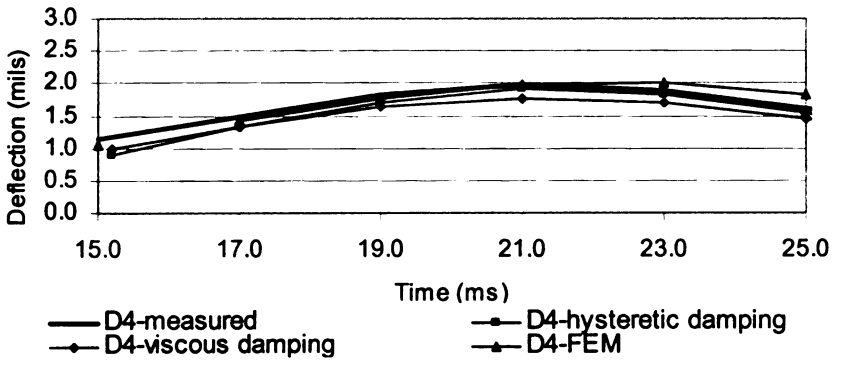

Figure 7.60 Comparison of measured and predicted deflection time history for sensor 4

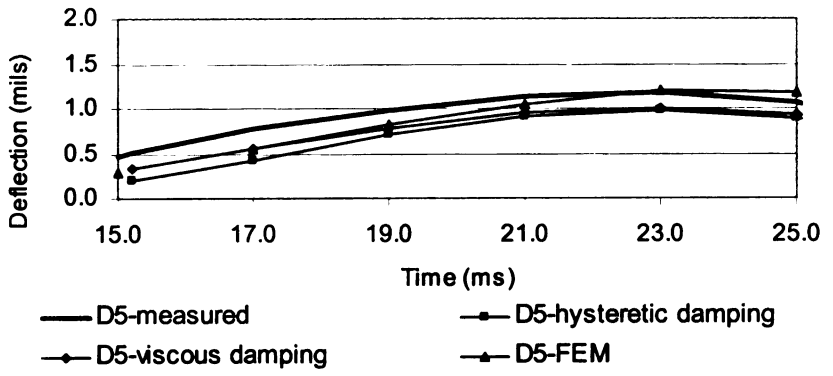

Figure 7.61 Comparison of measured and predicted deflection time histories for sensor 5

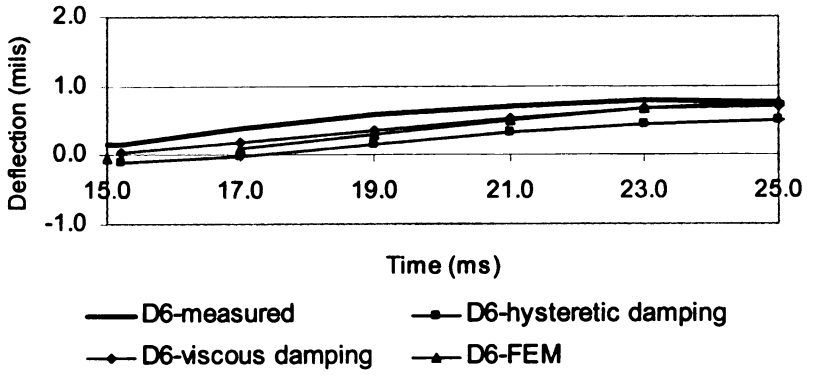

Figure 7.62 Comparison of measured and predicted deflection time histories for sensor 6

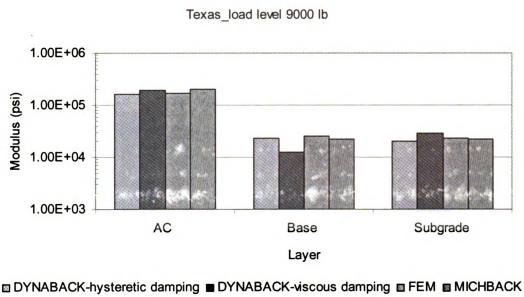

Figure 7.63 Comparison of layer modulus from different model

In the third part of the analysis, the uniqueness was analyzed. The different seed parameters that were used in the program are shown in Table 7.12. The backcalculated results are shown in Figure 7.64.

Table 7.12 Seed values used for Texas data

Layer	Case 1		Case 2		Case 3	
Layer	Seed Modulus (ksi)	Seed Damping	Seed Modulus (ksi)	Seed Damping	Seed Modulus (ksi)	Seed Damping
AC	350	0.10	850	0.15	250	0.20
Base	70	0.10	90	0.05	10	0.15
Subgrade	70	0.02	90	0.05	8	0.10

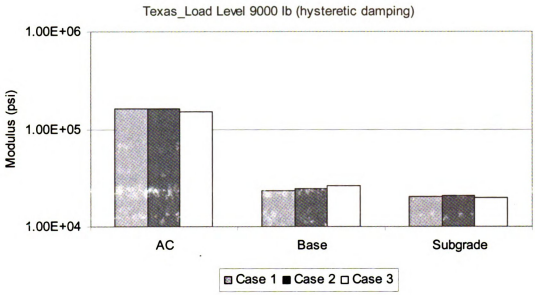

Figure 7.64 Comparison of backcalculated layer moduli using different seed values

In the fouth part of the analysis, only the hysteretic damping model is used. The thicknesses of base and subgrade layer are combined, and the modulus of AC, base, and stiff layers were backcalculated. Various combinations of damping ratios for the base and subgrade layer were used, as listed in Table 7.7. Figure 7.65 through Figure 7.69 show the backcalculation results. It can be seen that the backcalculated AC damping ratio deceases with the increasing damping ratios of base and subgrade layers because of compensation. The thickness of the AC layer varies from -12% to 4% from the true value (a good result). Also layer moduli are not significantly affected by the different assumptions of damping ratios for base and subgrade layer.

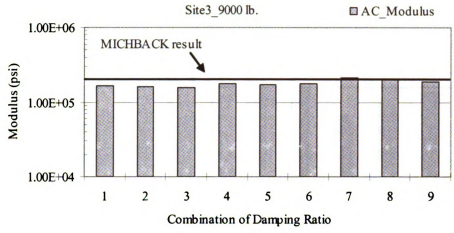

Figure 7.65 Comparison of backcalculated AC modulus for different damping ratio combinations for base and subgrade layers

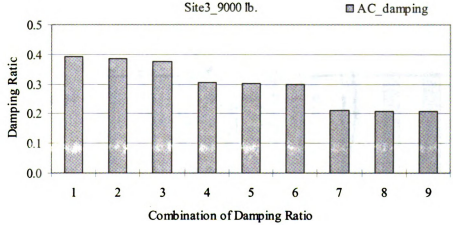

Figure 7.66 Comparison of backcalculated AC damping for different damping ratio combinations for base and subgrade layers

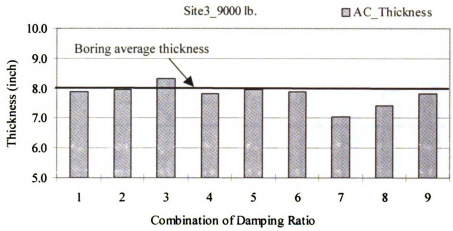

Figure 7.67 Comparison of backcalculated AC thickness for different damping ratio combinations for base and subgrade layers

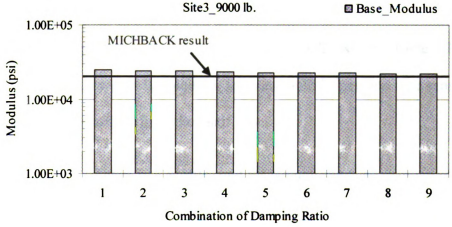

Figure 7.68 Comparison of backcalculated base modulus for different damping ratio combinations for base and subgrade layers

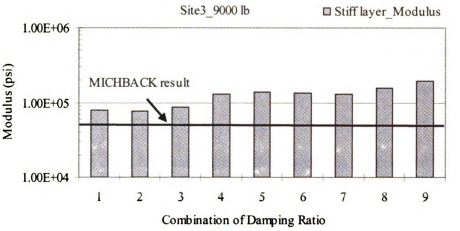

Figure 7.69 Comparison of backcalculated subgrade modulus for different damping ratio combinations for base and subgrade layers

7.2.3 Cornell Site

Table 7.13 shows the pavement cross-section of the Cornell test site. Table 7.14 shows the FWD sensor layouts, which is unique in the sense that it includes nine sensors with the farthest sensor at almost 6 ft from the load.

Table 7.13 Profile used for Cornell site

Layer Name	Thickness (in)	Unit Weight (pcf)	Poisson Ratio
AC	4.5	145	0.3
Base	15	135	0.35
Subbase	110	135	0.40
Subgrade	∞	125	0.45

Table 7.14 Sensor layout (distances are in inches) for Cornell site

D1	D2	D3	D4	D5	D6	D7	D8	D9
0	8	12	18	24	36	47	59	71

7.2.3.1 Comparison of Dynamic and Static Backcalculation for Four-layer System

The analysis was first conducted on a 4-layer pavement system. However, the results for dynamic analysis compare reasonably well with those from MICHBACK as shown in Table 7.15, with the exception of the subgrade modulus. Both analyses predict a very low modulus for the base layer and a high subgrade modulus which is not reasonable from an engineering point of view. Also, the backcalculated damping ratios for the unbound materials are unreasonably high. This may be indicative of non-linear behavior for these materials.

Figure 7.70 shows the measured and calculated deflections in frequency. The match is better for real deflections at low frequencies while it is better for imaginary deflection at intermediate frequencies. Figure 7.71 shows the comparison of measured and predicted peak deflections and time lags. The match is fairly good for peak deflections and poor for the time lags.

Table 7.15 Comparison of frequency and time-domain backcalculation results with those from MICHBACK- Cornell site

	Frequency-domain Bckcalculation		Time-domain Bckcalculation		Static Backcalculation
	Modulus (ksi)	Damping	Modulus (ksi)	Damping	Modulus (ksi)
AC	1752	0.10	1972	0.10	2013
Base	7	0.11	8	0.42	7
Subbase	29	0.08	20	0.13	21
Subgrade	216	0.24	58	0.14	34

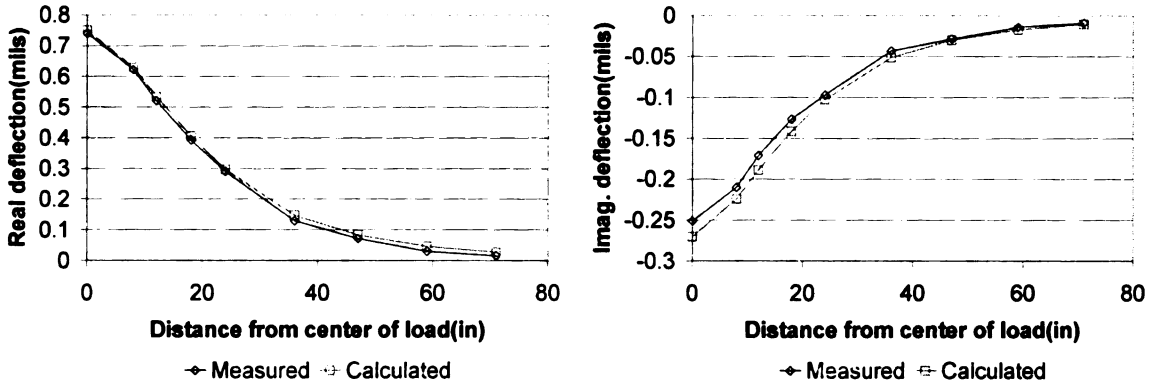

(a) Real and imaginary deflection basins at 2.44 Hz

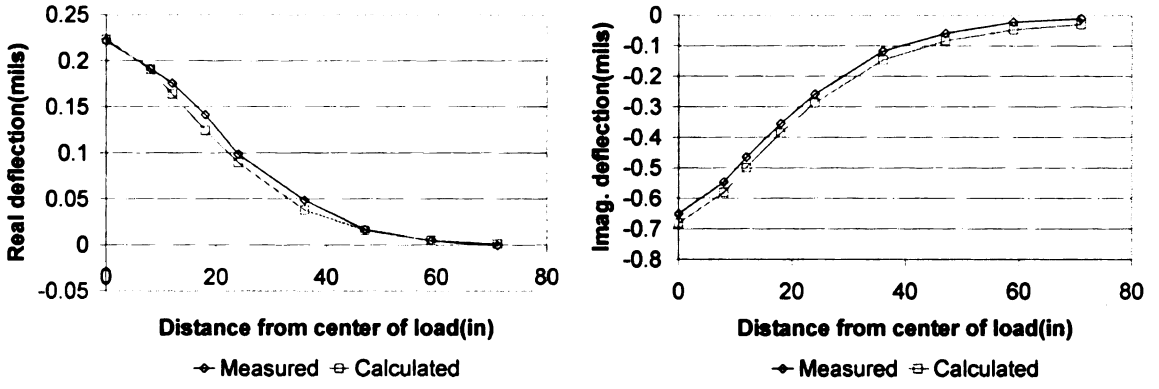

(b) Real and imaginary deflection basins at 9.77 Hz

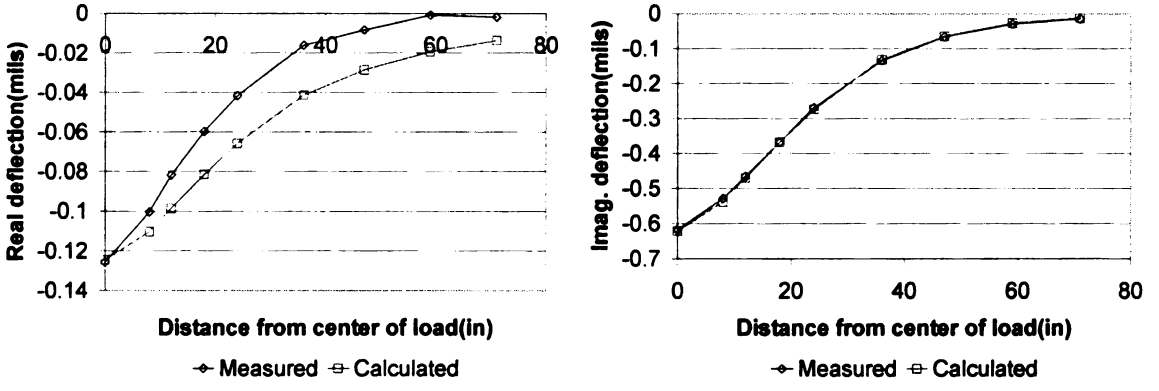

(c) Real and imaginary deflection basins at 14.65 Hz

Figure 7.70 Comparison of measured and predicted deflection basins – Cornell site

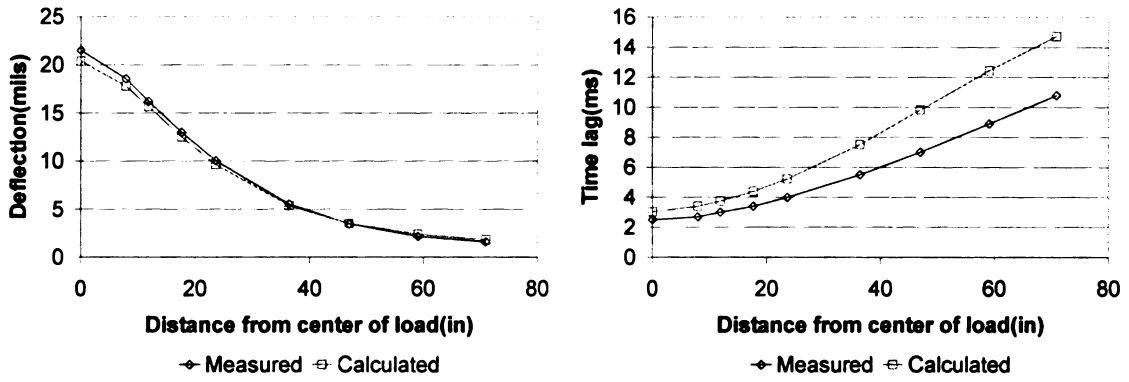

Figure 7.71 Comparison of measured and predicted deflection basins and time lags

7.2.3.2 Dynamic Time-domain Backcalculation for Three-layer System

In this section, the base and subbase layers were combined and the program was allowed to backcalculate the layer thicknesses. The time-domain backcalculation results are listed in Table 7.16. The error in the backcalculated thicknesses was about 33% for the AC layer and about -40% for the combined base and subbase layer. The effect of thickness backcalculation on layer moduli was significant for the AC layer as well as the subgrade. Also, the backcalculated damping ratio values are unreasonably high for the AC and base layers. The backcalculated subgrade modulus and damping ratio for the case when thickness backcalculation was allowed are unacceptable. Comparisons of measured and simulated deflections and time lags are shown in Figure 7.72 and Figure 7.73, for the cases with and without thickness backcalculation. The matching is not good, in both cases.

Table 7.16 Backcalculation results from time-domain analysis – Cornell site

	Dynamic Backcalculation (without thickness backcalculation)		Dynamic Backcalculation (with thickness backcalculation)		
	Modulus (ksi)	Damping	Modulus (ksi)	Damping	Thickness(in.)
AC	1903	0.11	687	0.21	6
Base	17	0.38	14	0.14	74
Subgrade	23	0.05	400	0.001	---

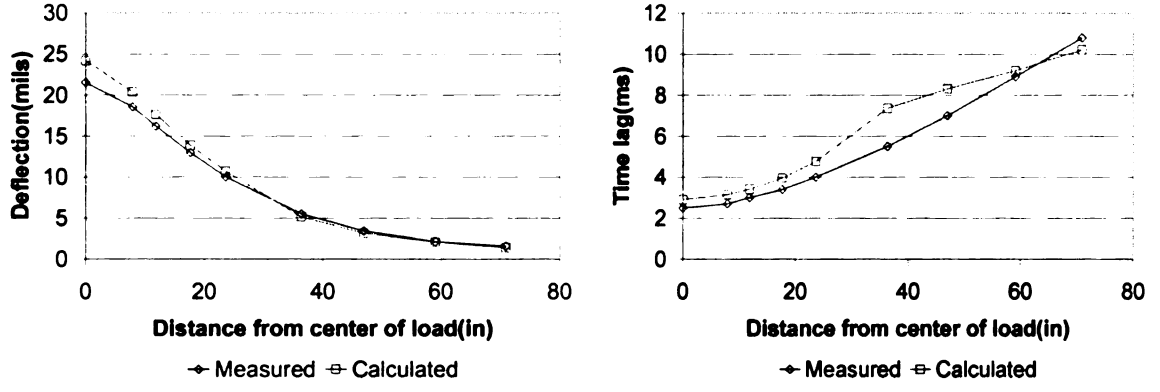

Figure 7.72 Comparison of measured and predicted deflections and time lags (with thickness backcalculation)

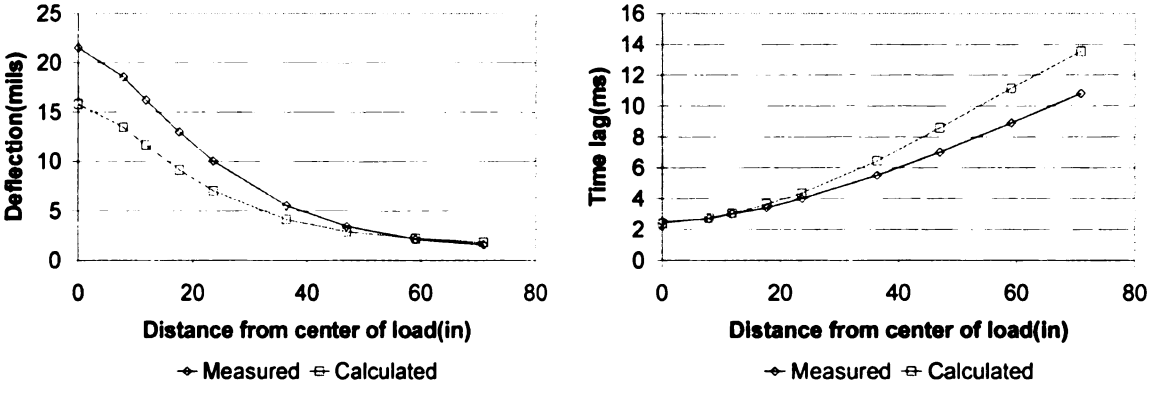

Figure 7.73 Comparison of measured and predicted deflections and time lags (without thickness backcalculation)

7.2.3.3 Dynamic Time-domain Backcalculation using Traces of Time History

In the first part, Figure 7.74 shows the relationship of α versus iteration number, and a value for α of 3 or 4 can be considered to be appropriate for this site.

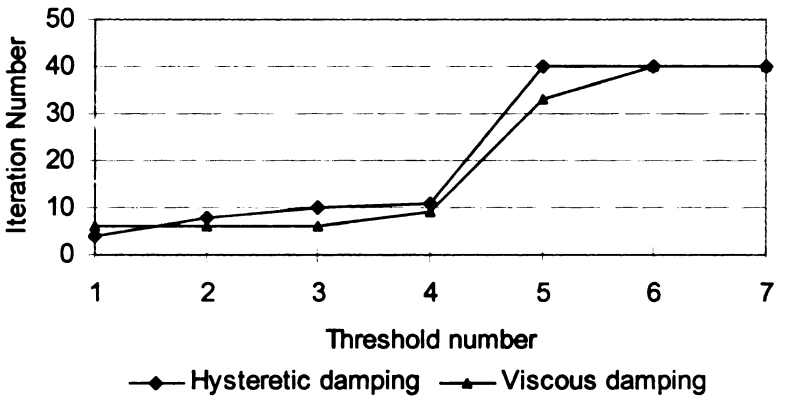

Figure 7.74 Iteration number to convergence versus α for Cornell site

In the second part of the analysis, a four-layer system is employed for backcalculation purposes. Traces of time history are used in the analysis. Figure 7.75 through Figure 7.82 show measured and predicted deflections for the various sensors. The backcalculated layer moduli from various models are compared to see the similarities and differences in Figure 7.84. The comparisons show that the relative difference for layer modulus between the hysteretic and viscous damping is –2% for AC layer, 20% for base, -7% for subgrade and –69% for stiff layer. The difference between the FEM method and DYNABACK with hysteretic damping is 1% for AC layer, -32% for base, 47% for subgrade, and –48% for stiff layer. The value seems to show a very good consistency for modulus in this site.

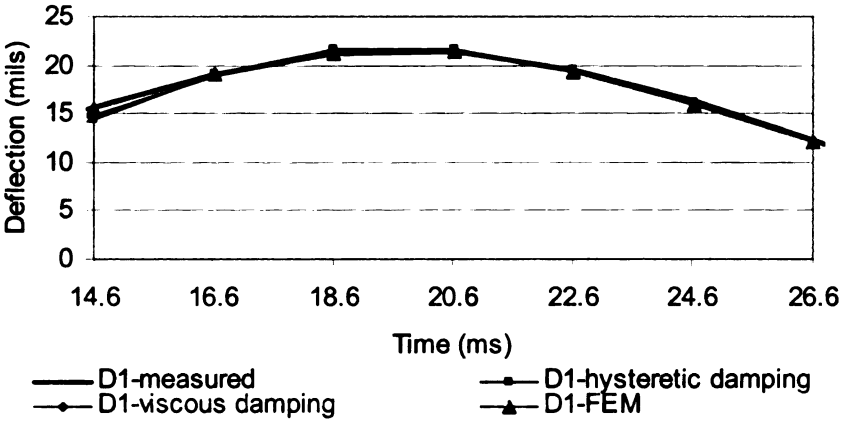

Figure 7.75 Comparison of measured and predicted deflection time histories for sensor 1

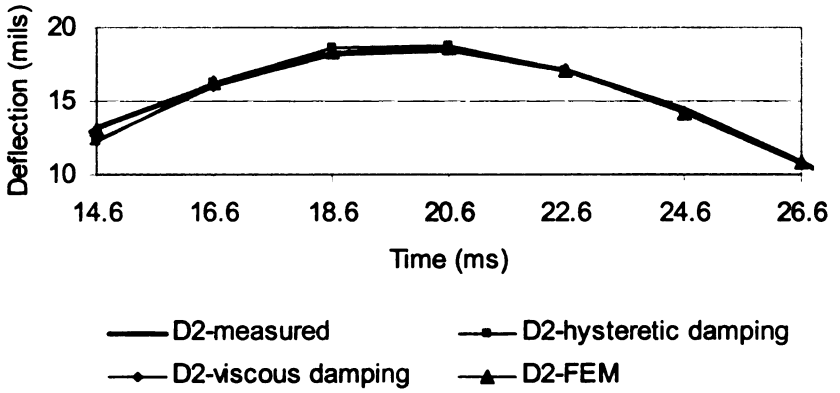

Figure 7.76 Comparison of measured and predicted deflection time histories for sensor 2

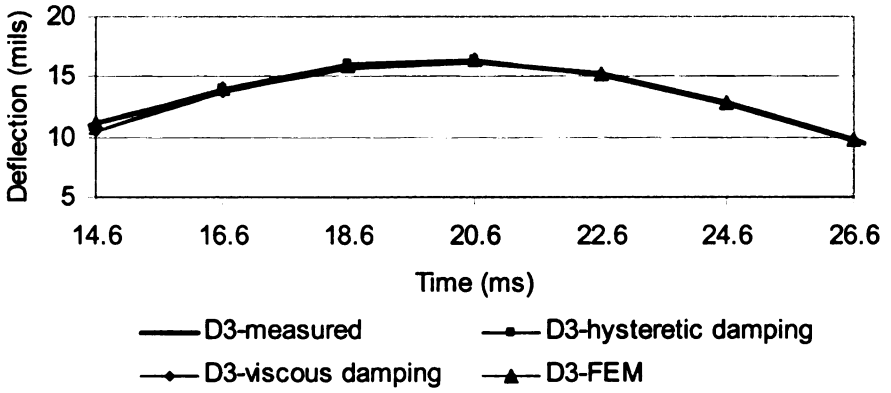

Figure 7.77 Comparison of measured and predicted deflection time histories for sensor 3

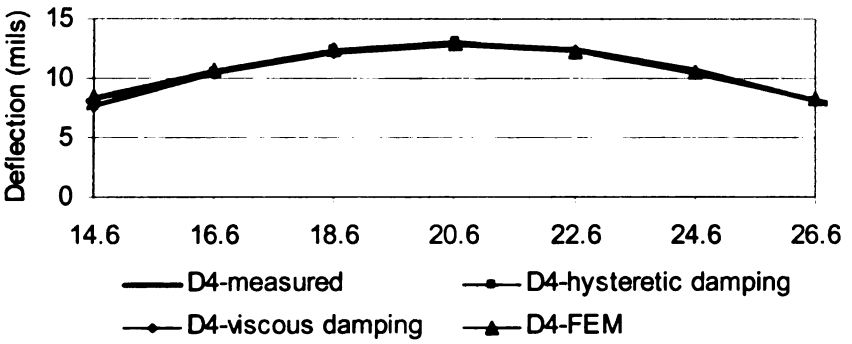

Figure 7.78 Comparison of measured and predicted deflection time histories for sensor 4

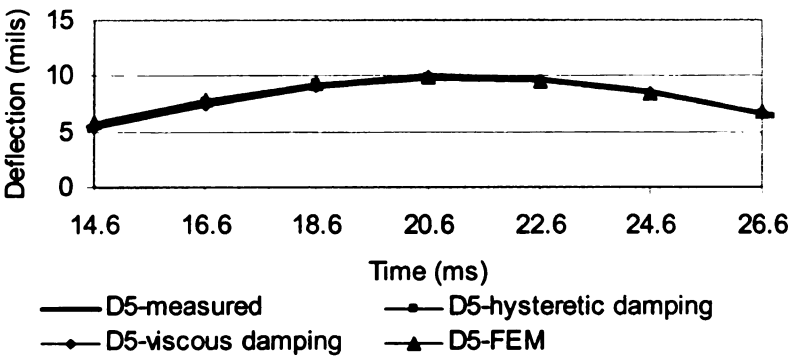

Figure 7.79 Comparison of measured and predicted deflection time histories for sensor 5

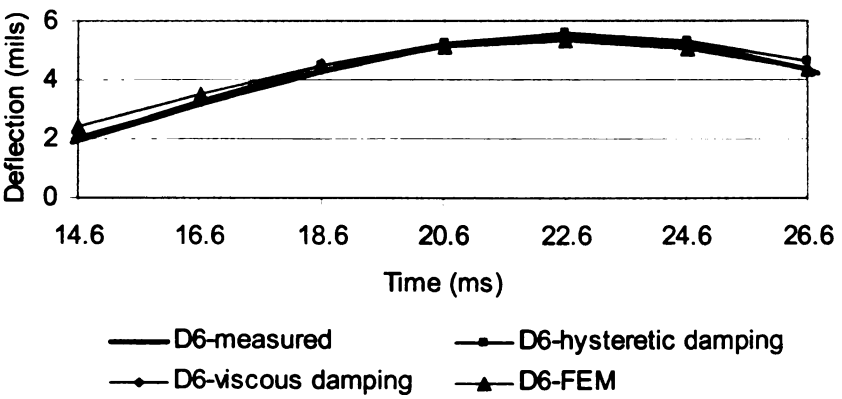

Figure 7.80 Comparison of measured and predicted deflection time histories for sensor 6

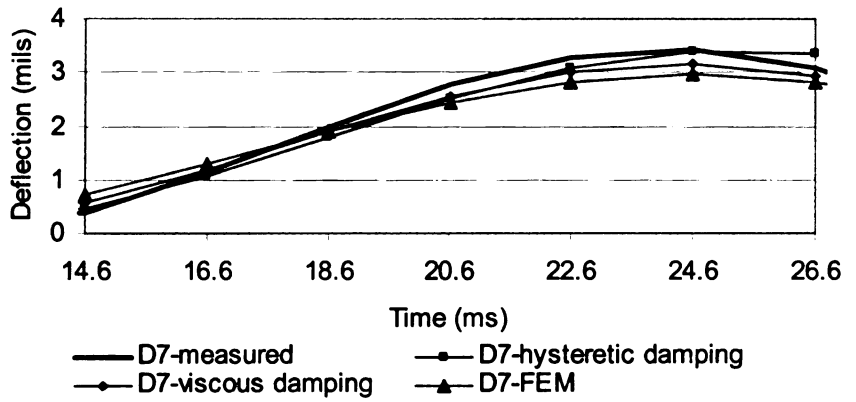

Figure 7.81 Comparison of measured and predicted deflection time histories for Sensor 7

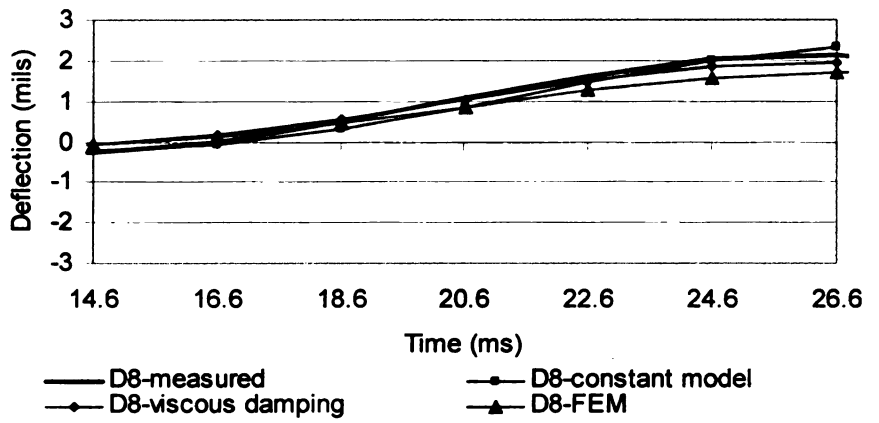

Figure 7.82 Comparison of measured and predicted deflection time histories for Sensor 8

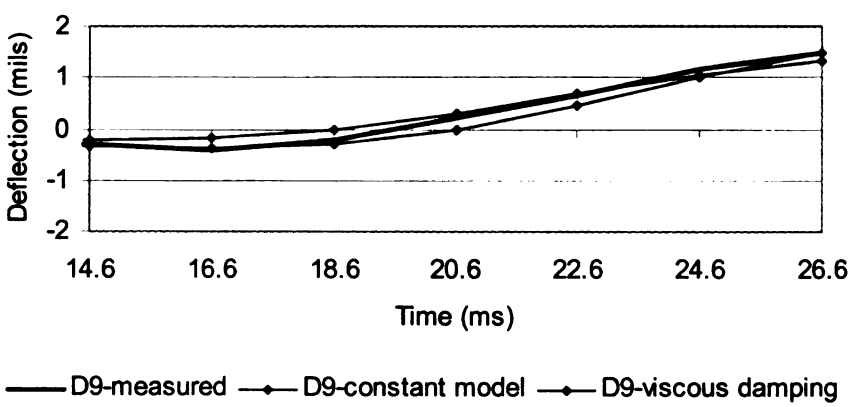

Figure 7.83 Comparison of measured and predicted deflection time histories for Sensor 9

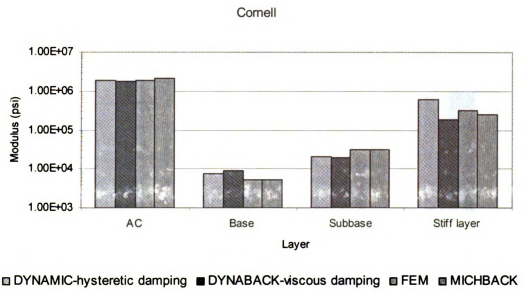

Figure 7.84 Comparison of backcalculated modulus from different models

In the third part of the analysis, the uniqueness was analyzed for the four layer pavement system. The different seed parameters that were used in the program are shown in Table 7.17. The backcalculated results using different seeds that are listed show the excellent agreement in Figure 7.85.

Table 7.17 Different seed Specifications – Cornell data

Layer	Case 1		Case 2		Case 3	
Layer	Seed Modulus (ksi)	Seed Damping	Seed Modulus (ksi)	Seed Damping	Seed Modulus (ksi)	Seed Damping
AC	450	0.1	250	0.2	850	0.3
Base	80	0.08	10	0.05	100	0.08
Subgrade	60	0.05	10	0.05	90	0.05
Stiff layer	50	0.03	30	0.03	10	0.03

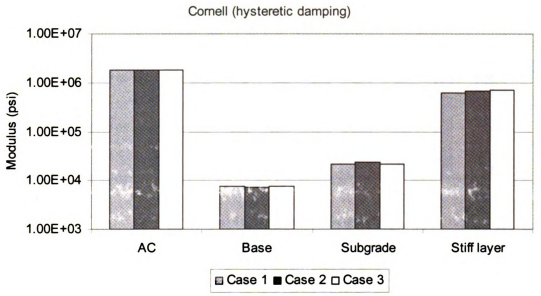

Figure 7.85 Comparison of backcalculated layer moduli using different seeds

In the fourth part of the analysis, a three-layer pavement system with unknown AC thickness and hysteretic damping was used. Various damping ratio combinations of base and subgrade layer as shown in Table 7.7. Six parameters are backcalculated, including modulus of AC. base, and subgrade and damping ratio and thickness for AC. Figure 7.86 through Figure 7.90 show the backcalculation results. Figures show the AC damping ratio deceases with the increasing of damping ratio for base and subgrade. The AC thickness varies from 25% to 46% from the true value. The AC, base and subgrade moduli were not affected.

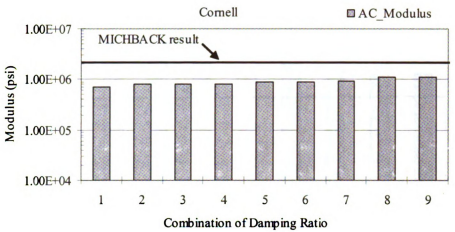

Figure 7.86 Comparison of backcalculated AC modulus for different damping ratio combinations for base and subgrade

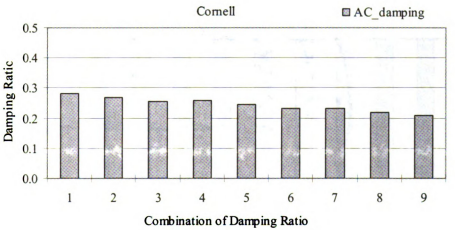

Figure 7.87 Comparison of backcalculated AC damping ratio for different damping ratio combinations for base and subgrade layers

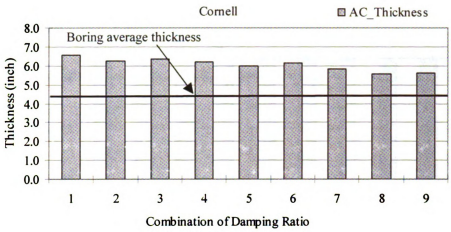

Figure 7.88 Comparison of backcalculated AC thickness for different damping ratio combinations for base and subgrade layers

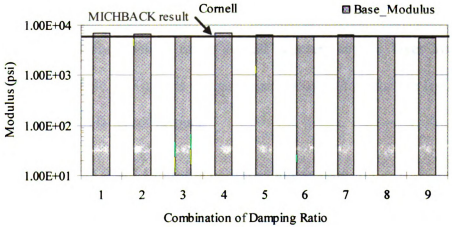

Figure 7.89 Comparison of backcalculated base modulus for different damping ratio combinations for base and subgrade layers

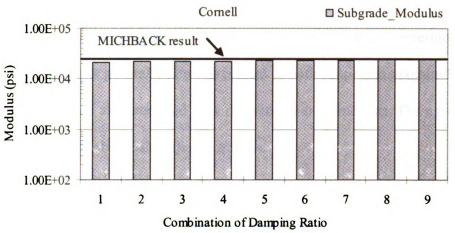

Figure 7.90 Comparison of backcalculated subgrade modulus for different damping ratio combinations for base and subgrade layers

7.2.4 Florence Site

The site in Florence, Italy, consists of an asphalt concrete surface layer overlying a cement-treated base. Table 7.18 shows the pavement cross-section for the test site, and Table 7.19 shows the FWD sensor layouts.

Table 7.18 Profile used for Florence site

Layer Name	Thickness (in)	Unit Weight (psf)	Poisson Ratio
AC	4	138	0.35
CTB	5.5	150	0.20
Subgrade	90	116	0.45
Stiff layer	∞	120	0.15

7.2.4.1 Comparison of Dynamic and Static Backcalculation for Four-layer System

Table 7.20 shows the backcalculation results. The results from time-domain analysis are somewhat more reasonable than those for frequency-domain analysis, while the results for static backcalculation are not reasonable, showing low values for the cement-treated base and bedrock moduli and a very high value for the subgrade modulus. The damping

ratios (for dynamic analysis) for the AC layer and subgrade are also unreasonably high. Figure 7.91 shows the measured and predicted deflection basins at low, intermediate and high frequencies. There is generally poor agreement in both shape and magnitude. Figure 7.92 shows the measured and predicted peak deflections and time lags. The agreement is fair but not acceptable for backcalculation purposes.

Table 7.19 Sensor layout (distances are in inches) for Florence site

D1	D2	D3	D4	D5	D6	D7
0	12	18	24	35	47	59

Table 7.20 Comparison of frequency and time-domain backcalculation results with those for MICHBACK – Florence site

	Frequency-domain Backcalculation		Time-domain Backcalculation		Static Backcalculation
	Modulus (ksi)	Damping	Modulus (ksi)	Damping	Modulus (ksi)
AC	300	0.32	562	0.52	440
CTB	495	0.01	624	0.01	200
Subgrade	11	0.13	9	0.27	124
Bedrock	124	0.05	1989	0.03	27

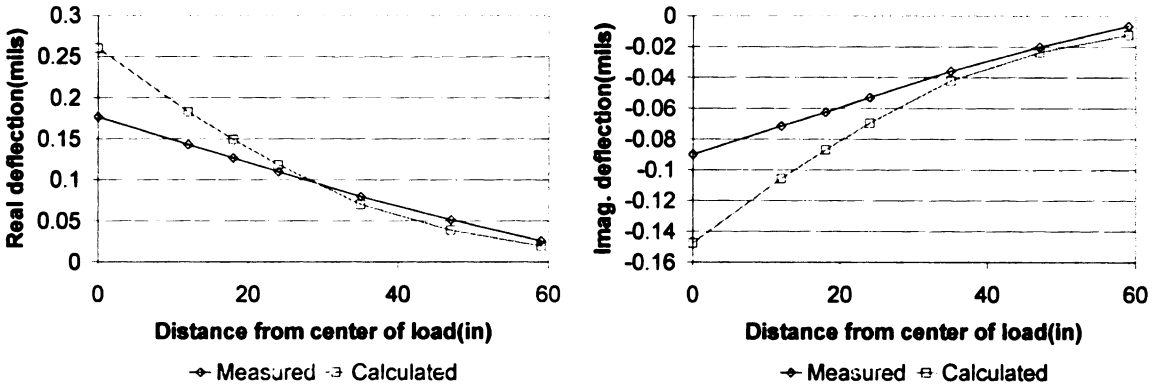

(a) Real and imaginary deflection basins at 3.66 Hz

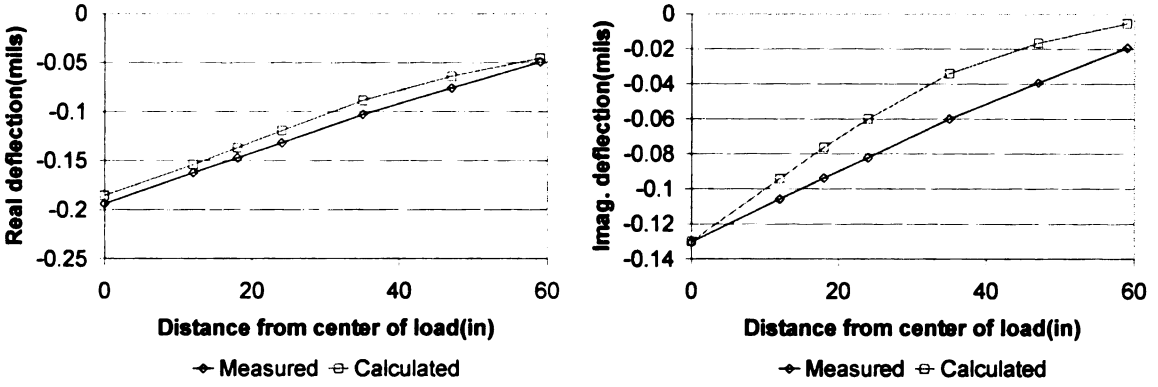

(b) Real and imaginary deflection basins at 15.89 Hz

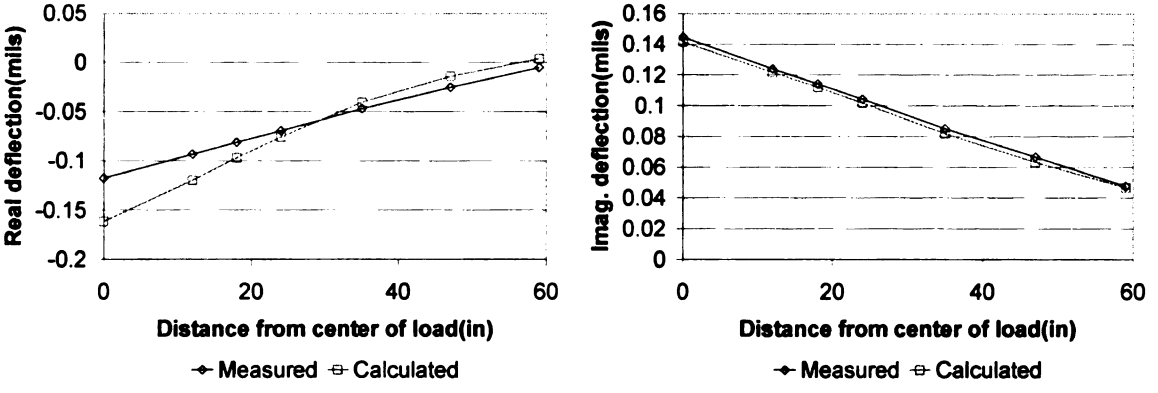

(c) Real and imaginary deflection basins at 23.19 Hz

Figure 7.91 Comparison of measured and predicted deflection basins– Florence site

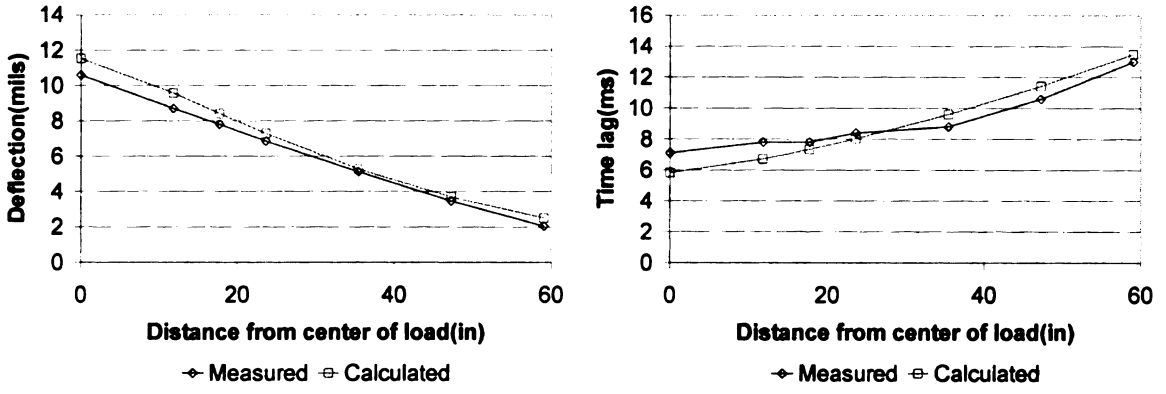

Figure 7.92 Comparison of measured and predicted deflection basins and time lags – Florence site

7.2.4.2 Dynamic Time-domain Backcalculation for Three-layer System

In this analysis, the AC and CTB layers were combined again and the program was allowed to backcalculate layer thicknesses. The time-domain backcalculation results are listed in Table 7.21. The error in the backcalculated thicknesses was about 17% for the combined AC and CTB layer and about 31% for the subgrade layer above the bedrock. The effect of thickness backcalculation on layer moduli was significant for all layers with the difference ranging from -55% to 34%. The backcalculated damping ratios are unreasonably high. Comparisons of measured and simulated deflections and time lags are listed in Figure 7.93 and Figure 7.94, for the cases with and without thickness backcalculation. Matching of peak deflections is better than that for time lags, and the results are slightly better when layer thicknesses are known.

Table 7.21 Thickness backcalculation in time-domain

	Dynamic Backcalculation				
	Without Thickness Backcalculation		With Thickness Backcalculation		
	Modulus (ksi)	Damping	Modulus (ksi)	Damping	Thickness(in.)
AC + CTB	862	0.11	547	0.23	11.1
Subgrade	9	0.18	12	0.12	118.2
Bedrock	118	0.47	52	0.50	---

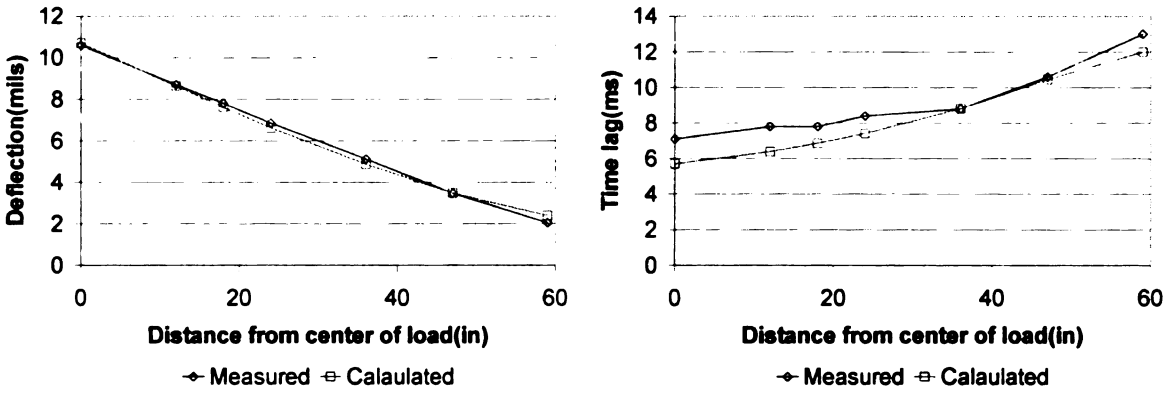

Figure 7.93 Comparison of peak deflections and time lags (with thickness backcalculation) – Florence site

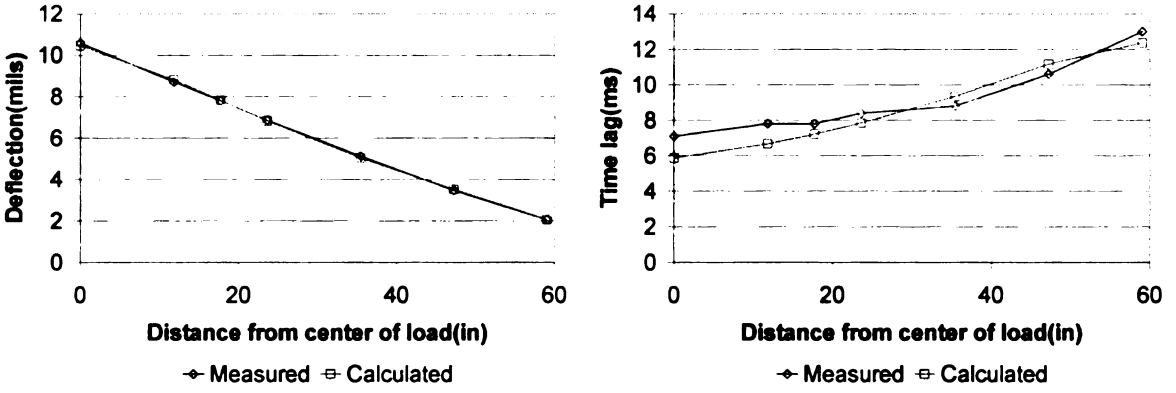

Figure 7.94 Comparison of peak deflections and time lags (without thickness backcalculation) – Florence site

7.2.4.3 Dynamic Time-domain Backcalculation using Traces of Time History

In the first part, the relation of α versus iteration number is shown in Figure 7.95. An α–Value of 3 or 4 is appropriate for this site.

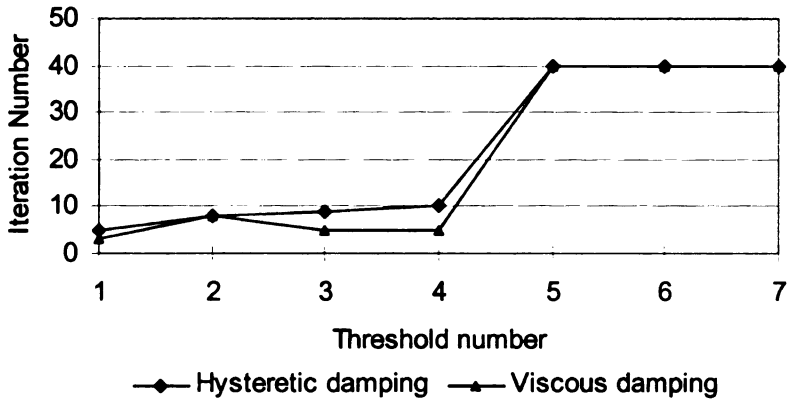

Figure 7.95 Iteration number to convergence versus α for Florence site

In the second part of the analysis, a three-layer pavement system consists of the AC layer, a cement treated base (CTB) and a subgrade layer is used. Figure 7.96 to Figure 7.102 show the comparisons of predicted and measurement time histories for different sensors. Figure 7.103 shows the backcalculated values for different layers using different models. The difference in backcalculated moduli using hysteretic and viscous damping is -21% for AC, 75% for base, and -21% for subgrade. The difference between the backcalculated moduli from the FEM method and DYNABACK with hysteretic damping is –33% for the AC and 50% for the base, and -5% for the subgrade.

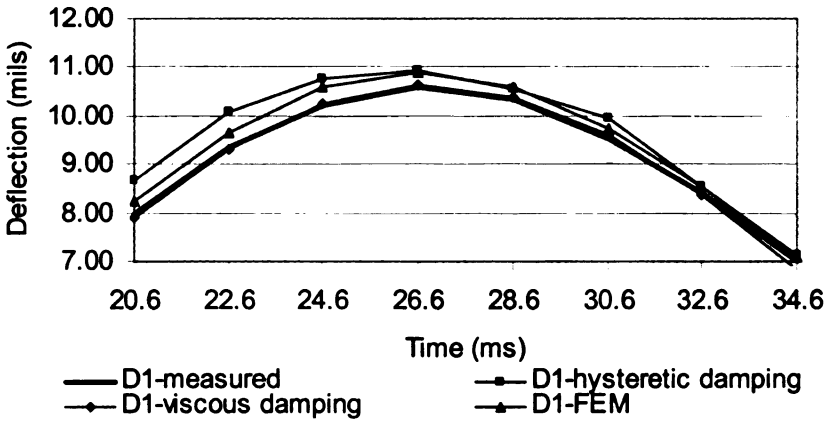

Figure 7.96 Comparison of measured and predicted deflection time histories for sensor 1

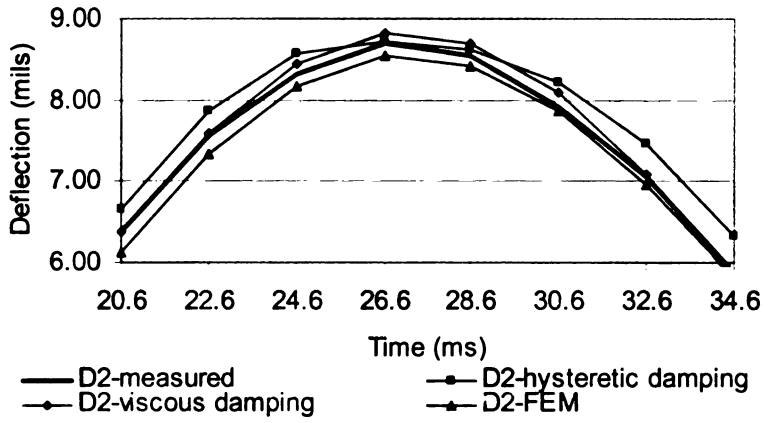

Figure 7.97 Comparison of measured and predicted deflection time histories for sensor 2

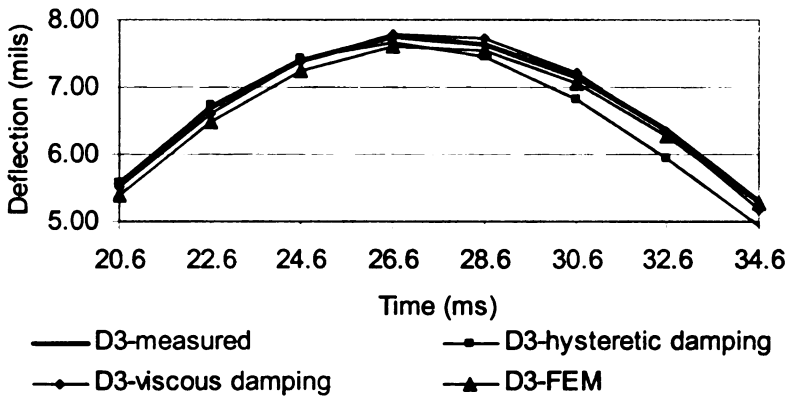

Figure 7.98 Comparison of measured and predicted deflection time histories for sensor 3

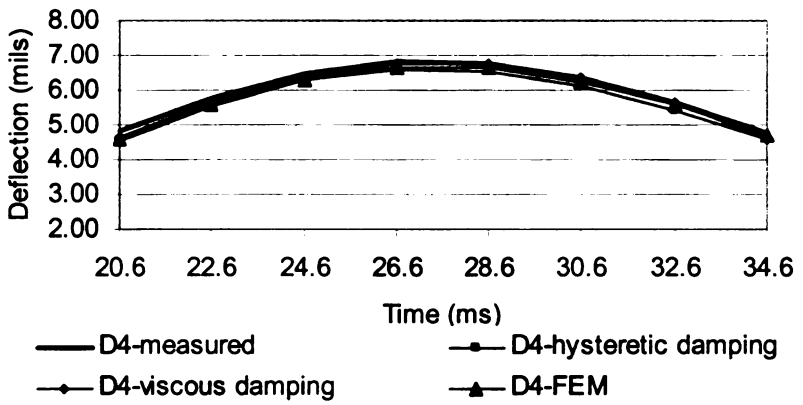

Figure 7.99 Comparison of measured and predicted deflection time histories for sensor 4

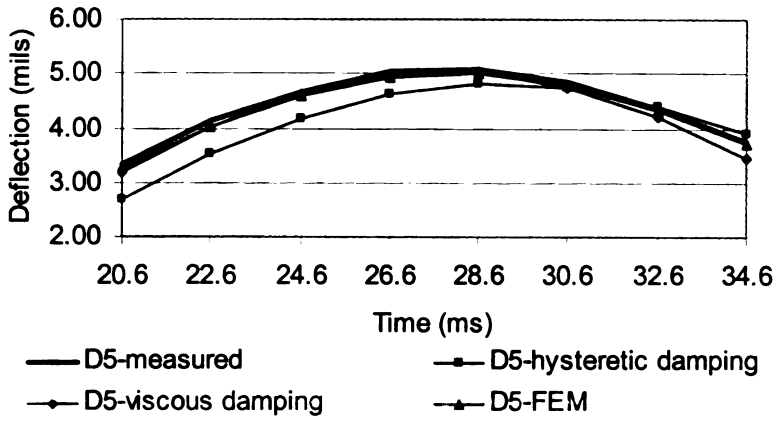

Figure 7.100 Comparison of measured and predicted deflection time histories for sensor 5

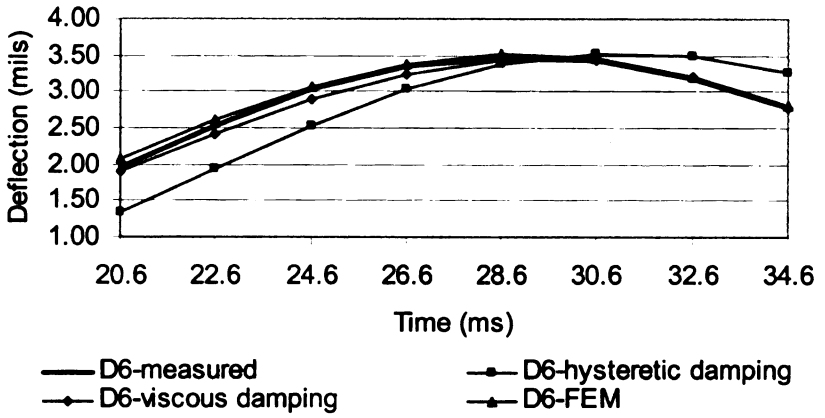

Figure 7.101 Comparison of measured and predicted deflection time histories for sensor 6

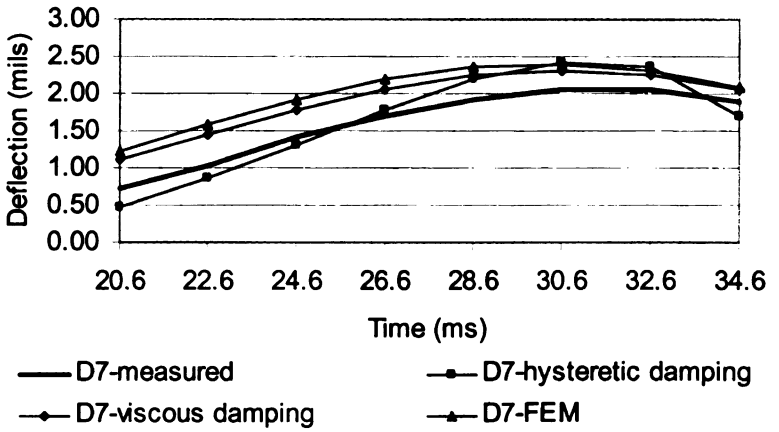

Figure 7.102 Comparison of measured and predicted deflection time histories for sensor 7

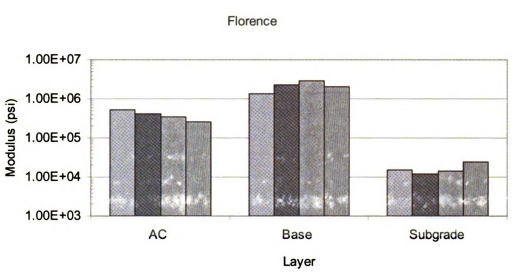

Figure 7.103 Comparison of backcalculated layer moduli from different models

In the third part of the analysis, the uniqueness of the backcalculated results was analyzed for three layers including AC, base and subgrade. The random seed parameters that were used in the program are shown in Table 7.22. Figure 7.104 shows that the backcalculation results are not affected by random seed values.

Table 7.22 Seed value used for Florence data

Layer	Case 1		Case 2		Case 3	
Layer	Seed Modulus (ksi)	Seed Damping	Seed Modulus (ksi)	Seed Damping	Seed Modulus (ksi)	Seed Damping
AC	300	0.4	530	0.2	230	0.3
Base	140	0.08	180	0.05	400	0.03
Subgrade	13	0.08	15	0.05	15	0.08

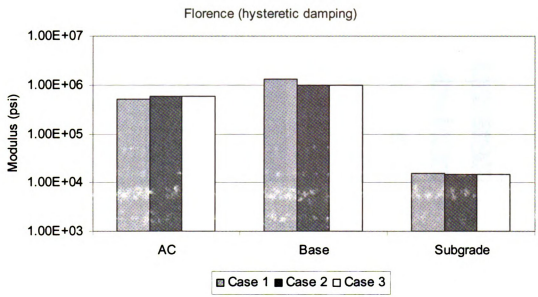

Figure 7.104 Comparison of backcalculated layer moduli using different seed value

In the fourth part of the analysis, a three-layer pavement system was used. The AC thickness is left unknown, and various damping ratio combinations for base and subgrade layers were used (see Table 7.7). The aggregate base and subgrade were combined as one layer base. Figure 7.105 through Figure 7.109 show the backcalculation results using hysteretic damping. The figure shows that the layer moduli are not significantly affected by the chain of damping ratio for the base and subgrade. The AC damping ratio is somewhat more affected, however its variation is not of practical significance. The error in AC thickness backcalculation varies from 23% to 49%; this is may not be acceptable for field application.

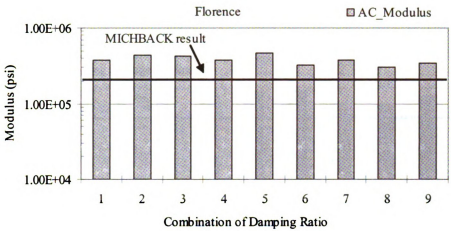

Figure 7.105 Comparison of backcalculated AC modulus for different damping ratio combinations for base and subgrade layers

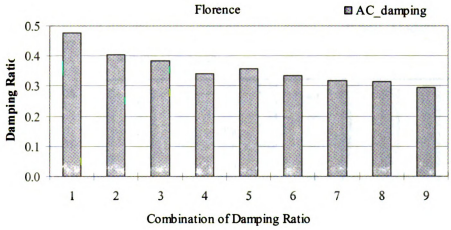

Figure 7.106 Comparison of backcalculated AC damping ratio for different damping ratio combinations for base and subgrade layers

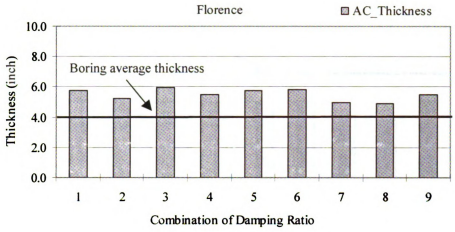

Figure 7.107 Comparison of backcalculated AC thickness for different damping ratio combinations for base and subgrade layer

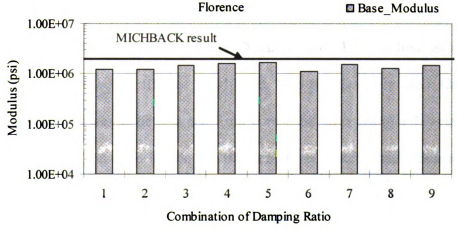

Figure 7.108 Comparison of backcalculated base modulus for different damping ratio combinations for base and subgrade layers

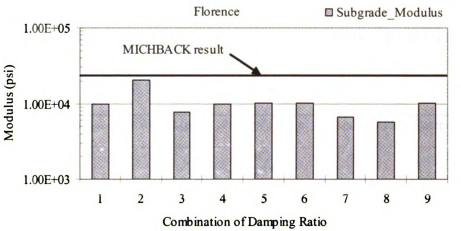

Figure 7.109 Comparison of backcalculated subgrade modulus for different damping ratio combinations for base and subgrade layers

7.2.5 Kansas Site

Backcalculation was also performed using FWD data collected in the field as a part of LTPP study in Kansas (Section ID No. 20-0103-1). Two profiles were used: One using four layers with thicknesses as determined from cores; the other using a 3-layer system with the combined AC and ATB layers. For the three-layer system, backcalculation was done with and without assuming layer thicknesses. Again, the MICHBACK program was used to perform static backcalculation for comparison purposes. The FWD data contained eight deflection time histories for sensors located at r = 0, 8, 12, 18, 24, 36, 48 and 60 inches from the load. The accuracy of each sensor was about ± 0.1 μm.

7.2.5.1 Dynamic Time-domain Backcalculation for Four-layer System

The four-layer pavement profile and backcalculation results are shown in Table 7.23. The results appear to be reasonable, although the subgrade modulus is higher than the base modulus. This is typical of backcalculation results, but is not necessarily realistic. The

damping ratio values are also unrealistic. The measured and calculated peak deflections and time lags are shown in Figure 7.110. The match is poor, especially for the time lags.

Table 7.23 Profile used for Kansas site

Layer Name	Thickness (in)	Unit Weight (pcf)	Poisson's Ratio	Modulus (ksi)	Damping ratio
AC	3.6	145	0.3	640	.33
Base	7.7	135	0.35	436	.54
Subbase	6	135	0.35	18	.09
Subgrade	∞	125	0.45	25	.29

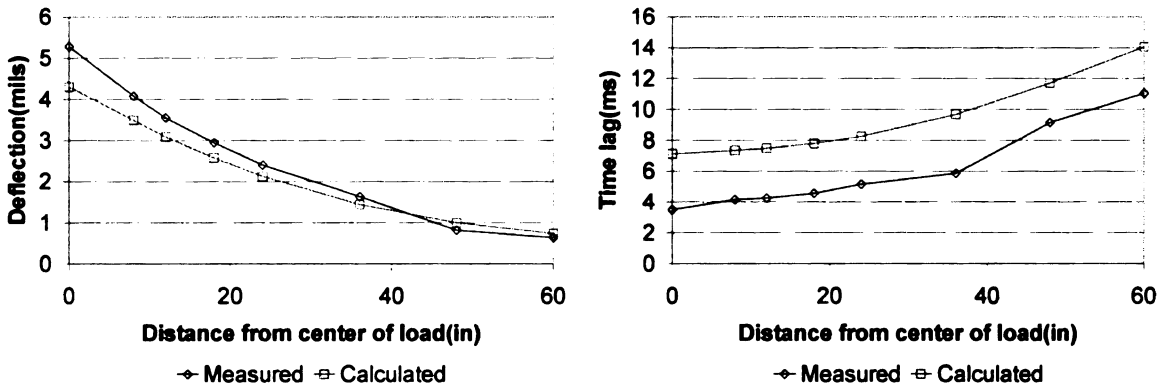

Figure 7.110 Comparison of measured and calculated peak deflections and time lags (four layer backcalculation)

7.2.5.2 Comparison of Dynamic and Static Backcalculation for Three-layer System

For the combined profile in Table 7.24, the results of the dynamic and static backcalculation are given in Table 7.25. The errors in the backcalculated AC and base thicknesses in Case 2 compared to the thicknesses reported from cores are shown within parentheses. In the dynamic backcalculation, the AC modulus decreases by 14% between Cases 1 and 2 mainly because the backcalculated AC thickness for Case 2 is 22% larger than the AC thickness used in Case 1. The backcalculated base thickness in Case 2 is 9.5% larger than the reported thickness from cores.

The measured and predicted surface peak deflections and time lags are shown in Figure 7.111 and Figure 7.112. The following observations are made from these figures.

The magnitude of the peak displacement and the time of its occurrence are very well matched by the simulation whether the layer thicknesses are assumed to be known (Figure 7.111), or when the layer thickness are assumed to be unknown (Figure 7.112).

Table 7.24 Profile used for Kansas site with combined AC and ATB layer

Layer Name	Thickness (in)	Unit Weight (pcf)	Poisson's Ratio
AC	11.3	145	0.3
Base	6	135	0.35
Subgrade	∞	125	0.45

Table 7.25 Backcalculation results for Kansas site

	True Value	Seed Value	Dynamic Backcalculation		Static Backcalculation using MICHBACK
			Excluding Thicknesses (Case 1)	All Parameters (Case 2)	
AC modulus (ksi)	Unknown	350	446.6	383.1	479.4
AC damping ratio	Unknown	0.2	0.15	0.21	—
AC thickness (in.)	11.3	8 (Case 2 only)	—	13.80 (22.1%)	—
Base modulus (ksi)	Unknown	20	5.43	5.50	4.25
Base damping ratio	Unknown	0.1	0.22	0.18	—
Base thickness	6	12.3 (Case 2 only)	—	6.57 (9.5%)	—
Subgrade modulus (ksi)	Unknown	10	42.1	41.4	53.21
Subgrade damping ratio	Unknown	0.1	0.19	0.21	—

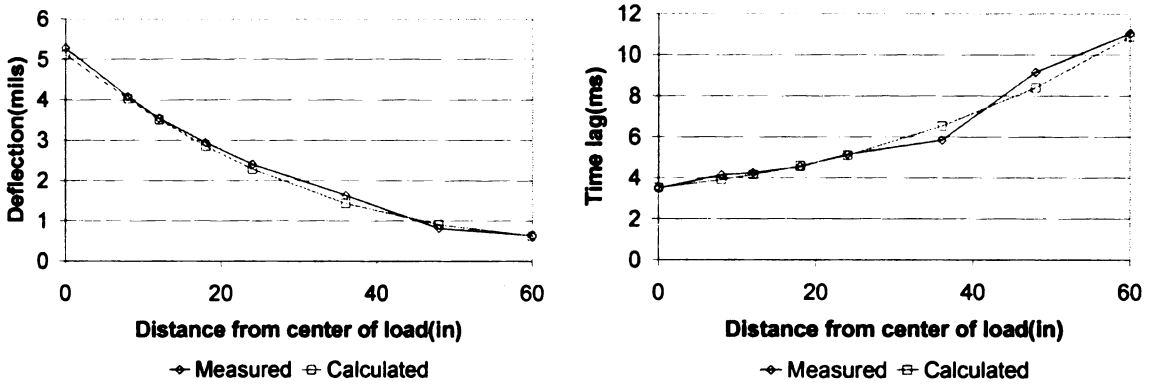

Figure 7.111 Comparison of measured and calculated peak deflections and time lags for case 1 (three layer backcalculation)

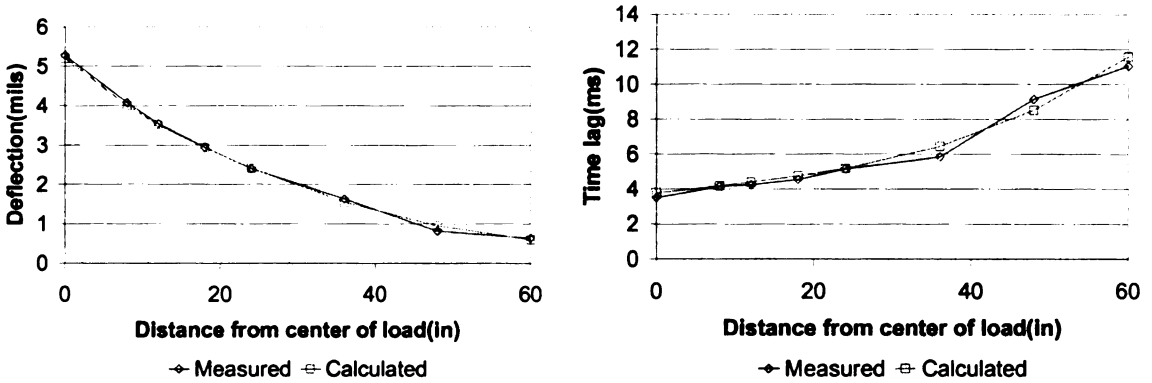

Figure 7.112 Comparison of measured and calculated peak deflection and time lag for case 2 (three layer backcalculation)

7.2.5.3 Dynamic Time-domain Backcalculation using Traces of Time History

First, the relation between convergence and α is investigated; Figure 7.113 shows that an α–value of 3 or 4 is appropriate.

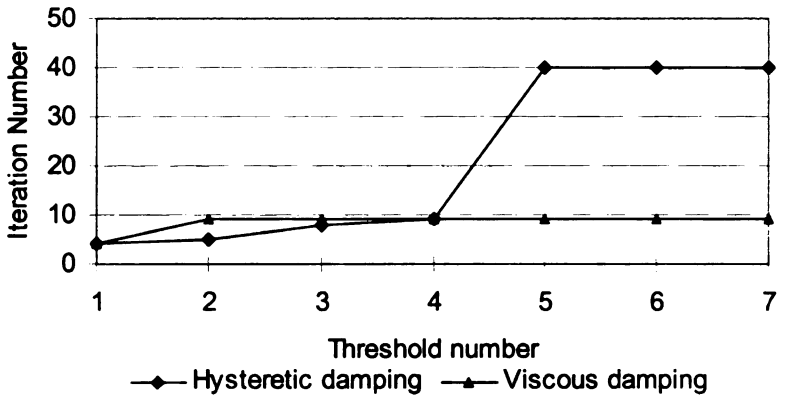

Figure 7.113 Iteration number to convergence versus α for Kansas site

In this following section, the combined profile listed in Table 7.24 will be used in the backcalculation analysis. Figure 7.114 to Figure 7.121 show the traces of time histories for different sensors. Figure 7.122 demonstrates that the three models give close prediction for this site. The difference between the DYNABACK with hysteretic and viscous damping is -3% for AC, -3% for base, and 4% for subgrade. The difference between the backcalculated moduli from FEM and those from DYNABACK with hysteretic damping is –2% for AC, and 45% for base, and –6% for subgrade.

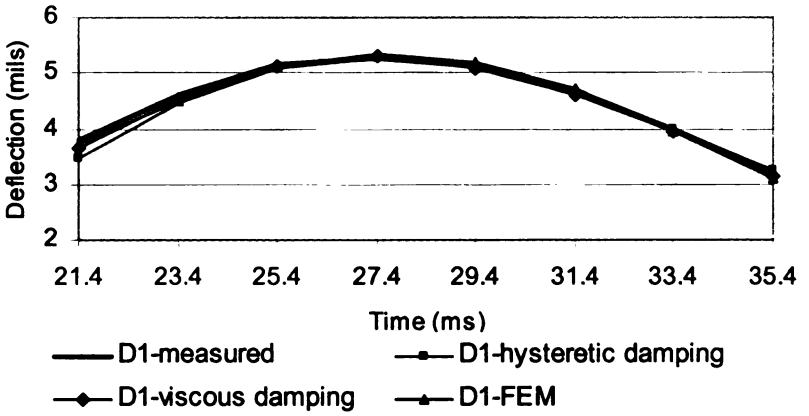

Figure 7.114 Comparison of measured and predicted deflection time histories for sensor 1

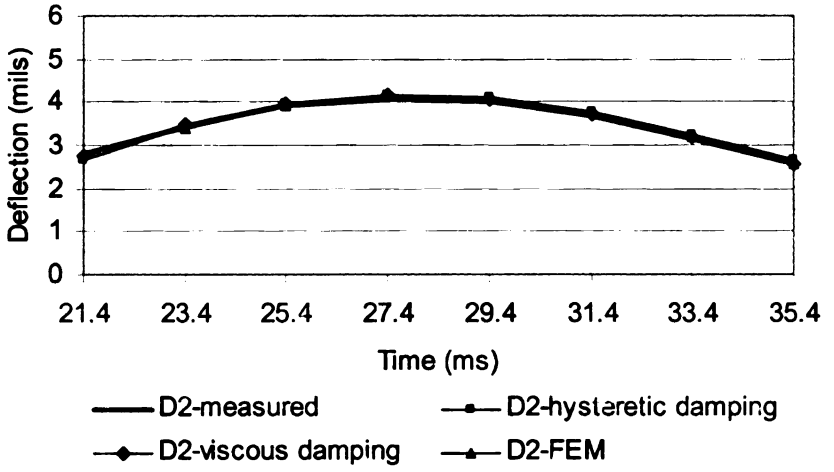

Figure 7.115 Comparison of measured and predicted deflection time histories for sensor 2

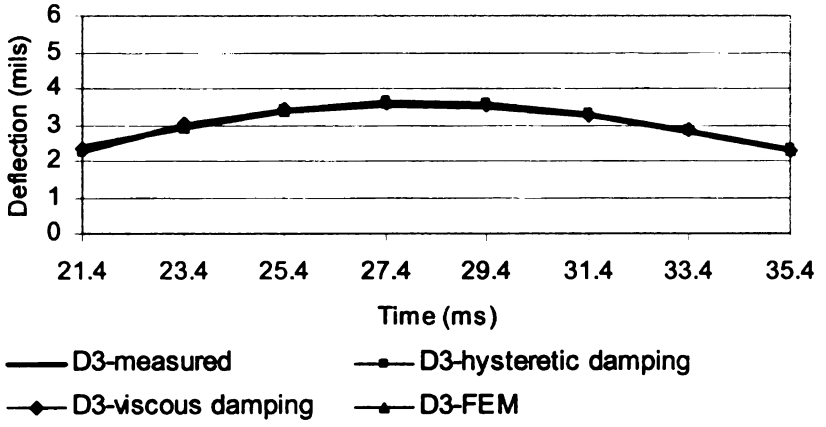

Figure 7.116 Comparison of measured and predicted deflection time histories for sensor 3

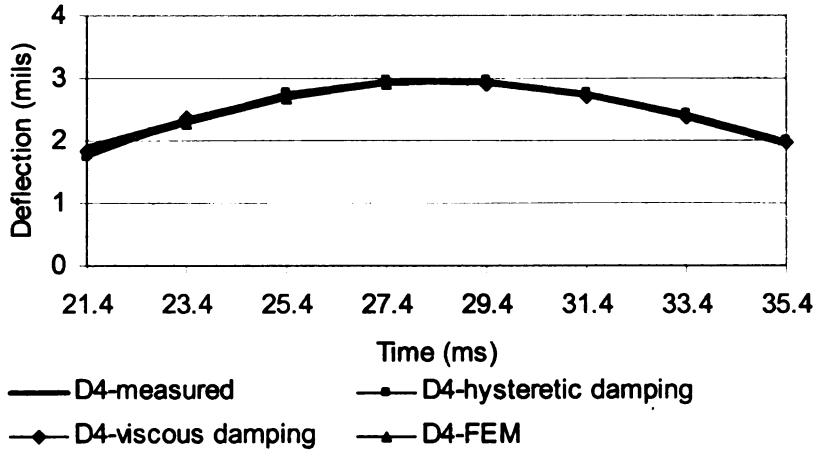

Figure 7.117 Comparison of measured and predicted deflection time histories for sensor 4

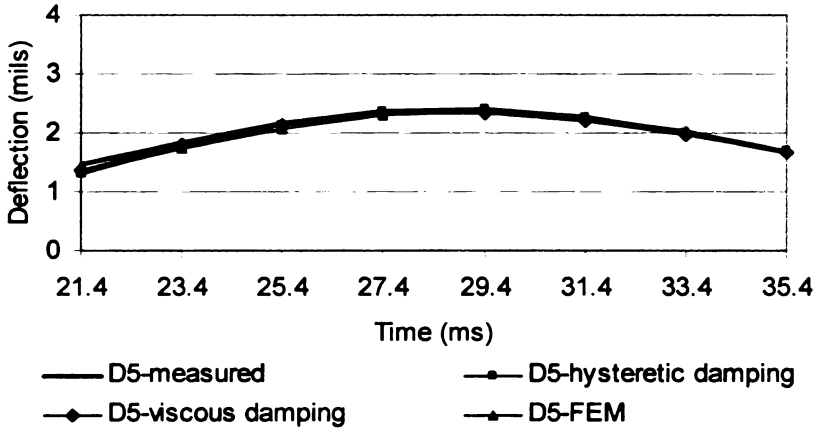

Figure 7.118 Comparison of measured and predicted deflection time histories for sensor 5

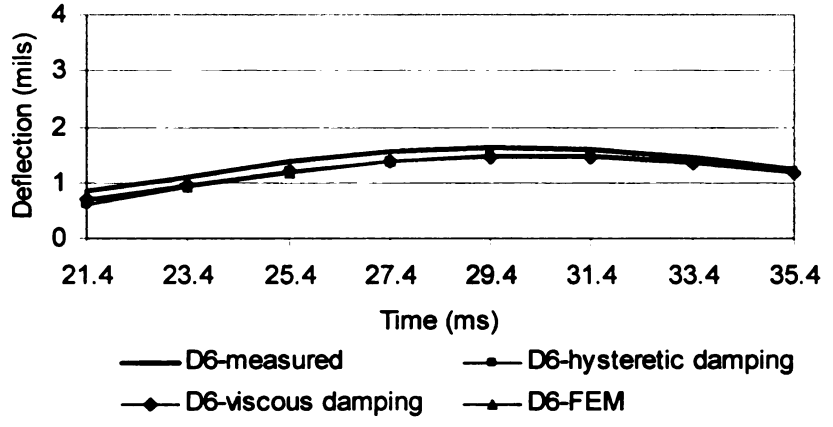

Figure 7.119 Comparison of measured and predicted deflection time histories for sensor 6

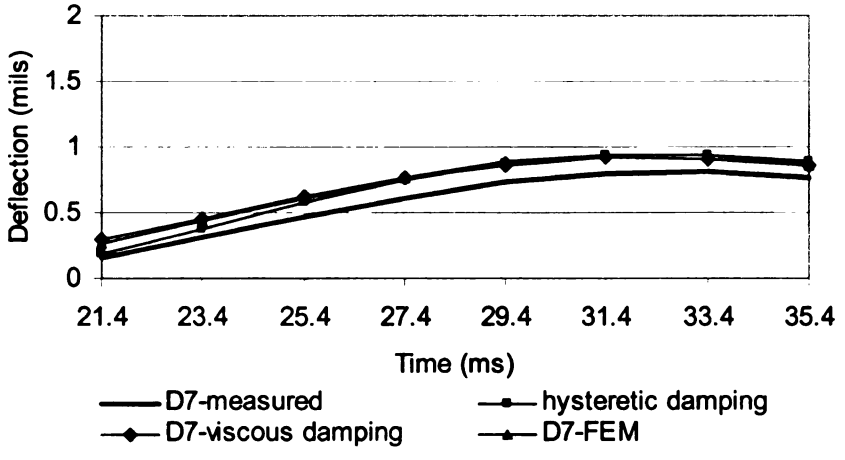

Figure 7.120 Comparison of measured and predicted deflection time histories for sensor 7

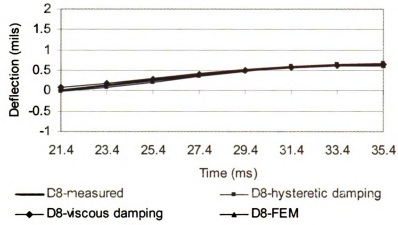

Figure 7.121 Comparison of measured and predicted deflection time histories for sensor 8

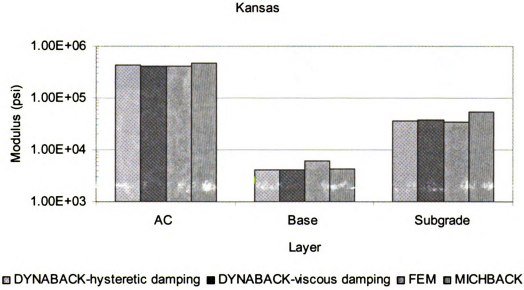

Figure 7.122 Comparison of backcalculated moduli from different models

In the second part of the analysis, different seed parameters were used for the uniqueness analysis (see Table 7.26). The backcalculated results are shown in Figure 7.123.

Table 7.26 Seed values used for Kansas data

Layer	Case 1		Case 2		Case 3	
Layer	Seed Modulus (ksi)	Seed Damping	Seed Modulus (ksi)	Seed Damping	Seed Modulus (ksi)	Seed Damping
AC	250	0.1	850	0.15	100	0.2
Base	70	0.05	10	0.08	15	0.1
Subgrade	70	0.03	10	0.05	15	0.05

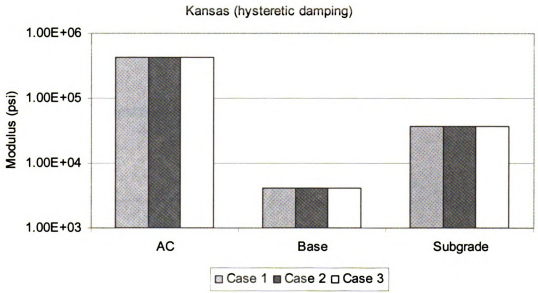

Figure 7.123 Comparison of backcalculated layer moduli using different seed values

In the third part of the analysis, the same profile is used except that the AC layer thickness is unknown. Various combinations of damping for base and subgrade, as listed in Table 7.7, are used for the backcalculation. The results are shown in Figure 7.124 through Figure 7.128. Backcalculated moduli for all combinations are in agreement with the reference case (Figure 7.122) meaning that for this site the choice of base and subgrade damping ratio did not affect the backcalculated layer moduli. Also, the AC damping ratio did not vary much (16% to 24%). Finally, the backcalculated thickness AC varies from 4% to 8% from the true value, which is an excellent result.

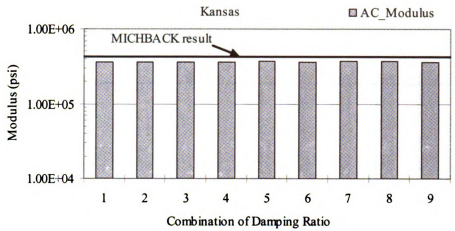

Figure 7.124 Comparison of backcalculated AC modulus for different damping ratio combinations of base and subgrade layers

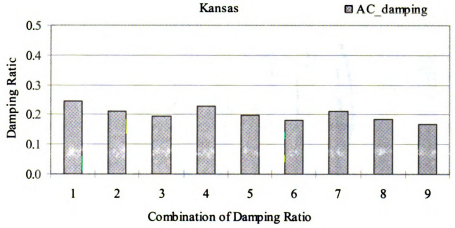

Figure 7.125 Comparison of backcalculated AC damping ratio for different damping ratio combinations of base and subgrade layers

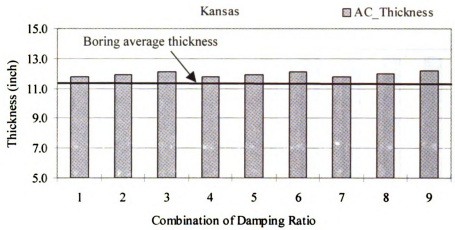

Figure 7.126 Comparison of backcalculated AC damping ratio for different damping ratio combinations of base and subgrade layers

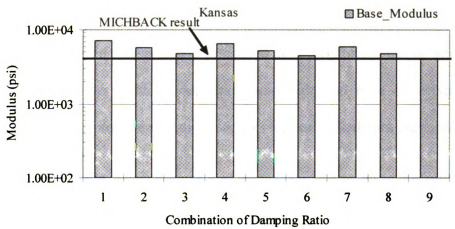

Figure 7.127 Comparison of backcalculated AC damping ratio for different damping ratio combinations of base and subgrade layers

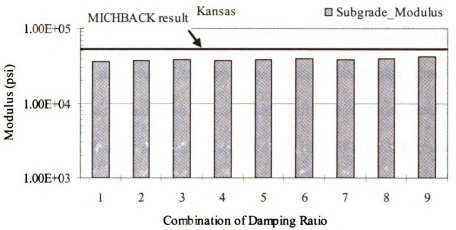

Figure 7.128 Comparison of backcalculated AC damping ratio for different damping ratio combinations of base and subgrade layers

7.3 Discussion

The discrepancies between measured and calculated deflection basins can be attributed to either measurement errors (both in deflection amplitude and time or arrival) or the inability of the theory to produce realistic responses for backcalculation purposes.

Measurement errors could be random or systematic. No matter what the nature of the error is, the consequence is a variation in the deflection. Moreover, truncated time records cause systematic errors in the frequency-based backcalculation solution. This will result in deflection basins that are different enough to change the backcalculation results.

While the program can theoretically backcalculate more parameters than typically allowed, the use of field data causes the program not to coverage. The program will then select the parameters corresponding to the lowest RMS automatically, which will potentially cause errors in the backcalculation results.

When using field data, time-domain backcalculation is preferred over frequency-domain backcalculation because the inaccurate regions of the FWD response time histories can be ignored and because of the truncations typically imposed on sensor time records. However, time-domain backcalculation is computationally much more intensive than frequency-domain backcalculation. Finally the use of an interpolation scheme and a cut off frequency in the forward calculation may potentially cause some errors in time-domain backcalculation results.

Ill conditioning is a serious issue in dynamic backcalculation when using field data. How to deal with it will determine not only the convergence in the backcalcultion process but also the quality of matches between measured and calculated deflection time histories. The use of the singular value decomposition (SVD) method with the appropriate truncation of the smaller singular value does improve the convergence of dynamic backcalculation solution and achieve better matches between measured and calculated deflections. The recommended threshold for the relative allowable error is about 10^{-3} to 10^{-4} when using field data. It should be noted that there is no need for truncation using synthetic FWD data since the same forward program is used for backcalculation. The field backcalction results show that viscous damping does not necessary lead to more accurate result than hysteretic damping. It may mean that viscous damping does not describe flexible pavement response better than hysteretic damping. While other rheologic method may be better suited for describing the real response of pavement materials, then use in the backcalculation problem is not possible at this time because of the increased number of parameters to be backcalculated.

In summary, dynamic backcalculation of layer parameters using field data presents some serious challenges. The frequency-domain method can lead to large errors if the measured FWD records are truncated before the motions fully decay in time, and the time-domain methods produce mixed results. At this point, it is recommended that time-domain solutions should be further explored when analyzing field data, mainly because of the truncation problem associated with the frequency-domain solution.

Simultaneous backcalculation of layer moduli and thicknesses is a difficult problem to solve when using field data. The results presented in this chapter showed that it is possible to backcalculate the AC thickness (with some error) when using three-layer pavement systems with assumed damping values for the base and subgrade. However, this problem needs to be fully studied.

CHAPTER 8 - CONCLUSIONS AND RECOMMENDATIONS

8.1 Summary

In this study, a new method for backcalculating flexible pavement layer parameters based on dynamic interpretation of FWD deflection time histories using frequency and time-domain solutions have been developed. The method allows for theoretically backcalculating the layer moduli, damping ratios and thicknesses for a three to five- layer system. The new associated program called DYNABACK has been written in the FORTRAN 77 language, and offers two options: (i) frequency-domain analysis, and (ii) time-domain analysis.

The new program uses the SAPSI program (Chen, 1987) as its forward routine. SAPSI models the pavement structure as a system of layers that are infinite in the horizontal direction and underlain by an elastic half-space. The materials are assumed to be isotropic and linearly elastic with hysteretic damping. Full interface bonding is assumed at the layer interfaces. The mass densities and elastic moduli are assumed to be constant within each layer. The steady-state solution in SAPSI is used for the frequency-domain backcalculation, while the transient solution is used for the time-domain backcalculation.

The dynamic backcalculation procedure is based on the modified Newton-Raphson method originally adopted in the MICHBACK program (Mahmood, 1993). Either the least squares method or singular value decomposition (SVD), with scaling and truncation can be used to solve the over determined set of equations. In the MICHBACK solution, this set of equations is real-valued and correspond to the peak deflection values, since the

backcalculation scheme uses a static solution (CHEVRONX) to predict the deflection basin. In the frequency-domain solution, the equations are complex-valued and correspond to the steady-state solution at one or multiple frequencies. In the time-domain solution, the real-valued equations are expanded to correspond to the peak transient deflections and their corresponding time lags relative to the peak load or to include traces of time history near the peaks.

In addition, methods for estimating the depth to stiff layer and the seed subgrade modulus, proposed by Roesset (1995) and Lee et.al. (1998), respectively, have been adopted with some modifications and are implemented in the new program.

The new program has been incorporated into the Windows^{TM} based MFPDS program, which allows for user–friendly features including interactive input and output screens, and the ability to view and process the deflection data before analyzing it.

The new program was theoretically verified using synthetic data, and its application to mechanistically-based pavement design and rehabilitation was evaluated using field FWD data.

For the theoretical verifications, time histories of FWD surface deflections generated from SAPSI were used to verify the capabilities of the newly developed dynamic backcalculation program. The backcalculation was done using both frequency and time-domain solutions. Various pavement profiles of different combinations of layer thicknesses and moduli with up to five layers were analyzed. Some profiles included cases where there was a shallow bedrock or ground water table. In addition to conducting

a sensitivity analysis, the effects of signal truncations in time and imprecision of the measured sensor deflections were also investigated theoretically.

To evaluate the applicability of the DYNABACK to interpret field tests, measured deflection time history data from several FWD tests conducted in Michigan and elsewhere were analyzed. The selected pavement test sections included sites in Texas, Cornell University, Florence (Italy), Michigan and a SPS-1 site in Kansas. For the Texas site, different load levels were considered. The analyses included the comparison of backcalculated layer moduli and damping ratios with MICHBACK results for various pavement sections and load levels. The backcalculation was done in both frequency and time domains, where the time-domain solution included backcalculating layer moduli and thicknesses. The data were obtained from tests involving KUAB and Dynatest FWD machines. Most pavement sections were analyzed as three- and four- layer systems with some sections involving a stiff layer at shallow depth.

8.2 Conclusions

Based on the theoretical verification analysis, the following conclusions were drawn for frequency-domain backcalculation:

1. The backcalculation results are all in excellent agreement with the true values. Both the average root mean square error (RMS) on the calculated and actual deflection basins, and the relative errors on layer moduli and thicknesses are practically zero, indicating that the program has the ability of backcalculate the moduli and thicknesses accurately.

2. Theoretical backcalculation shows that among the modulus, damping ratio, thickness and Poisson's ratio, the modulus is the easiest to backcalculate followed by damping ratio, thickness and Poisson's ratio.

3. Theoretical backcalculation shows that the frequency backcalculation program gives satisfactory convergence of layer moduli and thicknesses when using untruncated deflection time histories. However backcalculation results at higher frequencies are less accurate than those obtained at low frequencies.

4. Although Poisson's ratio of the AC layer is frequency-dependent, assuming a constant value for it will not affect the results significantly because the backcalculated results are not sensitive to reasonable variations in this parameter.

5. The frequency response-based backcalculation method can lead to large errors in deflection basins if the FWD records are truncated before the motions fully decay in time. The errors due to sensor imprecision were found to be less significant.

The following conclusions were drawn from the theoretical verification analysis for time-domain backcalculation:

6. Backcalculation based on synthetic time histories generated by SAPSI shows excellent stability and accuracy, therefore Newton-Raphson method could be used with the time-domain backcalculation.

7. The time-domain approach can match selected features of the measured time histories directly, and ignore the inaccurate measurement regions in time.

Therefore, from this point of view, the time-domain backcalculation is better than the frequency-domain backcalculation.

8. Numerical examples have illustrated that the method is able to backcalculate layer moduli and thicknesses accurately from synthetically generated FWD data for a three layer pavement system. Backcalculation of layer damping ratios are less accurate, but the influence of this error on the pavement response is insignificant.

In terms of field evaluation of the new backcalculation solutions, the results were not satisfactory. The discrepancies between measured and calculated deflection basins can be attributed to several factors including:

- Sensor measurement errors;
- Time synchronization errors in the data acquisition systems for sensor measurements;
- Truncated time records, which cause systematic errors in the frequency-based backcalculation solution;
- Improper characterization of damping effects.

While the program can theoretically backcalculate more parameters than typically allowed, using field data causes the program not to converge. The program will instead select the parameters corresponding to the lowest RMS automatically, which will potentially cause errors in the backcalculation results.

The following conclusions were reached from the analysis involving field FWD data:

1. When using field data, time-domain backcalculation is preferred over frequency-domain backcalculation because the inaccurate regions of the FWD response time histories can be ignored and because of the truncations typically imposed on sensor time records.

2. Ill conditioning is a serious issue in dynamic backcalculation when using field data. The use of singular value decomposition (SVD) method with scaling and appropriate truncation of the smallest singular values does improve the convergence of the solution and achieve better matches between measured and calculated time histories. The recommended threshold for the relative allowable error is about 10^{-3} to 10^{-4}.

3. Simultaneous backcalculation of layer moduli and thicknesses is a difficult problem to solve when using field data. However, the results presented in this research show that it is possible to backcalculate the AC layer thickness (with some error) when using three-layer pavement system with assumed damping value for the base and subgrade.

8.3 Recommendations

Based on the results from this research, the following recommendations are made:

1. Dynamic backcalculation of layer parameters using field data presents some serious challenges. The frequency-domain method can lead to large errors if the measured FWD records are truncated before the motions fully decay in time, and the time-domain methods produce mixed results. At this point, it is recommended

that time-domain solutions are used when analyzing field data, mainly because of the truncation problem associated with the frequency-domain solution.

2. Simultaneous backcalculation of layer moduli and thicknesses is a difficult problem to solve when using field data. This problem needs to be studied further.

3. Determining the depth to bedrock and the depth to ground water table requires the recording of free vibrations from FWD tests. The recorded time histories from existing FWD system usually not long enough for this purpose. Therefore their duration need to be increased to allow for at least two free vibration cycles.

4. Temperature is a very important factor affecting the behavior of asphalt concrete layer. Incorperating the variation of AC layer modulus as a function of temperature with depth should be considered in the future research.

5. SAPSI computer program is based on the assumption of linear viscoelastic behavior. In reality asphalt concrete is a nonlinear viscoelastic material, and its response depends on load level and duration as well as temperature. Also nonlinear characteristics for unbound granular materials and fine-grained soil materials should be considered. This non-linear effect should be considered in future research.

6. The effect of Poisson's ratio is another factor for backcalculation. Poisson's ratio is a function of temperature and frequency of loading. The current backcalculation solution assumes a constant real value for poisson's ratio. Other

rhelogic model that account for frequency-dependent complex moduli and poisson's ratio should be considered.

7. There is a need for investigating the relationship between damping obtained from backcalculation and pavement distress.

BIBLIOGRAPHY

1. Acum, W. E. A., Fox, L., "Computation of Load Stresses in a Three-Layer Elastic System," Geotechnique, Vol. 2(4): 293~300,1951.

2. Al-Khoury, R., Scarpas, A., Kasbergen, C. and Blaauwendraad, J., "Spectral Forward and Inverse Models for Parameter Identification of Layered Media," The International Journal of Geomechanics, Vol 1 (4) pp. 441-458, 2001.

3. Al-Khoury, R., Scarpas, A., Kasbergen, C. and Blaauwendraad, J., "Spectral Element Technique for Efficient Parameter Identification of Layered Media. Part I: Forward Calculation," International Journal of Solids and Structures, Vol 38, pp. 1605-1623, 2001.

4. Al-Khoury, R., Scarpas, A., Kasbergen, C. and Blaauwendraad, J., "Spectral Element Technique for Efficient Parameter Identification of Layered Media. Part II: Inverse Calculation," International Journal of Solids and Structures, Vol 38, pp. 8753-8772, 2001.

5. Al-Khoury, R., Scarpas, A., Kasbergen, C. and Blaauwendraad, J., "Spectral Element Technique for Efficient Parameter Identification of Layered Media. Part III: Viscoelastic Aspects," International Journal of Solids and Structures, Vol 39, pp. 2189-2201, 2002.

6. American Association of State Highway officials, " AASHO Interim Guide for Design of Pavement Structures 1972, " AASHO, AASHO Committee on Design, Washington, D. C., 1972.

7. American Association of State, Highway, and Transportation officials, "AASHTO Guide for Design of Pavement Structures," AASHTO, Washington, D.C., 1986.

8. Bentsen, R. A., Nazarian, S. and Harrison, J. A., " Reliability Testing of Seven Nondestructive Testing Devices" Nondestructive Testing of Pavements and Backcalculation of Moduli, ASTM STP 1026, A. J. Bush III and G. Y. Baladi, Eds., American Society for Testing and Materials, Philadelphia, pp 41 – 58, 1989.

9. Burmister, D. M., "The Theory of Stresses and Displacements in Layered Systems and Application to the Design of Airport Runways," Proceedings Highway Research Board, Vol. 23,1943.

10. Burmister, D. M., "The General Theory of Stress and Displacements in Layered Soil System," Journal of Applied Physics, 16(2): 89~94,1945.

11. Bush, A. J., "Computer Program BISDEF," U S Army Corps of Engineer Waterways Experiment Station, Vicksburg. Miss.,1985.

12. Bush, A. J., Alexander, D. R., "Pavement Evaluation Using Deflection Basin Measurements and Layered Theory," Transportation Research Record 1022, Transportation Research Board, National Research Council, Washington D C, 16~29,1985.

13. Chang D. W., Kang, Y. V., Roesset, J. M. and Stokoe II, K. H., "Effect of Depth to Bedrock on Deflection Basins Obtained with Dynaflect and Falling Weight Deflectometer Tests" Transportation Research Record 1355, pp 8-16, 1992.

14. Chatti, K. and Yun, K.K., "SAPSI-M: A Computer Program for Analyzing Asphalt Concrete Pavements Under Moving Arbitrary Loads", Transportation Research Record No. 1539, pp. 88-95, 1996.

15. Chatti, K., W.S. Haider, H.S. Lee, Y.G. Ji, and H. Salama. "Evaluation of Non-linear and Dynamic Effects on Pavement Response under FWD Loading". International Journal of Pavements, Vol. 2, pp. 88-99, 2003.

16. Chen, S. S. "The Response of Multilayered Systems to Dynamic Surface Loads. Ph.D. Dissertation, University of California, Berkeley, 1987.

17. Chou, Y. J. and Lytton, R. L., "Accuracy and Consistency of Backcalculated Pavement Layer Moduli", Transportation Research Record No. 1293, pp. 72-85, 1991.

18. Chua, K. M. and Lytton, R. L.," Load Rating of light Pavement Structures," Transportation Research Record 1043, Transportation Research Board, National Research Council, Washington D C, 1984.

19. Clough, R. W., and Penzien, J. Dynamics of Structure. McGraw-Hill, NY, 1975.

20. Dejong, D. L., Peutz, G. F., Korswagen, A. R., "Computer Program BISAR. Layered System under Normal and Tangential Surface Loads," Konink-Lijkel/ Shell-Laboratorium Amsterdam the Netherlands, External Report, ASMR.0006.73, 1973.

21. Haddad, Y. M., " Viscoelasticity of Engineering Materials," Chapman & Hall, London, 1995.

22. Harichandran, R. S., T. Mahmood, A. Raab, and G.Y. Baladi, "Backcalculation of Pavement Layer Moduli, Thicknesses and Bedrock Depth Using a Modified Newton Method." In Nondestructive Testing of Pavements and Backcalculation of Moduli (Second Volume), ASTM STP 1198, H. L. Von Quintus, A. J. Bush and G. Y. Baladi (eds.) American Society for Testing and Materials, Philadelphia, PA, pp. 68-82, 1994.

23. Huang, Y. H., "Pavement Analysis and Design," Prentice Hall, New Jersey, 1993

24. Hunt, H. E. M., "Stochastic Modeling of Traffic-induced Ground Vibrations," Journal of Sound and Vibration, Vol 144(1), pp. 53-70, 1991.

25. Irwin, L. H., Yang, W. S. and Stubstad, R. N., " Deflection Reading Accuracy and Layer Thickness Accuracy in Backcalculation of Pavement Layer Moduli," Nondestructive Testing of Pavements and Backcalculation of Moduli, ASTM STP 1026, A. J. Bush III and G. Y. Baladi, Eds., American Society for Testing and Materials, Philadelphia, pp. 229 – 244,1989.

26. Irwin, L. H., "Instructional Guide for Back-Calculation and the Use of MODCOMP, "CLRP Publication No. 94-10, Cornell University, Local Roads Program, Ithaca, NY, March 1994.

27. Jones, A., "Tables of Stresses in Three Layer Elastic Systems," Highway Res. Board. Bull., Vol 34(2): pp.176~214,1962.

28. Kausel, E. and Roesset, J. M., Stiffness Matrices for Layered Soils. Bulletin of the Seismological Society of America, Vol. 71 No. 6, pp.1743-1761,1981.

29. Kausel, E., Peek, R.," Dynamic Loads in the Interior of a Layered Stratum: An Explicit Solution," Bulletin of the Seismological Society of America, 72(5): pp.1459~1482, 1982.

30. Kang, Y. V., "Effect of Finite Width on Dynamic Deflections of Pavement," Ph. D Dissertation. University of Texas, Austin, 1990.

31. Kang, Y. V., "Multifrequency Back-Calculation of Pavement-Layer Moduli," Journal of Transportation Engineering vol. 124 (1): pp.73-81, 1998.

32. Kang, Y. V., "Use of Multifrequency Back-Calculation for Determining Moduli of a Pavement Structure," Nondestructive Testing of Pavements and Backcalculation of Moduli (Third Volume), ASTM STP 1375, S.D. Tayabji and E. O. Lukanen, Eds., American Society for Testing and Materials, West Conshohocken, pp. 383 –397, 2000.

33. Kopperman, S., Tiller, G., Tseng, M. T., "ELSYM5 Interactive Microcomputer Version, User's Manual," IBM-PC and compatible Version," FHWA, Final Report, Contract No. DTFH61-85-c-00051, September, 1985.

34. Lang, R., Zeng, S. P., "Efficient Dynamic Analysis of Multilayered System During Falling Weight Deflectometer Experiments," Journal of Transportation Engineering vol. 128 pp. 366-374, 2002.

35. Lee, Y. C., Kim, Y. R. and Ranjithan, S. R., " Dynamic Analysis-Based Approach to Determine Flexible Pavement Layer Moduli Using Deflection Basin Parameters," Transportation Research Record 1639, pp 36 - 42, 1998.

36. Loannides, A. M., Barenberg, E. J., Lary, J. A., "Interpretation of Falling Weight Deflectometer Results Using Principles of Dimensional Analysis," Proceedings 4th Conference on Concrete Pavement Design and Rehabilitation, Purdue University, West Lafayette, Indiana, pp.231~247,1989.

37. Losa, M., "The Influence of Asphalt Pavement Layer Properties on Vibration Transmission," Int. Journal of Pavements, Vol. 1, No. 1, pp. 67-76, 2002.

38. Luco J. E., Apsel R. J., "On the Green's Function for a Layered Half-Space, Part Ⅰ", Bulletin of the Seismological Society of America, Vol. 73, pp. 909-929,1983

39. Magnuson, A. H., Lytton, R. L., Briggs, R., "Comparison of Computer Predictions and Field Data for Dynamic Analysis of Falling-Weight Deflectometer Data," Transportation Research Record 1293, Backcalculation of Pavement Moduli, Transportation Research Board, National Research Council, Washington D C,pp. 61~71,1991.

40. Mahmood, T. Backcalculation of Pavement Layer Properties from Deflection Data. ; Ph.D. dissertation, Michigan State University , 1993.

41. Matsui K., Nishizawa T. and Kikuta Y., "Time Domain Backcalculation of Pavements", Structual Materials Technolodgy III: An NDT Conference. Editor(s) Ronald D. Medlock, David C. Laffrey, San Antonio, TX, vol. 3400, pp. 410-419, 1998.

42. Meier, R. W., Rix G. J.," Backcalculation of Flexible Pavement Moduli Using Artificial Neural Networks," paper No. 940678, 73 Annual Meeting of the Transportation Research Board, Washington, D. C., 1994.

43. Meier, R. W., Rix G. J.," Backcalculation of Flexible Pavement Moduli From Dynamic Deflection Basins Using Artificial Neural Networks," paper No. 950900, 74 Annual Meeting of the Transportation Research Board, Washington, D. C., 1995.

44. Nazarian, S., and Stokoe, K. H., "Non-destructive Testing of Pavements using Surface Waves" Transportation Research Board 993, pp. 67-79,1993.

45. Odemark, N.," Investigations as to the Elastic Properties of Soils Design of Pavements According to Theory of Elasticity," Staten Vaeginstitut, Stockholm, Sweden, 1949.

46. Ong Cheng Ling, David, E. N. and Raj Siddharthan, "Comparison of Dynamic and Static Backcalculation Moduli for Three-Layer Pavements," Transportation Research Record 1293, pp 86-92, 1991.

47. Olard F., and Di Benedetto H. "General 2S2D1D model and relation between the linear visoelastic behaviors of bituminous binders and mixes," Road Materials and Pavement Design Volume 4, pp.185-224, 2003.

48. Raad, L. and Figueroa," Load Response of Transportation Support Systems," Transportation Engineering Journal ASCE, Vol. 106 (1), pp. 111-128, 1980.

49. Pitchumani, R., "Applications of Computer Codes to the Analysis of Flexible Pavements," Proceedings, Third International Conference on the Structural Design of

Asphalt Pavements, University of Michigan, Ann Arbor, Vol 1, pp. 506-520, September 1972.

50. Press, W.H., Flannery, B.P., Teukolsky, S.A., Vetterling, W.T., "Numerical Recipes". Cambridge University Press, Cambridge, 1989.

51. Roesset, J. M., "Computer Program UTFWIBM," The University of Texas at Austin, TX, 1987.

52. Roesset J. M. and Kenneth H. Stokoe II, and Chia-Ray Seng, "Determination of depth to bedrock from Falling weight Deflectometer Test Data" Transportation Research Record 1504, pp. 68-78, 1995.

53. Sebaaly, B., Davis, T.G., and Mamlouk, M. S., "Dynamics of Falling Weight Deflectometer. Journal of Transportation Engineering, ASCE, 116(6), pp. 618-632, 1985.

54. Seed, H. B. ,Wong, R.T. , Idriss, I. M. and Tokimatsu, K., "Moduli and Damping Factors for Dynamic Analysis of Cohesive Soils," Journal of Geot. ENG., ASCE, Vol. 117(8) pp. 1133-1151, 1991.

55. Shames, I. H. and Cozzarelli, F. A., " Elastic and Inelastic Stress Analysis" Pretice Hall,1992.

56. Sivaneswaran, N., Steven, L. K. and Mahoney, J. P., "Advance Backcalculation Using a Nonlinear Least Square Optimization Technique," Transportation Research Record 1293, pp. 93-102, 1991.

57. Sousa, J. B., "Dynamic Response of Paving Materials," Ph.D. Dissertation. University of California, Berkeley, 1986.

58. Sousa, J. B. and Monismith, C.L., "Dynamic Response of Paving Materials," Transportation Research Record 1136, TRB, National Research Council, Washington, D. C., pp. 57-68, 1987.

59. Stubbs, N., Torpunuri, V. S., Lytton, R. L., Magnuson, A., "A Methodology to Identify Material Properties in Pavements Modeled as Layered Visco-Elastic Halfspace (Theory)," Nondestructive Testing of Pavements and Backcalculation of Moduli (Second Volume), ASTM STP 1198, American Society for Testing and Materials, (H. L. Von Quintus, A. J. Bush and G. Y. Baladi eds.), Philadelphia, pp.53~67, 1994

60. Tajirian, F. T., Impedance Matrices and Interpolation Techniques for 3-D Interaction Analysis by the Flexible Volume Method, Ph.D. dissertation, University of California, Berkeley, 1981.

61. Torpunuri, V. S., Stubbs, N., Lytton, R. L., et al, "Field Validation of a Methodology to Identify Material Properties in Pavements Modeled as Layered Visco-Elastic

Halfspace. Nondestructive Testing of Pavements and Backcalculation of Moduli (Second Volume)," ASTM STP 1198, American Society for Testing and Materials, (H. L. Von Quintus, A. J. Bush and G. Y. Baladi eds.), Philadelphia, pp.159~169, 1994.

62. Trevor, G. Davis and Mamlouk, M. S., "Theoretical Response of Multilayer Pavement System to Dynamic Nondestructive Testing," Transportation Research Record 1022, pp. 1–6, 1985.

63. Ullidtz, P., Battiato, G., et al, "Verification of the Analytical-Empirical Method of Pavement Evaluation Based on FWD Testing," Proceedings 6th International Conference on Structural Design of Asphalt Pavements, University of Michigan, Ann Arbor, Mich., Vol. 1, pp. 521~532, 1987.

64. Uzan J., Scullion, M., Paredes, C. H. and Lytton, P. L., "A Microcomputer Based Procedure for Backcalculating Layer Moduli from FWD Data," Texas Transportation Institute, July, 1988.

65. Uzan, J., "Dynamic Linear Backcalculation of Pavement Material Parameters." Journal of Transportation Engineering, ASCE ,Vol. 120(1), pp. 109-126, 1994.

66. Uzan, J., "Advanced Backcalculation Techniques" Nondestructive Testing of Pavements and Backcalculation of Moduli (Second Volume), ASTM STP 1198, American Society for Testing and Materials, (Harold L, Quintas V et al ed.), Philadelphia, PP. 3~37,1994.

67. Ullidtz, P., "Pavement Analysis". Elsevier, Amesterdam, 1987.

68. Wang, F. M., Lytton, R. L., "System Identification Method for Backcalculating Pavement Layer Properties," Transportation Research Record 1384, Transportation Research Board, National Research Council, Washington D C, pp. 1~7, 1993.

69. Waas G., Riggs H. R., Werkle H, "Displacement Solutions for Dynamic loads in Transversely-isotropic stratified media," Earthquake Engineering and Structure Dynamics, Vol. 13, pp.173-193,1985.

70. Warren, H., and Dieckmann, W. L., "Numerical Computation of Stresses and Strains in a Multiple-layer Asphalt Pavement System" Internal report, Chevron Research Corporation, Richmond, CA, 1963.

71. Wolf, J. P., "Dynamic Soil-Structure Interaction," Prentice-Hall, Inc. New York, 1985.

72. Yeh, M.S., Nonlinear finite element analysis and design of flexible pavements.: Ph.D. Dissertation. Michigan State University, 1989.

73. Zaghloul, S. M., White, T. D., Drnevich, V. P., and Coree, B., "Dynamic Analysis of FWD Loading and Pavement Response Using a Three Dimensional Dynamic FiniteElement Program", Nondestructive Testing of Pavements and Backcalculation

of Moduli (Second Volume), ASTM STP 1198, American Society for Testing and Materials, (Harold L, Quintas V et al ed.), Philadelphia, 1994, pp.125-142

74. Zhou, H. P., Hicks, R. G., Bell, C. A., "BOUSDEF: A Backcalculation Program for Determining Moduli of Pavements Structure," Transportation Research Record 1260, Transportation Research Board, National Research Council, Washington D. C., pp.166~179,1990.